Cholesterol dysregulation in the neuron astrocyte unit as an early contributor to neuronal dysfunction in Alzheimer's Disease

by

Hemant Kumar Mistry

Sheffield Institute for Translational Neuroscience
The University of Sheffield

Department of Neuroscience

Submitted for the degree of Doctor of Philosophy (PhD)

Date: September 2020

Contents

List of Figures

List of Tables

Acknowledgements

Firstly, I would like to acknowledge and thank my supervisors Prof Stephen Wharton and Dr Julie Simpson for providing me with this opportunity to develop as a scientific researcher and academic. I am forever grateful for the support and guidance throughout this journey and for encouraging me to maintain this pursuit, even when things were looking bleak. I would also like to thank my sponsors Alzheimer's Research UK and the Denise Coates Foundation for funding this PhD.

I am forever grateful to Dr Paul Heath, Dr Claire Garwood, Dr Annabelle Chambers, Dr Rachel Waller and Dr Irina Vázquez-Villaseñor for providing experimental expertise and guidance and for providing a forum to develop scientific ideas. I would also like to extend my thanks to the rest of the Neuropathology group and technical team at SiTraN, with a special thanks to Lynne Baxter and Dan Fillingham for always providing me with sections when needed.

I would also like to thank my fellow PhD students at SiTraN, only we know about the joys and pains that accompany this arduous process.

Finally, and most importantly, I would like to thank my parents for all their sacrifices to get me to where I am today, I am forever grateful. I would also like to thank my Gurus and my extended network of family and friends for the endless support, motivation and blessings throughout this journey. Without you, I would not have survived to tell the tale.

ॐ Tat sat

Abstract

Cholesterol is essential for normal neuronal function, but high blood cholesterol is a risk factor for Alzheimer's disease (AD). Astrocytes undertake the bulk of cholesterol synthesis in the brain; however, under stress conditions neurons can also synthesise cholesterol. Previous work showed that the neuronal DNA damage response is associated with lower cognitive function at the earliest stages of AD neuropathology, and this is associated with reduced expression of genes for cholesterol biosynthetic enzymes. The hypothesis for this study was that cholesterol dysregulation in neurons and astrocytes contributes to dementia and to the progression of AD. This study sought to determine the changes in expression of cholesterol biosynthetic enzymes in neurons and astrocytes with AD progression in post-mortem human tissue and in human neuronal and astrocytic monocultures.

Expression of HMG CoA reductase (HMGCR), the rate-limiting enzyme for cholesterol synthesis, and Sterol Regulatory Element Binding-Protein 2 (SREBP2), a key transcription factor regulating expression of cholesterol biosynthetic enzymes was examined by immunohistochemistry in the temporal cortex (Brodmann area 21/22) in an ageing population-based sample derived from a sub-cohort (n=99) of the Cognitive Function and Ageing Study (CFAS). Expression of HMGCR was predominantly associated with cortical pyramidal neurons within the cortex, although HMGCR expression was also associated with cells morphologically resembling astrocytes and oligodendrocytes in the cortex and white matter border regions of some cases. Quantification by determining HMGCR percentage immunoreactivity demonstrated population variation in HMGCR expression but no significant association with dementia status, AD neuropathology, oxidative DNA damage or neuroinflammation. SREBP2 was localised to neurons and astrocytes in temporal cortex and white matter regions.

Further work in post-mortem human tissue determined the expression of four key genes (*HMGCR, CYP46A1, ABCA1* and *SREBP2*) involved with cholesterol biosynthesis and metabolism; in neuronal and astrocyte cell populations isolated from temporal cortex tissue by laser capture microdissection, from a sub-set of cases that included all Braak and Braak neurofibrillary tangle stages (n=32). Staging for tau pathology correlated with changes in neuronal gene expression of *HMGCR*,

SREBP2 and *ABCA1*. Cholesterol concentration per mg of tissue was also determined in temporal cortex tissue using the Amplex Red cholesterol assay (n=63). Variation in tissue cholesterol concentration showed no significant association with dementia status, AD neuropathology, oxidative DNA damage or neuroinflammation. Furthermore, variation in HMGCR immunoreactivity and cholesterol biosynthetic gene expression in enriched samples of neurons and astrocytes isolated from temporal cortex did not correlate with temporal cortex cholesterol concentration. When tissue cholesterol concentration was categorically divided into tertiles and modelled using logistic regression analysis, moderate (OR:1.58, 95% CI: 0.39-6.43) and high (OR:1.44, 95% CI: 0.35-5.85) tissue cholesterol concentration was associated with dementia. However, the confidence intervals around these estimates were wide, indicating a high degree of uncertainty around the estimate.

In vitro work carried out in human neurons (LUHMES) and astrocytes (primary human foetal astrocytes) to determine the changes in expression of these genes in response to acute and a more chronic oxidative stress via a single and double exposure to H_2O_2. Both *in vitro* astrocytes and neurons expressed genes involved in cholesterol biosynthesis during neuronal proliferation, differentiation and in a post-mitotic state. Single and double exposure to 50 μM of H_2O_2 led to oxidative DNA damage in neurons and astrocytes, which persisted for 24 hrs and 96 hrs respectively. Preliminary data from stress experiments showed that the four key genes involved in cholesterol biosynthesis and metabolism (*HMGCR, ABCA1, SREBP2* and *APOE*) were expressed in both cell types following a single and double exposure to H_2O_2. However; due to the COVID-19 pandemic, these experiments could not be completed.

In conclusion, this study has demonstrated that neurons possess the machinery to carry out *de novo* cholesterol biosynthesis *in vivo* and *in vitro*. Changes in gene expression of key regulators of cholesterol biosynthesis and metabolism alter with increasing tau pathology. However, these changes do not translate to changes in tissue cholesterol levels. This suggests that whilst there may be some dysregulation of cholesterol biosynthetic gene expression with increasing tau pathology, brain

cholesterol itself is not altered by AD neuropathology and the association of altered brain cholesterol and dementia is weak.

Abbreviations

24(S)-OHC/ 24-OHC - 24(S)-hydroxycholesterol

3'UTR - 3' untranslated region

8-OHdG- 8-hydroxydeoxyguanosine

ABCA1 - ATP Binding Cassette A1

ABCA7 - ATP Binding Cassette A7

ABC-AP - Alkaline Phosphatase-conjugated Avidin-Biotin Complex

ABC-HRP - Horseradish Peroxidase-conjugated Avidin-Biotin Complex

ACH - Amyloid Cascade Hypothesis

AD - Alzheimer's Disease

ADAS-cog - Alzheimer Disease Assessment Scale-Cognitive

AGD - Argyrophilic grain disease

AICD - Amyloid Precursor Protein Intracellular Domain

ALDH1L1 - Aldehyde dehydrogenase L 1

ANOVA - Analysis of Variance

APA - American Psychiatric Association

APOE - Apolipoprotein E

APP - Amyloid Precursor Protein

APS - Ammonium Persulphate

ATP - Adenosine Triphosphate

Aβ - Amyloid Beta

BACE1 - β-site APP-Cleaving Enzyme 1

BBB - Blood Brain Barrier

BER - Base Excision Repair

bFGF - basic Fibroblast Growth Factor

bHLH - basic-Helix-Loop-Helix-Leucine

BRCA1 - Breast Cancer Type 1 Susceptibility Protein

BSA - Bovine Serum Albumin

CAA - Cerebra Amyloid Angiopathy

CAD - Coronary Artery Disease

CBD - Corticobasal Degeneration

cDNA - Complimentary DNA

CE - Cholesterol Esterase

CERAD- Consortium to Establish a Registry for Alzheimer's Disease

CFAS - Cognitive Function and Ageing Study

CI - Confidence Intervals

CLU - Clusterin

CNS - Central Nervous System

CO - Cholesterol Oxidase

CSF - cerebrospinal fluid

Ct - Cycle threshold

CYP46A1 - Cytochrome P Subunit 46 A1

DAB - 3,3'-diaminobenzidine

DDR - DNA Damage Response

DEPC - Diethylpyrocarbonate

DMSO - Dimethyl sulphoxide

DNA - Deoxyribonucleic Acid

DS - Down's Syndrome

DSBs - double stranded breaks

DSM V- Diagnostic and Statistical manual of Mental Disorders 5th edition

DTT - Dithiothreitol

ECL - Enhanced chemiluminescent substrate

EOAD - Early-Onset Alzheimer's Disease

ER - Endoplasmic Reticulum

FAD - Familial Alzheimer's Disease

FBS - Foetal Bovine Serum

FFPE - Formalin Fixed Paraffin Embedded

FPP – Farnesyl pyrophosphate

FTD - Frontotemporal Dementia

GFAP - Glial Fibrillary Acidic Protein

GGPP – Geranylgeranyl pyrophosphate

H2AX - Histone 2AX

HD - Huntington's disease

HMG-CoA - β hydroxy-β-methyl glutaryl Co A

HMGCR - β hydroxy-β-methyl glutaryl Co A Reductase

HPRT1 – Phosphoribosyl transferase 1

HRP - Horseradish Peroxidase

IgG - Immunoglobulin G

IHC - Immunohistochemistry

IHD - Ischaemic Heart Disease

IL-1β - Interleukin-1β

IL-6 - Interleukin -6

INSIG-1 - Insulin-Induced Gene 1

INSIG-2 - Insulin-Induced Gene 2

IPSCs - induced pluripotent stem cells

JT - Jonckheere-Terpstra

KS - Kolmogorov-Smirnov

KW - Kruskal-Wallis

LCM - laser capture microdissection

LDH - Lactate dehydrogenase

LDL - low density lipoprotein

LOAD - Late-Onset Alzheimer's Disease

LRP1 - Low density lipoprotein receptor-related protein 1

LUHMES - Lund human mesencephalic cells

LXR-α - liver X receptor-α

MAP - Microtubule Associated Protein

MAP2 – Microtubule Associated Protein 2

MCI - Mild Cognitive Impairment

MDA - Malondialdehyde

mRNA - Messenger Ribonucleic acid

MST - Minimum Spanning Tree

MW - Mann-Whitney

NADPH - Nicotinamide Adenine Dinucleotide Phosphate

NDRG2 - N-myc downstream regulated gene 2

NFT - Neurofibrillary Tangles

NMDA - N-methyl-D-aspartate

NTC - Non-Template Control

OR - Odds Ratio

PBS - Phosphate Buffered Saline

PBS-T - Phosphate buffered Saline-Tween

PCR - Polymerase Chain Reaction

PET - Positron Emission Tomography

PHF - Paired Helical Filaments

pLo - Poly-L-Ornithine hydrobromide

PMD - Post-mortem delay

Prx3 - peroxiredoxin-3

PSEN - Presenilin

PSP - Progressive Supranuclear Palsy

qRT-PCR - quantitative real-time PCR

RGC - Retinal Ganglion Cells

RIN - RNA Integrity Number

ROS - Reactive Oxygen Species

RT - Room Temperature

SCAP - SREBP Cleavage-Activating Protein

SDS - Sodium Dodecyl Sulphate

SEM - standard error of the mean

SNP - single nucleotide polymorphism

SREBP - Sterol Regulatory Element-Binding Proteins

TAE - Tris-acetate-Ethylenediaminetetraacetic acid

TBS - Tris-buffered Saline

TCx - Temporal Cortex

TDP-43 - Transactive Response DNA-Binding Protein 43

TEMED - Tetramethyl ethylenediamine

Tet - Tetracycline

TNF-α - Tumour Necrosis Factor Alpha

TREM2- Trigger Receptor Expressed on Myeloid Cells 2

Trx2 - Thioredoxin-2

TTa - Tetracycline-controlled Trans activator

WHO - World Health Organisation

X-XOD - Xanthine Oxidase

γH2AX -Phosphorylated Histone 2AX

1.0 Introduction to Alzheimer's disease and cholesterol in the brain

1.1.1 Dementia

Dementia is a clinical syndrome that is characterised by a significant decline in cognition causing an interference with the independence of the individual in everyday activities (Gale, Acar and Daffner, 2018). According to a report published by the World Health Organisation (WHO) in April 2016, there are approximately 45.7 million people in the world who have dementia (WHO 2016). This shows that dementia is becoming an ever-increasing burden on society, especially as the ageing population increases. According to the American Psychiatric Association (APA) dementia is classified as a major neurocognitive disorder (DSM V) (American Psychological Association (APA), 2013).

The multiple pathological causes for dementia can be categorised into two broad categories: non-neurodegenerative and neurodegenerative. Non-neurodegenerative causes of dementia include: nutrient deficiency such as vitamin B12, thiamine and folic acid; toxic causes such as exposure to lead, arsenic or pesticides; metabolic causes such as hypothyroidism, chronic uraemia and hypercortisolism; and vascular dementia (Gale, Acar and Daffner, 2018). Vascular dementia accounts for approximately one third of all dementias with several causes of which stroke and cerebral amyloid angiopathy are major contributors (O'Brien *et al.*, 2003; Gale, Acar and Daffner, 2018). Cerebral amyloid angiopathy (CAA) is the accumulation of amyloid proteins in cerebral blood vessels causing micro-bleeds and lobar haemorrhages (Xiong *et al.*, 2018).

Neurodegenerative causes of dementia include frontotemporal lobar degeneration (also known as frontotemporal dementia (FTD)), dementia with Lewy bodies and Alzheimer's disease (Gale, Acar and Daffner, 2018). FTD is characterised by the degeneration of the frontal and temporal lobes resulting in changes in behaviour and language and pathologically abnormal accumulations of tau and transactive response DNA binding protein 43 (TDP-43) (Finger, 2016). Dementia with Lewy bodies is characterised by the accumulation of alpha-synuclein aggregates within the brain and is the second most common cause of dementia (Finger, 2016; Gale, Acar and Daffner, 2018). Alzheimer's disease is characterised by the accumulation of

neuritic plaques and neurofibrillary tangles and it is the most common cause of dementia (Hebert *et al.*, 2013).

1.1.2 Alzheimer's Disease

The first recorded description of the symptoms of Alzheimer's disease (AD) was reported by Alois Alzheimer in 1907, where a 51-year old woman who had been admitted into an insane asylum in Munich portrayed a rapid loss of memory, disorientation and changes in her behaviour (Stelzmann, Norman Schnitzlein and Reed Murtagh, 1995). Post mortem analysis of her brain using Bielschowsky's silver staining method showed that abnormal neurofibrils were present in the atrophic brain alongside minute miliary foci which were deposited in the upper layers of the cortex (Stelzmann, Norman Schnitzlein and Reed Murtagh, 1995). These observations were later characterised to be neurofibrillary tau tangles (neurofibrils) and β-amyloid plaques (Aβ) (minute miliary foci) and are considered the classical hallmarks of the disease.

Since characterisation of the classical pathological hallmarks described by Alzheimer, new evidence has elucidated further neuropathologies observed in AD. Neuropathological assessment of AD patient brains has shown moderate atrophy in association cortex, limbic lobe structures and hippocampus followed by atrophy of the gyri within the frontal and temporal cortices (Perl, 2010). This atrophy can lead to the enlargement of the lateral ventricles within the frontal and temporal lobes and a decrease in brain weight, this atrophy is attributed to white matter loss (Piguet *et al.*, 2009). These observations are not specific to AD but help in cases where other macroscopic changes associated with other neurodegenerative disease are not present (Deture and Dickson, 2019).

A definitive diagnosis of AD is based on microscopic evaluation of post-mortem tissue. Alongside the presence of classical AD pathologies, such as senile plaques formed from aggregated amyloid peptide and neurofibrillary tangles formed for hyperphosphorylation of tau. Other cellular pathologies such CAA, granulovacuolar degeneration, Hirano bodies, neuroinflammation, gliosis and synaptic loss are also associated with AD (Perl, 2010; Deture and Dickson, 2019). Granulovacuolar degeneration are intraneuronal vacuoles found in the cytoplasm of pyramidal neurons of the hippocampus. The small vacuoles measure approximately 2-4 μm in

diameter and contain a dense basophilic granule (Ball and Lo, 1977). Recent studies have shown that the abundance of granulovacuolar bodies correlates to neurofibrillary tangle density suggesting that the presence of these vacuoles may be a cellular response to neuronal damage (Hou *et al.*, 2018). Hirano bodies are rod-like structures localised to neuronal dendrites within the hippocampus and formed from F-actin and actin proteins. The exact role Hirano bodies play in AD pathogenesis is unclear however, recent studies suggest an association with impaired synaptic response and a reduced spatial working memory (Gibson and Tomlinson, 1977; Hirano, 1994; Serrano-Pozo, Frosch, *et al.*, 2011; Furgerson *et al.*, 2014). Neuroinflammation is characterised by the activation of microglia and astrocytes in response to stress leading to an inflammatory response. In AD, activated microglia and reactive astrocytes have been observed around Aβ plaques and neurofibrillary tangles (Wake *et al.*, 2009; Serrano-Pozo, Mielke, *et al.*, 2011; Steele and Robinson, 2012; Heneka *et al.*, 2015). The loss of synapses precedes the loss of neurons and this synaptic loss appears to be the strongest correlate of a decline in cognition in AD (Terry *et al.*, 1991; Overk and Masliah, 2014). The major contributor to synaptic loss has been associated with defects in axonal trafficking as studies suggest that hyperphosphorylated tau within dendritic spines in the pre-synaptic terminal disrupts synaptic function by inhibiting the trafficking of glutamate receptors or impairing synaptic anchoring resulting in impaired synaptic transmission (Hoover *et al.*, 2010).

1.1.3 Classical AD Pathology

Aβ is formed from proteolytic cleavage of the amyloid precursor protein (APP). APP is a type 1 trans-membrane glycoprotein that is located on chromosome 21. The function of APP is not determined but a number of studies suggest that it could be involved in cell growth (Dawkins and Small, 2014). APP mRNA has been found to be expressed in many cells and is modified post-translationally by cleavage enzymes called secretases (α, β, γ). The site of cleavage on the c-terminal of APP and length of the final protein depends on which enzyme is used, α-secretase, β-secretase (β-site APP-cleaving enzyme 1/ BACE) and γ-secretase (encoded by the presenilin genes *PSEN1* & *PSEN2*) (Dawkins and Small, 2014).

There are two main pathways in which APP undergoes proteolytic processing: the non-amyloidogenic pathway, which prevents Aβ formation; and the amyloidogenic pathway, which generates the Aβ fragment necessary for amyloid plaque formation

(Figure 1.1). To generate the Aβ fragment that aggregates in AD, firstly APP is cleaved by β-secretase on the extra-cellular portion, which produces ~100kDa fragment called sAPPβ/APPsβ and has been shown to be involved in synaptic pruning during development (Nikolaev *et al.*, 2009; Galvão *et al.*, 2019). β-secretase cleavage is followed by cleavage in the hydrophobic transmembrane domain by γ-secretase generating the Aβ peptide which can vary in length between 37-43 amino acids long depending on the exact location of cleavage by γ-secretase. Consecutive cleavage of APP results in the release of Aβ peptide into the lumen or the extra cellular domain (Haass *et al.*, 2012). The action of γ-secretase enzymes generates an intracellular fragment known as amyloid precursor protein intracellular domain (AICD) which is considered to act as a transcription factor (Müller and Zheng, 2012). The Aβ42 fragment is thought to be the most amyloidogenic and is commonly found in plaques in AD brains (Herrup, 2015). The non-amyloidogenic pathway is characterised by cleavage of APP by α-secretase within the extra-cellular region forming the sAPPα/APPsα fragment. Subsequent cleavage by γ-secretase leads to the formation of AICD and p3 fragment, a truncated form of the Aβ peptide released into the lumen or extra cellular domain (Haass *et al.*, 2012).

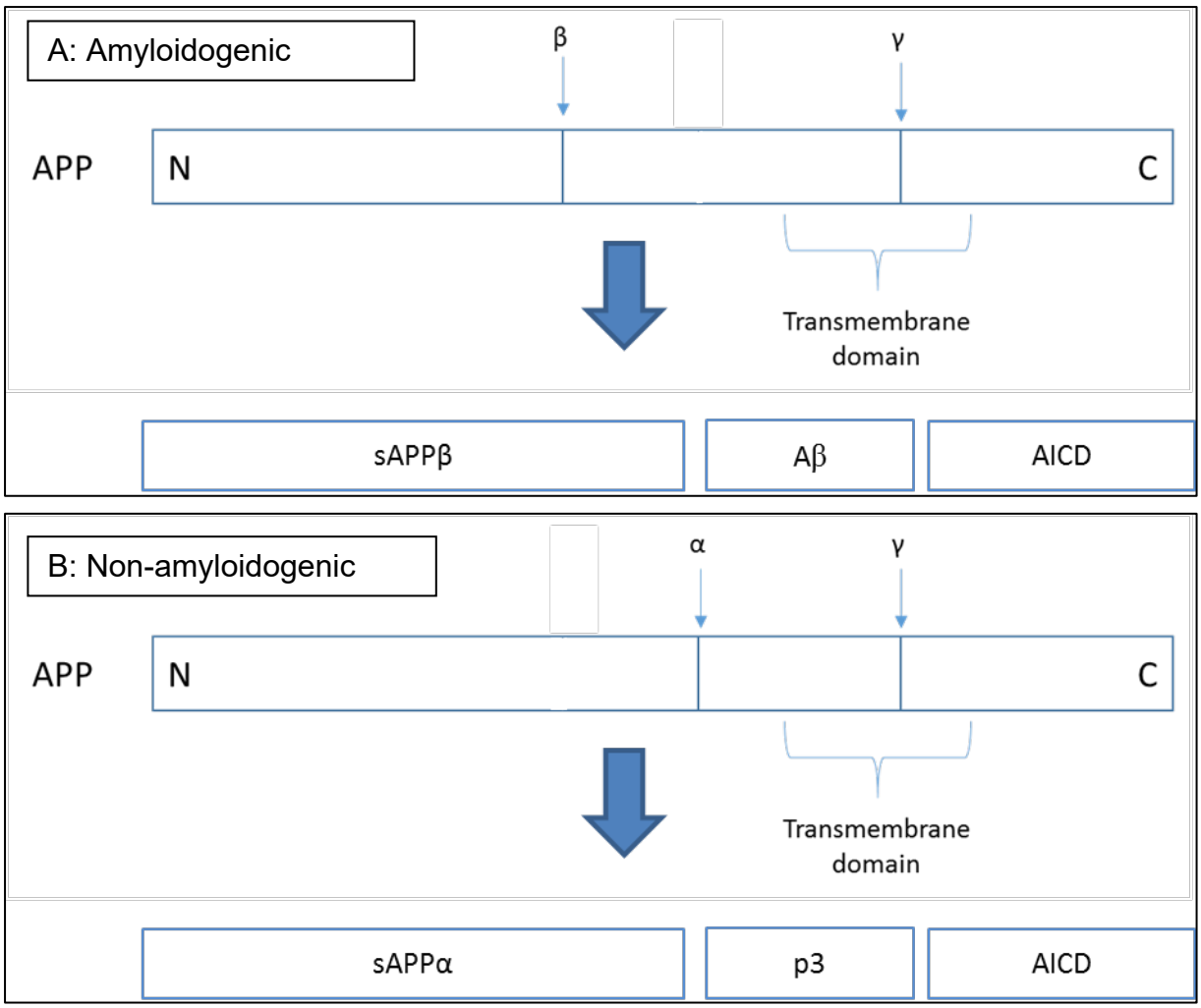

Figure 1.1: Cleavage sites of the secretase enzymes for APP. The amyloidogenic pathway involves a cleavage by β-secretase followed by cleavage by γ-secretase to produce the Aβ peptide (A). Non-amyloidogenic pathway includes an initial cleavage by α-secretase followed by a cleavage by γ-secretase (B). Not drawn to scale.

1.1.4 Amyloid cascade hypothesis

The amyloid cascade hypothesis (ACH) has been used to describe the pathogenesis of AD (Hardy and Higgins, 1992). This hypothesis is based on the finding that mutations in APP, in familial AD, lead to the formation of Aβ in neurons which significantly outweighs the clearance of Aβ and leads to accumulation of Aβ within the brain (Selkoe, 2000; A. Armstrong, 2014). In the original paper by Hardy & Higgins, they suggested that, due to the accumulation of Aβ there is an increase in Ca^{2+} which causes the hyperphosphorylation of tau proteins to create tangles; furthermore this increase in intracellular Ca^{2+} also signals for apoptosis (Hardy & Higgins 1992; Selkoe 2000). However, the hypothesis has been updated, missense mutations in *APP* and *PSEN1/2* increase Aβ42 production throughout life leading to accumulation and oligomerisation within cortices. More recent evidence is suggesting that oligomeric forms of Aβ are the more toxic forms and start to accumulate before the formation of Aβ plaques (Gyure *et al.*, 2001; Hayden and Teplow, 2013; Selkoe and Hardy, 2016; Roher *et al.*, 2017). Oligomeric Aβ has been shown to have a neurotoxic effect as studies suggest that Aβ oligomers can directly insert into membranes, causing disruption by acting like a pore (Arispe, 2004; Cline *et al.*, 2018). Aβ42 oligomers have subtle effects on synaptic efficacy and depostion of diffuse plaques occurs, which activate microglial and astrocytic inflammatory responses altering neuronal ionic homeostasis. This leads to oxidative damage, which changes the activity of kinases and phosphatases forming tau tangles. This results in neuronal and synaptic dysfunction resulting in neuronal loss and eventually dementia (Selkoe and Hardy, 2016).

One study found that a mutation in the *APP* gene was found to be protective of AD and prevented a decline in cognition. A single nucleotide polymorphism resulting in a substitution of alanine to threonine at position 673, which is adjacent to β-secretase cleavage site, lead to a 40% reduction in amyloidogenc peptides *in vitro,* providing further supporting evidence to this hypothesis (Jonsson *et al.*, 2012). Further evidence supporting this hypothesis is shown in patients with Down syndrome (DS) who have an extra copy of the APP gene as it is found on choromsome 21 (Head *et al.*, 2018). In brains from DS patients, Aβ levels are significantly increased compared to control brains and further studies have shown that neuropathology accumulates between the ages of 30 and 40 years leading to an AD diagnosis by the age of 40

years (Wisniewski, Wisniewski and Wen, 1985; Teller *et al.*, 1996). This early onset of AD has been attributed to an extra copy of the APP gene and increase levels of β-secretase homologue (BACE-2) which is also found on chromosome 21 (Hussain *et al.*, 2000; Barbiero *et al.*, 2003).

1.1.4.1 Amyloid cascade hypothesis - Refutation

In recent years ACH has undergone a great deal of scrutiny. The main weakness to ACH is the fact that there is a big overlap in Aβ plaque burdens between demented and non-demented individuals. The burden of plaques is a poor indicator for predicting dementia status, studies have shown that the burdens of tangles and plaques between demented and non-demented individuals converges at the oldest age so that the relationship of pathology to dementia status is attenuated; NFT are a better predictor of dementia compared to plaques however, they do not predict all of dementia (Matthews *et al.*, 2009b; Savva *et al.*, 2009; Wharton *et al.*, 2011). Furthermore, the removal of Aβ plaques does not improve the symptoms of dementia (Holmes *et al.*, 2008; Serrano-Pozo *et al.*, 2010; Herrup, 2015). Clinical trials in which patients with AD were immunised for Aβ42 showed that amyloid plaques were cleared, however this clearance did not prevent the progression of cognitive impairment (Holmes *et al.*, 2008). Furthermore, a recent phase 3 clinical trials for the Solanezumab (humanised analogue for m266), a monoclonal antibody which binds to Aβ, failed to improve cognition and functional ability in mild-to-moderate AD patients as a result of reduced clearance of aggregated Aβ (Doody *et al.*, 2014). Studies in mice showed that the m266 antibody was selective for the central domain of soluble Aβ and reduced Aβ burden by improving clearance of Aβ from the brain and plasma however, this was not the case in human trials (DeMattos *et al.*, 2001; Doody *et al.*, 2014).

1.1.4.2 Amyloid cascade hypothesis – Anti-amyloid therapeutics

Other anti-amyloid therapies also do not improve the clincial outcomes in AD patieints. For example in phase 3 clinical trials of Bapineuzumab, a monoclonal antibody, showed no significant difference between treated and placebo groups in cognitive tests scores, indicating that cognition had not improved (Salloway *et al.*, 2014). Studies using the murine homologue of Bapineuzumab (3D6) show that the antibody is targeted to the n-terminus of Aβ protein and can interact with both soluble and insoluble forms of Aβ (Zago *et al.*, 2012). Within the trial both carriers and non

carriers of the apolipoprotein E (*APOE*) ε4 allele were also investigated. They found that within *APOE* ε4 carriers, that were given the drug, there was a decrease in the rate of accummulation of amyloid within the brain. However, this was not significant compared to the non-carrier group (Salloway *et al.*, 2014). Aducanumab, another anti-amyloid antibody, which binds to both soluble oligomers and insoluble fibrils. During phase 1 clinicals trials, they found that aducanumab reduced overall Aβ within the brain and also showed improvements in cognitive tests (Sevigny *et al.*, 2016). However, as this drug approached phase 3 clinical trials, the trial had been stopped. The exact reason for terminiating this trial has not yet been published however, there is speculation that the drug does not slow down cognitive decline (Alzforum). This suggests that targetting Aβ cannot be the only form of treatment but rather a combination of treatments might be needed to slow down or halt cognitive decline (Selkoe, 2019).

Other potential therapeutic targets could exploit the inhibition of γ-secretase. Small molecules such as semagacestat and avagacestat are used to inhibit the action of the enzyme. A phase 3 clinical trial for semagacestat had to be terminated before completion as this drug did not improve cognitive decline and caused the patients adverse side effects such as weight loss, skin cancers and infections (Doody *et al.*, 2013). Similarly a more recent phase 2 clinical trial for avagacestat showed that progression of dementia was not different compared to the placebo and brain atrophy rates were higher particullary in hippocampal regions (Coric *et al.*, 2015).

One study suggested that the failure of semagacestat in trials could be due to it being a non-competitive inhibitor. Tagami *et al* (2007) found that semagacestat caused an increase in intracellular γ-secretase cleavage by-products and Aβ, and that it decreased extracellular Aβ levels (Tagami *et al.*, 2017). Other studies found that the inhibition of γ-secretase, via avagacestat, leads to the an increase in presenilin-1 (PS1) levels, the catalytic subunit of the γ-secretase enzyme (Sogorb-Esteve *et al.*, 2018). Rats treated with avagacestat for 21 days showed an increase in PS1 which increase the activity of γ-secretase and APP processing (Sogorb-Esteve *et al.*, 2018).

Another possible avenue that could be explored to remove Aβ aggregates is the use of scyllo-inositol, a stereoisomer of inositol which, along with other stereoisomers,

prevents the formation of Aβ fibrils (McLaurin *et al.*, 2000). This study also found that when primary human neuronal cell cultures were incubated with Aβ and scyllo-inositol there was an increase in cell survival compared to incubation with Aβ alone. The authors suggested that this reduction in toxicity of Aβ could be a result of altering the distribution of the fibrils preventing aggregation (McLaurin *et al.*, 2000). Phase 2 clinical trials involving the use of scyllo-inositol as a treatment for mild-moderate AD showed no significant difference in the neuropsychological test scores between the placebo and scyllo-inositol groups (Salloway *et al.*, 2011; Ahmed *et al.*, 2019).

The lack of successful therapies for the removal of Aβ and having an improvement on cognitive function suggests that there may be more factors at work within the pathogenesis of AD or that the therapies need to be administered at pre-clinical stages of the disease to be effective (Selkoe, 2019).

1.1.5 Tau pathology

Tau is a major protein component of the neurofibrillary tangles within AD brains. Tau is a microtubule associated protein (MAP) expressed primarily in the axon of mammalian neurons (Binder, Frankfurter and Rebhun, 1985). The gene encoding for tau (*MAPT*) is found on chromosome 17 and due to alternative splicing of its mRNA, six molecular isoforms of tau exist within the human brain (Figure 1.2) (Iqbal *et al.*, 2009). Tau has many functions within these cells including: polymerisation and stabilisation of microtubules; fast transport of organelles along the microtubules; regulating microtubule dynamics at the distal portion of the axon; determining the polarity of the neuron during development, migration and morphology of neurons; and intracellular mitochondrial transport (Witman *et al.*, 1976; Caceres and Kosik, 1990; Stamer *et al.*, 2002; Dixit *et al.*, 2008; Sapir *et al.*, 2012; Khan and Bloom, 2016).

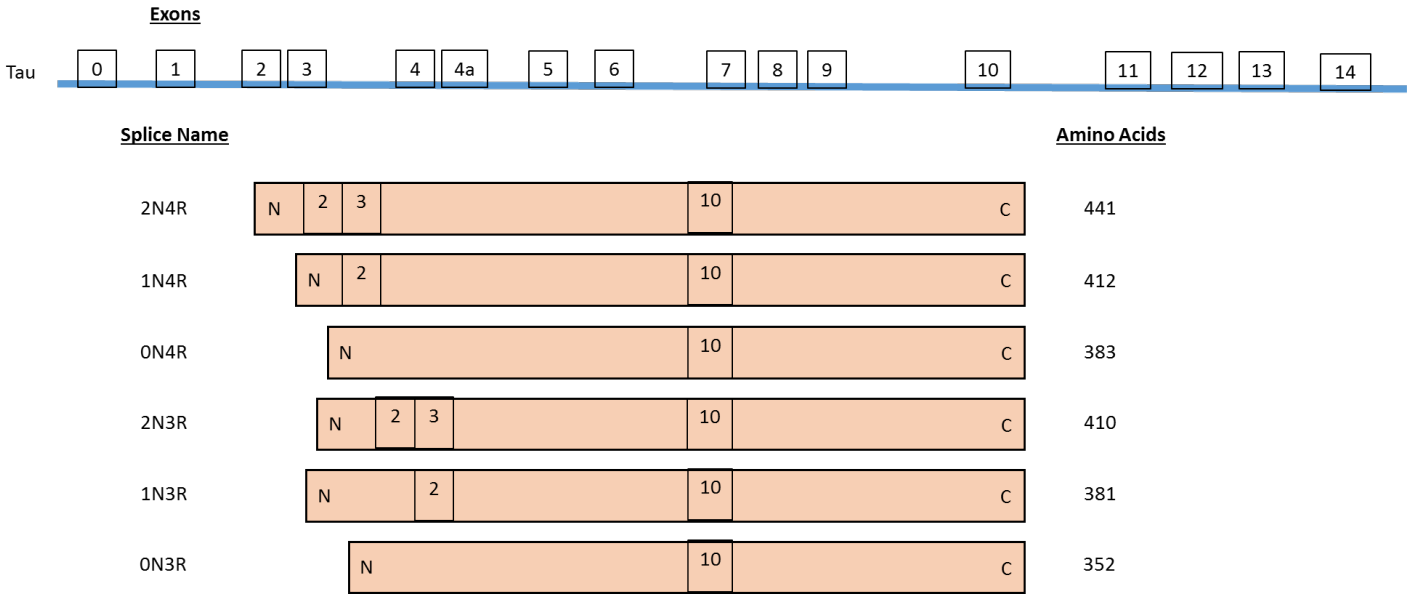

Figure 1.2: Six isoforms of Tau. The N number refers to the number of exons expressed within the N-terminus of the isoform. The R number refers to the number of microtubule binding repeat domains found within the C-terminus. Not drawn to scale.

In AD, tau is abnormally hyper-phosphorylated, causing a conformational change which then aggregates to form paired helical filaments (PHF) and neurofibrillary tangles (NFT) within neurons (Iqbal *et al.*, 2009). The ACH suggests that Aβ and tau interact with each other to cause AD like pathology; with Aβ molecular pathology being upstream; however, this sequence has not yet been proven and is not fully explained within the hypothesis. According to the hypothesis, the formation of Aβ leads to the hyper-phosphorylation of tau proteins forming NFT (Boutajangout and Wisniewski, 2014). The formation of NFT or pre-tangles can have a toxic effect upon the neurons. The toxicity of tau depends on the isoform that undergoes hyper-phosphorylation; studies have found that the 4R-tau isoform (2N4R isoform) has a cytotoxic effect in rat primary hippocampal neurons. Co-culturing primary rat hippocampal neurons with a murine fibroblast cell line, modified to express human 4R-tau isoform, saw an increase in cell death. (Klenyaeva *et al.*, 2014; Tatarnikova, Orlov and Bobkova, 2015). The biogenesis of NFTs involves tau oligomerisation, a toxic intermediate found within the cytosol, this mechanism has been observed to occur on the surface of microtubules when tau dissociates from microtubules leading to tau aggregation and the formation of NFTs (Makrides *et al.*, 2003; Gendreau and Hall, 2013). One study has shown that soluble tau is associated with cognitive impairment within post mortem human AD brains and that oligomeric tau can be a good predictor of cognitive scores (Koss *et al.*, 2016).

1.1.5.1 Tauopathies

Tau pathology and NFT are not just confined to AD, the deposition of tau has also been found in other neurodegenerative diseases and are known as tauopathies (Kovacs, 2015). Studies have demonstrated that two tau isoforms, 3R and 4R, have been commonly associated with tauopathies (Huefner *et al.*, 2013; Medina, Hernández and Avila, 2016). One study investigated the isoform specific phenotype of the two human tau isoforms 3R and 4R in a *Drosophila* model (Sealey *et al.*, 2017). Sealey *et al* (2017) found that flies expressing the 3R isoform had impaired locomotion compared to the 4R isoform. However, the 4R isoform was associated with a decrease in learning and memory, increase in oxidative stress and stronger neurodegenerative phenotype and compared to 3R. This data suggests that the differences in isoform specific phenotype could be attributed to different interactions between the isoforms within the brain (Sealey *et al.*, 2017).

In adult human brains the ratio of 3R:4R isoform is approximately 1, in tauopathies this ratio is altered as certain isoforms are predominantly found within aggregates (Andreadis, 2005; Sealey *et al.*, 2017). Picks Disease is characterised by the presence of Pick bodies within the neuronal cytoplasm. Pick bodies are tau filaments made from the 3R tau isoform and form straight tubules and twisted filaments approximately 15-18 nm and 22-24 nm in diameter, respectively. These Pick bodies are localised to granule cells of the dentate gyrus followed by the hippocampus and temporal and frontal cortical and subcortical structures (Zhukareva *et al.*, 2002; Arima, 2006; Dickson, 2006). Progressive supranuclear palsy (PSP) is another tauopathy comprising of NFTs made up from the 4R tau isoform forming filaments and straight tubules in tufted astrocytes and oligodendroglial coiled bodies in the subthalamic nucleus, basal ganglia and brainstem (Arima, 2006; Dickson, Rademakers and Hutton, 2007). Corticobasal degeneration (CBD) is characterised by tau positive lesions formed from the 4R tau isoform. These tau lesions are localised to cortical and striatal neurons and glia, thread-like lesions are found in focal cortical regions and substantia nigra (Dickson *et al.*, 2002). Argyrophilic grain disease (AGD) is characterised by the presence of argyrophilic and tau grains formed from the 4R tau isoform. These grains are localised pre-tangles and oligodendroglial coiled bodies in hippocampal and peri-amygdaloid white matter (Kovacs, 2015). Tau pathology has been observed in normal ageing brain and is made up from a combination of both 3R and 4R isoforms and has pathological overlap with the burdens seen in AD (Kovacs, 2015). A recent study assessed tau pathology in cognitively normal patients using positron emission tomography (PET) tau radiotracers and found greater retention of tau radiotracer in the entorhinal cortex, which was associated with a steeper decline in memory performance. This suggests that the early accumulation of pathological tau may influence changes in cognitive domains that are affected in AD and in cognitively normal individuals (Ziontz *et al.*, 2019).

1.1.6 Neuropathological diagnosis of AD

Neuropathological assessment of patient brains confirms AD diagnosis. Moderate atrophy in association cortex, limbic lobe structures and hippocampus followed by atrophy of the gyri within the frontal and temporal cortices has been observed in AD brains (Perl, 2010). This atrophy can lead to the enlargement of the lateral ventricles

and an overall decrease in brain weight (Piguet *et al.*, 2009). The Consortium to Establish a Registry for Alzheimer's Disease (CERAD) was created to develop a standardised and validated measures to asses AD. The measures include clinical, behavioural, neuropsychological and neuropathological assessments (Fillenbaum *et al.*, 2008). The neuropathological assessment consists of semi-quantitative histological analysis of microscopic sections from the neocortex (frontal, parietal, temporal and occipital cortices), hippocampus and amygdala. Semi-quantitative analysis assessed the frequency of senile plaques and neurofibrillary tangles in these brain regions and categorically scored into groups i.e. no pathology, mild/neuritic pathology, moderate-severe/diffuse pathology. In conjunction with clinical history, neuropathological assessment using CERAD can help indicate the certainty of AD diagnosis (Fillenbaum *et al.*, 2008).

Thal phase reflects the severity of β-amyloidosis and follows Aβ deposition across the brain as AD progresses (Thal *et al.*, 2002). Thal *et al* (2002) demonstrated the sequence of Aβ deposition within the brain and allocated five phases. Aβ depositions in phase 1 were localised to neocortical regions such as frontal, parietal, temporal and occipital lobes. Phase 2 sees Aβ depositions extend from the neo-cortex to the entorhinal and insular cortex. Phase 3 is characterised by Aβ deposits within the midbrain regions such the thalamus and hypothalamus. Phases 4 and 5 are characterised by Aβ deposits progressing to the brainstem and cerebellum respectively (Thal *et al.*, 2002).

Another method used to determine AD progression is by Braak and Braak staging (Braak and Braak, 1991). Braak and Braak staging reflects (relevant to the spectrum of ageing and AD) the hierarchy of tau deposition within the brain; this scheme is based on the localisation of NFTs within the allo- and isocortex to determine the stage of AD. The depositions of NFT have a closer correlation to dementia progression than Aβ deposition. Nevertheless, there is still an overlap with NFT deposition in demented and non-demented individuals which increases with age (Savva *et al.*, 2009). There are six stages in total, progression through the stages indicate an increase in NFT deposition. During stages I and II, NFT are localised to the transentorhinal and entorhinal regions; during stages III and IV, NFT spread into the limbic structures such as the hippocampus; stages V and VI, NFT spread

extends into neocortical regions such as association cortex (V) and primary cortex (VI) (Braak and Braak, 1991; Braak *et al.*, 2006).

1.2.1 Genetics

AD can be categorised into early onset (EOAD) and late onset (LOAD). EOAD accounts for approximately 5-6% of all AD and one in ten patients with EOAD is associated with familial AD (FAD) and tends to have mutations in three key genes: presenilin 1 (*PSEN1*), presenilin 2 (*PSEN2*) and amyloid precursor protein (*APP*). FAD accounts for 0.5% of all AD cases and 50% of FAD cases have a mutation in one of the genes mentioned above (Cruts, Theuns and Van Broeckhoven, 2012; Zhu *et al.*, 2015; Shea *et al.*, 2016; Mendez, 2019). The average age of onset of familial AD is usually around 65 (Wu *et al.*, 2012; Shea *et al.*, 2016). Mutations in these genes (Table 1.1) lead to enhanced production of Aβ42 leading to EOAD, although they may have other effects. (Shea *et al.*, 2016).

1.2.2 Genes associated with early onset AD

PSEN1 is a gene that is found on chromosome 14 and its protein product is involved in post translational modification of APP via γ-secretase. Approximately 215 pathogenic mutations in *PSEN1* have been found, the majority of which are missense mutations (Cruts, Theuns and Van Broeckhoven, 2012). These mutations cause an increase in the levels of Aβ42 compared to Aβ40 leading to the formation of Aβ plaques (Giri, Zhang and Lü, 2016).

PSEN2 is a gene located on chromosome 1 and like *PSEN1* it is involved in the post translational modification of APP. *PSEN2* codes for the main complex of γ-secretase hence mutations in *PSEN2* affect the activity of γ-secretase leading to an increase in the production of Aβ (Giri, Zhang and Lü, 2016). Only 19 pathogenic mutations in *PSEN2* have so far been found to cause AD, as mutations in *PSEN2* are rare (Cruts, Theuns and Van Broeckhoven, 2012). Studies have shown that mutations in *PSEN2* have an increased activity of β-secretase due to activation of protein kinases in the presence of reactive oxidative species (ROS) (Park *et al.*, 2012).

APP codes for a transmembrane glycoprotein whose specific function is yet to be determined. So far 49 mutations have been found in *APP*, if these mutations are located near the cleavage sites, they tend to have an impact on the size of the fragment that is cleaved by the secretase enzymes (Cruts, Theuns and Van

Broeckhoven, 2012; Giri, Zhang and Lü, 2016). A rare variant (A637T) has also been found to be protective against the development of AD. Here a substitution mutation in β-secretase region has been found, this mutation makes cleavage by β-secretase less favourable leading to a decrease in Aβ production (Jonsson *et al.*, 2012; Maloney *et al.*, 2014). *APP* is found on chromosome 21, studies in Down syndrome patients (trisomy 21) have shown to have an earlier onset of AD pathology compared to normal AD individuals (Prasher *et al.*, 1998). This early onset of AD has been attributed to an extra copy of the APP gene and increase levels of β-secretase homologue (BACE-2) which is also found on chromosome 21 (Hussain *et al.*, 2000; Barbiero *et al.*, 2003).

1.2.3 Genes associated with late onset AD

Most LOAD cases are sporadic. They can have a combination of genetic and environmental factors however, the genetic component is considered to be a stronger risk factor (Barber 2012). The gene apolipoprotein E (*APOE)* was one of the first genetic risk factors that was identified and has shown the strongest and most reproducible association with LOAD (Barber 2012; Rosenthal & Kamboh 2014). *APOE* is found on chromosome 19 and has 3 alleles- ε2, ε3 and ε4 - of which ε2 is said to be protective of LOAD and ε4 increases the risk of both EOAD and LOAD (Corder et al. 1993; Strittmatter et al. 1993; Rosenthal & Kamboh 2014; Karch & Goate 2015). *APOE* codes for a glycoprotein which is 299 amino acid long and is involved in cholesterol transport, neuroplasticity and inflammation within the CNS (Kim, Basak and Holtzman, 2009; Karch and Goate, 2015). Further studies have also shown that APOE interacts with Aβ and is involved in the clearance, aggregation and metabolism of Aβ (Kim, Basak and Holtzman, 2009; Karch and Goate, 2015). *APOE* is mainly expressed in astrocytes and microglia however, neurons are also able to express this gene during AD, although at a lower level than astrocytes (Metzger *et al.*, 1996; Xu *et al.*, 2006; Kim, Basak and Holtzman, 2009).

Recent genome sequencing studies discovered mutations in *TREM2* can increase the risk of developing LOAD (Guerreiro *et al.*, 2013; Jonsson *et al.*, 2013). Trigger Receptor Expressed on Myeloid Cells 2 (*TREM2*) gene is found on chromosome 6 and encodes a single pass immunoglobulin domain-containing transmembrane protein that is expressed in mononuclear phagocytes, such as osteoclasts and microglial cells, and is involved in regulation of phagocytosis, promotion of cell

survival and inhibition of inflammatory signalling (Colonna, 2003; Replogle *et al.*, 2015; Colonna and Wang, 2016). One variant of *TREM2*, R47H, has shown to increase the risk of developing AD by 2-3- fold, due to a SNP which substitutes arginine to histidine at amino acid 47 (Guerreiro *et al.*, 2013; Jonsson *et al.*, 2013). Within microglia, TREM2 is required to increase mechanistic target of rapamycin signalling and to boost microglial metabolism (Ulland and Colonna, 2018). Modelling *TREM2* mutations in AD mice models have shown that microglia fail to accumulate around Aβ plaques and there is an increase in neuronal dystrophy in these regions compared to plaques covered with microglia. This may suggest that in AD mutations in *TREM2* leads to the impairment, survival and migration of microglia (Condello *et al.*, 2015; Yuan *et al.*, 2016; Ulland *et al.*, 2017; Ulrich *et al.*, 2017).

1.2.4 GWAS identifies genes involved with cholesterol metabolism in late onset AD

GWAS studies have identified around 20 different genes or loci that are associated with LOAD and involved in cholesterol metabolism, these genes include: *CLU*, *ABCA7* and *SORL1* (Rosenthal and Kamboh, 2014; Giri, Zhang and Lü, 2016). The Clusterin gene (*CLU*) is found on chromosome 8 and codes for the protein clusterin, which like apoE is an apolipoprotein that plays an important role in lipid transport. The function of *CLU* has not yet been fully characterised; however, it has been hypothesised that clusterin could function as a chaperone protein or a heat-shock protein (Michel *et al.*, 1997; Wilson and Easterbrook-Smith, 2000; Jones and Jomary, 2002; Giri, Zhang and Lü, 2016). *CLU* is expressed systemically as well as in the brain and that it may be a pro-apoptotic signal in a response to cellular stress (Jones and Jomary, 2002). In AD, clusterin levels are increased, and the levels of plasma clusterin are linked to the progression of AD (Deming *et al.*, 2016; Giri, Zhang and Lü, 2016). Like apoE, clusterin is found in Aβ plaques and interacts with it, indicating that the *CLU* may play a role in classical AD pathology; clusterin suppresses the deposition of Aβ and prevents an inflammatory response and it also reduces apoptosis and oxidative stress within AD (Deming *et al.*, 2016; Giri, Zhang and Lü, 2016).

Gene	Early onset (EO) or Late onset (LO)	Chromosome	Wild type function	Role in AD
ABCA7	LO	19	Lipid transport	Perturbed phagocytosis leading to a reduction in clearance of Aβ
APOE	LO	19	Cholesterol transport	Impaired cholesterol transport to neurons
CLU	LO	8	Lipid transport	Loss of suppression of Aβ deposition
SORL1	LO	11	Processing and trafficking of APP	Under-expression leads to over-expression of Aβ
TREM2	LO	6	Microglial activation	Reduced microglial activation and accumulation around Aβ plaques
APP	EO	21	Unknown	Forms Aβ plaques which are neurotoxic
PSEN1	EO	14	Post-translational modification of APP	Increase in the formation of Aβ plaques
PSEN2	EO	1	Post-translational modification of APP	Increase in β-secretase activity

Table 1.1: Genes associated with AD

ABCA7 is located on chromosome 19, this gene is part of the ATP-binding-cassette gene family which are involved in the transport of lipids, such as cholesterol, across membranes against a concentration gradient (Holton *et al.*, 2013; Giri, Zhang and Lü, 2016). *ABCA7* mRNA is highly expressed in microglial cells within the hippocampus and plays a crucial role in cholesterol homeostasis. However, studies also show that *ABCA7* regulates phagocytosis and is highly expressed in macrophages (Giri, Zhang and Lü, 2016). Within AD there seems to be a loss of function mutation in *ABCA7* which is associated with AD pathogenesis, currently the mechanisms are not fully understood but recent data suggests that mutations in *ABCA7* may lead to a reduction in clearance of Aβ as a consequence of perturbed phagocytosis within macrophages (Steinberg *et al.*, 2015; Giri, Zhang and Lü, 2016).

SORL1 is located on chromosome 11 and is a member of the Vsp10p domain receptor family (Giri, Zhang and Lü, 2016). *SORL1* has been shown to interact with APP and influence the proteolytic processing and trafficking of APP within the brain (Andersen *et al.*, 2005). The mechanisms by which *SORL1* participates in the pathogenesis of LOAD are yet to be established. Current data suggests that under-expression of *SORL1* leads to over-expression of Aβ and that *SORL1* is also involved in the processing of APP via endocytic pathways which are crucial pathways in the formation of Aβ plaques (Offe *et al.*, 2006; Giri, Zhang and Lü, 2016).

1.3.1 Cholesterol biology

Cholesterol is an organic molecule (Figure 1.3) found within animal cell membranes. It is a type of sterol (lipid) molecule and forms the precursor for many steroid hormones. A key role of cholesterol is the assembly and function of lipid rafts within the cell surface membrane (Simons and Ilonen, 2000). Lipid rafts are areas within the phospholipid bilayer of the cell membrane that are primarily made from cholesterol and sphingolipids. They are involved in the sub-compartmentalisation of the plasma membrane and help determine the cellular polarity. Lipid rafts can also contain glycoproteins and glycolipids which aid in cellular signalling pathways (Simons and Ilonen, 2000; Simons and Sampaio, 2011). They play a role in post-Golgi trafficking and endocytosis, as the lipid raft will form part of the vesicle during trafficking and endocytosis (Simons and Ikonen, 1997; Simons and Sampaio, 2011). Together cholesterol and lipid rafts play a role in the distribution of proteins across the cell and organelles, as well as signalling cascades and activating immune responses (Langlet *et al.*, 2000; Simons and Ilonen, 2000; Simons and Toomre, 2000).

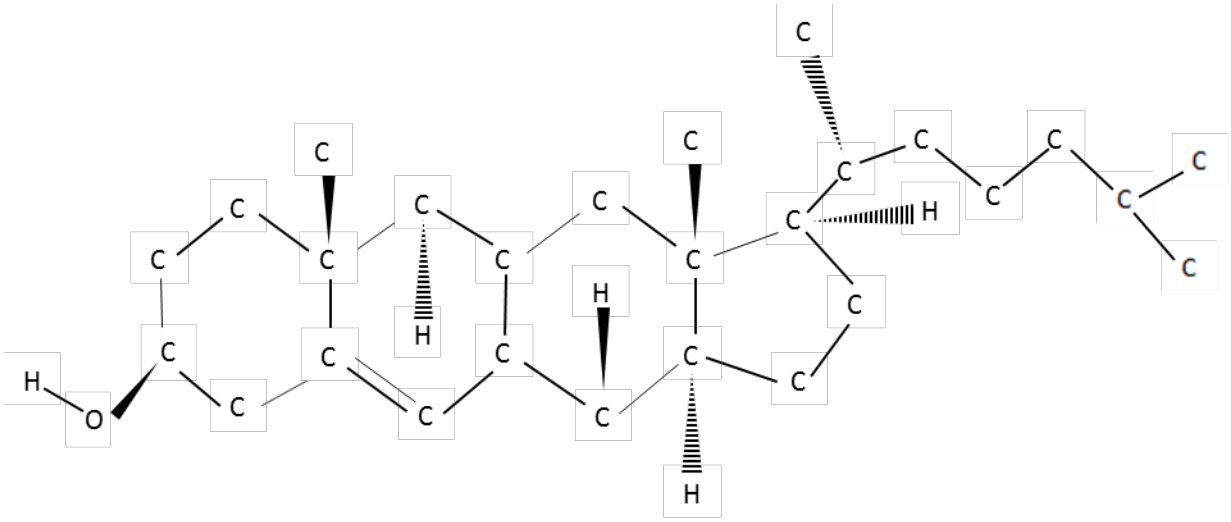

Figure 1.3: Molecular cholesterol: This diagram shows the molecular structure of cholesterol. Dark wedges represent bonds out of the page and dashed wedges represent bonds into the page Not all Hydrogen molecules are shown. Not drawn to scale

1.3.2 Cholesterol in the brain

The brain is a cholesterol rich organ; approximately 23% of the total cholesterol within the body is found within the brain (Dietschy, 2009; Vitali, Wellington and Calabresi, 2014). From this 23%, approximately 70-80% of the cholesterol is used in myelination of axons by oligodendrocytes (Dietschy, 2009; Hayashi, 2011; Vitali, Wellington and Calabresi, 2014). Myelin is made primarily from plasma membrane enriched with cholesterol and without myelination all major brain functions would be considerably slower causing a negative effect on survival (Snaidero and Simons, 2014).

Cholesterol is an essential component in dendrite and synapse formation, as well as axonal guidance (Zhang and Liu, 2015). Cholesterol derived from glial cells plays a crucial role in synaptogenesis. A study in postnatal rat retinal ganglion cells (RGC) found that cholesterol is required for dendrite differentiation, which directly promotes presynaptic differentiation. When RGC were cultured in glial cultured media or with cholesterol there was an increase in MAP2 positive dendrites compared to controls, showing the importance of both cholesterol and the neuronal-glia interaction in synaptogenesis (Goritz, Mauch and Pfrieger, 2005; Zhang and Liu, 2015). Depletion of cholesterol within neurons leads to: impairment of exocytosis of synaptic vesicles; impairment of neuronal activity and neurotransmission; and the degeneration of dendritic spines (Zhang and Liu, 2015).

Unlike other organs within the body, the brain cannot absorb cholesterol from the blood due to the blood brain barrier (BBB); so, the brain carries out *de novo* cholesterol biosynthesis to meet its cholesterol demand. Astrocytes and other glial cells undertake the bulk of cholesterol synthesis (Björkhem, Meaney and Fogelman, 2004; Zhang and Liu, 2015). Cholesterol synthesis within the brain occurs via the cholesterol biosynthesis pathway (Figure 1.4).

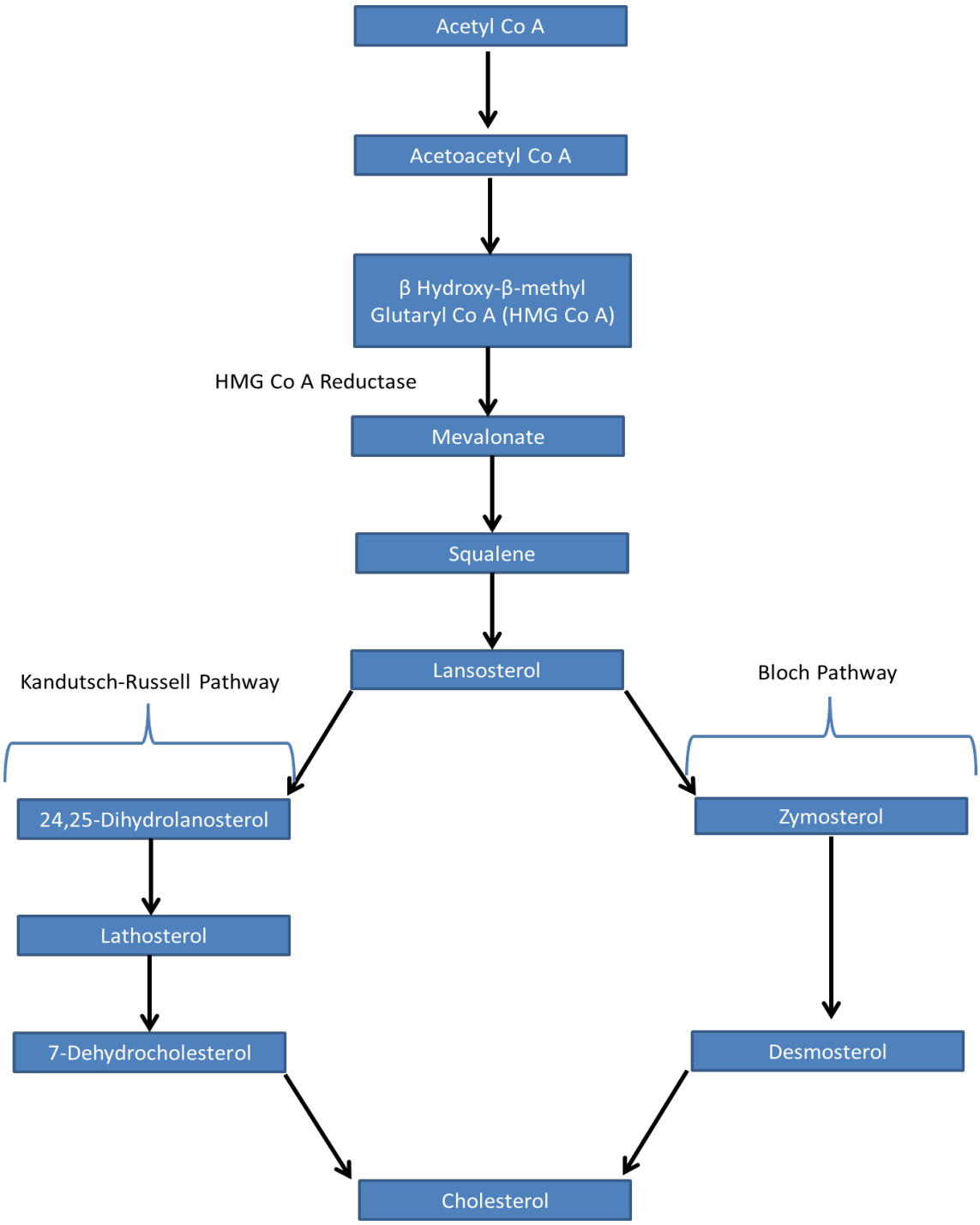

Figure 1.4: Cholesterol Biosynthesis Pathway: This diagram shows a brief summary of the cholesterol synthesis pathway. Condensation of Acetyl Co A into Mevalonate is known as the mevalonate pathway. Post-squalene cholesterol production can occur via two pathways: Kandutsch-Russell and Bloch pathway.

1.3.3 Cholesterol biosynthesis

Cholesterol biosynthesis is a complicated pathway and takes place within the peroxisome and the endoplasmic reticulum (ER) of a cell. The pathway begins with the condensation of acetyl Co A into mevalonate. During condensation, β hydroxy-β-methyl glutaryl Co A (HMG-CoA) is produced, with the action of HMG CoA reductase (HMGCR) enzyme HMG-CoA is converted into mevalonate. This conversion is the rate-limiting step for the cholesterol biosynthesis pathway. Mevalonate is then converted into squalene in the ER via a series of condensation reactions. Squalene is subsequently converted into cholesterol; this can occur via two biochemical routes, the Bloch or Kandutsch-Russell pathways (Mazein *et al.*, 2013). Both pathways have similar catalytic steps and products. They are distinguished by the penultimate reaction: in the Bloch pathway, cholesterol is produced by the reduction of desmosterol, whereas in the Kandutsch-Russell pathway cholesterol is preceded by 7-dehydrocholesterol. Studies have shown that during cholesterol synthesis within the brain, a hybrid of both of the pathways are used, where cholesterol biosynthesis after lansosterol occurs according to the Bloch pathway and then after a certain number of steps switches to the Kandutsch-Russell pathway (Mitsche *et al.*, 2015).

Astrocytes have been shown to undertake the bulk of cholesterol biosynthesis for post-mitotic neurons. (Pfrieger, 2003). The expression of *APOE* within astrocytes indicates that cholesterol transport to neurons is via apolipoproteins (Pfrieger and Ungerer, 2011). The literature suggests that cholesterol transport to the neurons could be a similar mechanism to the one found in hepatocytes i.e. assembly of a core particle in the ER which is then transported to the Golgi for further modification before secretion (Vance and Vance, 1990; Pfrieger and Ungerer, 2011). Neurons possess receptors for apoE (LRP1) suggesting that transport via cholesterol is by apoE and disruption to the apoE system could lead to an imbalance in cholesterol homeostasis within the neurons (Pfrieger and Ungerer, 2011; van den Kommer *et al.*, 2012). A study by Clement *et al* (2009) found that exposure to oxidative stress causes an increase in the expression of HMGCR in neuronal cells; showing that neurons are also capable of synthesising cholesterol (Clement et al. 2009).

1.3.4 Cholesterol homeostasis

To maintain cholesterol homeostasis, cholesterol can be metabolised into the oxysterol 24-hydroxycholesterol (24-OHC). This conversion is catalysed by the enzyme cholesterol 24-hydroxylase which is encoded by *CYP46A1* (Hughes *et al.*, 2013; Zhang and Liu, 2015). Compared to cholesterol, 24-OHC is more lipophilic and can easily pass through the BBB by simple diffusion making it an ideal molecule to measure cholesterol homeostasis within the brain via a simple blood test (Hughes *et al.*, 2013). Studies have shown that high concentrations of 24-OHC (25-50μM) increases the production of free radicals within the brain, which leads to oxidative stress (Kölsch *et al.*, 2001a; Gamba *et al.*, 2015).

Cholesterol homeostasis can also be achieved by regulating cholesterol biosynthesis in the ER by regulating SREBPs (sterol regulatory element-binding proteins). SREBPs are membrane bound proteins which cycle between the ER or Golgi body to the nucleus to regulate transcription of the genes involved in cholesterol biosynthesis (Simons and Ilonen, 2000; Goldstein, DeBose-Boyd and Brown, 2006). The cycling of SREBP is dependent on SCAP (SREBP cleavage-activating protein) which cleaves SREBPs twice allowing translocation from the Golgi to the nucleus.

When cholesterol levels are normal, SREBP2 is found within the ER membrane and is bound to SCAP (Goldstein, DeBose-Boyd and Brown, 2006). SCAP is an ER membrane embedded protein which is involved in activating SREBP2 by proteolytic cleavage and chaperones SREBP2 from the ER to the Golgi (Sakai *et al.*, 1997). SCAP consists of 8 membrane spanning domains which also contains a sterol sensing domain, the C-terminus contains a WD-repeat domain allowing binding of SCAP to SREBP2 (X. Hua *et al.*, 1995; Brown and Goldstein, 1997).

When cholesterol levels are low, translocation of the SREBP2/SCAP complex to the Golgi occurs. Within the Golgi, proteolytic cleavage activity of SREBP2 by SCAP releases the N-terminus of SREBP2 and translocate to the nucleus which increases the transcription of genes, such as *HMGCR,* which in turn leads to an increase in cholesterol synthesis (Sakai *et al.*, 1996; Simons and Ilonen, 2000; Goldstein, DeBose-Boyd and Brown, 2006). When an increase in cellular cholesterol levels is detected by SCAP, translocation of the SREBP2/SCAP to the Golgi is inhibited preventing cleavage of SREBP2 (Sun *et al.*, 2005). In addition, at high cellular

cholesterol levels the binding of HMGCR to INSIG-1 (Insulin-Induced Gene 1) and INSIG-2 (Insulin-Induced Gene 2) marks HMGCR for ubiquitination and degradation leading to the rapid suppression of cholesterol synthesis within the brain (Goldstein, DeBose-Boyd and Brown, 2006; DeBose-Boyd, 2008; Dietschy, 2009).

Maintaining cholesterol homeostasis within the brain is crucial as studies in animals and cells suggest a link between excess brain cholesterol and an increase in amyloid production (Hughes *et al.*, 2013). Hypercholesterolemia increases the chances of cleavage by γ-secretase of the C99 terminal of APP to release the Aβ polypeptide; however, the exact mechanisms by which Aβ production is affected by cholesterol still remains unknown (Fassbender *et al.*, 2002). Other studies have shown that APP may regulate cholesterol turnover within neurons (Pierrot *et al.*, 2013a). APP down-regulates neuronal cholesterol levels via SREBP pathway in rat cortical neurons; however, in astrocytes APP does not influence cholesterol biosynthesis.

Altered cholesterol metabolism has also been found in Huntington's disease (HD). Studies have found that the levels of 24-OHC decrease in HD post mortem brain tissue with a reduction in the levels of cholesterol 24-hydroxylase (Kreilaus *et al.*, 2015). The production of 24-OHC in neurons has been hypothesized to initiate cholesterol transport from astrocytes to the neurons as a method of maintaining homeostasis (Pfrieger, 2003). Disruption within cholesterol synthesis or transport within astrocytes could contribute to neuronal dysfunction. In a study by Valenza et al (2014), they found that astrocytes are responsible for cholesterol dysfunction within HD as the supply of cholesterol to the neurons has decreased (Valenza *et al.*, 2014).

1.4.1 The Blood Brain Barrier

The blood brain barrier (BBB) is a physical barrier between the central nervous system and the periphery and is crucial in maintaining homeostasis within the brain. The BBB consists of capillary endothelial cells and a basement membrane which is surrounded by pericytes and astrocytic endfeet (Sweeney, Sagare and Zlokovic, 2018). The presence of tight junctions within brain endothelial cells restricts the paracellular exchange of molecules and allows small lipid-soluble molecules or compounds with a molecular weight of less than 400 Da to diffuse across the BBB (Pardridge, 2015).

1.4.2 The Blood Brain Barrier in AD

BBB dysfunction is a feature of neurodegeneration and can contribute to the pathogenesis of AD (Cai *et al.*, 2018; Ajikumar *et al.*, 2019). BBB dysfunction is characterised by an increase in permeability which could be caused by degeneration of cells that form the BBB. A study in transgenic mice carrying the *APOE* E4 allele demonstrated accelerated BBB breakdown and pericyte degeneration (Halliday *et al.*, 2016). Another study observed BBB breakdown within the hippocampus in patients with MCI compared to age matched controls. CSF analysis found a correlation between BBB breakdown and increased levels of soluble platelet-derived growth factor receptor-β, a marker of pericyte injury (Montagne *et al.*, 2015). These studies show that pericyte injury contributes to the breakdown of BBB within the hippocampus. Furthermore, hippocampal BBB breakdown was observed before hippocampal atrophy suggesting that BBB breakdown occurs before the onset of neurodegeneration (Montagne *et al.*, 2015; Sweeney, Sagare and Zlokovic, 2018).

The degeneration of endothelial cells can also contribute to BBB dysfunction, particularly a decrease in expression of tight junction proteins. Tight junctions are an integral part of the BBB, they form a diffusion barrier between capillary endothelial cells preventing substances from peripheral circulation entering the brain (Ballabh, Braun and Nedergaard, 2004). Nishitsuji *et al* (2011) used a triple co-culture system including primary murine brain endothelial cells, pericytes and astrocytes to model the BBB and to investigate the effects of astrocytic *APOE* knockout and expressing different *APOE* alleles on tight junction integrity. This study found that transendothelial electric resistance, a marker of tight junction integrity, was reduced in apoE4 mice compared to apoE3, indicating an increase BBB permeability (Nishitsuji *et al.*, 2011). This suggests that astrocytic apoE expression can regulate the permeability of the BBB through tight junction integrity.

The accumulation and toxicity of Aβ can contribute to BBB disruption by causing direct damage to pericytes, astrocytes and endothelial cells (Cai *et al.*, 2018; Sweeney, Sagare and Zlokovic, 2018). One study assessed the effects of Aβ on the interaction between astrocytes and endothelial cells in mono and co-culture (Spampinato *et al.*, 2017). Spampinato *et al* (2017) found that in a co-culture system, incubation with Aβ leads to endothelial barrier dysfunction, characterised by reduced claudin-5 expression and increased permeability to FITC-conjugated dextran. The

dysfunction of endothelial cells has been attributed to an increase in matrix metalloprotease 9 activity, caused by increased astrocytic expression of vascular endothelial growth factor, which leads to the disruption of claudin-5 and therefore BBB dysfunction (Spampinato *et al.*, 2017).

1.4.3 The Blood Brain Barrier and cholesterol transport in AD

Due to the large size of cholesterol molecule, it cannot easily diffuse through the BBB, thus the use of cholesterol transporters, such as ATP-binding cassette 1 (ABCA1), contribute to cholesterol efflux at the BBB (Do *et al.*, 2015). A study by Do *et al* (2015) used a triple transgenic mouse model of AD to investigate the expression of ABCA1 at the BBB. An increase in ABCA1 expression was observed at all timepoints in transgenic mice compared to age matched wildtype controls. In addition, Do *et al* (2015) observed a significant increase in cholesterol efflux in transgenic mice aged 3 and 6 months compared to the controls (Do *et al.*, 2015). This suggests that in AD, BBB dysfunction can lead to an increase in cholesterol efflux from the CNS.

1.5.1 Changes in the brain during ageing

Ageing, one of the greatest risk factor for developing AD, is characterised by the accumulation of cellular damage over time; leading to the loss of physiological integrity, impairing function and increasing the vulnerability to death (López-Otín *et al.*, 2013). The process of ageing affects many cellular processes, some of which are involved in development of AD; however, many suggestions have been put forward to describe the process of ageing that occurs within the brain (Martin, Dotti and Dolores, 2010; López-Otín *et al.*, 2013). Myelin breakdown is a common phenomenon that occurs during the progression of ageing and has been observed in mild cognitive impairment (MCI) and dementia. Myelin breakdown releases cholesterol and other nutrients into the CSF and extracellular space causing an increase in cholesterol levels which leads to neuronal death (Bartzokis, 2011; Hughes *et al.*, 2013).

Changes in mitochondria have also been associated with advancing age. Studies suggest that, during normal ageing, mitochondrial mass increases and there is a decline in the activity of complex I and complex IV and an increase in manifestation of oxidative stress markers (Barrientos *et al.*, 1997; Navarro and Boveris, 2007;

Boveris and Navarro, 2008; Bartzokis, 2011). In AD brains the activity of complex I and complex IV decreases, leading to a depletion in ATP stores which prevents APP cleavage by α-secretase and promotes cleavage with β-secretase to produce Aβ (Gabuzda *et al.*, 1994; Tamagno *et al.*, 2002; Swerdlow, 2011).

During natural ageing there is loss of brain cholesterol, however the amount of cholesterol that is lost does not correlate with age; and the rate of change in cholesterol levels varies depending on the brain region (Martin, Dotti and Dolores, 2010). The distribution of apoE during ageing is yet to be fully elucidated; studies in rats have shown that there is a decrease in apoE protein expression in the hypothalamus and cortex but an increase within the hippocampus (Jiang *et al.*, 2001; Terao *et al.*, 2002). During ageing there is an increase in the amount of cholesterol 24-hydroxylase enzyme leading to an increase in production of oxysterols, this down-regulates cholesterol synthesis within astrocytes and reverse cholesterol transport (E G Lund, Guileyardo and Russell, 1999; Clement *et al.*, 2009; Martin, Dotti and Dolores, 2010).

1.5.2 Cholesterol changes in the brain during AD

During AD, it has been suggested that there is an imbalance in cholesterol homeostasis, but the exact mechanisms by which this occurs are still unknown. Some studies suggest that there is a decrease in brain cholesterol due to a reduction in cholesterol synthesis. This reduction in synthesis is due to a decrease in expression of the gene for 3β-hydroxysterol Delta 24-reductase (Selective AD indicator 1- seladin1) – the enzyme involved in converting desmosterol to cholesterol (Greeve *et al.*, 2000; Waterham *et al.*, 2001; Martin, Dotti and Dolores, 2010). Cholesterol transport from glial cells to neurons is also altered in AD. The apoE ε4 allele is a genetic risk factor for AD, this allele has a lower ability to release cholesterol from glial cells resulting in a decrease in cholesterol level within the neurons (J.-S. Gong *et al.*, 2002; Martin, Dotti and Dolores, 2010). Studies in mice have shown that apoE is involved in BBB integrity; expression of human apoE4 in mice, showed BBB breakdown by activation of proinflammatory signalling in pericytes, leading to neurotoxic proteins from the blood entering neurons (Bell *et al.*, 2012). The ε4 allele also has a decreased activity in clearance leading to Aβ accumulation (Lomnitski *et al.*, 1999; DeMattos, 2004; Martin, Dotti and Dolores, 2010). The 24-hydroxylase enzyme is present in neuritic plaques in AD and is

deficient in neurons making them more susceptible to stress and its expression is increased in the presence of oxidative stress (Brown, Theisler, Silberman, Magnuson, Gottardi-Littell, John M Lee, *et al.*, 2004; Ohyama *et al.*, 2006; Martin, Dotti and Dolores, 2010). The levels of 24-OHC are also decreased in AD brains, studies show that 24-OHC favour the non-amyloidogenic processing of APP however, the mechanisms by which this is achieved are still unknown (Sparks *et al.*, 1994; Heverin *et al.*, 2004; Martin, Dotti and Dolores, 2010).

1.5.3 Oxidative stress in the brain during ageing

Oxidative stress is a feature of brain ageing and may contribute to the pathogenesis of AD. It is defined as the imbalance between biochemical processes leading to ROS being produced and those processes responsible for the removal of ROS (Harman, 1981; Recuero *et al.*, 2009). Accumulation of ROS within neurons causes DNA damage and induces a DNA damage response, which leads to cellular senescence and may contribute to neuronal dysfunction. Previous work in our lab has demonstrated that oxidative DNA damage is associated with lower cognitive measures at early stages of AD pathology (Simpson *et al.*, 2015). Further work investigated the changes in gene expression in neurons in high vs low DNA damage responses using gene microarray analysis. This study identified that an overexpression in six out of the ten genes probes involved in cholesterol biosynthesis was associated with a high DNA damage response (Simpson *et al.*, 2016). Studies also indicate that neuronal loss in AD may be due to an increase in oxidative stress (Moreira *et al.*, 2005; Recuero *et al.*, 2009). In the presence of oxidative stress cholesterol biosynthesis is induced. This was shown in a study by Recuero *et al* (2009) they induced oxidative stress by treating neuroblastoma cells with xanthine oxidase and found that HMGCR expression within neurons was increased which caused damage to the cells (Recuero *et al.*, 2009).

1.6 Overall aims of this thesis

Currently, we are aware of the importance of maintaining cholesterol homeostasis within the brain for normal brain function and evidence is further suggesting that cholesterol may have a role in the processing of APP to produces Aβ plaques; however, the exact mechanisms remain unknown. This thesis aims to characterise how cholesterol production and cholesterol metabolism change during the progression of AD. The overall hypothesis is that cholesterol dysregulation in the brain contributes to dementia and to progression of Alzheimer's disease (Figure 1.5). We further hypothesise that dysregulation of cholesterol biosynthesis occurs at the earliest stages of AD, with an initial compensatory stage that fails. We also will investigate the hypothesis that dysregulation of cholesterol biosynthesis in the neuron-astrocyte unit contributes to dementia by impairing neuronal function due to impaired cholesterol metabolism and through generation of pro-oxidative stress metabolites.

Objectives:

- Define changes in the expression of genes that encode cholesterol biosynthesis pathway enzymes in neurons and astrocytes in an ageing population-representative neuropathology cohort in relation to AD progression and oxidative DNA damage. This was carried out by isolating neurons and astrocytes using laser capture micro-dissection to produce an enriched sample from frozen temporal cortex sections. The cell extractions were used for quantitative real time PCR to measure the expression of genes involved in cholesterol biosynthesis.
- Examine the effects of acute and chronic stress on cholesterol metabolism in the neuron-astrocyte unit using astrocyte and neuron monocultures. This was carried out by culturing Lund human mesencephalic cells (LUHMES), a neuronal cell line, and primary human foetal astrocytes separately in monoculture examining the effect of a single and double exposure to hydrogen peroxide on the cholesterol biosynthetic gene expression.

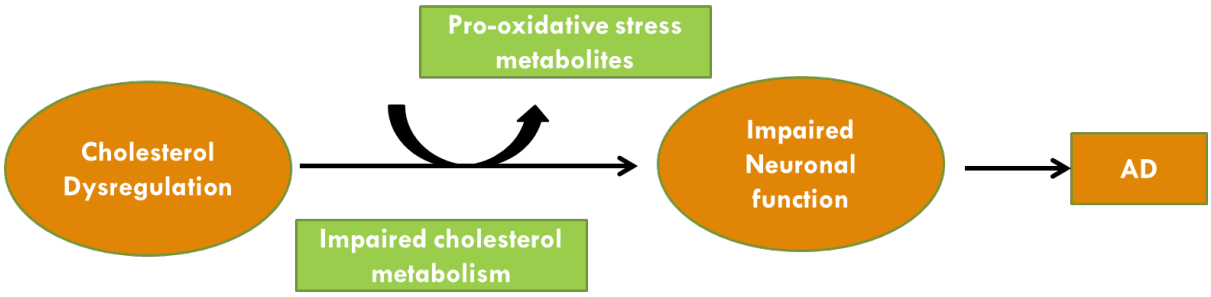

Figure 1.5: Diagram illustrating the hypothesis of the project: Dysregulation of cholesterol biosynthesis in the neuron-astrocyte unit contributes to dementia by impairing neuronal function due to impaired cholesterol metabolism and through generation of pro-oxidative stress metabolites.

2.0 Histological characterisation of key regulators of cholesterol biosynthesis in the ageing brain

2.1 Introduction

Due to the significance of cholesterol in maintaining optimum neuronal function, the control of cholesterol production within the brain is of paramount importance. *De novo* cholesterol production in the brain occurs via the cholesterol biosynthesis pathway mainly in astrocytes (Pfrieger, 2003; Maria Giudetti *et al.*, 2015), and the rate of cholesterol production is regulated by the action of the HMG-CoA reductase (HMGCR) enzyme (Sharpe and Brown, 2013a). HMGCR is a trans-membrane glycoprotein which is found within the endoplasmic reticulum (ER) membrane and catalyses the conversion of HMG-CoA into mevalonate (Figure 1.4 and Figure 2.1) (Hwang *et al.*, 2016). It is encoded by the *HMGCR* gene, which is found on chromosome 5 and generates a monomer consisting of 888 amino acids (Kumar *et al.*, 2019). The HMGCR monomer contains three domains: The N-domain (N-terminal); S-domain and L-domain (C-terminal). The catalytic portion of the enzyme consists of four monomers to form a tetramer and substrate binding occurs within the S and L domains at the junction between monomers (Istvan and Deisenhofer, 2000).

Sterol Regulatory Element-Binding Proteins (SREBP) regulate the expression of *HMGCR*. SREBP's are transcription factors that are localised to the ER membrane which regulate cholesterol production within cells (Sakai *et al.*, 1997). Three isoforms of SREBP are expressed in mammals, SREBP-1a, SREBP-1c and SREBP2 (Goldstein, DeBose-Boyd and Brown, 2006). All three isoforms are incorporated into the ER in the same orientation, with both N-terminus and COOH-terminus facing the cytosol which is also where SREBP Cleavage-Activating Protein (SCAP) binds to SREBP after synthesis (Sakai *et al.*, 1997). SREBP-1a and SREBP-1c are encoded by a gene located on chromosome 17 and is involved in the activation of transcription of genes involved in cholesterol, fatty acid and triglyceride synthesis (Xianxin Hua *et al.*, 1995; Horton, Goldstein and Brown, 2002). The gene encoding SREBP2 is found on chromosome 22 and is specifically involved in the activation of transcription of genes involved in cholesterol biosynthesis (Xianxin Hua *et al.*, 1995; Horton, Goldstein and Brown, 2002). All SREBP isoforms have a similar structure, the N-terminus is a transcription factor belonging to the basic-helix-loop-helix-leucine

(bHLH) zipper family, followed by a transmembrane domain and the C-terminus contains a regulatory domain (Sakai *et al.*, 1997).

Regulation of the cholesterol biosynthesis pathway occurs via cleavage and trafficking of SREBP2. When cholesterol levels are low, SCAP cleaves SREBP2 which migrates to the nucleus to promote the transcription of genes involved in cholesterol biosynthesis, such as *HMGCR*, upregulating cholesterol synthesis (Simons and Ilonen, 2000; Goldstein, DeBose-Boyd and Brown, 2006). When cholesterol levels increase, HMGCR binds to INSIG-1 (insulin-induced gene 1) and INSIG-2 (insulin-induced gene 2) which mark HMGCR for ubiquitination and degradation which leads to the rapid suppression of cholesterol synthesis within the brain (Goldstein, DeBose-Boyd and Brown, 2006; DeBose-Boyd, 2008; Dietschy, 2009).

The processing of APP within membranes is also influenced by cholesterol levels found within the membranes (Grimm, Rothhaar and Hartmann, 2012). One study found that in SHSY-5Y cells, cleavage with β-secretase was favoured within cholesterol enriched lipid rafts suggesting that α-secretase cleavage is favoured within cholesterol-depleted regions of the membrane (Cordy *et al.*, 2003; Grimm, Rothhaar and Hartmann, 2012). A study by Pierrot *et al.*, (2013) demonstrated the role APP plays in cholesterol biosynthesis regulation. In primary rat cortical neurons, moderate expression of APP was found to decrease cholesterol biosynthesis as well as a decrease in SREBP mRNA expression (Pierrot *et al.*, 2013b). APP was found to inhibit the site-2 mediated release of SREBP preventing the nuclear localisation of the SREBP transcription factor domain. However, in primary rat cortical astrocytes APP did not interact with SREBP suggesting that within astrocytes APP does not play a role in the regulation of cholesterol biosynthesis (Pierrot *et al.*, 2013b). These results were further confirmed *in vivo*, where transgenic mice expressing different APP mutants, showed a downregulation in SREBP expression (Pierrot *et al.*, 2013b). Furthermore, an SNP found within the promoter region of the HMGCR gene was found to increase the risk of AD and accelerate progression of AD (Porcellini *et al.*, 2007). These studies further reinforce the link between cholesterol biosynthesis and AD.

1) HMG-CoA + NADPH ➔ Mevaldyl-CoA + $NADP^+$

2) Mevaldyl-CoA + H^+ ➔ Mevaldehyde + CoASH

3) Mevaldehyde + NADPH +H^+ ➔ Mevalonate

Figure 2.1 Cholesterol biosynthesis rate determining step: The three steps involved in the formation of mevalonate from HMG-CoA, which is catalysed by the HMGCR enzyme.

For this study, post-mortem human tissue was obtained from the Cognitive Function and Ageing Study (CFAS). CFAS is a prospective multicentre epidemiological study of the ageing population (>65 years of age) in the UK which represents the spectrum of age-related neurodegenerative pathologies and range of cognitive impairment, enabling neuropathological correlates of dementia to be determined (http://www.cfas.ac.uk). The study was based around six centers across the UK (Cambridgeshire, Oxford, Nottingham, Newcastle, Liverpool and Gwynedd) with an initial screening process including a mini-mental state examination and an automated geriatric examination for computer-assisted taxonomy to assess cognitive impairment in candidates, this was followed up after 6 years with a total of 3145 patients that had been screened and interviewed as part of the study (Ince, 2001; Brayne, McCracken and Matthews, 2006; Matthews *et al.*, 2009; Wharton *et al.*, 2011). The neuropathology cohort consists of 525 brain donations from all six centers, from which the Cambridge cohort consists of 100 brains with both frozen and fomalin fixed samples available (Wharton *et al.*, 2011).

CFAS is a longitudinal ageing population representative study which means that there is a wide range of cases with and without dementia, making it a valuable resource for studying the progression of dementia in a population. This approach reveals the variability within a population and provides an idea of the spectrum that is encompased within this disorder. Furthermore, due to the nature of this study it facilitates an unbiased assessment of relationships between pathology and dementia, as cases are not pre-selected based on clinical groups and are free from sampling biases. This provides complementary information to classical case-control studies. Studies on the CFAS neuropathology cohort have shown that AD pathology is the commonest association with dementia and multiple pathologies also associate and coexist with dementia with age being the biggest risk factor, especially over 90 years of age. Additionaly, a smaller brain weight, small vessel disease and hippocampal atrophy, increase the risk of dementia. The study also found that both demented and non-demented individuals had classical AD pathology and the overlap in Aβ plaque burden increases at the oldest ages however, a severe tangle score was only observed in 20% of demented patients and was a better discriminator in both demented and non-demented individuals (Matthews *et al.*, 2009; Savva *et al.*, 2009; Wharton *et al.*, 2011).

Previous population-based studies involving CFAS have demonstrated that oxidative DNA damage is associated with lower cognitive measures at early stages of AD pathology (Simpson *et al.*, 2015). Further work investigated the changes in gene expression in neurons in high vs low DNA damage responses using gene microarray analysis. This study identified that an overexpression in six out of the ten genes probes involved in cholesterol biosynthesis was associated with a high DNA damage response (Simpson *et al.*, 2016). A fold change of 4.5 (p=0.0008) for *HMGCR* and a down-regulation in *SREBF2* with a fold change of -1.1 (p=0.001) was observed. This study also found an association with neuronal DNA damage response and the levels of the cholesterol metabolite 24(S)-hydroxycholesterol (24(S)-OHC) in the cerebrospinal fluid (CSF) (r=0.30. p=0.033) and 24(S)-OHC negatively correlated with increasing Braak and Braak stage (r=-0.29, p=0.040). This data suggests that at early Braak and Braak stages, oxidative DNA damage is associated with increased cholesterol biosynthesis. This may be a compensatory mechanism that fails as AD progresses.

Cholesterol has a vital role in maintaining normal neuronal function during development and throughout adult life and given that oxidative stress is a feature of brain ageing, it is important to characterise changes in cholesterol biosynthesis that occur as the brain ages. To determine if a decline in HMGCR expression occurs at older ages, suggesting a reduction in cholesterol biosynthetic capacity at older ages, post-mortem human brain tissue was obtained from Edinburgh Medical Research Council Sudden Death Brain Bank. Donors to this cohort had no history of neurological disorders and spanned a large age range (16-75 years of age), making the cohort ideal to assess the changes in cholesterol synthesis during ageing. This cohort will help determine if there are changes in HMGCR expression during ageing regardless of dementia or AD and will determine if changes in cholesterol synthesis occur as the brain ages, potentially contributing to impaired brain function. The CFAS neuropathology cohort is an aging population representative cohort and recruited patients who were 65 years old and above and so contains a wide spectrum of pathology and dementia status allowing the assessment of cholesterol biosynthesis over disease progression. The use of Edinburgh cohort, an ageing series, allow characterisation of cholesterol biosynthesis in relation to the effects of old age.

2.2 Aims and Objectives

The aim of this study was to investigate how the expression of HMGCR and SREBP2, key regulators of cholesterol biosynthesis, vary in the ageing brain and how the expression of these regulators are affected by dementia status, Alzheimer's neuropathology, DNA damage and neuroinflammation.

We hypothesise that changes in the expression of the key regulators of cholesterol biosynthesis are associated with increased Alzheimer's neuropathological change, oxidative DNA damage and neuroinflammation leading to dysfunction of cholesterol synthesis within the ageing brain.

The objectives for this chapter are:

- Characterise cellular localisation of HMGCR using immunohistochemistry
- Validate HMGCR antibody expression.
- Provide a quantitative analysis of the immunoreactivity of HMGCR expression within temporal cortex tissue from the CFAS Cambridge Cohort.
- Carry out non-parametric analysis to determine if variation in HMGCR immunoreactivity is associated with dementia status and Alzheimer's neuropathological change.
- Carry out further statistical analysis to determine if variation in HMGCR immunoreactivity correlates to markers of oxidative stress and neuroinflammation.
- Characterise and quantify expression of HMGCR in an aging cohort.
- Determine if variation in HMGCR immunoreactivity is associated with the effects of ageing.
- Characterise the expression of SREBP2 using immunohistochemistry within temporal cortex tissue from the CFAS Cambridge Cohort.

2.3 Methods

List of materials can be found in Appendix **6.1.1**

2.3.1 Human Brain Tissue

Post-mortem human brain tissue was obtained from the Cambridge centre of CFAS (n=99). One hemisphere was sampled and fixed using formalin and stored at RT. The other hemisphere was sliced in the coronal plane and snap frozen, and stored at -80°C. For both frozen and fixed sections the temporal cortex (Brodmann area 20/21) was investigated and the ethical approval (15/SW/0246) can be found in the appendix (appendix 6.3) alongside the cohort demographics (appendix table 6.3.1).

Post-mortem formalin fixed human prefrontal association cortex (Brodmann area 8/9) was obtained from the Edinburgh Medical Research Council Sudden Death Brain Bank. Neuropathology was specifically assessed in Brodmann area 8/9 using the immunoreactivity of Aβ and tau to determine if any neurodegenerative features were present. The cohort represented various age groups such as 16-30yrs (n=3), 31-45 yrs (n=3), 46-60 yrs (n=5), 61-75 yrs (n=4) and 75+ yrs (n=1). Ethical approval can be found (TR75/19) in the appendix (appendix 6.4) alongside the cohort demographics (appendix 6.4.1).

2.3.2 Immunohistochemistry

Immunohistochemistry (IHC) was carried out using the standard horseradish peroxidase-conjugated avidin-biotin complex (ABC-HRP) IHC technique (Vectastain Elite kit, Vector Laboratories UK) with 3,3'-diaminobenzidine (DAB) (Vector laboratories, UK) as substrate. Formalin fixed paraffin embedded (FFPE) sections (5μM) were de-waxed in two changes of xylene (Fisher Scientific, UK) and rehydrated through a graded series of ethanol (absolute, 95%, 70%) (VWR Chemicals, France) and placed in a pressure cooker in the corresponding buffer (Table 2.1) (Menarini Diagnostics, UK). Antigen retrieval was carried out (125°C at 20psi for 30 seconds), before sections were cooled to RT in running tap water and blocked for endogenous peroxidase in 3% (v/v) H_2O_2/Methanol (Fisher Scientific UK) for 20 minutes at RT. The sections were blocked, followed by primary antibody incubation (Table 2.1). Following incubation, sections were washed with TBS for 5 minutes at RT and incubated with 0.5% (v/v) biotinylated (50 μl in 10ml of 1.5% (v/v) goat serum) secondary antibody for 30 minutes, followed by another wash with TBS

for 5 minutes at RT. The sections were then incubated with 2% (v/v) ABC-HRP (100 µl of both reagent A and B in 10 ml of TBS, prepared 30 minutes prior to use) for 30 minutes followed by a wash with TBS for 5 minutes at RT. The antibody binding was visualised by incubating the sections with DAB for 5 minutes at RT and the reaction was stopped with d.H_2O. The sections were washed in tap water, counterstained in Harris's haematoxylin for 30 seconds and blued in Scotts Tap water for 10 seconds. The sections were dehydrated in a graded series of ethanol (70%, 95%, absolute) and cleared in xylene before mounting with DPX and glass coverslips. Once mounted the sections were placed in an oven overnight at 37°C to dry. Rabbit isotype controls and omission of primary antibody (negative controls) were included to confirm antibody specificity. HMGCR antibody optimisation can be found in the appendix (appendix 6.1).

Antibody (Catalogue number)	Species, optimised dilution and incubation conditions	Antigen retrieval
HMGCR (Abcam, UK) (ab174830)	Rabbit monoclonal, 1/100, overnight at 4°C	pH 9.5 buffer, pressure cooker, 1hr
HMGCR (Atlas Antibodies, Sweden) (AMAb90619)	Mouse Monoclonal, 1/100, overnight at 4°C	pH 9.5 buffer, pressure cooker, 1hr
SREBF2 (Abcam, UK) (ab28482)	Rabbit IgG polyclonal, 1/100, 1hr at RT	pH 6 buffer, microwave 10 minutes
GFAP (Dako, Denmark) (Z033401-2)	Rabbit IgG polyclonal, 1/500, overnight at 4°C	n/a

Table 2.1: Antibodies used for Immunohistochemistry

2.3.3 Frozen Immunohistochemistry

Frozen cryosections (7µm) were warmed to RT within the lamina hood for 5 minutes. The sections were fixed and permeabilised in ice cold acetone (VWR chemicals, France) for 3 minutes and air-dried briefly at RT. The sections were blocked in 1.5% (v/v) goat normal serum for 30 minutes at RT, followed by an overnight incubation at 4°C with HMGCR (Table 2.3) (Abcam, UK). The sections were washed with TBS for 5 minutes at RT and incubated with 0.5% biotinylated secondary antibody for 30 minutes, followed by a wash with TBS for 5 minutes at RT. The sections were

incubated with 2% (v/v) ABC-HRP for 30 minutes followed by a wash with TBS for 5 minutes at RT. The antibody binding was visualised by incubating the sections with 3,3'-diaminobenzidine for 5 minutes at RT and the reaction was quenched with d.H_2O. The sections were washed in tap water, counterstained in Harris's haematoxylin for 30 seconds and blued in Scotts Tap water for 10 seconds. The sections were dehydrated in a graded series of ethanol (70%, 95%, absolute) and cleared in xylene before mounting with DPX and glass coverslips. Once mounted the sections were placed in an oven overnight at 37°C to dry. Rabbit isotype controls and omission of primary antibody (negative controls) were included to confirm antibody specificity.

2.3.4 Quantification and statistical analysis of variation of HMGCR expression

For quantification, two parallel ribbons were imaged throughout all layers of the cortex of each stained section. These images were quantified using the Analysis^D software (Figure 2.2A). This programme counted the number of pixels that had been stained and compared them to the total number of pixels in the image producing a percentage immunoreactivity value for each case. The programme was set so that specific immunolabelling of HMGCR was detected above a threshold value and non-specific background staining was excluded from the final percentage (Figure 2.2B and C). For each case, the average percentage of immunoreactivity was recorded and used for statistical analysis.

Statistical analysis was carried out using SPSS Statistics v25 (IBM, UK). A Kolmogorov Smirnov test was carried out to determine if the data was normally distributed. To investigate the associations between AD neuropathology and HMGCR immunoreactivity a Kruskal-Wallis (KW) test was carried out. The Jonckheere-Terpstra (JT) test was carried out to identify any trends between groups. Spearman rank correlation test was used to investigate correlations between percentage HMGCR immunoreactivity and DNA damage response, AD neuropathology progression, brain pH, inflammation and post-mortem delay. Data from previous publications and studies were used for statistical analysis (Savva *et al.*, 2009; Simpson *et al.*, 2015). AD neuropathology progression was measured using Braak and Braak group staging and Thal β-Amyloid phase. For statistical analysis, Braak and Braak stages were combined to allow comparisons between Braak and Braak groups, Thal phases were also grouped to allow for comparison between and

Thal phases. Groups were defined as follows: for Braak and Braak, group 1 contained stages 0-II (entorhinal), group 2 contained stages III-IV (limbic) and group 3 contained stages V-VI (isocortical); for Thal, group 1 contained phases 1-2, group 2 contained phases 3-4 and group 3 contained phases 5-6. To determine if the variation in neuronal expression of HMGCR associated with dementia status a Mann-Whitney U test was carried out. The effect of HMGCR immunoreactivity on risk of dementia was analysed using logistic regression. Statistical analysis in relation to dementia status was carried out by Connor Richardson, University of Newcastle. All tests were two tailed and the $p<0.05$ was set as the level for significance.

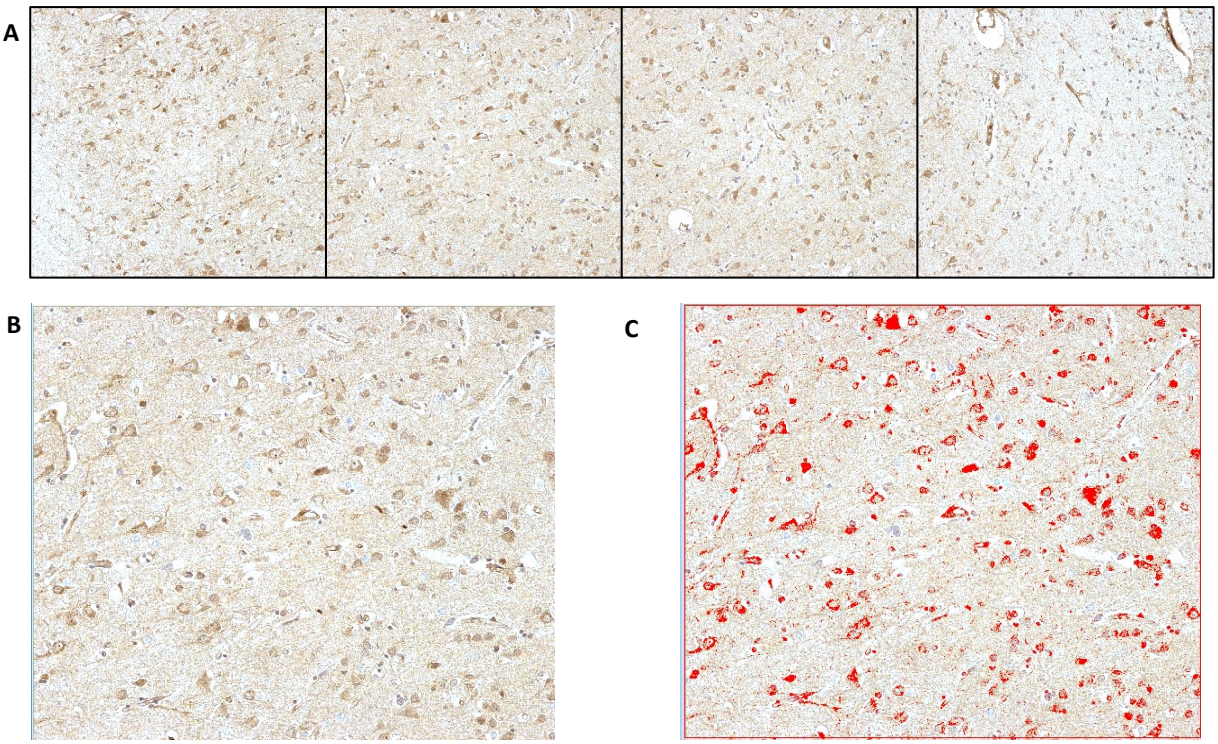

Figure 2.2. Quantification of HMGCR expression: A set of images was taken across the all layers of the cortex ranging from just below the pia-surface (LHS) all the way to the white matter regions (RHS) for each section (A). Using Analysis^D software to set colour thresholds and calculate percentage immunoreactivity, original image (B) and the image highlighting the areas with positive immunoreactivity (C).

2.3.5 Dual Labelling IHC of co-localisation of HMGCR with astrocytes

To confirm co-localisation of HMGCR with astrocytes dual labelling was performed. IHC for HMGCR was carried out as outlined above (2.3.2) using the ABC-HRP technique and Vectastain Elite Kit (Vector Laboratories, UK) with DAB (Vector Laboratories, UK) as substrate. After DAB incubation, the sections were blocked in 1.5% (v/v) goat normal serum for 30 minutes at RT, followed by 15 minutes incubation with avidin at RT (first component of avidin/biotin blocking kit, Vector Laboratories, UK). After blocking, the sections were washed with TBS once and then incubated with biotin (second component of the avidin/biotin blocking kit, Vector Laboratories, UK) for 15 minutes at RT. The excess biotin was removed and the sections where incubated with GFAP antibody (1:500 dilution) overnight at 4°C. The sections were washed in TBS for 10 minutes, prior to the addition of biotinylated anti-rabbit secondary antibody (50µl in 1.5% (v/v) goat serum) for 1hr at RT. The sections were washed in TBS for 10 minutes, prior to the addition of the alkaline phosphatase-conjugated avidin-biotin complex (ABC-AP, Vector Laboratories, UK) (100µl of reagent 'A', 100µl of reagent 'B' in 5 ml TBS, prepared at least 30 minutes prior to use) for 1hr at RT and washed with TBS for 10 minutes, ensuring all TBS was removed after the wash. The sections were incubated in the alkaline phosphatase substrate (Vector Red, Vector Laboratories, UK) (100 µl reagent 1, 2, and 3 in 5 ml Tris-HCL, 100mM) for 10-20 minutes, allowing enough time for the reaction to develop. The reaction was stopped by washing the slides with d.H_2O. The sections were washed in tap water, counterstained in Harris's haematoxylin for 30 seconds and washed in tap water. The sections were dehydrated in a graded series of ethanol (70%, 95%, absolute) and cleared in xylene before mounting with DPX and glass coverslips. Once mounted, the sections were placed in an oven overnight at 37°C to dry. Rabbit and mouse isotype controls and omission of primary antibody (negative controls) were included to confirm antibody specificity.

2.3.6 Bicinchoninic acid assay (BCA)

LUHMES and astrocyte cell pellets were obtained as outlined in chapter 4.3.1 and 4.3.3 HeLa cell pellet was obtained from Dr Emma Smith and was used as a positive control. The cell pellets were lysed in ice-cold extra-strong lysis buffer followed by centrifugation at 16,000 g at 4°C for 5 minutes. Tissue protein extracts were obtained from previous studies carried out within the lab (Viggars *et al.*, 2011). To determine the protein concentration of the cell and tissue protein extract, a BCA protein assay

was performed according to the manufacturer's instructions (ThermoFisher Scientific, USA). BSA protein standards were freshly prepared at concentrations ranging from 0-2 mg/ml using extra strong lysis buffer. Absorbance of samples was measured at 550 nm wavelength using PHERAStar spectrophotometer and protein concentration values were interpolated from the protein standard curve. Samples were diluted using extra strong lysis buffer to ensure equal proteins concentrations were used.

2.3.7 SDS-polyacrylamide gel electrophoresis (SDS-PAGE)

Samples were mixed with (4x) Laemmli sample buffer and heated at 100°C for 5 minutes and centrifuged at 10,000g for 1 minute. The samples were loaded 12% (v/v) polyacrylamide gel with 4% (v/v) stacking gel (Table 2.2). Molecular weight standard, Precision Plus Dual Colour Protein Standard (Bio-Rad Laboratories Ltd, UK) was also loaded with the protein samples. Gels were electrophoresed at 120V for approximately 1.5 hrs or until the dye front had reached the bottom of the gel.

	5% Stacking gel	12% Resolving gel
Acrylamide	1.7ml	4ml
Resolving buffer	-	2.5ml
Stacking buffer	2.5ml	-
10% (w/v) APS	50µl	50µl
TEMED	20µl	20µl
dH_2O	5.8ml	3.5ml

Table 2.2: Composition of stacking and resolving gel

2.3.8 Western Blotting

Following electrophoresis, gels were placed onto nitrocellulose membranes (GE Healthcare, UK), which was sandwiched between sponges and filter paper (Whatman Laboratories) in an X-Cell transfer module (Life Technologies) and submerged in transfer buffer. Protein transfer was carried out at 300 mA for 2 hrs and the success of the transfer was checked using Ponceau Red. The membrane was blocked for non-specific binding in 5% (v/v) milk in PBS-T for 1 hr at RT, followed by a primary antibody (Table 2.3) incubation at 4°C overnight. Following primary antibody incubation, the membranes were washed 3 times in 1x PBS-T for 10 minutes followed by an incubation with species-specific HRP conjugated secondary antibody (Table 2.3) for 1 hr at RT. Following secondary antibody

incubation, the membranes were washed 3 times in 1x PBS-T for 10 minutes prior to incubating with enhanced chemiluminescent substrate (EZ-ECL Biological Industries, Israel) and visualising the membranes using the G-box Chemi-XT CCD Gel imaging system (Syngen, UK).

Antibody (Catalogue number)	Species, optimised dilution and incubation conditions
HMGCR (Abcam, UK) (ab174830)	Rabbit monoclonal, 1/1000, overnight at 4°C
α-tubulin (clone DM1A), (Sigma Aldrich, UK) (T6199)	Mouse monoclonal, 1/10,000, overnight at 4°C
Anti-rabbit HRP (Promega, UK) (W4011)	Goat polyclonal, 1/5000, 1hr at RT
Anti-mouse HRP (Promega, UK) (W4021)	Goat polyclonal, 1/5000, 1hr at RT

Table 2.3: Antibodies used for western blotting

2.4 Results

2.4.1 HMGCR is expressed in pyramidal neurons in the temporal cortex

Immunohistochemistry showed that the HMGCR enzyme was expressed in pyramidal neurons of the temporal cortex. Positive immunostaining in neurons was observed in all cases throughout the cohort, with some variation in intensity of immunolabelling between cases. The expression was punctate and localised to the cytoplasm of neuronal cell bodies and proximal processes (Figure 2.3 A and B). The variation in HMGCR expression was not normally distributed (Kolmogorov-Smirnov p=0.092) with a mean percentage immunoreactivity across the cohort of 3.90, standard deviation of 2.86, median of 3.87 and an interquartile range of 3.56 (Figure 2.3 C). To ensure that the variation in immunostaining was not an artefact of brain donation, correlations between brain pH (r=0.094, p=0.405) and post-mortem delay (r=-0.026, p=0.813) were determined.

To determine if the variation in neuronal expression of HMGCR changed with AD neuropathology we examined variation across Braak and Braak groups as a measure of NFT progression (KW p=0.559) (JT p=0.578) (Figure 2.3 D) (Table 2.4). We found that HMGCR expression did not vary with Braak and Braak stage. Variation between HMGCR immunoreactivity did not vary with Thal Aβ staging for the cohort. Thal Aβ staging was examined as a measure of Aβ progression (KW p=0.311) (JT p=0.171) (Table 2.5). To further assess the relationship to AD neuropathology, variation in HMGCR immunoreactivity was also assessed according to local measures of AD neuropathology in temporal cortex. There were no significant differences in HMGCR immunoreactivity between different neuritic plaque density groups (KW p=0.791) (JT p=0.551), or neurofibrillary tangle score groups (KW p=0.430) (JT p=0.741). No significant correlations were found between neuronal HMGCR immunoreactivity and Aβ percentage immunoreactivity (r=-0.027, p=0.800), and phosphorylated tau (AT8) percentage immunoreactivity (r=-0.083, p=0.434).

Data from previous studies in our lab was used to study correlations with HMGCR immunoreactivity and markers of oxidative stress, DNA damage and neuroinflammation (Simpson *et al.*, 2015). To determine if HMGCR immunoreactivity correlated with markers of DNA damage response we examined

γH2AX immunoreactivity in both neurons (r=-0.039, p=0.706) and astrocytes (r=0.060, p=0.563). Furthermore, protein expression of malondialdehyde, was assessed by western blotting, was also examined as a measure of oxidative stress (r=-0.008, p=0.966). This shows that neuronal HMGCR percentage immunoreactivity does not vary with markers of DNA damage response and oxidative stress. To investigate correlations between neuroinflammation and HMGCR immunoreactivity, we examined CD68 immunoreactivity (r=-0.034, p=0.752) and MHCII immunoreactivity (r=-0.055, p=0.617) as a measure of microglial activation. This data shows that the variation in neuronal HMGCR percentage immunoreactivity does not correlate with markers of neuroinflammation.

Braak and Braak Groups	N	Mean	SD	SEM	Median	Range
1 (0-II)	30	3.64	3.02	0.553	3.41	14.60
2 (III-IV)	51	4.14	2.84	0.398	3.98	14.35
3 (V-VI)	18	3.66	2.73	0.287	4.01	10.31

Table 2.4: Case summaries of average percentage immunoreactivity of HMGCR in temporal cortex according to Braak and Braak groups

Thal Aβ Phase	N	Mean	SD	SEM	Median	Range
0	13	3.20	2.14	0.593	3.26	6.64
1	9	3.92	4.21	1.403	2.73	14.09
2	17	4.24	3.64	0.882	2.67	13.53
3	24	3.37	2.81	0.574	3.18	10.75
4	19	4.70	1.92	0.441	4.93	7.35
5	17	3.93	2.71	0.657	4.02	10.31

Table 2.5: Case summaries of average percentage immunoreactivity of HMGCR in temporal cortex according to Thal Aβ phase.

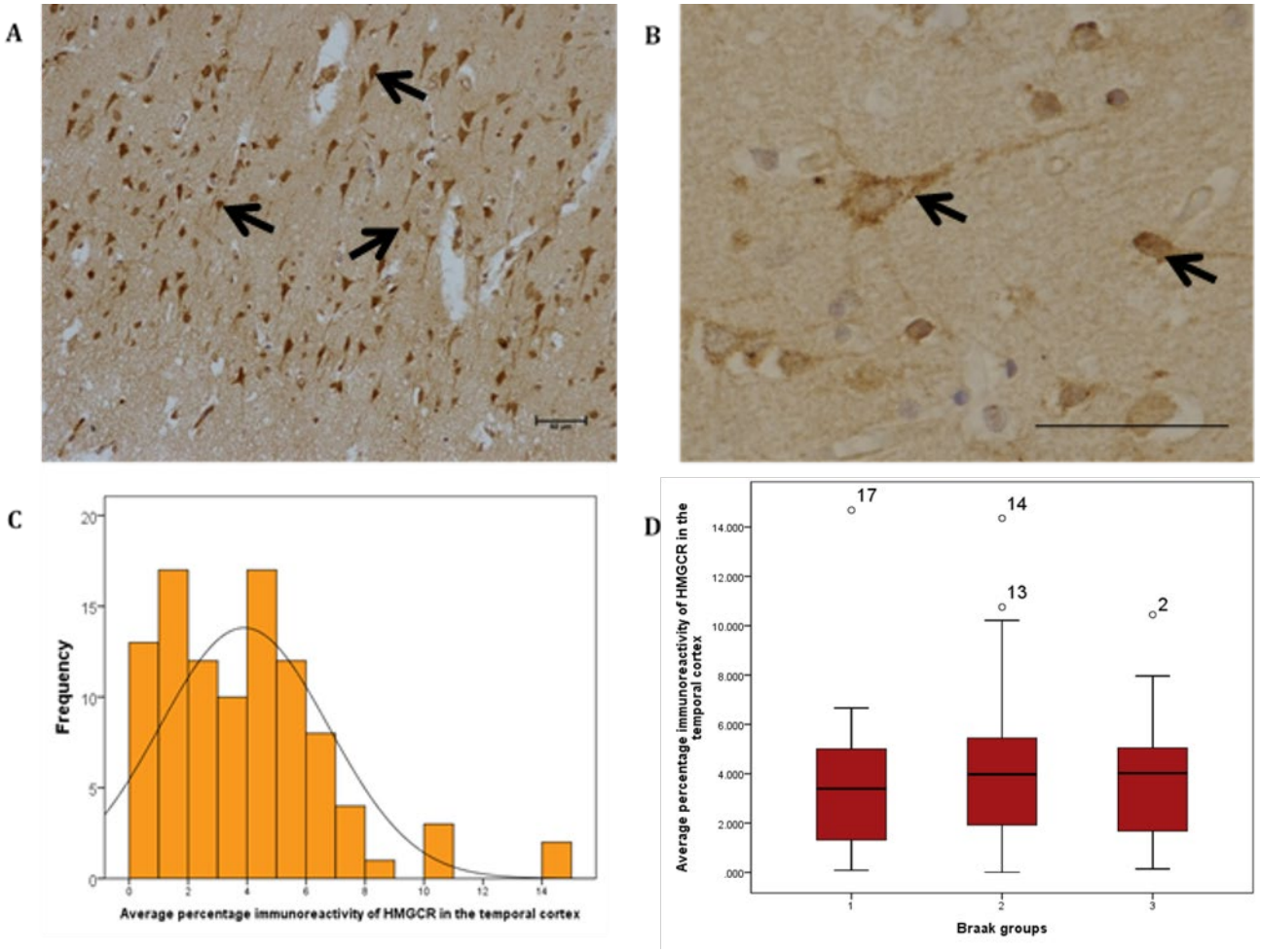

Figure 2.3. HMGCR is expressed in pyramidal neurons in the temporal cortex. Representative images from the cohort show that HMGCR expression was associated with pyramidal neurons throughout all layers of the temporal cortex (A, black arrow). HMGCR immunoreactivity was predominantly detected in the cytoplasm of neuronal cell bodies and proximal processes (B, black arrows). Histogram of the average immunoreactivity of HMGCR shows that the distribution of HMGCR expression does not follow a normal distribution throughout the cohort (C). Boxplot of the percentage area of immunoreactivity indicated that expression of HMGCR does not show an association with Alzheimer-type neuropathology in the ageing brain (D). Scale bar represents 50μm.

2.4.2 Validating HMGCR expression

Positive immunolabelling for HMGCR was found in pyramidal neurons. The expression was punctate and localised to the cytoplasm of neuronal cell bodies and proximal processes The literature suggests that astrocytes are responsible for cholesterol biosynthesis within the brain thus expression would be preferentially expected in astrocytes (Pfrieger, 2003; Maria Giudetti *et al.*, 2015). Hence, to validate this novel finding and confirm HMGCR expression observed in the CFAS tissue, the optimised HMGCR staining protocol was repeated in frozen tissue sections to confirm that the fixation process of the tissue did not affect the binding of the HMGCR antibody. Frozen temporal cortex sections from the Cambridge CFAS cohort were used and the HMGCR antibody was incubated overnight at 4°C. This also demonstrated HMGCR immunopositive pyramidal neurons in the temporal cortex, with immunoreactivity localised to the cytoplasm of neuronal cell bodies and proximal processes, an identical pattern to that observed in the FFPE tissue (Figure 2.4 A). Further validation was carried out by repeating the optimised IHC protocol on FFPE tissue from the CFAS cohort, using an alternative anti-HMGCR monoclonal antibody purchased from another company (Atlas Antibodies). This antibody targeted an epitope from 484-497 amino acids compared to the Abcam antibody, which targeted an epitope from 400-500 amino acids. IHC staining using this antibody confirmed the punctate immunolabelling pattern localised to the cytoplasm and proximal processes of pyramidal neurons (Figure 2.4 B).

To further confirm the Abcam antibody specificity a western blot was carried out (Figure 2.4 C). Cell lysates from Hela cells, cultured neurons (LUHMES) and astrocytes (primary human foetal astrocytes) and human post-mortem temporal cortex protein extract (TCx) were used. Neuronal and astrocytic cell lines were used to confirm neuronal and astrocytic HMGCR expression *in vitro* and validate staining pattern observed in temporal cortex tissue. Temporal cortex protein extract was used to confirm antibody specificity and expression of HMGCR in temporal cortex and validates that the immunoreactivity observed in temporal cortex sections. HeLa cell lysates were used as a positive control. A band was present around 97kDa for all samples, at the expected size for HMGCR, confirming the specificity of the HMGCR antibody. α-tubulin was used as a loading control.

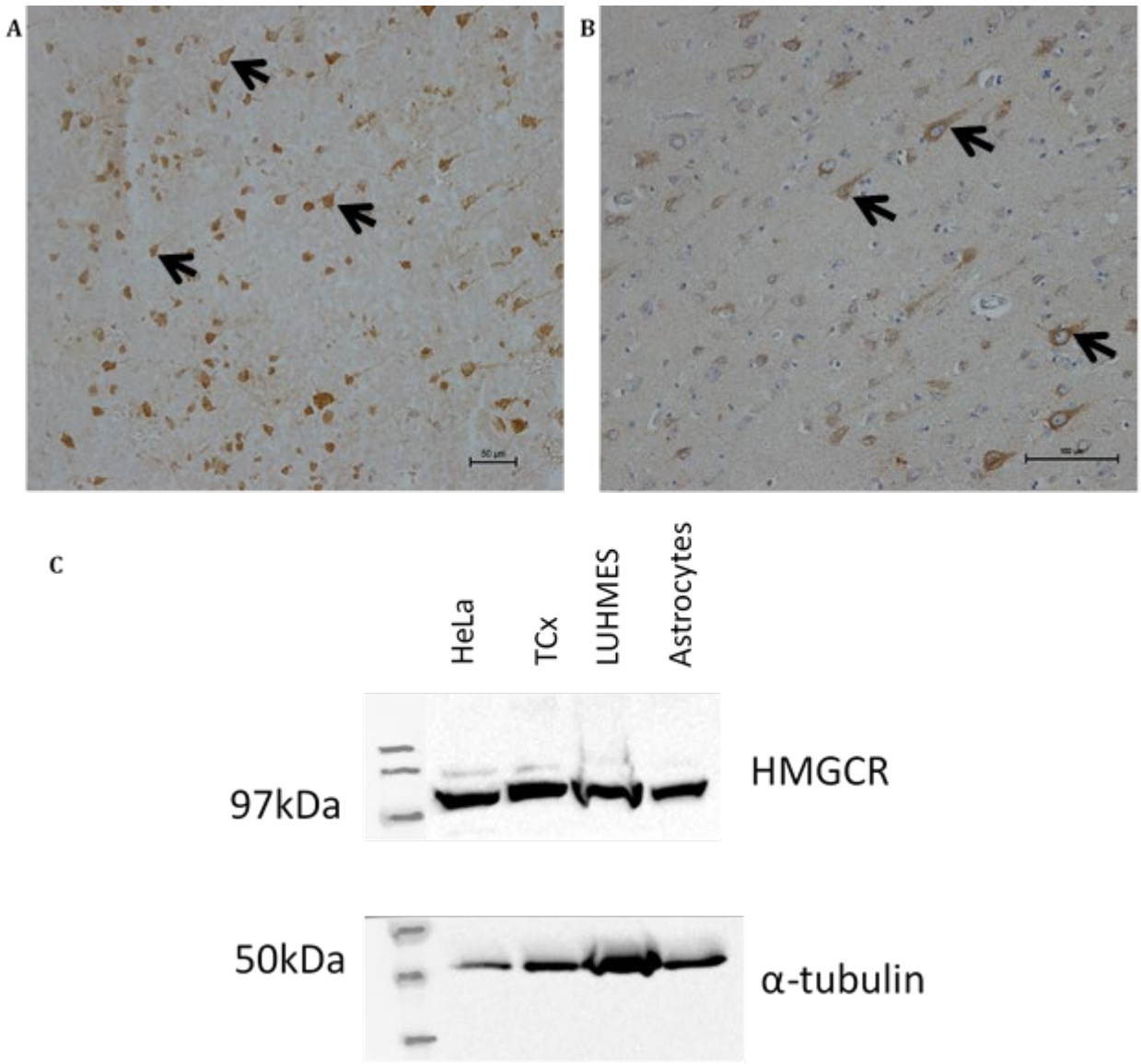

Figure 2.4. Validation of HMGCR expression. HMGCR expression was validated by carrying out the optimised staining protocol in frozen tissue (A) and using another antibody that had been purchased from another company (Atlas Antibodies) (B). In both images, HMGCR expression was associated with pyramidal neurons of the temporal cortex in frozen tissue sections (black arrows). HMGCR immunoreactivity was punctate and found within the cytoplasm of the cell soma and proximal processes (black arrows) HMGCR immunoreactivity was detected in the cytoplasm of the neuronal cell bodies and proximal processes. (C) Shows a western blot for the HMGCR antibody (Abcam, UK) for HeLa cells, post-mortem human temporal cortex protein extract, LUHMES astrocyte lysates. (A) Scale bar represents 50μm. (B) Scale bar represents 100μm.

2.4.3 Glial expression of HMGCR

The pattern of HMGCR immunoreactivity within the temporal cortex of the Cambridge cohort varied between cases. Within the cortex and white matter border regions of some cases, HMGCR expression was associated with cells morphologically resembling glial cells (Figure 2.5 A). In approximately 35% of the cohort, positive glial expression was observed in what appeared morphologically to be astrocytes and oligodendrocytes within the white matter regions of the temporal cortex sections. To confirm that these positive cells were glial, double–staining IHC was carried out for HMGCR and GFAP (astrocytic marker). HMGCR did not co-localise with GFAP expressing astrocytes in the temporal cortex and white matter regions (Figure 2.5 B and C).

2.4.4 HMGCR expression does not vary with ageing

To investigate if pyramidal neuronal HMGCR declines with ageing, which may imply a decline in cholesterol biosynthesis, further IHC was carried out on young, middle aged and old subjects. Formalin fixed prefrontal association cortex (Brodmann area 8/9) tissue samples from the Edinburgh medical Research Council Sudden Death Brain Bank were used. The optimised HMGCR staining protocol was performed on each case (n=16). The cases showed positive immunolabelling in pyramidal neurons of the prefrontal association cortex, with immunoreactivity localised to the cytoplasm of neuronal cell bodies and proximal processes (Figure 2.6 A). Quantification was carried out as previously described in 2.3.4. HMGCR neuronal expression did not vary significantly between age groups (KW p=0.206), and there was no trend to increased or decreased expression with increasing age (JT p=0.641). To ensure that the immunostaining was not an artefact of brain donation, correlations between brain pH (r=-0.031, p=0.210) and post-mortem delay (r=-0.243, p=0.364) were determined.

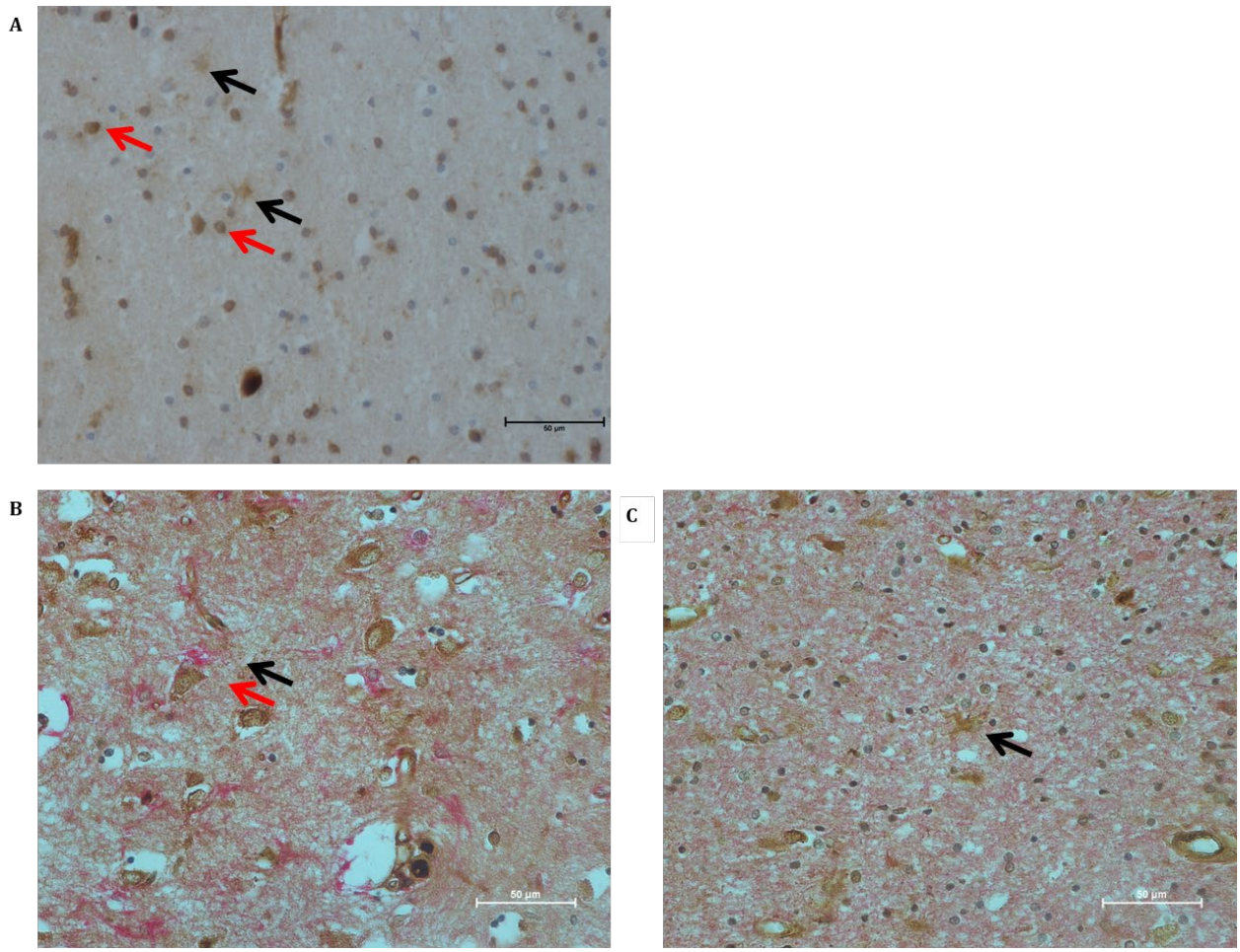

Figure 2.5. HMGCR does not correlate with GFAP expressing astrocytes: Immunopositive glial cells in the cortex were detected in approximately 35% of the cohort and was associated with cells morphologically resembling astrocytes (A, black arrows) and glia (A, red arrows).Using dual labelling, HMGCR immunoreactivity (B, red arrow) does not co-localise with GFAP positive astrocytes in temporal cortex (A, black arrow). In white matter regions of temporal cortex, GFAP positive astrocytes did not co-localise with HMGCR, however astrocyte like morphology was observed in HMGCR positive cells (B, black arrow). Scale bar represents 50µm.

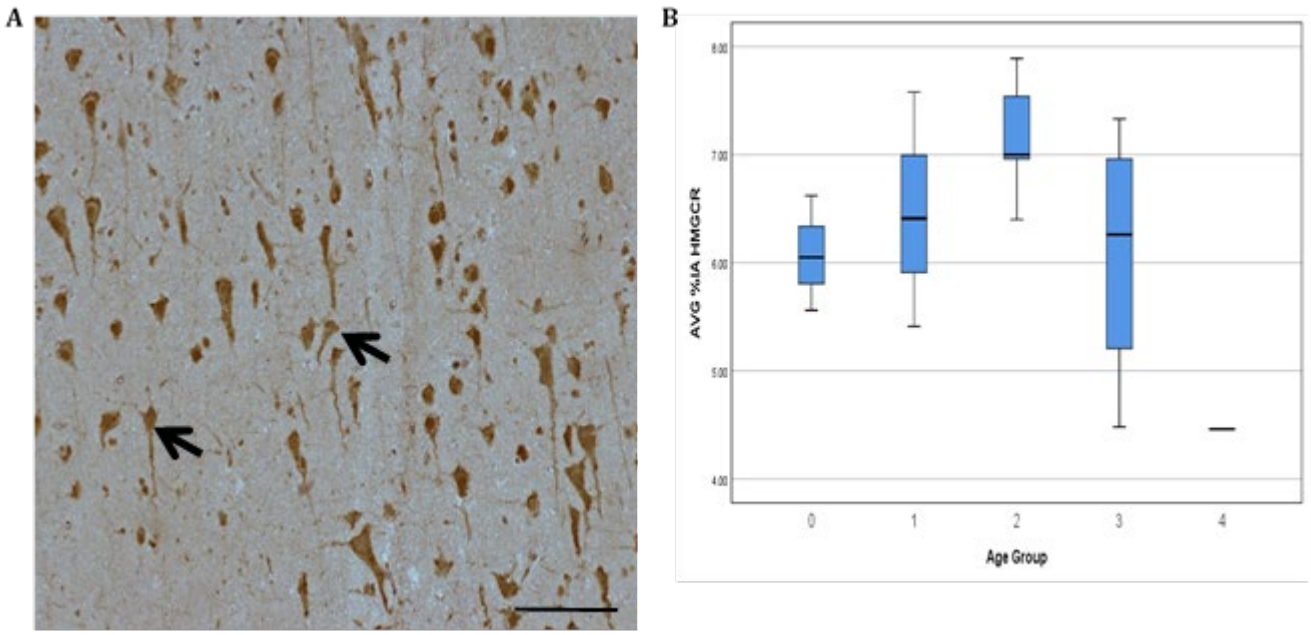

Figure 2.6. HMGCR expression does not change with age: HMGCR immunoreactivity is associated with pyramidal neurons in the prefrontal cortex (Brodmann area 8/9) (A). HMGCR immunoreactivity was predominantly detected in the cytoplasm of neuronal cell bodies and proximal processes. Scale bar represents 100 µm. HMGCR expression is not associated with ageing (n=16) (B). Ages were grouped accordingly 0= 16-30yrs (n=3), 1= 31-45 yrs (n=3), 2= 46-60 yrs (n=5), 3= 61-75 yrs (n=4) and 4= 75+ yrs (n=1).

2.4.5 HMGCR immunoreactivity does not change with dementia status

To determine if the variation in neuronal expression of HMGCR was associated with dementia status a Mann-Whitney U test was carried out. From the cohort 58 cases had a dementia diagnosis before death (median=3.70, IQR= 1.69-4.96) and 38 cases had no dementia (median=3.70, IQR= 1.64-6.10) (Figure 2.7 A). There was no significant difference between HMGCR immunoreactivity between demented and non-demented individuals (MW, p=0.59). The distribution of HMGCR immunoreactivity by dementia status across specific Braak and Braak stages and Thal phases was determined (Figure 2.9 B and C). A pairwise comparison of means using Tukey's adjustment found no significant difference between HMGCR immunoreactivity and dementia status at specific Braak and Braak stages and Thal phases. The effect of HMGCR immunoreactivity on risk of dementia was analysed using logistic regression (Figure 2.7 D). A univariate model adjusted for only age at death and sex as covariates, as well as a multivariate model adjusted for Braak and Braak, Thal and CAA pathology was produced. HMGCR immunoreactivity was analysed as continuous scales and categorically divided into tertiles. None of HMGCR models showed any effect on risk of dementia. Statistical analysis in relation to dementia status was carried out by Connor Richardson, University of Newcastle.

2.4.6 SREBP2 is expressed in both astrocytes and neurons

SREBP2 immunoreactivity was present in both neurons and astrocytes. SREBP2 immunoreactivity within the temporal cortex was associated with neurons and localised to the cytoplasm and proximal process within cortical regions (Figure 2.8 A). At the cortical and white matter border SREBP2 immunoreactivity was associated with astrocytes and localised to the cytoplasm and astrocytic processes (Figure 2.8 B). As no significant correlations between HMGCR and AD and other pathologies were observed, the sole aim of this study was to confirm expression and localisation of the key regulator within the brain, hence quantification of SREBP2 immunoreactivity was not carried out.

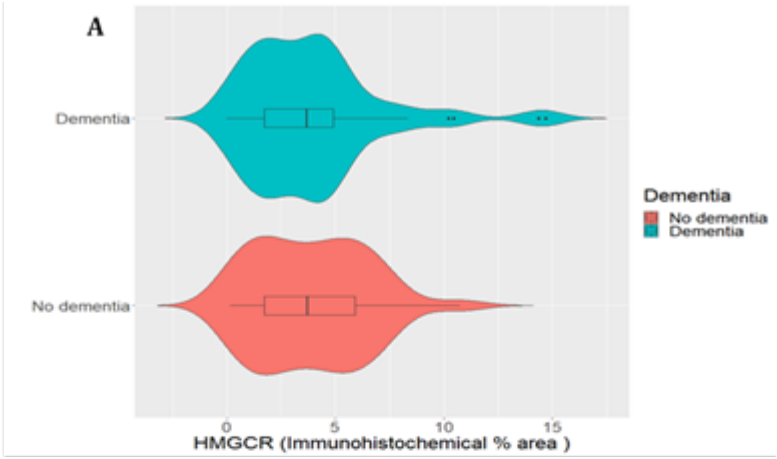

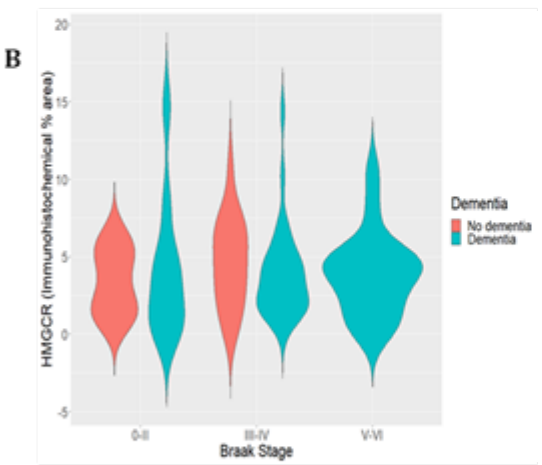

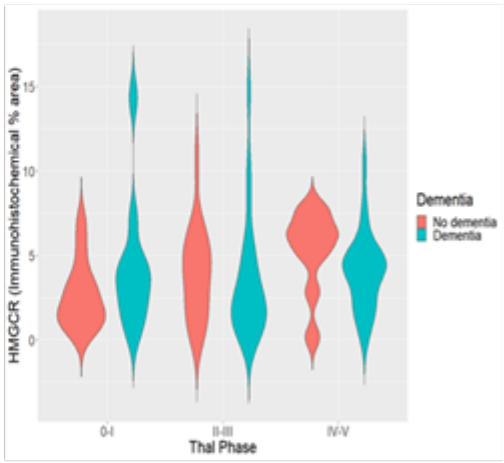

D

	Unadjusted (univariate)			Adjusted (multivariate)		
	OR	95% CI	p=	OR	95% CI	p=
HMGCR	0.96	0.82-1.12	0.58	0.96	0.82-1.13	0.94
Tertiles						
Moderate	0.81	0.26-2.53	0.72	0.69	0.2-2.47	0.72
High	0.47	0.15-1.4	0.18	0.4	0.11-1.42	0.18

Figure 2.7. HMGCR expression does not change with dementia status: HMGCR percentage immunoreactivity was compared to dementia status. Box and violin plots displaying the distribution and probability density of HMGCR immunoreactivity by dementia status (A). Box plots show median, IQR and range, area around the box displays the probability density. Wider sections of the violin plots represent a higher probability that members of the population will take on the given value; narrower sections represent a lower probability. Violin plots showing the distribution of HMGCR immunoreactivity by dementia status at specific Braak and Braak stage (C) and Thal phase (D). No significant difference between HMGCR immunoreactivity and dementia status was found. Table D shows the output from logistic regression modelling (D). A univariate model adjusted for age at death and sex, multivariate models adjusted for Braak and Braak, Thal and CAA pathology. HMGCR immunoreactivity was modeled on a continuous scale and categorically by tertiles. Results are presented as odd ratios (OR) with 95% confidence intervals (CI) and p values. Statistical analysis and violin plots courtesy of Connor Richardson, University

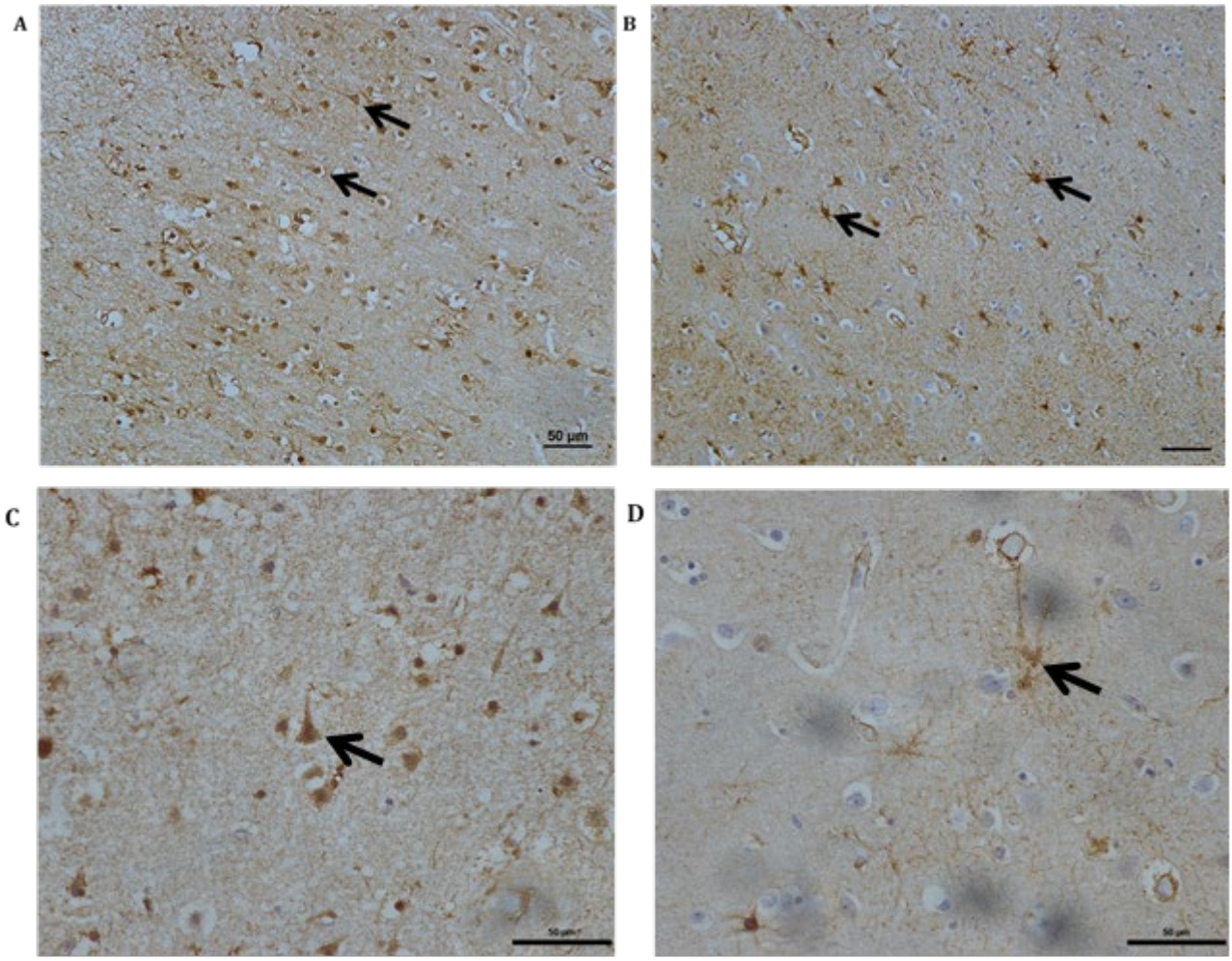

Figure 2.8. SREBP2 is expressed in both neurons and astrocytes: SREBP2 immunoreactivity was associated with pyramidal neurons within the temporal cortex (A) and (C). SREBP2 immunoreactivity was also present in astrocytes within the white matter and grey matter border regions of the temporal cortex (B) and (D). Scale bar represents 50 µm.

2.5 Discussion

The cholesterol biosynthesis pathway has a vital role in maintaining normal neuronal function. In this chapter the expression of key regulatory proteins in cholesterol biosynthesis were characterised using IHC. HMGCR was localised to pyramidal neurons in both temporal and prefrontal association cortex. SREBP2 was localised to both astrocytes and neurons in the temporal cortex. This study found that the variation in the expression of HMGCR, determined by IHC, did not alter with dementia status, increasing AD neuropathology, neuronal DNA damage, neuroinflammation or ageing.

2.5.1 Neuronal expression of HMGCR in the temporal cortex

Immunohistochemical characterisation of HMGCR in human post-mortem temporal cortex tissue showed positive immunolabelling in pyramidal neurons in all cases and positive immunoreactivity in oligodendrocytes and astrocytes was observed in approximately 35% of the cohort. The presence of this key rate-limiting enzyme and its regulator SREBP2 suggests that the pyramidal neurons of the temporal cortex may synthesise cholesterol. This is a significant finding as many studies have shown glial cells to undertake the bulk of the cholesterol production within the brain (Pfrieger, 2003; Nieweg, Schaller and Pfrieger, 2009; Pfrieger and Ungerer, 2011; Zhang and Liu, 2015). There is experimental data to suggest that neurons can synthesis cholesterol as well as glial cells. In murine hippocampal cells, resistant to oxidative stress from H_2O_2, a decrease in the mRNA levels of HMGCR was observed however, these cells also showed an increase in total cholesterol levels. This shows that neurons express HMGCR and are able to synthesise cholesterol (Clement *et al.*, 2009). Rat pyramidal neurons have also been shown to express enzymes involved in neurosteroidogenesis, which suggests that neurons synthesise cholesterol as a precursor molecule for other steroid hormones (Tsutsui *et al.*, 2000). Further studies using primary rat neurons have shown that neurons are able to uptake radioactively labelled acetate (a precursor molecule for cholesterol synthesis) and synthesise cholesterol. However, the efficiency of cholesterol synthesis is lower in neurons compared to glial cells (Nieweg, Schaller and Pfrieger, 2009)

The cholesterol biosynthesis pathway comprises of the mevalonate, Bloch and Kandutsch-Russell pathway. In neurons a hybrid between the Bloch and Kandutsch-

Russell pathways have been shown to be involved in cholesterol production (Mitsche *et al.*, 2015). New evidence suggests that murine cortical neurons retain an active mevalonate pathway and redirect its resources to maintaining activity within this pathway rather than producing cholesterol (Moutinho, Nunes and Rodrigues, 2017). By studying the RNA-Seq transcriptome in murine cortical neurons, the expression of genes involved in both pre and post squalene pathways were down regulated in comparison to astrocytes. However, genes involved in the non-sterol pathway were upregulated. This suggests that within murine cortical neurons, the mevalonate pathway is maintained and used in the production of isoprenoids rather than cholesterol (Cahoy *et al.*, 2008b; Zhang *et al.*, 2014; Moutinho, Nunes and Rodrigues, 2017). This data would suggest that one possible reason for HMGCR expression within neurons is to allow the production isoprenoids such as farnesyl pyrophosphate (FPP) and geranylgeranyl pyrophosphate (GGPP) rather than cholesterol (Eckert *et al.*, 2009).

FPP and GGPP are isoprenoids which are involved in the prenylation of proteins, a post-translational modification, allowing insertion into membranes and determining their function and localisation. FPP is formed from the mevalonate arm of the cholesterol biosynthesis pathway and is a precursor for both cholesterol and GGPP (Eckert *et al.*, 2009). The literature suggests that prenylated proteins such as FPP and GGPP may have a role in AD pathogenesis. One study reported the involvement of GGPP in γ-secretase activity in SH-SY5Y neuroblastoma cells; and FPP and GGPP increase the Aβ levels in H4 neuroglioma cells by increasing γ-secretase activity (Kukar *et al.*, 2005; Urano *et al.*, 2005).

Further studies have shown that levels of FPP and GGPP are altered in AD. Using post-mortem human frontal cortex tissue, Eckert *et al* (2009), found that FPP and GGPP levels were increased in male AD patients compared to controls, whereas cholesterol levels and HMGCR gene expression did not differ between the two groups (Eckert *et al.*, 2009). Inhibition of HMGCR, using statins, in mice showed a reduction in FPP, GGPP and cholesterol levels (Eckert *et al.*, 2009). This suggests that within neurons the mevalonate arm of the cholesterol biosynthesis pathway is diverted to isoprenoid synthesis rather than cholesterol, providing a possible explanation as to why HMGCR expression is observed in pyramidal neurons.

2.5.2.1 HMGCR expression in relation to AD pathologies

The neuronal expression of HMGCR did not correlate with Braak and Braak stages or Thal phase in this study. Furthermore, the expression of HMGCR did not correlate with markers of DNA damage or neuroinflammation. A study found that both APP and β-amyloid interact with cholesterol and catalyse the metabolism of it into 7β-hydroxycholesterol, which is neurotoxic (Nelson and Alkon, 2005). However, our data suggests that there is no correlation between HMGCR expression and amyloid plaque expression. Aβ can exist in multiple forms: monomeric, oligomeric, fibrils and aggregates, hence it's crucial that when measuring Aβ it's important that the relevant form is investigated (Ladanza et al., 2018). In the study by Simpson *et al* (2010) from which the β-amyloid immunoreactivity data was obtained, an antibody which labelled residues 8-17 of the N-terminal of the Aβ peptide was used and this labelled β-amyloid plaques (J. E. Simpson *et al.*, 2010). This antibody labels both diffuse and compact forms of tissue deposits but does not provide a measure of oligomeric Aβ.

Oxidative stress is a feature of brain ageing and may contribute to the pathogenesis of AD. It is defined as the imbalance between biochemical processes leading to ROS being produced and those processes responsible for the removal of ROS (Harman, 1981; Recuero *et al.*, 2009). Accumulation of ROS within neurons causes DNA damage and induces a DNA damage response which leads to cellular senescence and may contribute to neuronal dysfunction (Simpson *et al.*, 2015). Neuroinflammation is the activation of microglia as a response to brain injury, pathogens, neurotoxins and abnormal stimulation within the CNS (Bradl and Hohlfeld, 2003; Carson *et al.*, 2006; Park *et al.*, 2011). Prolonged activation of microglia leads to secretion of cytokines and neurotoxins leading to chronic neuroinflammation and contributing to neurodegeneration (Lyman *et al.*, 2014). Neuroinflammation has been shown to be involved in the pathogenesis of AD (Shabab *et al.*, 2017). Studies suggest that mitochondrial dysfunction in microglia results in excess ROS production and stimulates pro-inflammatory cytokine release, which induces neuroinflammation and promotes neuronal damage (Vyas *et al.*, 2016; Wu *et al.*, 2016).

To assess variation with DNA damage, HMGCR immunoreactivity was compared to γH2AX immunoreactivity in the temporal cortex (J. E. Simpson *et al.*, 2010). H2AX is a core histone molecule, which forms part of the nucleosome complex, and is

recruited at sites of double stranded breaks (DSBs) where it is phosphorylated on the 139th serine residue to form γH2AX foci. The presence of foci aids in the recruitment of DNA repair machinery and acts as an indicator of DSBs in a 1:1 manner allowing assessment of DNA damage (Kuo and Yang, 2008). Our data suggests that there is no correlation between HMGCR expression and neuronal γH2AX expression suggesting that the variation in expression in HMGCR does not correlate to DNA damage.

Previous studies from our lab have shown that at low Braak and Braak stages there is an increase in oxidative stress markers compared to high Braak and Braak stages. Furthermore, high levels of oxidative stress was associated with a DNA damage response (DDR) (J. E. Simpson *et al.*, 2010). Further work based on gene expression showed that there was an overexpression of HMGCR in cases with high neuronal DDR suggesting that there is a link with oxidative DNA damage (Simpson *et al.*, 2016). The results from the study by Simpson *et al* (2016) do not contradict the findings from this current study however; there are differences between the two studies, which could account for the differing results. The work carried out in this study was on temporal cortex regions of brain compared to the frontal cortex tissue that was used for the study by Simpson *et al,* (2016). Another key difference is that in the study by Simpson *et al,* (2016) measured RNA quantitatively whereas in *this current study* HMGCR was measured using immunohistochemistry. Quantifying using immunohistochemistry has limitations as this method only takes into account the number of pixels that contain the chromogen and not the density of chromogen present, it is difficult to quantify the protein amount, as the number of pixels is not directly proportional to the amount of antigen (Matkowskyj *et al.*, 2003).

The deposition of Aβ plaques is a source of oxidative stress leading to DNA damage within neurons. The base excision repair (BER) system is a mechanism responsible for repairing DNA damage caused by oxidative stress (Kwiatkowski *et al.*, 2016). One study found that patients with AD showed an increase in the level of DNA damage compared to control patients. They also observed polymorphisms in genes involved in the BER response which may contribute to the increase in DNA damage (Kwiatkowski *et al.*, 2016).

HMGCR immunoreactivity was compared to CD68 immunoreactivity in the temporal cortex to assess whether it was affected by neuroinflammation. CD68 is a glycosylated type 1 transmembrane glycoprotein localised to endosomal/lysosomal compartments and is expressed on the surface of macrophages (Chistiakov *et al.*, 2017). Within the brain, the microglia play the role of macrophages and act as a first line of defence against pathogens and changes to homeostasis (Hendrickx *et al.*, 2017). CD68 is located in the lysosmal compartments near the nucleus in ramified and amoeboid microglia and its expression increases during phagocytosis, suggesting that it is a marker of microglial activation, and for neuroinflammation (Hendrickx *et al.*, 2017). Our study found that the immunoreactivity of HMGCR did not correlate with immunoreactivity of CD68. One study looked at the effect of a high cholesterol diet in young and old mice and found that in aged mice on a normal diet microglial activation was observed and in mice fed with a high cholesterol diet showed a further increase in microglial activation and secretion of inflammatory cytokines such a IL-1β, IL-6 and TNF-α (Chen *et al.*, 2018). This suggests that a high cholesterol diet could cause neuroinflammation via microglial activation, however the data from this study does not demonstrate this relationship.

2.5.2.2 HMGCR as a potential therapeutic target for AD

Statins are a class of drugs that inhibit the action of HMGCR and are prescribed to patients with hypercholesterolemia. Considering the fact that the prescription of statins is increasing, especially amongst the ageing population, it is important to assess the effect they have on AD progression (Trusler, 2011). Statins are competitive inhibitors which target the active site of the HMGCR enzyme. When bound, statins result in a conformational change of the active site preventing the binding of its endogenous substrate and disabling functional structure (Stancu and Sima, 2001). Studies have shown that cholesterol-lowering drugs reduce the levels of Aβ. However, the use of statins as a therapy for AD needs further research (Refolo *et al.*, 2001; McGuinness *et al.*, 2014). BBB permeability of statins depends on the type of statin, lipophilic statins can easily cross the BBB compared to hydrophilic statins (Daneschvar, Aronson and Smetana, 2015). A trial showed that atorvastatin had a positive effect on cognition in patients with mild-to-moderate AD compared to a placebo (Sparks *et al.*, 2006). After 6 months there was an improvement in the Alzheimer Disease Assessment Scale-Cognitive (ADAS-cog)

score and this therapy was more effective in patients that carried the apoE ε4 allele. However, this study only had 63 participants all of which had been diagnosed with AD (Sparks *et al.*, 2006). Another trial found that simvastatin did not have an effect on ADAS-cog and had no effect on the progression of AD symptoms (Sano *et al.*, 2011). Within the CFAS cohort a few cases had been recorded to take stains, however due to the lack of data and few n numbers any relationships between HMGCR immunoreactivity and statin use was not assessed.

One study using a transgenic mouse model has shown that cholesterol lowering drugs can reduce the levels of β-amyloid (Refolo *et al.*, 2001). This study used a compound called BM15.766 which inhibits the activity of 7-dehydrocholesterol-Δ7-reductase which is involved in the conversion of 7-dehyrocholesterol to cholesterol (Mazein *et al.*, 2013). They found that treatment with this drug reduced the levels of Aβ42 and Aβ40 as well as a reduction is plasma cholesterol levels and induced hypocholesterolaemia. Unfortunately the drug compound used caused a toxic build-up of sterols making it an unviable option for human clinical trials however, it is a good proof of principle that by using pharmacological intervention to lower cholesterol levels can cause a reduction in Aβ levels (Refolo *et al.*, 2001). Currently there is no convincing evidence that statins provide an effective treatment for AD and so further research into this avenue needs to be carried out.

2.5.3 Glial expression of HMGCR in the temporal cortex

In cortical and white matter boundary areas, positive immunolabelling for HMGCR was found in glial cells such as astrocytes and oligodendrocytes in approximately 35% of the cohort. One study showed that both rat retinal ganglion cells and rat astrocytes cells synthesise cholesterol. However, cholesterol synthesis in neurons was inefficient compared to cholesterol synthesis within glial cells, possibly due to the lack of enzymes involved further downstream (Nieweg, Schaller and Pfrieger, 2009; Moutinho, Nunes and Rodrigues, 2017). Astrocytes use the Bloch pathway to carry out cholesterol synthesis following the synthesis of Lansosterol via the mevalonate pathway; and the synthesised cholesterol is transported to neurons using apolipoproteins (Nieweg, Schaller and Pfrieger, 2009; Pfrieger and Ungerer, 2011). As a result, expression of HMGCR in glial cells within the cortex might be expected but this was not demonstrated in our study.

Approximately 80% of total brain cholesterol is incorporated into myelin membranes. Myelin is an extension of the oligodendrocyte plasma membrane which encompasses axons allowing fast transduction of neuronal signals across a large distance, critical for essential brain functions (Saher and Stumpf, 2015). Cholesterol which contributes to the formation of myelin is synthesised by oligodendrocytes, in a study which conditionally knocked out *fdft1,* a gene involved in the condensation of squalene synthase (part of the mevalonate arm of the cholesterol biosynthesis pathway), in mice oligodendrocytes. They found that in the conditional knockout, the mice exhibited motor deficits such as ataxia and impaired control of hind limbs (Saher *et al.*, 2005). Histological characterisation showed severe demyelination in white matter tracts in brain and spinal cord, providing evidence of the importance of cholesterol synthesis in oligodendrocytes for myelin synthesis (Saher *et al.*, 2005). This suggests that HMGCR is expressed in oligodendrocytes and could be responsible for the positive immunoreactivity observed in our study.

Our study found that HMGCR did not co-localise with GFAP expression in the temporal cortex. GFAP is a protein, which makes up the intermediate filaments of the astrocytic cytoskeletal, in reactive astrocytes this protein is overexpressed (Carter *et al.*, 2019). However, studies have found that GFAP only accounts for 15% of the astrocyte volume and 40% of astrocytes within the adult rat hippocampus do not express GFAP (Walz and Lang, 1998; Bushong *et al.*, 2002). This suggests that carrying out staining with a different marker may be more appropriate, such as NDRG2 or ALDH1L1. Aldehyde dehydrogenase L 1 (ALDH1L1) is an astrocytic marker which is present in astrocytic cell bodies and extensive processes, immunohistochemical staining in rat tissue has shown an increased number of ALDH1L1 positive astrocytes compared to GFAP positive astrocytes (Neymeyer, Tephly and Miller, 1997; Cahoy *et al.*, 2008a). NDGR2 is a gene associated with cell differentiation and proliferation, which is specifically expressed in mature, nonreactive and non-proliferating astrocytes (Shen *et al.*, 2008; Flügge *et al.*, 2014). One study found that NDRG2 is a more appropriate marker for cortical astrocytes in mouse cerebral regions compared to GFAP however, GFAP is better at labelling astrocytic processes and branches in the white matter regions such as the corpus callosum and cerebral peduncles (Z. Zhang *et al.*, 2019). Recent work carried out in our lab has also demonstrated that NDGR2 positively correlates with tau pathology

within the aging brain (Fadul *et al.*, 2020). This study shows that not all astrocytes are NDGR2 positive, so no matter which markers are selected, not all astrocytes will be labelled. Use of multiple astrocytic markers would allow more astrocytes to be labelled and further determine co-localisation with HMGCR.

2.5.4 HMGCR expression during ageing

Since cholesterol plays such a vital role in maintaining neuronal function, therefore cholesterol synthesis becomes crucial during development. A study in mice demonstrated that during the first three weeks of life the rate of cholesterol synthesis is 250 µg/day, however after three weeks, the rate drops to 25-35 µg/day (Quan *et al.*, 2003). Conversely, most of the cholesterol produced during development, contributed to myelin formation and therefore, the cholesterol is synthesised by oligodendrocytes (Dietschy, 2009).

Neurons are capable of synthesising cholesterol during development. A study in mice where cholesterol biosynthesis in forebrain projection neurons was ablated showed that cholesterol demand is maintained by microglial cholesterol production and delivery, however they found that after birth neuronal degeneration occurred (Fünfschilling *et al.*, 2012). *In vitro* studies showed that the ablation of cholesterol synthesis in forebrain projection neurons lead to neuronal death in 2-4 days *in vitro* (Fünfschilling *et al.*, 2012). Further evidence demonstrating neuronal *de novo* cholesterol synthesis *in vitro* where primary murine cortical neurons were cultured in cholesterol free medium, cholesterol accumulation within the neurons was observed (Genaro-Mattos *et al.*, 2019a).

During ageing, there is an overall decrease in cholesterol levels however; the degree of change depends on the specific region. In a study that looked at human post-mortem brains they found that in grey and white matter regions there was a significant decreases in cholesterol content compared to younger brains whereas, in the pons there was very little change in cholesterol content over ageing (Söderberg *et al.*, 1990). These changes in cholesterol have been suggested to be caused by synapse loss and a reduction in neuron size (de Chaves and Narayanaswami, 2008).

Over the course of life cholesterol synthesis within the brain decreases. One study examined the concentrations of various intermediate sterols from the cholesterol biosynthesis pathway in the hippocampus from post-mortem human tissue. In both

young and elderly group, the cholesterol concentrations remained constant. However, the concentration of lathosterol and lanosterol (cholesterol precursors) was significantly higher in the younger group compared to the elderly group (Thelen *et al.*, 2006). This suggests that cholesterol synthesis is reduced during ageing. Further evidence supporting this was found by Raihan *et al.,* where microRNA miR-335-3p was elevated in murine hippocampal brain as well as aged murine primary astrocytes. MiR-335-3p was found to supress the action of HMGCS1 and HMGCR by binding to the 3' untranslated region (3'UTR) of mRNA preventing protein synthesis in astrocytes, thus reducing cholesterol production (Raihan *et al.*, 2018).

In our study, we found that HMGCR was expressed in the pyramidal neurons in prefrontal association cortex (Brodmann area 8/9). This suggests that the expression of HMGCR is uniform within the cerebral cortices as identical punctate staining within the cytoplasm and proximal processes in both temporal and prefrontal cortices was observed. The post-mortem tissue was obtained from the Edinburgh Medical Research Council Sudden Death brain bank; the cases that were used had no history of neurological disease and covered a large age range (16-75+ years of age). The expression of HMGCR did not show any correlation to an increase in age. However, this expression could be due to the neurons using the mevalonate arm of the pathway to synthesis isoprenoids. The isoprenoids FPP and GGPP have been shown to be significantly increased in 23-month old mice compared to 3-month-old mice at a protein level however; at gene expression level no difference was observed. Interestingly the levels on *HMGCR* gene expression was increased in older mice however, cholesterol levels remained unaffected (Hooff *et al.*, 2012). This suggests that HMGCR expression is used for isoprenoid production rather than cholesterol synthesis, as murine adult neurons *in vivo* have been shown to survive without endogenous cholesterol synthesis (Fünfschilling *et al.*, 2007).

2.5.5 HMGCR expression and dementia

Data from this current study showed that there was no significant association between HMGCR immunoreactivity within the temporal cortex and dementia status. A population-based prospective study called the Conselice study of brain ageing patients were recruited based on age. Biological and clinical data was collected from the patients over two interviews five years apart. Licastro *et al* (2010) applied a novel data mining process to identify consistent patterns and systematic relationships

between variables using a minimum spanning tree (MST) algorithm to determine any links. This study found that both variants of HMGCR genotype were relevant factors for developing dementia (Licastro *et al.*, 2010). Another epidemiological study found that the splice variant rs3846662 of *HMGCR* was a potent modifier of AD risk (Leduc *et al.*, 2015). *HMGCR* gene has two possible alleles G and A, alternative splicing leads to full length and a variant containing a single nucleotide polymorphism (SNP) at locus rs3846662 which results in alternative splicing of exon 13. The skipping of exon 13 (Δ13) is more common in A allele rather than the G allele. The exact effect of the SNP remains unknown but it is suggested that it may result in a reduced or lack of enzymatic activity (Johnson *et al.*, 2003; Burkhardt *et al.*, 2008; Medina and Krauss, 2009; Yu *et al.*, 2014). In the study by Leduc *et al* (2015) the *HMGCR* splice variant was studied in three case control cohorts and found that the G allele was a protective variant for sporadic AD and delayed the onset of sporadic AD in women (Leduc *et al.*, 2015). These studies suggest a clear link between HMGCR and dementia whereas *this current study* found no significant difference. It is important to note that, the studies by Licastro *et al* (2010) and Leduc *et al* (2015) measure HMGCR at a genetic level in a mixture of blood plasma and brain tissue. Whereas, in *this study* we have measured HMGCR at a protein level in a specific region of the brain this could account for the differences in results between the studies.

2.5.6 SREBP2 expression

In our study, we found SREBP2 to be localised in both astrocytes and neurons within the temporal cortex. SREBP2 is a membrane bound transcription factor, which is involved in the regulation of transcription of genes involved in cholesterol biosynthesis (Zhang and Liu, 2015). Within neurons, SREBP2 was localised to the cytoplasm and the proximal processes, within astrocytes positive immunolabelling was found in the cytoplasm and astrocytic processes. Astrocytic immunoreactivity was absent within the cortical layers however, it was present within the cortical and white matter boundary. The presence of SREBP2 suggests that cholesterol levels have depleted within the cells and cholesterol biosynthesis is trying to be upregulated (Horton *et al.*, 2003).

When the level of cellular cholesterol is low, SREBP2 forms a complex with SCAP (SREBP cleaving-activating protein) and is translocated from the endoplasmic reticulum (ER) membrane to the Golgi apparatus membrane, where it undergoes

proteolytic cleavage by proteases. This cleavage produces two fragments, one of which can translocate to the nucleus and switches on genes for cholesterol biosynthesis (HMGCR) and cholesterol uptake through low-density lipoprotein (LDL) receptors (Goldstein, DeBose-Boyd and Brown, 2006).

When an increase in sterols is detected within the ER, cholesterol binds to SCAP, which leads to a conformational change and causing it to bind with INSIG. INSIG is an ER protein which binds to the SCAP/SREBP2 complex preventing translocation from the ER to the Golgi (Yang *et al.*, 2002). This prevents the proteolytic processing and cholesterol biosynthetic gene expression decreases (Goldstein, Rawson and Brown, 2002). Furthermore, during high cholesterol levels, HMGCR is degraded as a result of INSIG-1 binding to the sterol sensing domain of HMGCR, leading to accelerated ubiquitination (Sever *et al.*, 2003).

The data sheet provided by the antibody supplier (Abcam, UK) states that the antibody is specific to amino acids 876-890 of SREBP2 peptide. This falls within the COOH-terminal of the protein forming part of the regulatory domain within the cytosolic portion of the protein (Horton, Goldstein and Brown, 2002). When cholesterol levels are normal SCAP binds to the COOH-terminal keeping it within the ER (Sakai *et al.*, 1997). This suggests that the cytosolic expression of SREBP2 in both astrocytes and neurons suggest that there are no changes in cellular cholesterol, as expression is not localised to Golgi body or nucleus.

The expression of SREBP2 has been demonstrated in neurons and astrocytes in previous studies. One study found that insulin activates the cholesterol biosynthesis pathway in mouse primary cortical neurons, where a significant increase in SREBP2 gene expression was observed at 100 nM of insulin. In type-1 insulin deficient mice a decrease in SREBP2 expression was observed at both protein and mRNA levels suggesting that the absence of insulin was down regulating cholesterol biosynthesis (Suzuki *et al.*, 2010). Knockdown of SREBP2 in mouse hypothalamic cultured neurons showed a decrease in synaptic markers *in vivo* this hypothalamic knockdown translated to an increase in nocturnal food intake and affects the circulation of norepinephrine and glucagon (Suzuki *et al.*, 2010). Additionally, SREBP2 knockdown in cultured murine astrocytes shows a reduction in neurite outgrowth in co-culture, *in vivo* astrocytic knockdown leads to impaired brain

development and motor and behavioural defects (Ferris *et al.*, 2017). This demonstrates the crucial role SREBP2 plays in maintaining overall brain function and specifically maintaining normal neuronal function.

Studies have demonstrated that Aβ may have a role to play in cholesterol biosynthesis. One study found that oligomeric Aβ inhibited SREBP2 maturation in neurons *in vitro* (Mohamed *et al.*, 2018a). Incubating rat sympathetic, rat striatal (St14A) and cortical neurons with 20 μM of oligomeric Aβ a significant reduction in protein expression was observed in all cell types. Furthermore, in TgCRND8 mice (mouse model for AD) lower levels of SREBP2 were observed in frontal cortices, suggesting that Aβ may negatively regulate cholesterol biosynthesis (Mohamed *et al.*, 2018a). Further evidence demonstrating the regulatory role of Aβ was shown by Wang *et al* (2014) where, different ways of processing of Aβ had a different effect of cholesterol metabolism (Wang *et al.*, 2014). In a human astocytoma cell line and AD patient derived fibroblasts, cleavage of APP by α-secretase had a positive effect on SREBP2 leading to an increase in expression on cholesterol biosynthetic genes, whereas cleavage with β-secretase had the opposing effect (Wang *et al.*, 2014). In primary rat cortical neurons, oligomeric Aβ reduced cellular cholesterol by reducing cholesterol synthesis however, a change in SREBP2 expression was not observed, suggesting that cholesterol synthesis is inhibitied at a post-transcitional level (J. S. Gong *et al.*, 2002). Together, these studies demonstrate the role APP processing and Aβ has on cholesterol metabolism.

NFT may also play a role in SREBP2 mediated cholesterol synthesis. One study found that the N-terminal of SREBP2 was localised in the cytoplasm of pyramidal neurons from the hippocampus in AD brains, compared to age-matched control brains where the N-terminal of SREBP2 was localised to the nucleus (Wang *et al.*, 2019). The study also found that a negative assocaitation with AT8-positive NFTs and the nuclear localisation of SREBP2, suggesting that NFTs may be involved in the regulation of cholesterol synthesis (Wang *et al.*, 2019).

2.5.7 Limitations

The use of IHC has certain limitations; for example, the quantification method that is used, types of antibody used and the tissue type. Furthermore, the IHC method does not provide a linear assessment of protein concentration and cannot provide a measure of enzyme activity. This makes it difficult to assess if HMGCR is

enzymatically active to result in an increase in cholesterol biosynthesis - therefore a measure of brain cholesterol was carried out to see if HMGCR expression associated with brain tissue cholesterol levels (3.4.20). There are two main ways in which tissue for IHC can be prepared: firstly, and the most common is formalin-fixed paraffin embedded (FFPE) tissue; the second is by snap freezing the tissue using liquid nitrogen and fixing using acetone (S. R. Shi *et al.*, 2008). The use of FFPE tissue requires antigen retrieval, this reverses crosslinks between proteins leading to unmasking of the epitope however, sometimes this may alter the way in which the antigen is recognised by the antibody, making comparisons between studies difficult (Engel and Moore, 2011).

Other points to consider when comparing IHC studies include the type of antibody that is used. In this study a monoclonal antibody was used, these types of antibodies are more specific compared to polyclonal antibodies however; this may also become a limiting factor, as small changes in the epitope sequence, such as ones that may occur during antigen retrieval, would prevent binding (Lipman *et al.*, 2005). Polyclonal antibodies on the other hand can still recognise a host of antigenic epitope sequences, meaning that changes that may occur during antigen retrieval can still cause antibody/antigen complexes. However, this decrease in specificity can lead to cross reactivity and increase non-specific background staining (Lipman *et al.*, 2005).

The method of quantification will have a role to play when comparing studies. The method employed within this study was based on the percentage total immunoreactivity per image. However, as this method only takes into account the number of pixels that contain the chromogen and not the density of chromogen present, it is difficult to quantify the protein amount, as the number of pixels is not directly proportional to the amount of antigen (Matkowskyj *et al.*, 2003). In addition, the detection system used by the programme is not linear, which means that once a pixel exceeds the threshold value and is marked as positive the amount of protein that is present becomes irrelevant and is not considered in the final percentage value. Furthermore, the use of ABC/DAB to amplify and visualise the binding of the antibody plateaus at a certain maximum, this in turn prevents the further binding of antibody to antigen from being detected and therefore having an impact on quantification as the immunoreactivity is not a true representation of antigen

expression. One way in which this could be avoided is by using primary antibodies which are conjugated with a fluorophore or horseradish peroxidase, allowing for a more accurate representation, however it may be difficult to visualise if there is a low concentration of antigen expression (Matkowskyj *et al.*, 2003).

Other limitations that need to be considered for this study are the markers of oxidative stress and neuroinflammation that have been used. This study used markers that had been characterised using IHC so therefore the limitations of these needs to be considered. Furthermore, in this study correlation analysis was carried out on γH2AX as a marker for DNA damage from oxidative stress, other markers such as Malondialdehyde (marker of lipid peroxidation), 8-hydroxydeoxyguanosine (marker of oxidative DNA damage), thioredoxin-2 (marker of ROS induced oxidative stress) and peroxiredoxin-3 (marker of ROS induced oxidative stress). The use of multiple oxidative stress markers would further validate any associations with HMGCR immunoreactivity and oxidative stress. Similar limitations also apply to markers of neuroinflammation, correlation analysis was carried out on CD68 immunoreactivity as a marker of microglial activation, other markers such as major histocompatibility complex class 2 (marker of microglial activation) and GFAP (marker of gliosis) could be used to provide a more robust analysis of association of HMGCR immunoreactivity and neuroinflammation.

2.6 Conclusion

This study has found that HMGCR expression was associated with pyramidal neurons throughout all layers of the temporal cortex. This is a novel finding as currently the literature suggests that glial cells are responsible for cholesterol biosynthesis within the brain however, we have found that the key regulatory enzyme of the pathway is expressed in neurons. Neuronal expression of HMGCR is not altered by Alzheimer-type neuropathology, markers of oxidative stress and markers of neuroinflammation. No significant association between HMGCR immunoreactivity within the temporal cortex and dementia status were found. Positive immunolabelling was also observed in prefrontal association cortex and quantification showed that HMGCR expression did not change with age. HMGCR expression was localised to the cytoplasm and proximal process of pyramidal neurons and expression was also observed in cells morphologically resembling astrocytes and oligodendrocytes within

white matter regions of temporal cortex sections. Dual-IHC confirmed that HMGCR and GFAP positive astrocytes did not co-localise in the temporal white matter and cortical regions. One possible explanation for the neuronal expression of HMGCR, could be that neurons are using the mevalonate arm of the cholesterol biosynthesis pathway to synthesis isoprenoids and other molecules, rather than cholesterol. Furthermore, this study has also shown that SREBP2, a master gene regulator for the cholesterol biosynthesis pathway is expressed in both neurons and astrocytes in temporal cortex and white matter regions, respectively. SREBP2 is localised to the neuronal cytoplasm and proximal process and within astrocytic cytoplasm and processes, this suggests that cholesterol biosynthetic gene expression is not being upregulated.

3.0 Determining expression of key regulators of cholesterol homeostasis and measuring cholesterol concentration in the ageing brain

3.1 Introduction

Cholesterol homeostasis within the brain is achieved by balancing *de novo* cholesterol biosynthesis, cholesterol metabolism and cholesterol efflux. Maintaining cholesterol homeostasis within the brain is crucial as cholesterol is fundamental for development and during adult life (Zhang and Liu, 2015). Cholesterol biosynthesis is regulated by the action of two key enzymes, HMG CoA reductase (*HMGCR*) and Sterol Regulatory Element-Binding Protein 2 (*SREBP2*). *HMGCR* encodes for an enzyme which catalyses the conversion of HMG-CoA into mevalonate and is the rate determining step of the cholesterol biosynthesis pathway (Sharpe and Brown, 2013b). HMGCR is localised to the endoplasmic reticulum (ER) membrane and immunohistochemical analysis for *this* study has shown that HMGCR protein is expressed in the pyramidal neurons within the temporal cortex (2.4.1). *SREBP2* gene encodes for a transcription factor which is responsible for controlling the expression of genes involved with cholesterol biosynthesis such as *HMGCR* (Sakai *et al.*, 1996; Simons and Ilonen, 2000; Goldstein, DeBose-Boyd and Brown, 2006). Immunohistochemical analysis from *this* study has demonstrated that the SREBP2 protein was expressed in both the cytoplasm of neurons and astrocytes in the temporal cortex and cortical and white matter boundary respectively (2.4.6).

Within the brain, neurons and glia do not have the capability of breaking down cholesterol and so rely on the liver for degradation. However, the blood brain barrier (BBB) prevents cholesterol from entering the peripheral circulation and reaching the liver (Sun, Yu and Tan, 2015). One major excretion route of cholesterol within the brain is via conversion to oxysterols such as 24S-hydroxycholesterol (24S-OHC) and 27-hydroxycholesterol (27-OHC) which can easily pass through the BBB into the peripheral circulation and be further metabolised into bile acids within the liver (Sun, Yu and Tan, 2015; Zhang and Liu, 2015; Chang *et al.*, 2017). The conversion of cholesterol into 24S-OHC is catalysed by the enzyme cholesterol 24-hydroxylase which is encoded by the gene *CYP46A1*, which is a member of cytochrome P450 protein family (Erik G. Lund, Guileyardo and Russell, 1999). The conversion of

cholesterol into 27-OHC is catalysed by sterol 27-hydroxylase and is encoded by the gene *CYP27A* (Heverin *et al.*, 2005).

CYP46A1 gene is located on chromosome 14q32.1 and contains 15 exons, which result in a protein that contains approximately 500 amino acids. The enzyme is localised to the ER membrane and is preferentially expressed within neurons (Erik G. Lund, Guileyardo and Russell, 1999). Genetic association studies have found that a single nucleotide polymorphism (SNP) within an intron between exon 3 and 4 of the *CYP46A1* gene is significantly associated with AD compared to healthy controls and is also associated with an increase in 24S-OHC/cholesterol ratios in CSF (Kölsch *et al.*, 2002). Another study found that one allele of *CYP46* (TT allele) caused by a SNP in which a T is substituted for C 151 bases 5' to exon 3 (rs754203) was associated with increased Aβ peptide levels in both the brain and CSF of AD patients; and increased levels of phosphorylated tau within CSF of AD patients (Papassotiropoulos *et al.*, 2003). However, the same SNP did not show any significant associations with AD, brain Aβ or NFT levels in a different cohort (Ingelsson *et al.*, 2004). Further studies have shown that the TT-homozygote genotype in young healthy patients had the smallest parahippocampal and hippocampal volumes compared to heterozygotes and CC-homozygotes (Hänggi *et al.*, 2011). These studies suggest that SNPs in *CYP46A1* may be a risk factor for AD.

Studies *in vitro* have shown that 24S-OHC has a neurotoxic effect by producing free radicals leading to oxidative stress and eventual cell death via apoptosis (Kölsch *et al.*, 1999, 2001b). Human neuroblastoma cells exposed to exogenous 24S-OHC, showed a significant increase in α-secretase activity and a significant decrease in β-secretase activity (Famer *et al.*, 2007). This study suggests that the presence of 24S-OHC promotes the non-amyloidogenic pathway due to the activation of α-secretase. Another study found that treating human neuroblastoma cells expressing human APP with physiological concentrations of 24S-OHC resulted in a decrease in Aβ production, suggesting that the reduction in Aβ production could be due to 24S-OHC inhibiting the tracking of APP within the ER (Urano, Ochiai and Noguchi, 2013). This study further reinforced the protective effect 24S-OHC and hence *CYP46A1* expression on preventing the formation of Aβ peptides.

The *CYP27A1* gene is part of the cytochrome p450 family and encodes for a mitochondrial enzyme 27-hydroxylase. Within the liver, 27-hydroxylase is involved in catalysis of the first step of bile acid biosynthetic pathway and in other tissues 27-hydroxylase is involved in converting cholesterol into 27-OHC and 3β-hydroxy-5-cholestenoic acid (Dubrac *et al.*, 2005). 27-OHC is the most abundant oxysterols found within the peripheral circulation and flows into the brain as it can easily cross the BBB, but 27-OHC can also be synthesised within the brain as *CYP27A1* expression has been observed in neurons, astrocytes and oligodendrocytes (Lütjohann *et al.*, 1996a; Brown, Theisler, Silberman, Magnuson, Gottardi-Littell, John M. Lee, *et al.*, 2004; Pataj *et al.*, 2016).

Studies have found that 27-OHC may induce or exacerbate AD like pathology. Human neuroblastoma cells co-cultured with rat glioma cells showed a cytotoxic effect by inducing a significant reduction in cell viability and proliferation. Furthermore, a significant decrease in mRNA and protein expression of cholesterol biosynthetic genes such as *HMGCR* and *SREBP2* was observed and a significant increase in cholesterol transport genes expression such as ATP binding cassette A1 (ABCA1) and liver X receptor-α (LXR-α) (Wang *et al.*, 2016). This study suggests that an increase in 27-OHC may disrupt cholesterol homeostasis and could contribute to pathogenesis of neurodegenerative diseases. Further studies in APP/PS1 transgenic mice showed that treating the mice with 27-OHC produced a decline in learning and memory as well as increased Aβ plaque deposition in the hippocampus (X. Zhang *et al.*, 2019). Studies carried out in patients with mild cognitive impairment found significantly increased levels of plasma 27-OHC and plasma levels of 27-OHC correlated with plasma levels of Aβ1-40 (X. Zhang *et al.*, 2019). These studies suggest that 27-OHC levels and hence the action of 27-hydroxylase enzyme may contribute to AD pathology.

Oxysterols have the potential to be a diagnostic biomarker for neurodegenerative disease. 24S-OHC mainly originates from the brain and has a half-life of approximately 12 hours within the plasma, the plasma levels of 24S-OHC are dependent upon the rate of metabolism within the liver and rate of brain secretion (Bretillon *et al.*, 2000). One study found that plasma 24S-OHC levels were negatively correlated with Mini Mental Score, other studies have found that high levels of plasma oxysterols is correlated with larger hippocampal volumes in healthy middle-

aged individuals (Papassotiropoulos *et al.*, 2000; Koschack *et al.*, 2009). Furthermore, similar studies have found an increased plasma 24S-OHC was present in AD and vascular dementia patients; these contrasting findings could be explained by differences in the severity of disease (Lütjohann *et al.*, 2000; Leoni and Caccia, 2011). Considering the fact that the use of cholesterol lowering drugs, liver disease and body mass index and overall cholesterol levels can affect 24S-OHC levels within the plasma, plasma levels should be carefully interpreted before making correlations and diagnosis (Bretillon *et al.*, 2000; Brown and Jessup, 2009; Leoni and Caccia, 2011).

Targeting cholesterol metabolism could be a potential treatment for AD. A drug screening study in neuronal induced pluripotent stem cells (iPSCs) derived from AD patients found that allosteric activation of CYP46A1 enzyme using the small molecule efavirenz reduces the levels of phosphorylated tau within the neurons without altering astrocyte viability (van der Kant *et al.*, 2019). However, some studies suggest that inhibition of cholesterol 24-hydroxylase enzyme using small molecules such a imidazo(1,2-a)pyridines could be another potential therapeutic strategy (Uto, 2015). Repurposing of statins has been found to decrease the levels of plasma 24S-OHC in AD patients by approximately 20%, which suggests that statins may have a direct effect on brain cholesterol metabolism (Vega *et al.*, 2003). Further studies have demonstrated that statins (that can easily pass across the BBB), such as lovastatin have neuro-protective effects (He *et al.*, 2006). He *et al* (2006) induced brain injury in rats using kainic acid and found an increase in cholesterol and 24S-OHC levels in the hippocampus following exposure. In rats injected with both kainic acid and lovastatin, reduced cholesterol and 24S-OHC levels were observed; this reduction in oxysterols levels decreases the chance of free radical damage to neurons (Kölsch *et al.*, 1999; He *et al.*, 2006). These studies suggest that regulating oxysterols such as 24S-OHC could be a potential therapeutic target for neurodegenerative disease such as AD.

Regulating cholesterol efflux is important in maintaining cholesterol homeostasis. One enzyme involved in cholesterol transport is the ATP-binding cassette transporter A1 (ABCA1) and is encoded by *ABCA1* gene. *ABCA1* is located on chromosome 9q31.1 and contains approximately 50 exons and is ubiquitously expressed and localised to the plasma membrane (Dean, Hamon and Chimini, 2001). *ABCA1*

encodes a protein 2,261 amino acids long that contains two transmembrane domains and two nucleotide binding domains, and is involved in the ATP-dependent transport of lipids across membranes (Phillips, 2018).

For efficient ABCA1 dependent cholesterol efflux, lipid free apolipoproteins such as apoA1, apoAII and apoE are required. Within the CNS apoE is the major apolipoprotein, ABCA1 activity is critical to apoE protein lipidation, as ABCA1 chaperones intracellular cholesterol from endosomes into apoE to form the apoE HDL (Vance and Hayashi, 2010). The lack of lipidation of apoE4 makes it more prone to forming aggregates and developing AD pathology (Hatters *et al.*, 2006; Raulin *et al.*, 2019). A study using mouse astrocytes found that apoE4 expression lead to ABCA1 being retained in the late endosome, thus reducing ABCA1 activity and decreasing the lipidation of apoE4 (Rawat *et al.*, 2019). These studies suggest that ABCA1 has a critical role in transporting cholesterol from astrocytes to neurons via apoE proteins. The lack of ABCA1 activity can reduce apoE4 lipidation which prevents cholesterol transport as well as inhibiting Aβ degradation (Rawat *et al.*, 2019).

Further studies in *ABCA1* knockout mice found a decrease in cortical and CSF apoE levels; however, no changes in free and esterified cholesterol were observed in the mice (Wahrle *et al.*, 2004). This suggests that *in vivo* ABCA1 activity is not crucial for regulating brain tissue cellular lipid levels. Additionally, in primary mice astrocyte cultures, a marked reduction in secretion of cholesterol into the media was observed in *ABCA1* knockout cells and smaller apoE particles with reduced cholesterol content were also observed (Wahrle *et al.*, 2004). This suggests that there are ABCA1 independent pathways to apoE lipidation and release; however, ABCA1 is more efficient and effective.

Studies have indicated that *ABCA1* may play a role in AD pathogenesis. Microarray analysis of the hippocampus from AD patients showed an increase in expression of *ABCA1* (Blalock *et al.*, 2004; Carter, 2007). This was further consolidated by other studies that found a significant increase in both mRNA and protein levels of ABCA1 in the hippocampus of AD brains. Up-regulation of *ABCA1* was not observed in other brain areas such as the cerebellum, suggesting that this increase in *ABCA1* expression is associated with AD pathology (Kim *et al.*, 2010).

ABCA1 activity could be a potential novel drug target to treat AD. A study by Boehm-Cagan *et al* (2016) used transgenic mice expressing human analogues of apoE3 and apoE4 and treated the mice with a peptide (CS-6253) which stimulates ABCA1 activity. This study found that in apoE4 mice treatment with CS-6253 led to a significant reduction of Aβ and phosphorylated tau immunoreactivity in the hippocampus compared to control apoE4 mice (Boehm-Cagan *et al.*, 2016). Furthermore, mice treated with the peptide showed a significant improvement in performance of cognitive tests such as the Morris water maze. This data suggests that activation of ABCA1 may reverse the pathological effects of the apoE4 and reduce AD pathology, suggesting that AD pathology may arise due to lack of ABCA1 activity and reduced lipidation of apoE.

For *this* study, the assessment of changes in cholesterol biosynthetic and metabolism gene expression was conducted using frozen temporal cortex tissue from the CFAS Cambridge neuropathology cohort from which sub-populations of neurons and astrocytes were isolated using laser capture microdissection (LCM). LCM is a method that is used to isolate specific cell types or region of interest from a section of tissue. It combines immunohistological and histological methods to identify a sub-population of cells or regions of interest, with microscopy techniques allowing isolation of a specific sub-population of cells or a region of interest and producing an enriched sample. The LCM microscope has an infrared laser attached to it and in conjunction with an LCM cap, which has a thermoplastic film attached to the bottom of the cap. When the cap is placed on top of a tissue section and the laser is fired, this causes the thermoplastic film to melt and adhere to the tissue below. Therefore, when the cap is removed it also removes the region or cells of interest directly below, RNA/DNA can be extracted and used for gene expression studies (Simpson, Wharton and Heath, 2018). The LCM method was used to determine cholesterol biosynthetic gene expression in sub-populations of astrocytes and neurons isolated from the temporal cortex and investigating the specific changes that occur within the cells, rather than the entire tissue. This allows for a more detailed look at changes in cholesterol biosynthesis and metabolism at a cellular level and how AD pathology may alter this.

For this study four key genes involved in cholesterol homeostasis were investigated to assess changes in relation to AD progression. The genes selected were *HMGCR,*

SREBP2, CYP46A1 and *ABCA1*. Previous work from our lab carried out microarray analysis on neurons isolated from frontal cortex sections from CFAS Cambridge neuropathology cohort with low and high DNA damage response (DDR) (Simpson *et al.*, 2016). Importantly this study had included all low Braak and Braak stage (I-II) cases (n=39) within the cohort and so the variation was not accounted for by AD pathology and was not examined by the paper. That study found a fold change of 4.5 (p=0.0008) for *HMGCR* and a down-regulation in *SREBF2* with a fold change of -1.1 (p=0.001) was associated with a high DDR. It was further extended to investigate the levels of 24S-OHC in CSF samples from the CFAS neuropathology cohort and found that 24S-OHC negatively correlated with increasing Braak and Braak stage (r=-0.29, p=0.040) and a significant correlation between 24S-OHC levels in CSF and astrocyte DDR (r=-0.43, p=0.001) and neuronal DDR (r=-0.30, p=0.033) across all Braak and Braak stages. This study prompted the selection of the four key genes to further investigate individual changes in cholesterol homeostasis in astrocytes and neuronal sub-populations in relation to AD progression.

This current study also measured the levels of brain cholesterol within the temporal cortex to investigate if changes in cholesterol biosynthetic and metabolism genes lead to an over-all change in brain cholesterol levels and whether these changes are associated with AD progression and pathology. To determine brain tissue cholesterol levels the Amplex Red cholesterol assay was used. Amplex Red cholesterol assay is based on an enzyme-coupled reaction, which detects both cholesteryl esters and free cholesterol. Cholesterol esterase (CE) hydrolyses cholesteryl esters into cholesterol which is then oxidised by cholesterol oxidase (CO) to produce H_2O_2 and cholest-4-ene-3-one (Amundson and Zhou, 1999). H_2O_2 is detected using the Amplex Red reagent (10-acetyl,3,7-dihydroxyphenoxazine), in the presence of horseradish peroxidase (HRP) Amplex Red reagent has a 1:1 stoichiometry to H_2O_2 and produces resorufin. Resorufin has absorption and fluorescence emission maxima at approximately 571 nm and 585 nm respectively, this wavelength minimises the effect of auto-fluorescence from biological samples (Amundson and Zhou, 1999).

3.2 Aims and Objectives

The aim of this study was to define the changes in expression of genes involved in cholesterol biosynthesis, metabolism and efflux in neurons and astrocytes isolated from human temporal cortex tissue in relation to AD neuropathology progression, oxidative DNA damage and neuroinflammation. This study also aimed to measure the levels of brain cholesterol within temporal cortex tissue to see if changes in cholesterol biosynthetic gene expression impact overall brain cholesterol levels.

We hypothesise that changes in cholesterol biosynthetic gene expression in neurons and astrocytes are associated with AD neuropathology, oxidative DNA damage and neuroinflammation leading to a decrease in overall cholesterol levels in the temporal cortex.

The objectives of this chapter are:

- Optimise and validate LCM for isolating neurons and astrocytes from temporal cortex regions.
- Determine the expression of *HMGCR, SREBP2, CYP46A1* and *ABCA1* in astrocyte and neuronal populations isolated from the temporal cortex from a pan-Braak and Braak sub-cohort using qualitative real-time PCR.
- Determine if changes in cholesterol biosynthetic and metabolism gene expression is associated with AD neuropathology progression and pathology and other AD pathological markers such as oxidative stress and neuroinflammation.
- Measure levels of brain cholesterol using Amplex Red Cholesterol assay in frozen temporal cortex tissue.
- Determine if changes in tissue cholesterol levels associated with AD progression and neuropathology and other AD pathological markers such as oxidative stress, neuroinflammation and vascular pathologies.

3.3 Methods

List of materials can be found in Appendix **6.1.1**

3.3.1 Human brain tissue

Post-mortem human brain tissue was obtained from the Cambridge centre of CFAS and a sub cohort was used for this study (n=32). Cases were stratified according to Braak and Braak groups and selected based on pH and post-mortem delay (PMD). Braak and Braak groups were defined as follows: Braak and Braak, group 1 contained stages 0-II (entorhinal) (n=12), group 2 contained stages III-IV (limbic) (n=10) and group 3 contained stages V-VI (isocortical) (n=10). Freshly prepared frozen cryosections (7 µm) were used for Laser capture microdissection (LCM). Frozen sections of the temporal cortex (Brodmann area 20/21) were investigated for this study and the ethical approval can be found in the appendix (15/SW/0246) (appendix 6.2).

3.3.2 RNA extraction from post-mortem tissue

Total RNA extraction was carried out before LCM to assess the initial RNA quality of each tissue sample. A cryosection (10 µm) was collected into a sterile tube. The section was homogenised in 100 µl of TRIzol (Fisher Scientific, UK) using a handheld homogeniser. After homogenisation, an additional 900 µl of TRIzol and 200 µl of chloroform (Sigma-Aldrich, UK) was added and the samples vortexed for 15 seconds. The samples were incubated at RT for 3 minutes, before being centrifuged (Sigma-Aldrich, UK) at 12,000g at 4°C for 15 minutes. The upper aqueous layer of the supernatant was removed and transferred into a sterile tube. 500 µl of isopropanol (Fisher Scientific, UK) was added and samples left to stand at RT for 10 minutes. The samples were centrifuged at 12,000g at 4°C for 10 minutes and the supernatant was discarded. The RNA pellet was washed with 1 ml of ice-cold 75% ethanol (VWR Chemicals, France), vortexed and centrifuged at 7500g at 4°C for 5 minutes. The supernatant was carefully discarded and the pellet air dried for 5-10 minutes before re-suspending the pellet in 20 µl of RNAase free water (Zymo research, US). The samples were incubated at 65°C for 10 minutes and RNA stored at -80°C until required. The RNA concentration of each sample was determined using the NanoDrop Spectrophotometer (ThermoFisher Scientific, USA) and RNA

integrity was determined using the bioanalyzer and Agilent RNA 6000 Nano Chip (Agilent Technologies, USA).

3.3.3 Rapid immunohistochemistry for laser capture microdissection of astrocytes

Freshly prepared frozen cryosections (7µm) were collected onto uncharged glass slides. The sections were fixed and permeabilised in ice cold acetone (VWR Chemicals, France) for 3 minutes and air-dried briefly at RT. The sections were blocked in 1.5% goat normal serum for 3 minutes, followed by 3 minutes incubation at RT with primary rabbit anti-glial fibrillary acidic protein (anti-GFAP) antibody (Dako, Denmark [Z033401-2]) at a 1/50 dilution. The sections were washed with sterile TBS and incubated with 0.5% (v/v) biotinylated anti-rabbit secondary antibody for 3 minutes, followed by a brief wash with sterile TBS. The sections were incubated with 2% (v/v) ABC-HRP for 3 minutes followed by a wash with sterile TBS. The antibody binding was visualised with DAB for 5 minutes at RT and the reaction was stopped with sterile d.H_2O. The sections were dehydrated in increasing ethanol concentrations (70%, 95% and absolute) and cleared in xylene for 5 minutes and placed in a lamina flow hood to dry for a minimum of an hour.

3.3.4 Toluidine Blue staining for laser capture microdissection of neurons

Freshly prepared frozen cryosections (7µm) were collected onto uncharged glass slides. The sections were fixed and permeabilised in ice cold acetone (VWR Chemicals, France) for 3 minutes and air-dried briefly at RT. The slides were immersed in toluidine blue for 1 minute and then washed in Diethylpyrocarbonate (DEPC)-treated d.H_2O for 1 minute. The sections were dehydrated in graded series of ethanol (70%, 95% and absolute) and cleared in xylene for 5 minutes and then placed in a lamina flow hood to dry for a minimum of an hour.

3.3.5 Laser Capture Microdissection (LCM)

LCM was performed using Pixcell laser capture microdissection system (Arcturus, Thermofisher scientific, UK) at x20 magnification. An LCM cap was placed over the tissue section and an infrared laser fired to micro-dissect approximately 1000 $GFAP^+$ astrocytes and 1000 neurons per cap (laser power: 55 mW, laser pulse: 15 ms and laser spot size: 7.5 µm). The thermoplastic film was carefully removed from the cap using sterile forceps and placed in a 0.5 ml sterile tube for RNA extraction.

3.3.6 RNA extraction following LCM

Using the Picopure RNA isolation kit (Thermo fisher scientific, UK), 50 µl of extraction buffer was added to the 0.5 ml sterile tube containing thermoplastic film and the sample was incubated at 42°C for 30 minutes. 250 µl of conditioning buffer was added to the RNA extraction column and allowed to precondition at RT for 5 minutes before centrifugation (Thermofisher scientific, UK) at 13,000 g for 1 minute prior to use. Following the 42 °C incubation, 50 µl of 70% ethanol was added to each LCM extracted sample and samples transferred to the RNA extraction column; centrifugation was carried out at 100 g for 2 minutes to allow the RNA to enter the column followed by a faster spin at 13,000 g for 1 minute, all flow-through was discarded. The columns were washed with 100 µl wash buffer 1 and centrifuged at 8,000 g for 1 minute followed by 100 µl of wash buffer 2 at 8,000 g for 1 minute before a final wash step in 100 µl of wash buffer 2 centrifuged at 13,000 g for 2 minutes. The column was placed into a 1.5 ml sterile tube and 11 µl of elution buffer was added to the column; this was allowed to incubate for 1 minute at RT before centrifugation at 1000 g for 1 minute followed by a faster spin at 13,000 g for 1 minute. The eluted RNA was stored at -80°C. The RNA concentration of each sample was determined using the NanoDrop Spectrophotometer (ThermoFisher Scientific, USA) and RNA integrity was determined using the Agilent RNA 6000 Pico Chip (Agilent Technologies, USA).

3.3.7 Cell enrichment validation

To confirm cell enrichment of each extracted RNA sample RT-PCR was performed. Firstly, each RNA sample was synthesised into cDNA qScript cDNA mix (Quanta biosciences, US). Following the manufacturer's protocol 50 ng of RNA was placed into a labelled 0.2 ml sterile tube, followed by 2 µl of Q-script (Quanta biosciences, US) and samples were made up to 10 µl with RNAase free water. The samples were placed into the thermocycler (Peltier Thermal cycler, MJ Research, USA) and incubated at: 25°C for 5 minutes, 42°C for 30 minutes, 85°C for 5 minutes, before being held at 4°C.

To confirm cell enrichment relevant primers were prepared and aliquoted to create 5 pM/µl primer stocks (Solis Biodyne, Estonia) (Table 3.1). To 1 µl of each cDNA sample, 4 µl 5X Green Firepol PCR mix (Eurofins Genomics, Germany), 1 µl forward and 1 µl reverse primer and 13 µl RNAase free water was added and the samples

were briefly centrifuged and placed into the thermocycler. The PCR programme consisted of denaturation at 95°C for 10 minutes and products were amplified in 40 cycles (95°C 15 seconds, and 60°C for 1 minute) followed by a final incubation at 22°C for 10 minutes, before being held at 10°C. Non-template control (NTC) samples, in which cDNA was replaced with 1 µl of RNAase free water, was used to determine the specificity of primers.

Gene Name	Primer Sequence	Product size (bp)
GFAP	F 5'-GCA GAA GCT CCA GGA TGA AAC R 5'-TCC ACA TGG ACC TGC TGT C	213
NeuN	F 5'-ACG ATG GTA GAG GGA CGG AA R 5'-AAT TCA GGC CCG TAG ACT GC	127
β-Actin	F 5'-TCC CCC AAC TTG AGA TGT ATG AAG R 5'-AAC TGG TCT CAA GTC AGT GTA CAG G	100

Table 3.1: Primers used for cell enrichment validation

3.3.8 3% Agarose gel electrophoresis of PCR products

All PCR products were run on a 3% (w/v) agarose gel to check they were the expected size. A 3% (v/v) agarose gel was prepared by adding 3 g of agarose to 100 ml of x1 Tris-acetate-EDTA (TAE) buffer. The mixture was heated in the microwave on full power until all the agarose had completely dissolved. The solution was cooled to RT under a running tap and 1 µl of ethidium bromide was added. The gel mix was poured into the gel cast and a gel comb added, the gel was allowed to set for approximately 20 minutes at RT. The comb was removed, and the gel placed in the electrophoresis tank containing x1 TAE buffer. 10 µl of each cell specific cDNA samples and NTC samples were loaded into the wells and 7 µl of hyperladder V (Bioline, UK) was also loaded as a DNA base pair marker. The gel was run at constant (100 V) for 1 hr, after which the PCR products were visualised using a G-box Gel imaging system (Syngen, UK).

3.3.9 Quantitative real time PCR (q RT-PCR)

To measure changes in cholesterol biosynthetic gene expression q RT-PCR was carried out. Extracted RNA from post-mortem tissue cell isolations was synthesised into cDNA as outline above (refer to 3.4.7). cDNA was diluted to a concentration of 2.5 ng/µl. The PrimeTime qPCR assays (Integrated DNA Technologies) (Table 3.2) were used. PCR was performed using 50 ng cDNA, 500nM of forward and reverse primer, 250 nM probe and 1x LUNA universal probe qPCR master mix (New England

Biolabs, UK) in a total volume of 10 µl per sample. Each sample was assessed in triplicate and analysed in a 384 well PCR plate (BioRad) sealed with PCR film lid (BioRad) on a BioRad CFX384 Real time system. The PCR programme consisted of denaturation at 95°C for 5 minutes, products were amplified in 39 cycles of (95°C for 10 seconds and 60°C for 30 seconds), followed by a final cycle at 95°C for 1 minute, 55°C for 30 seconds, and 95°C for 30 seconds. Cycle threshold (Ct) values were determined by the number of cycles it takes for the fluorescence from gene probes to reach the threshold value, which is determined by 10 standard deviations above background florescence. Thus, increased expression of a gene has lower Ct values compared to a higher Ct value which indicates reduced gene expression. β-actin was also amplified on each plate to normalise the gene expression levels using the comparative Ct, (ΔΔCt) method of quantification. The relative concentration values for each gene were calculated relative to the mean ΔCt expression for Braak and Braak group 1 or Thal group 1 for each cell type.

3.3.10 Quantification and statistical analysis of cholesterol biosynthetic genes in LCM isolated neuron and astrocytes

Statistical analysis was carried out using SPSS Statistics v26 program (IBM, UK) (Figure 3.1). Gene expression data was normalised to β-actin expression and the relative concentration was calculated relative to Braak and Braak group 1 and Thal group1 for each cell type and gene. Gene expression was tested for normality using the Kolmogorov-Smirnov (KS) test and by visualisation of histograms, and the mean, median and interquartile range calculated. Non-parametric Kruskal-Wallis (KW) and Jonckheere-Terpstra (JT) tests were performed to determine whether any significant differences and trends between neuronal and astrocytic cholesterol biosynthetic gene expression and AD neuropathology progression (Braak and Braak group staging and Thal β-Amyloid phase).

Non-parametric analyses (KW and JT tests) were also used to determine any significant differences and trends in cholesterol biosynthetic gene expression in astrocytes and neurons with AD neuropathology within the temporal cortex (CERAD Aβ plaque and tangle scores). Spearman rank correlation was used to determine any relationships between neuronal and astrocytic cholesterol biosynthetic gene expression with total percentage HMGCR immunoreactivity, 24(S)-OHC levels in CSF, oxidative stress (ɣH2AX, 8-hydroxydeoxyguanosine [8-OHdG] and

Malondialdehyde [MDA] expression), β-amyloid, phosphorylated tau expression (AT8), brain pH, neuroinflammation (CD68, GFAP and MHCII), and post-mortem delay (PMD) in the cases. Data on Aβ, AT8, pH, PMD, oxidative and neuroinflammatory markers was obtained from previous studies on the same cohort in the temporal cortex (CFAS Cambridge Neuropathology cohort) (J E Simpson *et al.*, 2010; Simpson *et al.*, 2015). All tests were two tailed and the $p<0.05$ was set as the level for significance. Outliers were identified based on distribution displayed on a histogram and box plots and extreme data points with a relative concentration greater than 3 and one SD away from the upper quartile. Outliers must meet both conditions to be removed from subsequent reanalysis.

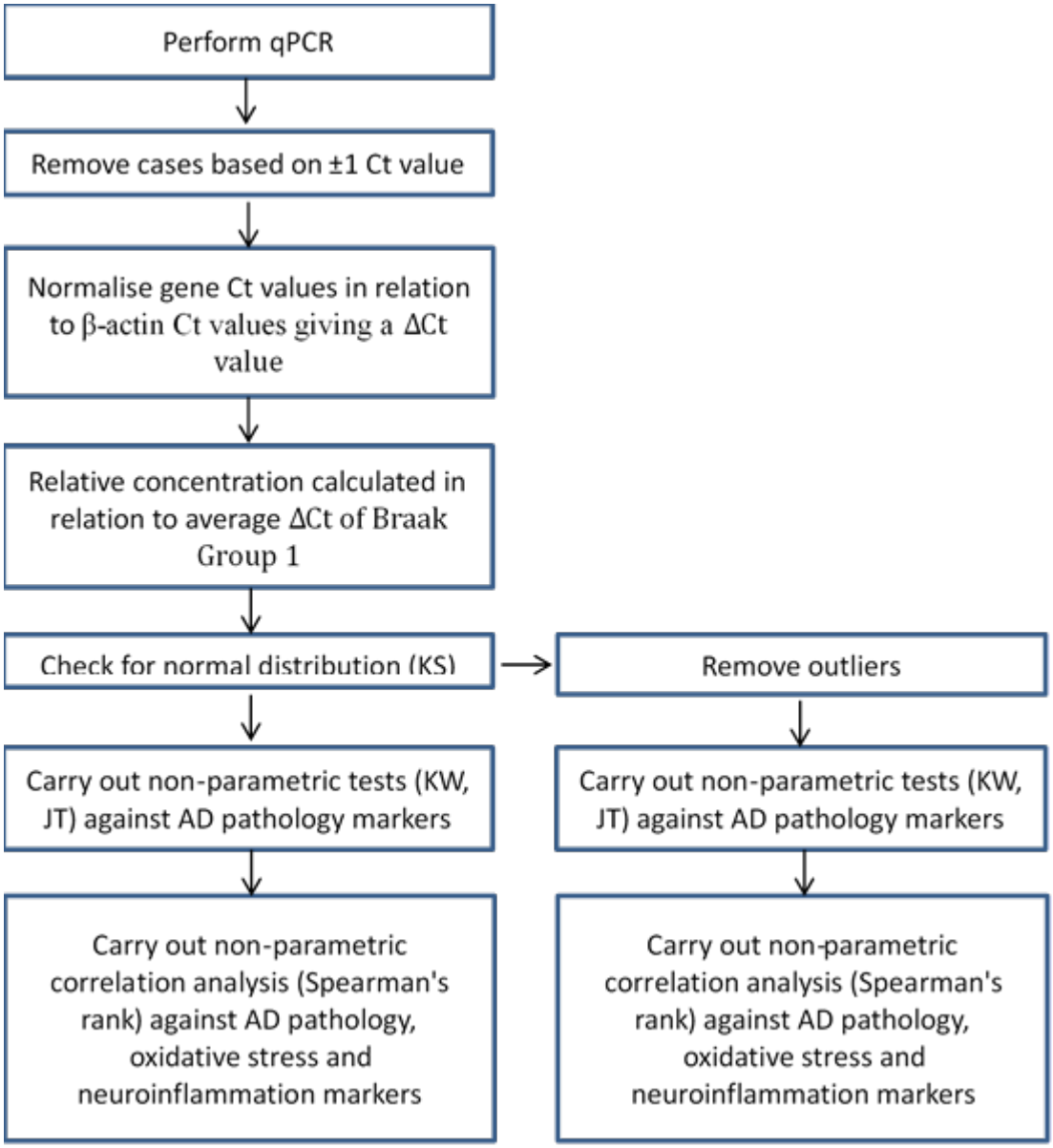

Figure 3.1. Quantification and statistical analysis of qPCR data: A flow chart outlining the methods of quantification and statistical analysis carried out.

Gene	Prime Time® Assay ID	Reference	Exon	Primer Sequence	Probe Sequence
HMG Co Reductase (HMGCR)	Hs.PT.58.4048748	NM_001130996	15-16	1) 5'-CCTTTATATCCGTTTCCAGTCCA-3' 2) 5'-CCACTAACGGCTAGAATCTGC-3'	5'-/56-FAM/ATGTTCATC/ZEN/CCCATGGCATCCCC/3IABkFQ/-3'
Cytochrome P450 46A1 (CYP46A1)	Hs.PT.58.26445892	NM_006668	12-13	1) 5'-AAGAGTCGCTGAGGCTGTA-3' 2) 5'-CCTCAAAGTATGTGTCCATCCG-3'	5'-/56-FAM/CTCCTCTTC/ZEN/CAGCAGGCGAAAGG/3IABkFQ/-3'
ATP Binding Cassette A1 (ABCA1)	Hs.PT.58.11955	NM_005502	49-50	1) 5'-TGCTACAATACCAGCTTCCATC-3' 2) 5'-GTCCTTGGCAAAGTTCACAA-3'	5'-56-FAM/TCTCCCAGA/ZEN/GCAAAAAGCGACTCC/3IABkFQ/-3'
Sterol regulatory element binding transcription factor 2 (SREBF2)	Hs.PT.58.39417166	NM_004599	16-17	1) 5'-TTCCTTCTGCCATTGCGA-3' 2) 5'-ACAGTAGCAGGTCACAGGT-3'	5'-56-FAM/CTATGGAGC/ZEN/AGCCTCAACGTCAGT/3IABkFQ/-3'
Beta-Actin (ACTB)	Hs.PT.39a.22214847	NM_001101	1-2	1) 5'-ACAGAGCCTCGCCTTTG-3' 2) 5'-CCTTGCACATGCCGGAG-3'	5'-56-FAM/TCATCCATG/ZEN/GTGAGCTGGCGG/3IABkFQ/-3'

Table 3.2: List of all Prime Time® qPCR Assays used for cholesterol biosynthetic gene expression investigation

3.3.11 Amplex Red cholesterol Assay

Post-mortem human brain tissue was obtained from the Cambridge centre of CFAS cohort and all available frozen temporal cortex tissue was used for this study (n=63). To extract cholesterol from post-mortem human brain tissue, freshly prepared frozen cryosections (10 µm) were collected into sterile tubes and mass of tissue was measured and noted. The section was homogenised in 200 µl of 1x reaction buffer (provided with the kit) (Thermo fisher scientific, UK) using a handheld homogeniser. After homogenisation, an additional 800 µl of 1x reaction buffer (Thermo fisher scientific, UK) was added and the samples vortexed for 15 seconds and stored at -80°C.

Amplex Red cholesterol assay was purchased from Thermo fisher scientific, UK and was carried out according to manufacturer's protocol. Briefly, brain tissue cholesterol samples were diluted 500-fold and 50 µl was pipetted into separate wells of a 96-well microplate (Merck, Germany). Cholesterol standards were also prepared by diluting cholesterol reference standard (provided with the kit) into 1x reaction buffer to produce cholesterol concentrations of 0-7.5 µM, alongside a positive control of 10 µM of H_2O_2 (provided with the kit). 50 µl of positive control and cholesterol standards were pipetted into separate wells of a 96-well microplate. Amplex red working solution was prepared using HRP, cholesterol oxidase, cholesterol esterase and Amplex red reagent in 1x reaction buffer according to manufacturer's protocol. 50 µl of Amplex red working solution was added to each well containing samples and controls. Each sample was ran in triplicate. The plate was incubated at 37 °C for 30 minutes and protected from light. The excitation fluorescence was measured at 540 nm and the emission was measured at 590 nm using the PHERAStar spectrophotometer. For each well, background fluorescence was corrected for by subtracting the no-cholesterol control. Cholesterol concentration was calculated by plotting a standard curve using the known cholesterol values and the cholesterol concentration for samples were interpolated from the curve. Cholesterol concentrations were divided by the mass of tissue that was used to extract cholesterol from to give cholesterol concentration per mg of tissue.

3.3.12 Statistical analysis of cholesterol concentration in whole tissue cholesterol extracts

Statistical analysis was carried out using SPSS Statistics v26 program (IBM, UK). Cholesterol concentration per mg of tissue was tested for normality using the Kolmogorov-Smirnov (KS) test and by visualisation of histograms, and the mean, median and interquartile range calculated. Non-parametric Kruskal-Wallis (KW) and Jonckheere-Terpstra (JT) tests were performed to determine whether any significant differences and trends between cholesterol concentration and AD progression (Braak and Braak group staging and Thal β-Amyloid phase). Non-parametric analysis (KW and JT tests) were also used to determine any significant differences and trends in cholesterol concentration with cortical microinfarcts. A Mann-Whitney (MW) test was carried out to determine any significant differences in cholesterol concentration and the presence of cerebral amyloid angiopathy (CAA). Spearman rank correlation was used to determine any relationships between cholesterol concentration with neuronal and astrocytic cholesterol biosynthetic gene expression, total percentage HMGCR immunoreactivity, 24(S)-OHC levels in CSF, oxidative stress (γH2AX and Malondialdehyde [MDA] expression), β-amyloid, phosphorylated tau expression (AT8), brain pH, neuroinflammation (CD68, GFAP and MHCII), and post-mortem delay (PMD) in the cases. Data on Aβ, AT8, pH, PMD, vascular pathology, oxidative and neuroinflammatory markers was obtained from previous studies on the same cohort in the temporal cortex (CFAS Cambridge Neuropathology cohort) (Ince, 2001; Matthews *et al.*, 2009b; J E Simpson *et al.*, 2010; Simpson *et al.*, 2015). Further non-parametric tests were carried out to determine differences and trends with further markers of oxidative stress (Trx2 and Prx3 immunoreactivity) (unpublished data). To determine if the variation in brain tissue cholesterol concentration associated with dementia status a Mann-Whitney U test was carried out. The effect of tissue cholesterol concentration on risk of dementia was analysed using logistic regression. All tests were two tailed and the $p<0.05$ was set as the level for significance. Statistical analysis in relation to dementia status and corresponding violin plots was carried out by Connor Richardson, University of Newcastle.

3.4 Results

3.4.1 Case selection

The CFAS Cambridge cohort contains a total of 100 frozen samples. From this a sub-cohort (n=32) were selected based on pH and post-mortem delay (PMD), to ensure better quality RNA before LCM as degradation occurs during the LCM process (Table 3.3). To characterise the changes in gene expression in relation to AD progression cases from all three Braak and Braak groups were also selected: Braak and Braak group 1 (n=12), group 2 (n=10) and group 3 (n=10).

3.4.2 LCM isolated enriched populations of astrocytes and neurons from frozen post-mortem human tissue

Large pyramidal neurons were clearly visible under a microscope using (toluidine blue) histological stain (Figure 3.2 A). Using immuno-LCM, $GFAP^+$ astrocytes were easily distinguishable under the microscope through their stellate morphology (Figure 3.2 B). Approximately 1000 astrocytes and 1000 neurons were captured to obtain approximately 50 ng extracted RNA (2.4-20 ng/µl).

Cell enrichment was assessed for each sample following LCM by RT-PCR analysis of glial and neuronal transcripts. All astrocyte samples showed a strong band for GFAP at 213 bp while neuronal samples showed a strong band for NeuN at 127 bp. β-actin (100 bp) was used as a positive control for both samples. A non-template control (NTC) containing no cDNA was used as a negative control (Figure 3.3).

3.4.3 RNA quality decreases following LCM

The RNA integrity number (RIN) of each frozen tissue block (n=32) was analysed pre-LCM and post-LCM using the Agilent RNA 6000 Pico Chip (Agilent Technologies, USA) (Figure 3.4). The mean RIN of the tissue blocks pre-LCM was 3.0 (range 1-6.9). Following LCM, a decrease in RIN was observed. For astrocyte RNA samples the mean RIN was 2.4 (range 1-2.9) and for neuron RNA samples the mean RIN was 2.7 (range 2.2-2.9).

Case	Braak stage	pH	PMD	Tissue RIN	Astrocyte isolate conc/ ng/µl	Astrocyte isolate RIN	Neuron isolate conc/ ng/µl	Neuron isolate RIN
2	5	-	7.00	5.1	7.04	n/a	13.10	n/a
4	3	7.02	-	N/A	3.58	n/a	7.74	2.8
6	2	6.69	11.0	N/A	4.30	n/a	9.13	n/a
7	4	6.06	-	N/A	9.73	3.0	13.02	2.9
8	5	-	10.0	N/A	32.25	5.1	7.14	2.8
13	3	6.56	32.0	3.5	15.34	n/a	7.44	n/a
15	3	6.01	24.0	6.9	7.67	n/a	8.64	n/a
20	5	6.56	16.0	N/A	16.39	n/a	8.32	n/a
21	5	6.59	15.0	N/A	11.06	2.4	11.86	2.7
22	4	7.07	24.0	2.4	18.04	2.2	8.41	2.6
23	1	6.85	23.00	5.2	5.40	2.2	9.22	2.7
27	6	6.65	24.0	N/A	15.85	1.0	10.08	2.4
28	0	6.49	20.0	N/A	35.86	n/a	43.02	n/a
30	1	6.86	17.0	1.2	4.80	n/a	8.24	n/a
31	3	6.29	24.0	2.4	7.74	n/a	7.55	n/a
36	4	-	8.0	1	2.63	2.2	4.73	n/a
40	1	6.46	8.0	3.7	18.45	n/a	28.17	n/a
41	4	6.08	7.0	2.2	7.35	2.5	10.04	n/a
43	2	6.50	17.0	1	9.67	2.3	6.96	n/a
48	2	6.00	3.00	N/A	28.57	2.4	7.42	n/a
64	6	7.04	36.0	1	8.83	1.1	6.11	n/a
66	2	6.40	36.0	N/A	6.31	n/a	11.87	2.90
67	5	6.32	47.0	2.4	10.82	n/a	73.21	n/a
68	6	5.97	35.0	N/A	27.21	n/a	8.89	n/a
69	4	6.43	35.0	N/A	22.10	2.5	15.59	n/a
75	6	6.05	13.0	N/A	11.64	n/a	15.26	n/a
76	2	7.34	12.0	4.7	13.03	2.4	20.16	2.8
77	2	6.18	20.0	2.3	4.00	2.6	7.08	n/a
79	2	6.53	15.0	N/A	11.29	2.4	14.26	2.2
90	2	6.40	36.0	N/A	4.82	2.3	17.3	n/a
92	3	-	13.0	N/A	6.18	n/a	10.98	2.8
96	5	5.80	48.0	N/A	7.66	n/a	8.57	n/a

Table 3.3. Sub-cohort case details used in the LCM study: RNA integrity was assessed in 32 cases of the CFAS Cambridge neuropathology cohort selected based on brain pH measured at the time of death and post-mortem delay (PMD). RNA quality was also assessed post-LCM for all neuronal and astrocytic enriched samples.

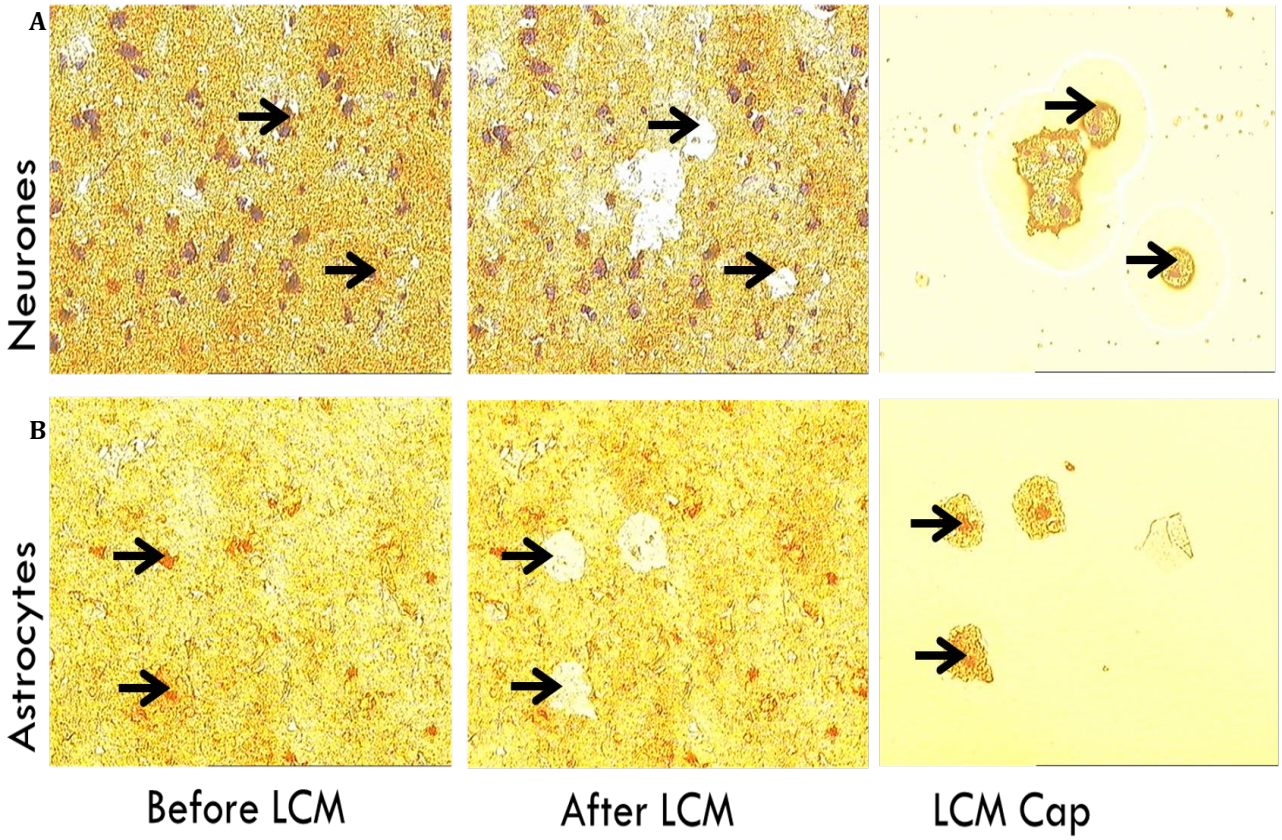

Figure 3.2. Isolation of neurons and astrocytes: Neurons identified by toluidine blue and GFAP^{+} astrocytes were isolated from temporal cortex sections of the CFAS Cambridge cohort. Isolation of neurons (A) (black arrows), isolation of astrocytes (B) (black arrows). Images taken at x200 magnification.

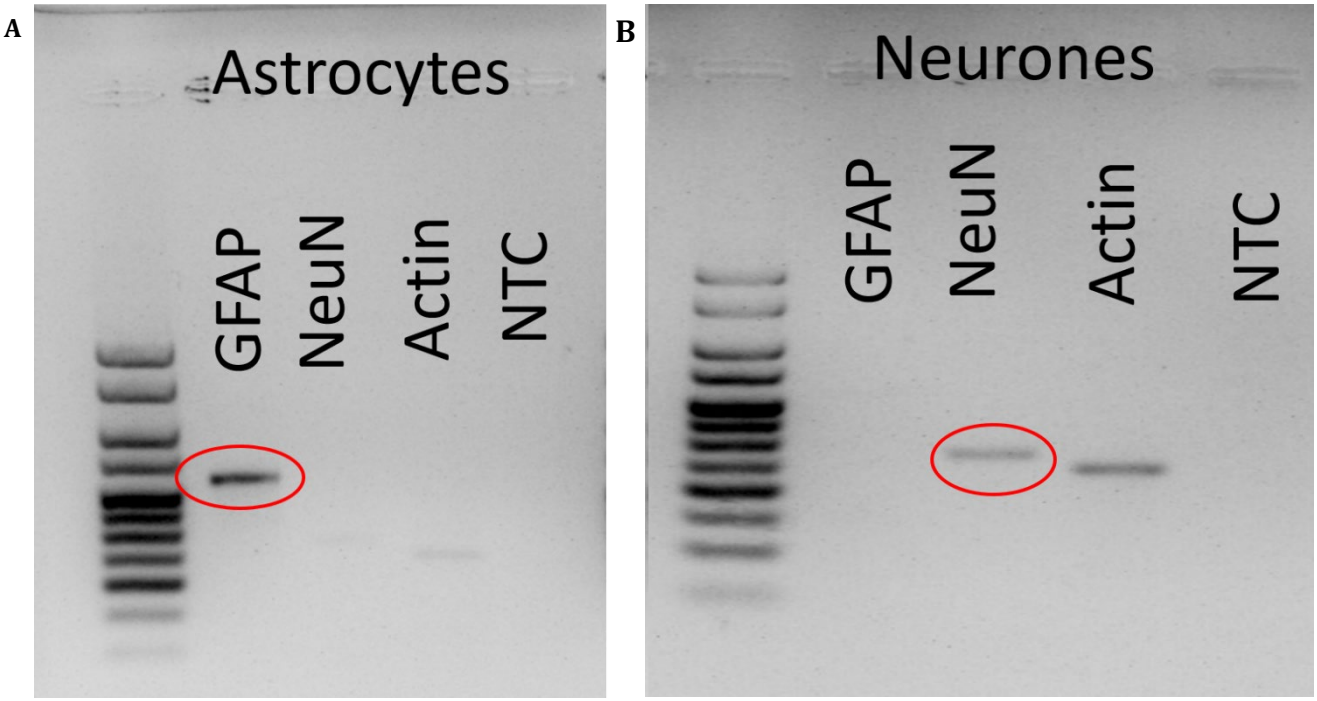

Figure 3.3. RT-PCR analysis of neurons and astrocytes isolated from post-mortem tissue using LCM: Astrocyte enriched samples are associated with high transcript levels of GFAP and low expression of NeuN (A, red ring). Neuronal enriched samples are associated with high transcript levels of NeuN and low expression of GFAP (B, red ring). Hyperladder V (Bioline, UK) was used to determine base pairs length and β-actin was used as a positive control.

3.4.4 Successful amplification of cholesterol biosynthetic genes using qPCR

qPCR was successfully carried out to determine the gene expression *HMGCR, CYP46A1, ABCA1* and *SREBP2* in astrocytes and neurons isolated from post-mortem human temporal cortex sections (Figure 3.5).

3.4.5 Relative concentration of cholesterol biosynthetic genes is not normally distributed in astrocytes and neurons

Distributions of relative concentration values for each gene were tested for normality using the Kolmogorov-Smirnov (KS) test. Histograms were also plotted to visualise the distribution of relative concentration values of the genes in astrocytes (Figure 3.6 B-E) and neurons (Figure 3.7 B-E). A non-parametric approach was used because although the KS values were not significant indicating a normal distribution however, inspection of histograms suggests that the data is not normally distributed. As a quality control measure the effect of pH and post-mortem delay (PMD) on the relative concentration values for the four genes was assessed using a Spearmen's rank correlation test for each cell type. No significant correlations between relative concentration in both astrocytes and neurons with pH and PMD (Table 3.4).

3.4.6 *SREBP2* relative concentration in astrocytes shows a trend to decrease with Braak and Braak stage

To determine how the relative concentration of cholesterol biosynthetic genes in astrocytes related to NFT progression, we examined the relationship to Braak and Braak groups. No significant differences or trends were observed for *HMGCR, CYP46A1* and *ABCA1* between Braak and Braak groups in astrocytes (Figure 3.8). However, a significant trend to decrease between *SREBP2* relative concentration and Braak and Braak groups was observed (JT; p= 0.031), but a significant difference between Braak and Braak groups was not observed (KW; p=0.120).

A

Pre-LCM

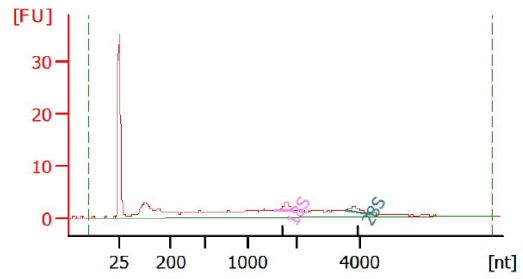

Overall Results for sample 5 : 76

RNA Area:	96.4
RNA Concentration:	431 pg/µl
rRNA Ratio [28s / 18s]:	0.8
RNA Integrity Number (RIN):	4.7 (B.02.08)
Result Flagging Color:	
Result Flagging Label:	RIN: 4.70

B

Post LCM

Astrocytes

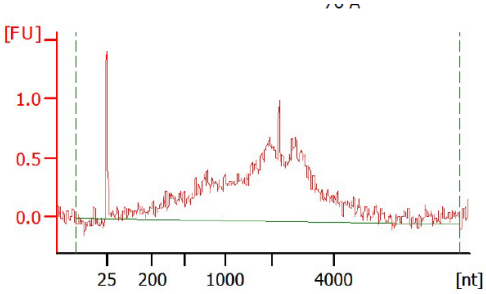

Overall Results for sample 4 : 76 A

RNA Area:	23.5
RNA Concentration:	144 pg/µl
rRNA Ratio [28s / 18s]:	0.0
RNA Integrity Number (RIN):	2.4 (B.02.08)
Result Flagging Color:	
Result Flagging Label:	RIN: 2.40

C

Post LCM

Neuron

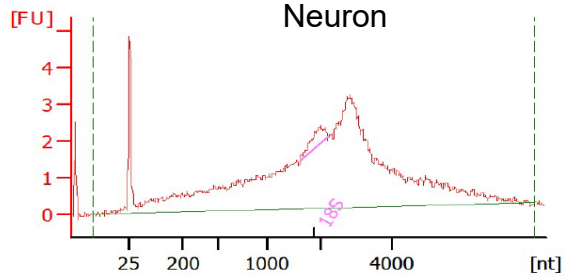

Overall Results for sample 5 : 76 N

RNA Area:	88.8
RNA Concentration:	544 pg/µl
rRNA Ratio [28s / 18s]:	0.0
RNA Integrity Number (RIN):	2.8 (B.02.08)
Result Flagging Color:	
Result Flagging Label:	RIN: 2.80

Figure 3.4. RNA quality human post-mortem CNS samples cases before and after LCM: The RNA quality of the frozen tissue samples was assessed on the Agilent 2100 bioanalyser, (A) represents a suitable sample for LCM with a RIN value of 4.7. LCM reduces the quality of RNA (B) astrocytic post-LCM RNA, RIN 2.4 and (C) neuronal post-LCM RNA, RIN 2.8.

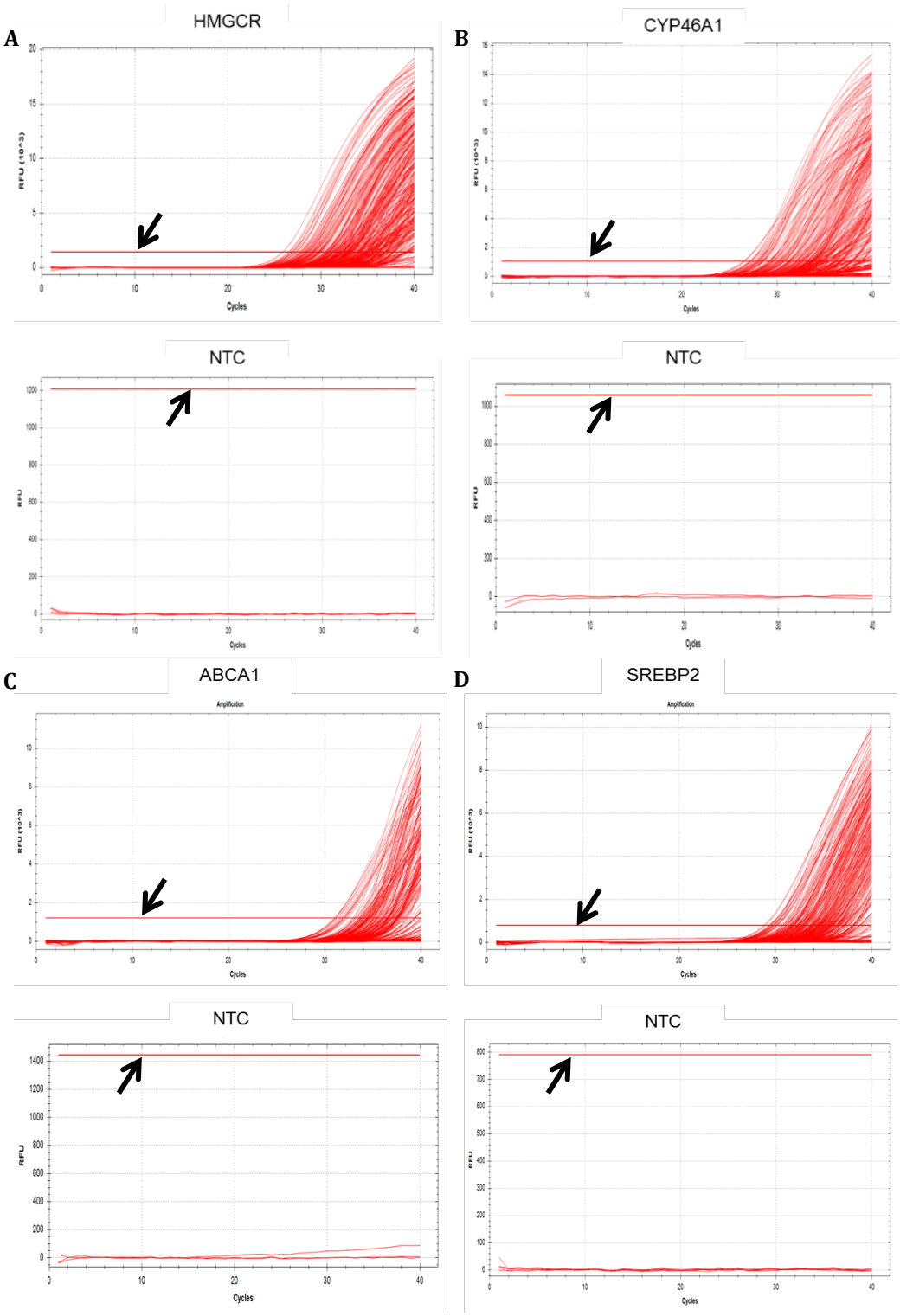

Figure 3.5. Successful gene amplification using qPCR: The qPCR amplification curves for astrocytes and neurons to determine gene expression for *HMGCR, CYP46A1, ABCA1* and *SREBP2* respectively and corresponding NTC curve (A-D). Threshold value (black arrow).

A

	HMGCR Astrocytes	CYP46A1 Astrocytes	ABCA1 Astrocytes	SREBP2 Astrocytes
n	15	9	8	9
Mean	1.14	1.17	1.64	1.00
SEM	0.27	0.23	0.47	0.23
Median	0.82	0.94	1.19	1.04
SD	1.06	0.70	1.34	0.69
IQR	0.52-1.48	0.76-1.32	0.89-2.38	0.45-1.30
KS	0.265	0.296	0.340	0.204

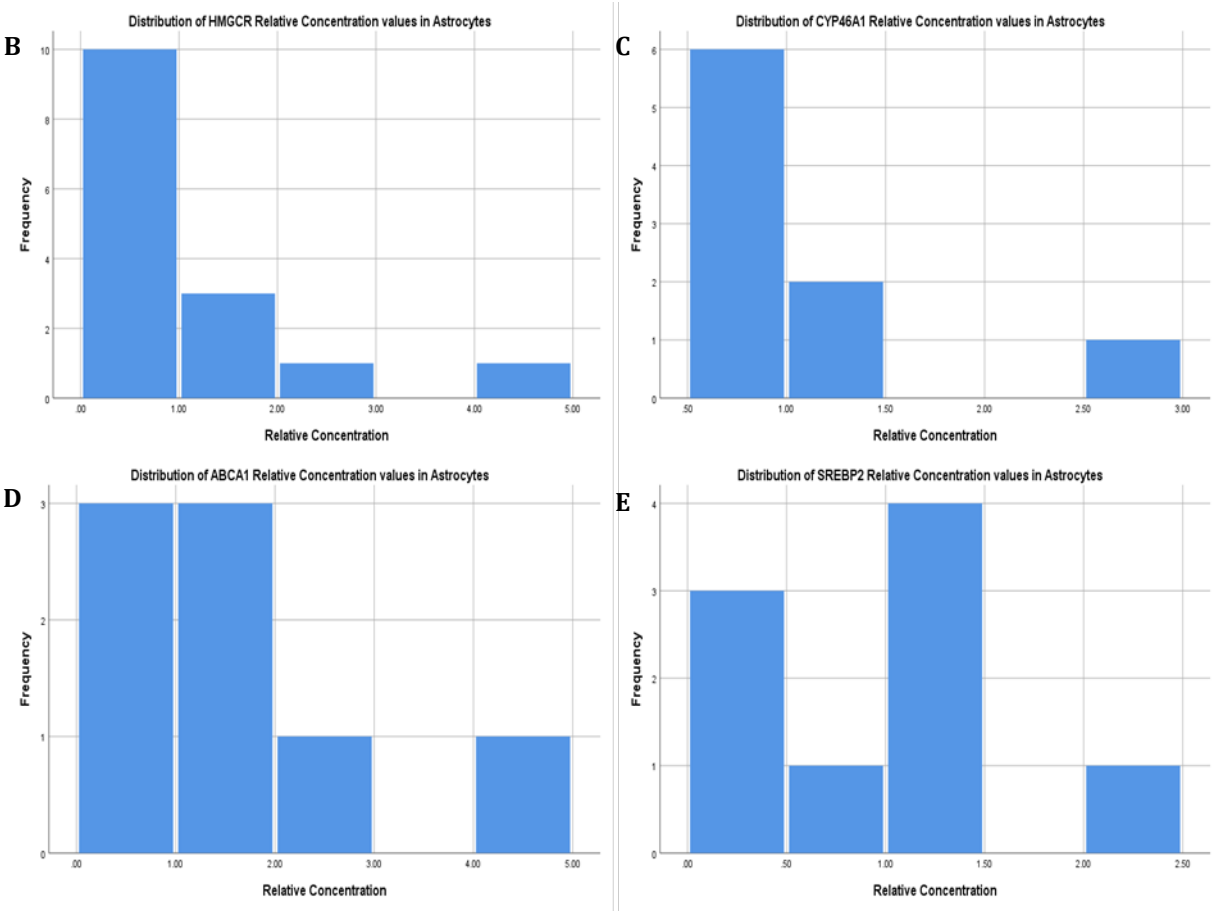

Figure 3.6. Distribution of the expression of key genes involved in cholesterol biosynthesis in isolated astrocytes: Relative concentration (RC) values for each gene were calculated relative to Braak and Braak Group 1, using the ΔΔCT calculations following normalisation to β-actin expression. The table shows the descriptive statistical values for each gene in astrocytes (A). Data was tested for normality using Kolmogorov-Smirnov (KS). The distribution of the RC values for HMGCR, CYP46A1, ABCA1 and SREBP2 respectively on a histogram (B-E).

A

	HMGCR Neurons	CYP46A1 Neurons	ABCA1 Neurons	SREBP2 Neurons
n	23	20	14	17
Mean	0.94	1.440	0.98	2.68
SEM	0.26	0.33	0.22	0.98
Median	0.61	1.02	0.76	0.83
SD	1.23	1.47	0.83	4.04
IQR	0.44-0.75	0.56-1.90	0.23-1.56	0.52-2.95
KS	0.371	0.210	0.184	0.276

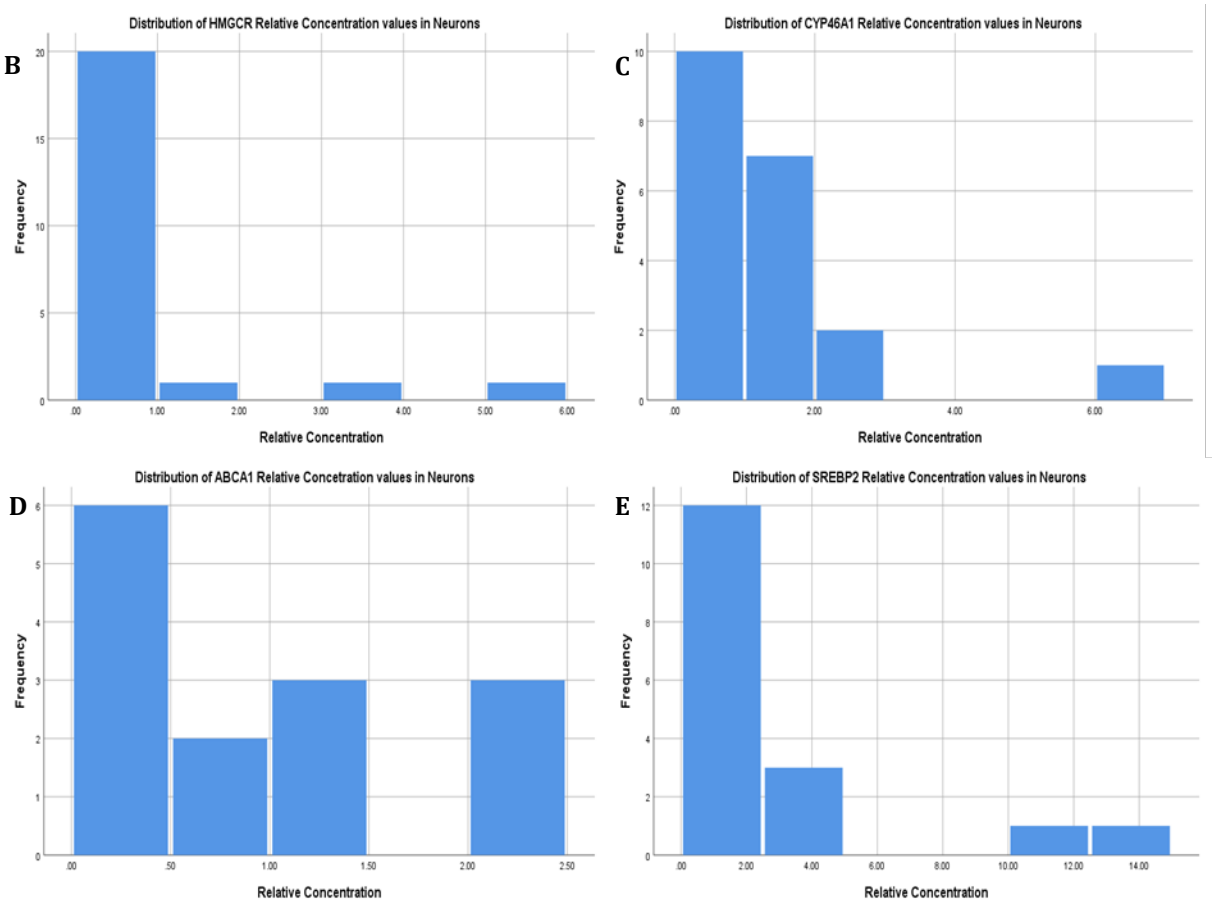

Figure 3.7. Distribution of the expression of key genes involved in cholesterol biosynthesis in isolated neurons: Relative concentration (RC) values for each gene were calculated relative to Braak and Braak Group 1, using the ΔΔCT calculations following normalisation to β-actin expression. The table shows the descriptive statistical values for each gene in neurons (A). Data was tested for normality using Kolmogorov-Smirnov (KS). The distribution of the RC values for HMGCR, CYP46A1, ABCA1 and SREBP2 respectively on a histogram (B-E).

A

	pH	PMD
HMGCR Astrocytes	r = 0.077 p = 0.802	r = 0.002 p = 0.994
CYP46A1 Astrocytes	r = 0.000 p = 1.000	r = -0.395 p = 0.293
ABCA1 Astrocytes	r = -0.464 p = 0.294	r = 0.108 p = 0.799
SREBP2 Astrocytes	r = 0.217 p = 0.606	r = 0.361 p = 0.339

B

	pH	PMD
HMGCR Neurons	r = 0.315 p = 0.177	r = -0.305 p = 0.179
CYP6A1 Neurons	r = -0.222 p = 0.376	r = 0.063 p = 0.805
ABCA1 Neurons	r = -0.517 p = 0.085	r = -0.025 p = 0.936
SREBP2 Neurons	r = -0.477 p = 0.062	r = -0.109 p = 0.699

Table 3.4. Correlation matrix between cholesterol biosynthetic gene expression in astrocytes and neurons with pH and PMD: Spearmen's rank correlation test was carried out to determine any correlations between relative concentration values for cholesterol biosynthetic genes from astrocytes (A) and neurons (B) with pH and post-mortem delay (PMD). Where r is the correlation coefficient and p is the significance value. Relative concentration values for each gene were calculated relative to Braak and Braak Group 1.

A

		Braak Groups			KW	JT
		0-II	III-IV	V-VI		
HMGCR Astrocytes	n	8	4	3	0.544	0.826
	Mean	1.40	0.74	1.01		
	SEM	0.49	0.28	0.16		
	Median	0.79	0.64	0.88		
	SD	1.38	0.57	0.28		
	Range	4.03	1.36	0.50		
CYP46A1 Astrocytes	n	4	3	2	0.539	0.571
	Mean	1.02	1.61	0.80		
	SEM	0.13	0.67	0.14		
	Median	0.92	1.22	0.80		
	SD	0.26	1.16	0.20		
	Range	0.56	2.22	0.28		
ABCA1 Astrocytes	n	5	1	2	0.747	0.469
	Mean	1.61	1.23	1.94		
	SEM	0.74	-	0.79		
	Median	0.90	1.23	1.94		
	SD	1.65	-	1.12		
	Range	4.09	-	1.58		
SREBP2 Astrocytes	n	6	1	2	0.120	0.031*
	Mean	1.29	0.60	0.33		
	SEM	0.27	-	0.12		
	Median	1.22	0.60	0.33		
	SD	0.66	-	0.17		
	Range	2.03	-	0.24		

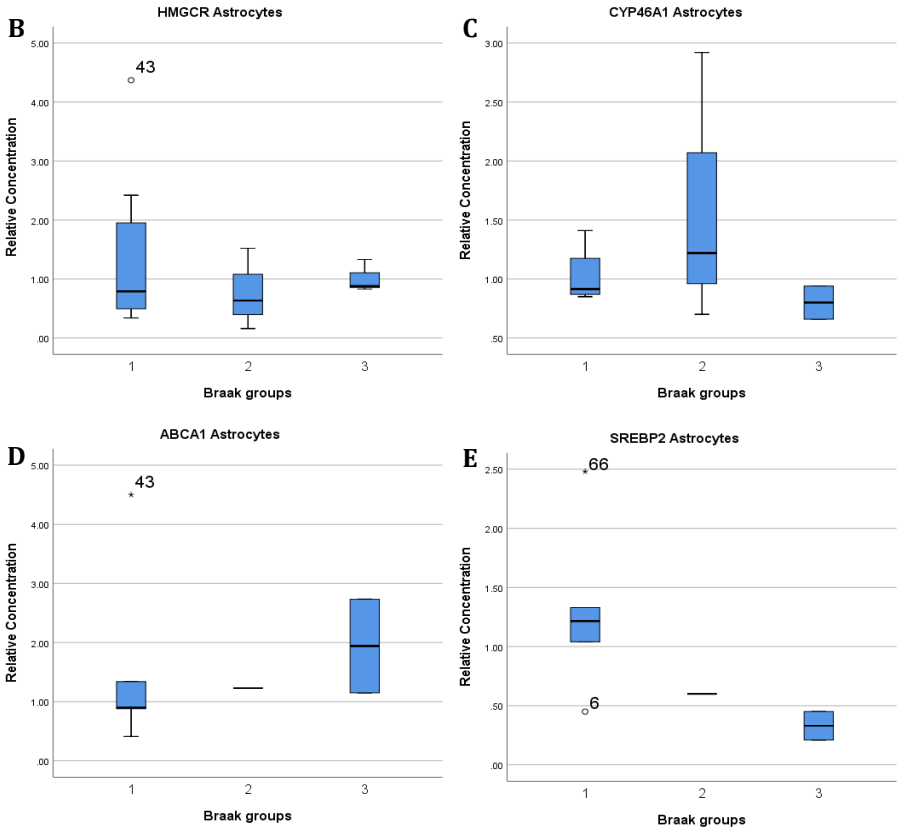

Figure 3.8. SREBP2 gene expression in astrocytes decreases with Braak and Braak groups: The table shows the descriptive statistical values for each gene in astrocytes in each Braak and Braak group. The table also shows the p values for KW and JT tests to assess differences between the RC values in astrocytes for cholesterol biosynthetic genes and Braak and Braak groups (A). Box plots show the distribution of astrocytic relative concentration for (y-axis) *HMGCR, CYP46A1, ABCA1* and *SREBP2* respectively across Braak and Braak groups (x-axis) (B-E). *SREBP2* expression in astrocytes suggests a significant trend to decrease as Braak and Braak group increases. No significant differences between *HMGCR, CYP46A1* and *ABCA1* astrocytic gene expression and Braak and Braak groups were identified. Relative concentration values for each gene were calculated relative to Braak and Braak Group 1.

A

		Braak Groups			KW	JT
		0-II	III-IV	V-VI		
HMGCR Neurons	n	9	8	6	0.115	0.079
	Mean	1.56	0.53	0.55		
	SEM	0.61	0.08	0.08		
	Median	0.67	0.48	0.51		
	SD	1.84	0.21	0.19		
	Range	5.43	0.65	0.48		
CYP46A1 Neurons	n	8	8	4	0.893	0.725
	Mean	1.33	1.74	1.09		
	SEM	0.26	0.78	0.40		
	Median	1.49	0.79	0.81		
	SD	0.74	2.20	0.81		
	Range	2.31	6.57	1.81		
ABCA1 Neurons	n	3	8	3	0.639	0.457
	Mean	0.75	0.93	1.32		
	SEM	0.28	0.32	0.63		
	Median	0.93	0.54	1.33		
	SD	0.48	0.90	1.09		
	Range	0.91	2.23	2.18		
SREBP2 Neurons	n	5	6	6	0.046*	0.011*
	Mean	0.89	1.41	5.43		
	SEM	0.45	0.62	2.41		
	Median	0.48	0.70	2.58		
	SD	1.00	1.51	5.91		
	Range	2.35	3.98	13.78		

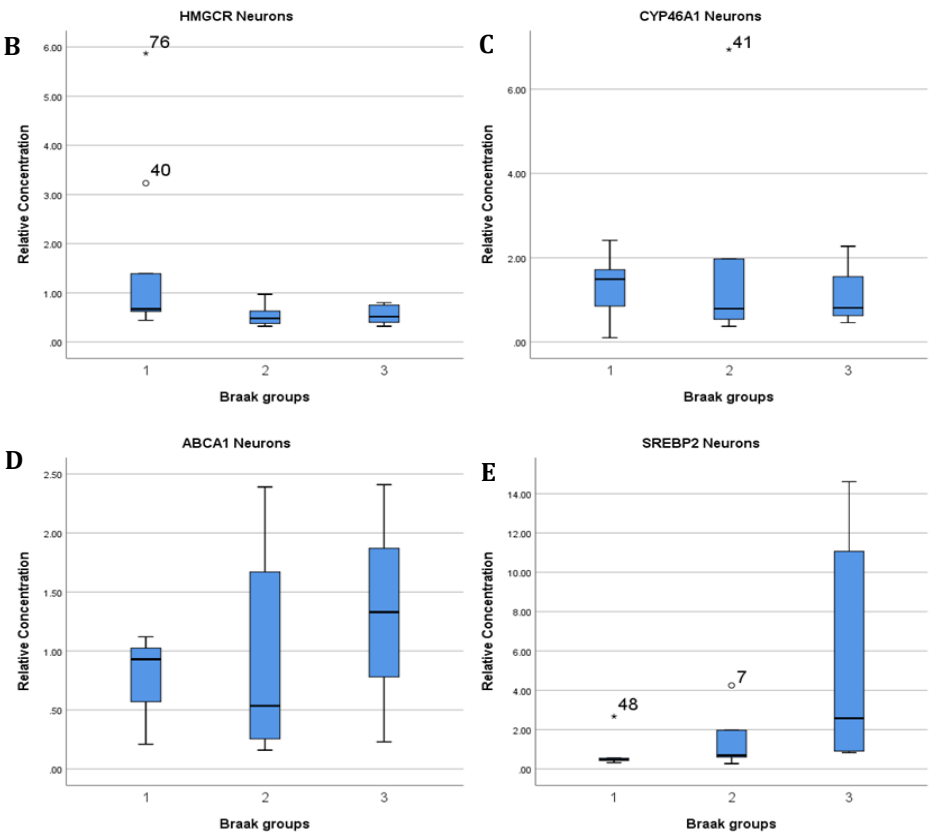

Figure 3.9. SREBP2 gene expression in neurons increases with Braak and Braak groups: The table shows the descriptive statistical values for each gene in neurons in each Braak and Braak group. The table also shows the p values for KW and JT tests to assess differences between the relative concentration values in neurons for cholesterol biosynthetic genes and Braak and Braak groups (A). Box plots show the distribution of neuronal relative concentration for (y-axis) *HMGCR, CYP46A1, ABCA1* and *SREBP2* respectively across Braak and Braak groups (x-axis) (B-E). *SREBP2* expression in neurons suggests a significant difference and trend to increase as Braak and Braak group increases. No significant differences between *HMGCR, CYP46A1* and *ABCA1* neuronal gene expression and Braak and Braak groups were identified. Relative concentration values for each gene were calculated relative to Braak and Braak Group 1.

3.4.7 *SREBP2* relative concentration in neurons increase with Braak and Braak stage

To determine how the relative concentration of cholesterol biosynthetic genes in neurons related to NFT progression, we examined the relationship to Braak and Braak groups. No significant differences or trends were observed between *HMGCR, CYP46A1* and *ABCA1* with Braak and Braak groups in neurons (Figure 3.9). However, a significant difference (KW; p=0.046) and a trend to increase (JT; p=0.011) was observed between *SREBP2* relative concentration and Braak and Braak groups was observed. Post hoc analysis following Bonferroni correction, showed a significant difference between Braak and Braak group 1 and Braak and Braak group 3 (KW; p=0.045).

3.4.8 *HMGCR* and *SREBP2* relative concentration in neurons decreases and increases with neurofibrillary tangle pathology respectively

To determine how the relative concentration of cholesterol biosynthetic genes in astrocytes and neurons related to tangle pathology, we examined the relationship to local CERAD neurofibrillary tangle score in the cortex (Savva *et al.*, 2009; Wharton *et al.*, 2011). No significant differences or trends were observed between any of the four genes with tangle score in astrocytes (Figure 3.10). No significant differences or trends were observed between *CYP46A1* and *ABCA1* neuronal relative concentration with tangle score (Figure 3.11). *HMGCR* expression in neurons also showed a trend to decrease (JT; p=0.022) as tangle score increases. Post hoc analysis following Bonferroni correction, showed no significant difference between tangle scores. A significant difference (KW; p=0.022) and a trend to increase (JT; p=0.005) was observed between *SREBP2* relative concentration and tangle score. Post hoc analysis following Bonferroni correction, showed a significant difference between tangle score of 3 and tangle score of 0 (KW; p=0.027) and trend (JT; p=0.021).

A

Genes	Tangle Score	
	KW	JT
HMGCR Astrocytes	0.221	0.660
CYP46A1 Astrocytes	0.828	0.910
ABCA1 Astrocytes	0.707	0.354
SREBP2 Astrocytes	0.161	0.127

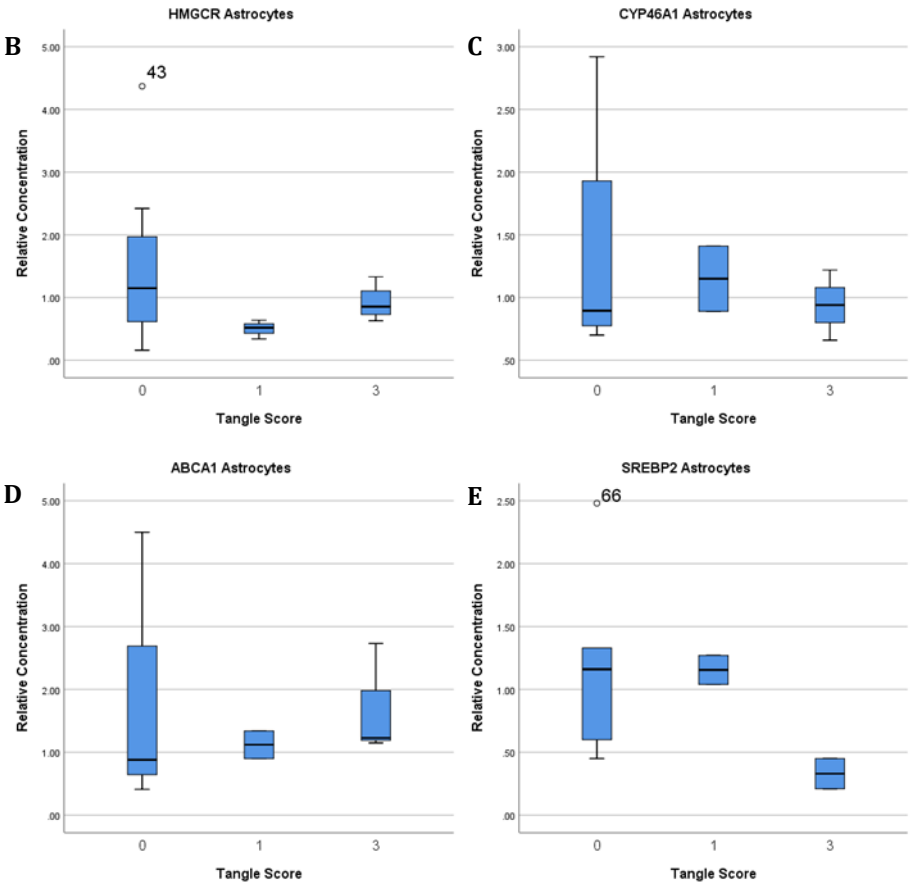

Figure 3.10. Cholesterol biosynthetic gene relative concentration changes in astrocytes do not change with tangle pathology: No significant differences between astrocytic gene expression and tangle scores were identified (A). Box plots showing the distribution of astrocytic relative concentration (y-axis) for *HMGCR, CYP46A1, ABCA1* and *SREBP2* respectively across tangle scores (x-axis) (B-E). 0= no tangles, 1= mild tangles 3=moderate-severe tangles. Relative concentration values for each gene were calculated relative to Braak and Braak Group 1.

A

Genes	Tangle Score	
	KW	JT
HMGCR Neurons	0.059	0.022*
CYP46A1 Neurons	0.418	0.171
ABCA1 Neurons	0.103	0.639
SREBP2 Neurons	0.022*	0.005*

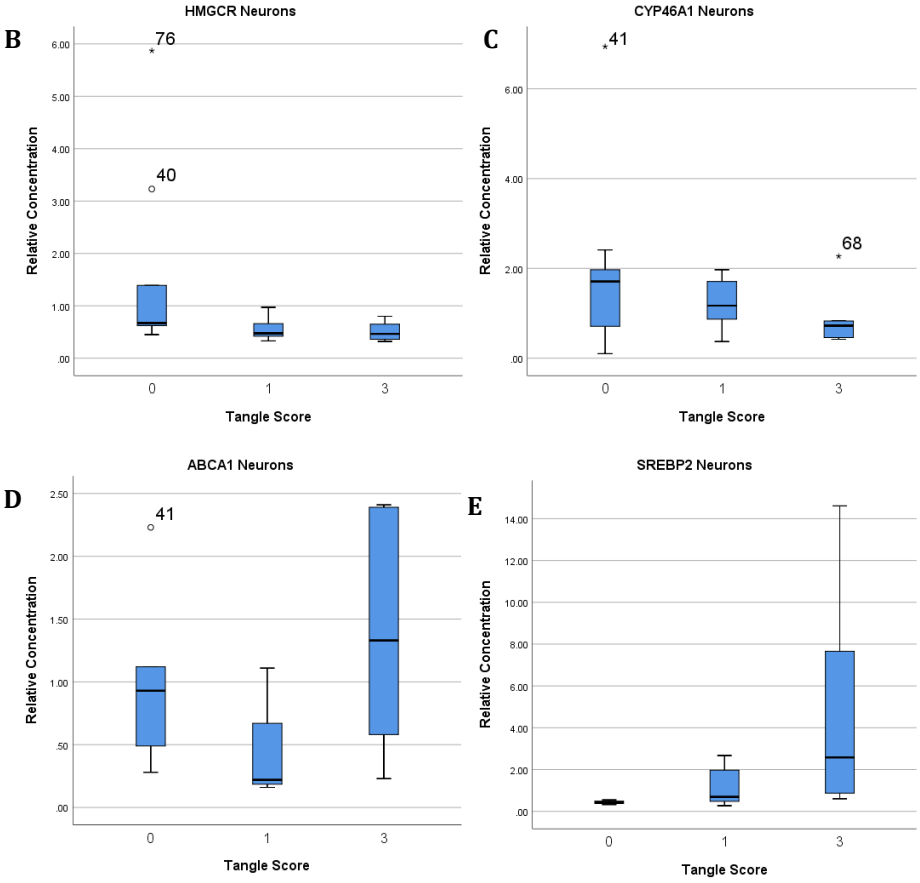

Figure 3.11. HMGCR and SREBP2 relative concentration in neurons decreases and increases with tangle pathology respectively: No significant differences between neuronal *CYP46A1* and *ABCA1* relative concentration and tangle scores were identified (A). *SREBP2* expression in neurons suggests a significant difference and trend to increase as tangle score increases. *HMGCR* expression in neurons suggests a significant trend to decrease as tangle score increases. Box plots showing the distribution of astrocytic relative concentration (y-axis) for *HMGCR, CYP46A1, ABCA1* and *SREBP2* respectively across tangle scores (x-axis) (B-E). 0= no tangles, 1= mild tangles 3=moderate-severe tangles. Relative concentration values for each gene were calculated relative to Braak and Braak Group 1.

3.4.9 Cholesterol biosynthesis gene expression in astrocytes and neurons does not change with Thal Aβ phases.

To determine whether the cholesterol biosynthesis gene expression in astrocytes and neurons relates to Aβ progression, we examined the relationship to Thal Aβ phases. Relative concentration values for each gene were calculated relative to Thal Group 1. No significant differences or trends were observed between any of the four cholesterol biosynthetic gene relative concentration with Thal Aβ groups in both astrocytes (Figure 3.12) and neurons (Figure 3.13).

3.4.10 *HMGCR* gene relative concentration in neurons decreases with plaque pathology

To determine how the relative concentration of cholesterol biosynthetic genes in astrocytes and neurons related to plaque pathology, we examined the relationship to local CERAD plaque score in the cortex (Savva *et al.*, 2009; Wharton *et al.*, 2011). No significant differences or trends were observed between any of the four genes with plaque score in astrocytes (Figure 3.14). No significant difference or trends were observed between *CYP46A1, ABCA1* and *SREBP2* gene relative concentration with plaque score in neurons (Figure 3.15). However, a significant difference (KW; p=0.022) and a trend to increase (JT; p=0.020) was observed between *HMGCR* relative concentration and plaque score. Post hoc analysis following Bonferroni correction, showed a significant difference between plaque score of 1 and plaque score of 0 (KW; p=0.042) and trend (JT; p=0.031). Relative concentration values for each gene were calculated relative to Thal Group 1.

A

		Thal Groups			KW	JT
		0-1	2-3	4-5		
HMGCR Astrocytes	n	7	3	5	0.600	0.483
	Mean	1.47	0.88	1.41		
	SEM	0.63	0.46	0.38		
	Median	0.89	0.73	1.00		
	SD	1.67	0.79	0.86		
	Range	4.73	1.56	2.13		
CYP46A1 Astrocytes	n	5	1	3	0.241	0.723
	Mean	1.13	0.57	1.07		
	SEM	0.32	-	0.15		
	Median	0.76	0.57	0.97		
	SD	0.71	-	0.26		
	Range	1.68	-	0.49		
ABCA1 Astrocytes	n	5	-	3	0.297	0.513
	Mean	1.40	-	1.86		
	SEM	0.64	-	0.46		
	Median	0.79	-	1.70		
	SD	1.44	-	0.80		
	Range	3.56	-	1.58		
SREBP2 Astrocytes	n	5	3	1	0.664	0.408
	Mean	1.07	1.15	0.52		
	SEM	0.16	0.70	-		
	Median	1.18	0.70	0.52		
	SD	0.36	1.21	-		
	Range	0.90	2.28	-		

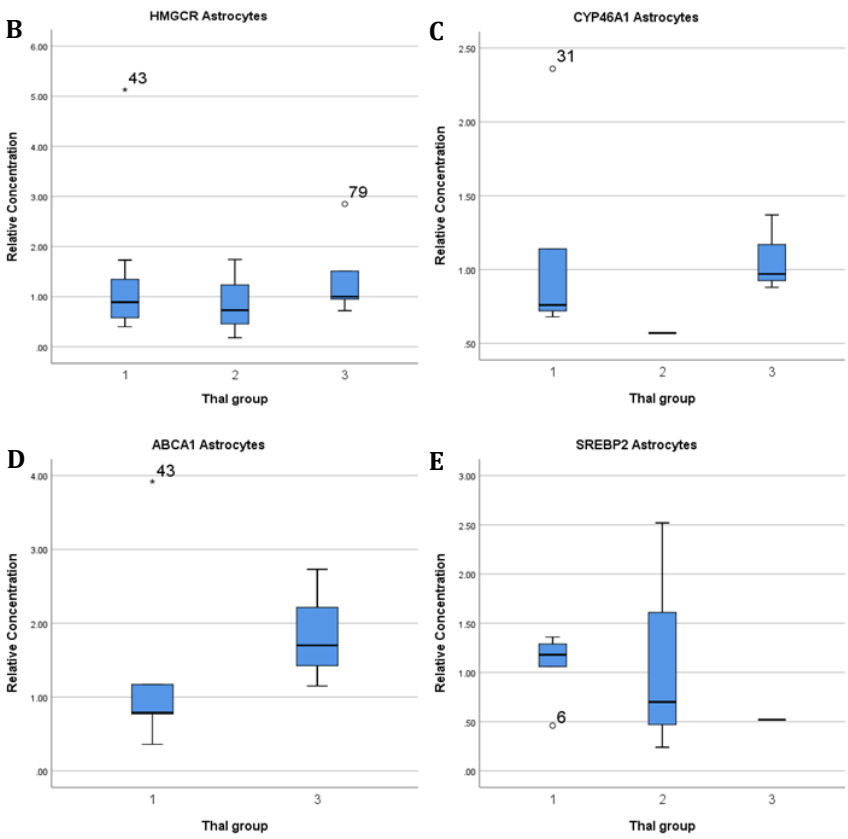

Figure 3.12. Cholesterol biosynthetic gene relative concentration in astrocytes does not change with Thal groups: The table shows the descriptive statistical values for each gene in astrocytes in each Thal group. The table also shows the p values for KW and JT tests to assess differences between the relative concentration values in astrocytes for cholesterol biosynthetic genes and Thal groups (A). Box plots show the distribution of astrocytic relative concentration for (y-axis) *HMGCR, CYP46A1, ABCA1* and *SREBP2* respectively across Thal groups (x-axis) (B-E). No significant differences between cholesterol biosynthetic gene relative concentration in astrocytes and Thal groups were identified. Relative concentration values for each gene were calculated relative to Thal Group 1.

A

		Thal Groups			KW	JT
		0-1	2-3	4-5		
HMGCR Neurons	n	7	9	7	0.075	0.051
	Mean	1.31	1.48	0.53		
	SEM	0.47	0.72	0.10		
	Median	0.76	0.81	0.50		
	SD	1.24	2.16	0.25		
	Range	3.43	6.76	0.80		
CYP46A1 Neurons	n	7	7	6	0.630	0.627
	Mean	1.35	2.29	0.98		
	SEM	0.29	0.97	0.32		
	Median	1.41	1.90	0.70		
	SD	0.76	2.56	0.77		
	Range	2.07	7.33	2.05		
ABCA1 Neurons	n	3	6	5	0.513	0.374
	Mean	1.24	1.52	2.17		
	SEM	0.59	0.58	0.70		
	Median	0.76	1.08	2.08		
	SD	1.02	1.42	1.57		
	Range	1.87	3.25	3.40		
SREBP2 Neurons	n	4	5	8	0.252	0.152
	Mean	1.02	5.50	5.19		
	SEM	0.11	3.10	2.60		
	Median	1.05	2.83	2.21		
	SD	0.22	6.93	7.36		
	Range	0.53	16.85	21.87		

B

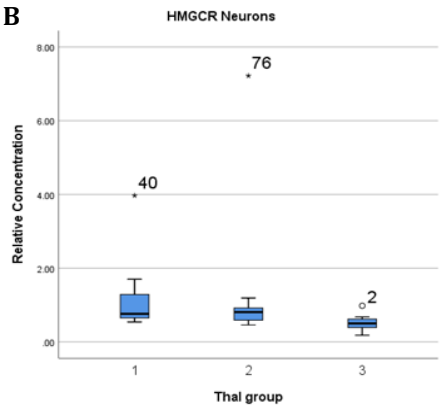

C

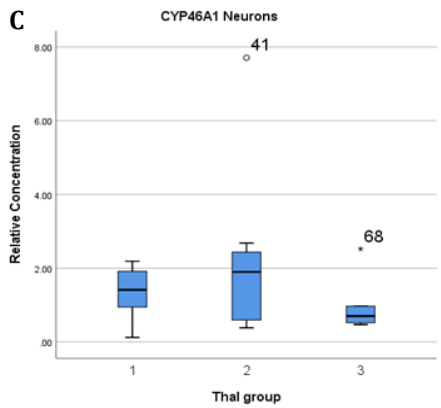

D

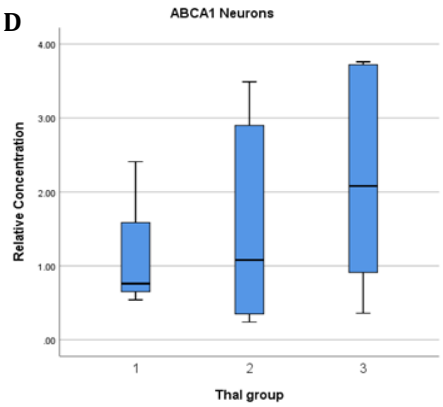

E

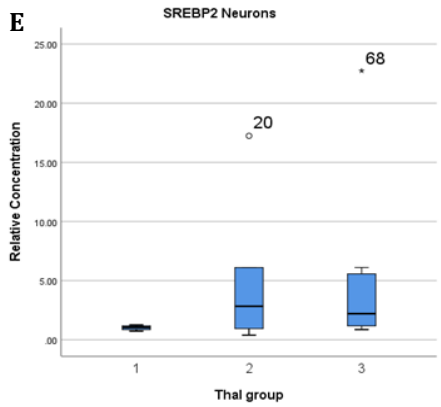

Figure 3.13. Cholesterol biosynthetic gene relative concentration in neurons does not change with Thal groups: The table shows the descriptive statistical values for each gene in neurons in each Thal group. The table also shows the p values for KW and JT tests to assess differences between the relative concentration values in neurons for cholesterol biosynthetic genes and Thal groups (A). Box plots show the distribution of astrocytic relative concentration for (y-axis) *HMGCR, CYP46A1, ABCA1* and *SREBP2* respectively across Thal groups (x-axis) (B-E). No significant differences between cholesterol biosynthetic gene relative concentration in neurons and Thal groups were identified. Relative concentration values for each gene were calculated relative to Thal Group 1.

A

Genes	Plaque Score	
	KW	JT
HMGCR Astrocytes	0.794	0.794
CYP46A1 Astrocytes	0.444	0.448
ABCA1 Astrocytes	0.297	0.297
SREBP2 Astrocytes	0.439	0.439

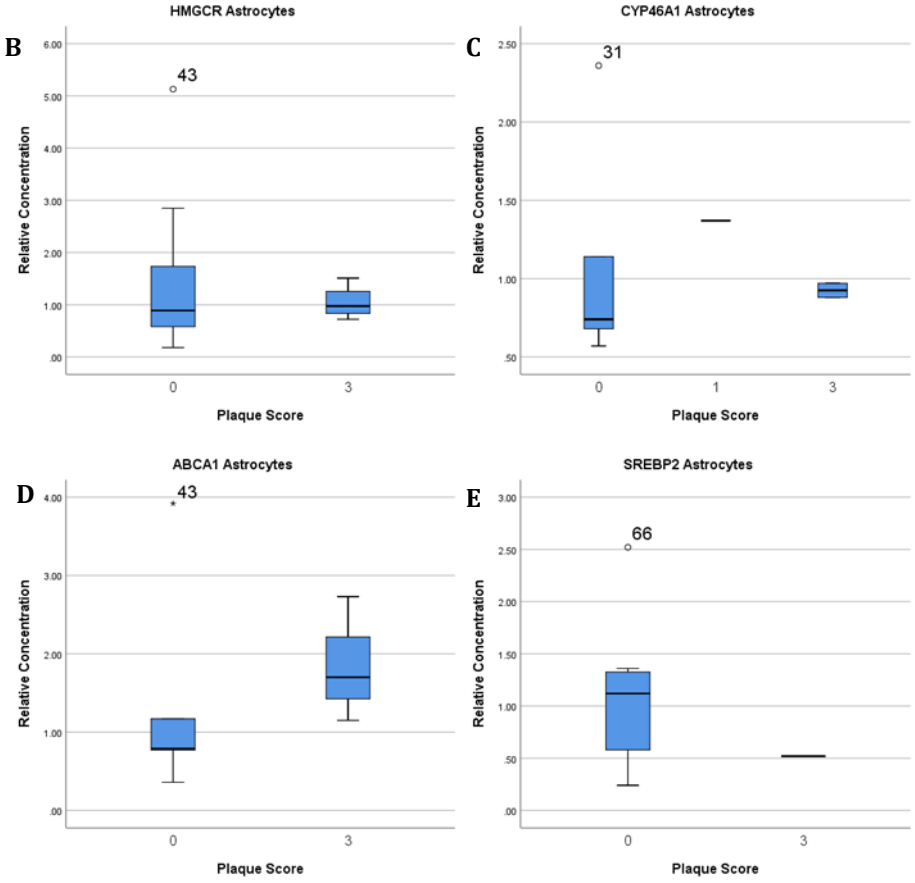

Figure 3.14. Cholesterol biosynthetic gene relative concentration changes in astrocytes do not change with plaque pathology: No significant differences between astrocytic gene expression and plaque scores were identified (A). Box plots showing the distribution of astrocytic relative concentration (y-axis) for *HMGCR, CYP46A1, ABCA1* and *SREBP2* respectively across plaque scores (x-axis) (B-E). 0= no plaques, 1= mild plaques 3= moderate-severe plaques. Relative concentration values for each gene were calculated relative to Thal Group 1.

Genes	Plaque Score	
	KW	JT
HMGCR Neurons	0.022*	0.020*
CYP46A1 Neurons	0.084	0.074
ABCA1 Neurons	0.383	0.953
SREBP2 Neurons	0.191	0.064

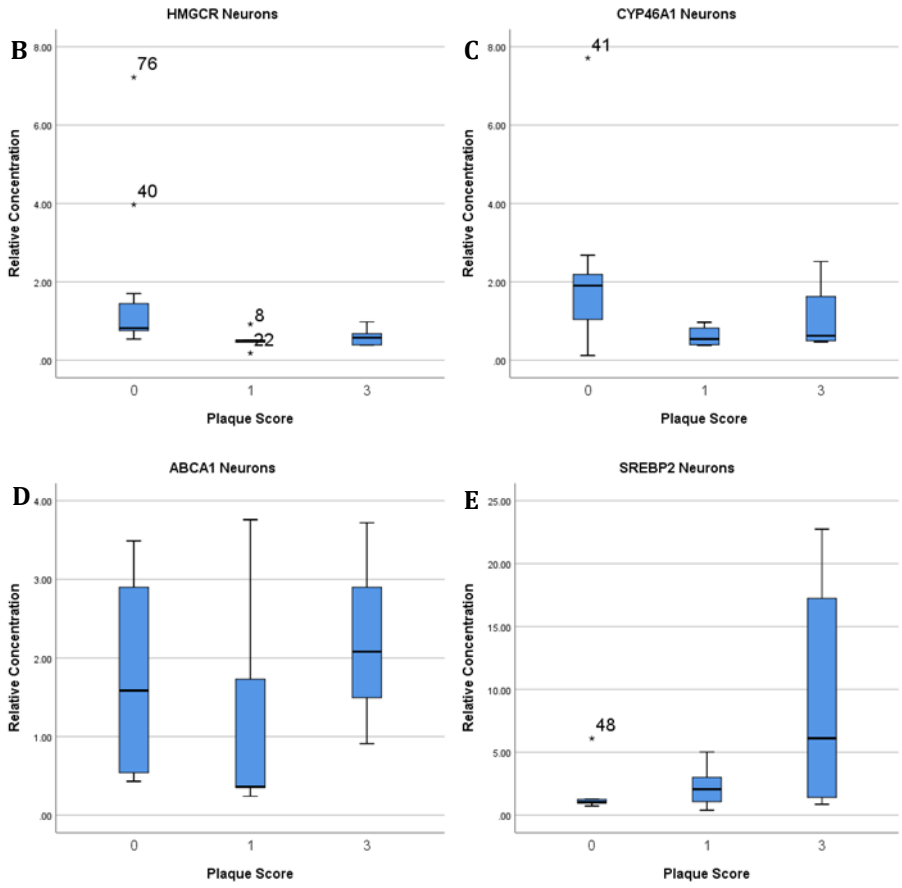

Figure 3.15. HMGCR gene relative concentration changes in neurons decreases with plaque pathology: No significant differences between *CYP46A1, ABCA1* and *SREBP2* neuronal gene expression and plaque scores were identified (A). *HMGCR* expression in neurons suggests a significant difference and trend to decrease as plaque score increases. Box plots showing the distribution of astrocytic relative concentration (y-axis) for *HMGCR, CYP46A1, ABCA1* and *SREBP2* respectively across plaque scores (x-axis) (B-E). 0= no plaques, 1= mild plaques 3= moderate-severe plaques. Relative concentration values for each gene were calculated relative to Thal Group 1.

3.4.11 *HMGCR, ABCA1* and *SREBP2* gene relative concentration in neurons correlate with AT8 immunoreactivity

To assess whether the cholesterol biosynthetic gene relative concentration in astrocytes and neurons were related to local AD pathology we examined the relationship of two classical markers of AD pathology; namely the extent of Aβ and AT8 pathology determined by percentage area immunoreactivity in the temporal cortex, previously determined in our lab group (J E Simpson *et al.*, 2010). No significant correlations between cholesterol biosynthetic gene relative concentration in astrocytes and markers of classical AD pathology were observed (Figure 3.16 A). No significant correlations between *CYP46A1* gene relative concentration in neurons and markers of classical AD pathology were observed (Figure 3.16 B). The relative concentration of *HMGCR* in neurons showed a moderate negative correlation with AT8 immunoreactivity (r=-0.458, p=0.032) (Figure 3.16 C). The relative concentrations of *ABCA1* and *SREBP2* in neurons showed moderate positive correlations with AT8 immunoreactivity (r=0.541, p=0.046; r=0.574, p=0.016 respectively) (Figure 3.16 D and E respectively).

3.4.12 *HMGCR* gene relative concentration in neurons correlates with markers of DNA damage in neurons

To assess whether the cholesterol biosynthetic gene relative concentration in astrocytes and neurons were related to markers of oxidative stress and DNA damage, we examined the relationship of oxidative stress markers (Malondialdehyde [MDA] and 8-hydroxydeoxyguanosine [8-OHdG]) and DNA damage markers (γH2AX), previously determined in our lab group (J. E. Simpson *et al.*, 2010). This study found that no significant correlations between cholesterol biosynthetic gene relative concentration in astrocytes and MDA protein expression and 8-OHdG immunoreactivity. Furthermore, we found no significant correlations cholesterol biosynthetic gene relative concentration in astrocytes and γH2AX immunoreactivity in astrocytes and neurons (Figure 3.17 A). This study also found that no significant correlations between cholesterol biosynthetic gene relative concentration in neurons and MDA protein expression and 8-OHdG immunoreactivity. We also found no significant correlations in *CYP46A1, ABCA1* and SREBP2 gene relative concentration in neurons and γH2AX immunoreactivity in astrocytes and neurons (Figure 3.17 B). However, the relative concentration of *HMGCR* in neurons showed a moderate positive correlation with γH2AX immunoreactivity in neurons (r=0.419,

p=0.046) but no significant correlation was observed with γH2AX immunoreactivity in astrocytes (Figure 3.17 C).

3.4.13 *HMGCR* gene relative concentration in neurons correlates with markers of neuroinflammation

To assess whether the cholesterol biosynthetic gene relative concentration in astrocytes and neurons were related to markers of neuroinflammation and gliosis, we examined the relationship of neuroinflammation markers (MHC class 2 and CD68) and gliosis markers (GFAP), previously determined in our lab group (J. E. Simpson *et al.*, 2010). This study found that no significant correlations between cholesterol biosynthetic gene relative concentration in astrocytes and MHCII and CD68 immunoreactivity. Furthermore, we found no significant correlations cholesterol biosynthetic gene relative concentration in astrocytes and GFAP immunoreactivity (Figure 3.18 A). This study also found that no significant correlations between *CYP46A1, ABCA1* and SREBP2 gene relative concentration in neurons and MHCII, CD68 and GFAP immunoreactivity (Figure 3.18 B). The relative concentration of *HMGCR* in neurons showed a moderate positive correlation with MHCII immunoreactivity (r=0.490, p=0.039) but no significant correlation was observed with CD68 and GFAP immunoreactivity (Figure 3.18 C).

3.4.14 Cholesterol biosynthetic gene relative concentration in astrocytes and neurons does not correlate with markers of cholesterol biosynthesis and metabolism

To assess whether the cholesterol biosynthetic gene relative concentration in astrocytes and neurons was related to markers of cholesterol biosynthesis and metabolism, we examined the relationship of HMGCR immunoreactivity and 24S-OHC levels in CSF, previously determined in our lab group (Simpson *et al.*, 2016). This study found that no significant correlations between cholesterol biosynthetic gene relative concentration in astrocytes and neurons and HMGCR immunoreactivity and 24S-OHC CSF levels (Table 3.5).

A

	A Beta	AT8
HMGCR Astrocytes	r = 0.325 p =0.237	r = -0.138 p = 0.637
CYP46A1 Astrocytes	r = -0.151 p = 0.699	r = -0.455 p = 0.257
ABCA1 Astrocytes	r = 0.167 p = 0.693	r = -0.286 p = 0.535
SREBP2 Astrocytes	r = -0.485 p = 0.185	r = -0.690 p = 0.058

B

	A Beta	AT8
HMGCR Neurons	r = -0.351 p = 0.101	r = -0.458* p = 0.032*
CYP6A1 Neurons	r = -0.372 p = 0.106	r = -0.211 p = 0.387
ABCA1 Neurons	r = 0.172 p = 0.557	r = 0.541* p = 0.046
SREBP2 Neurons	r = 0.414 p = 0.098	r = 0.574* p = 0.016*

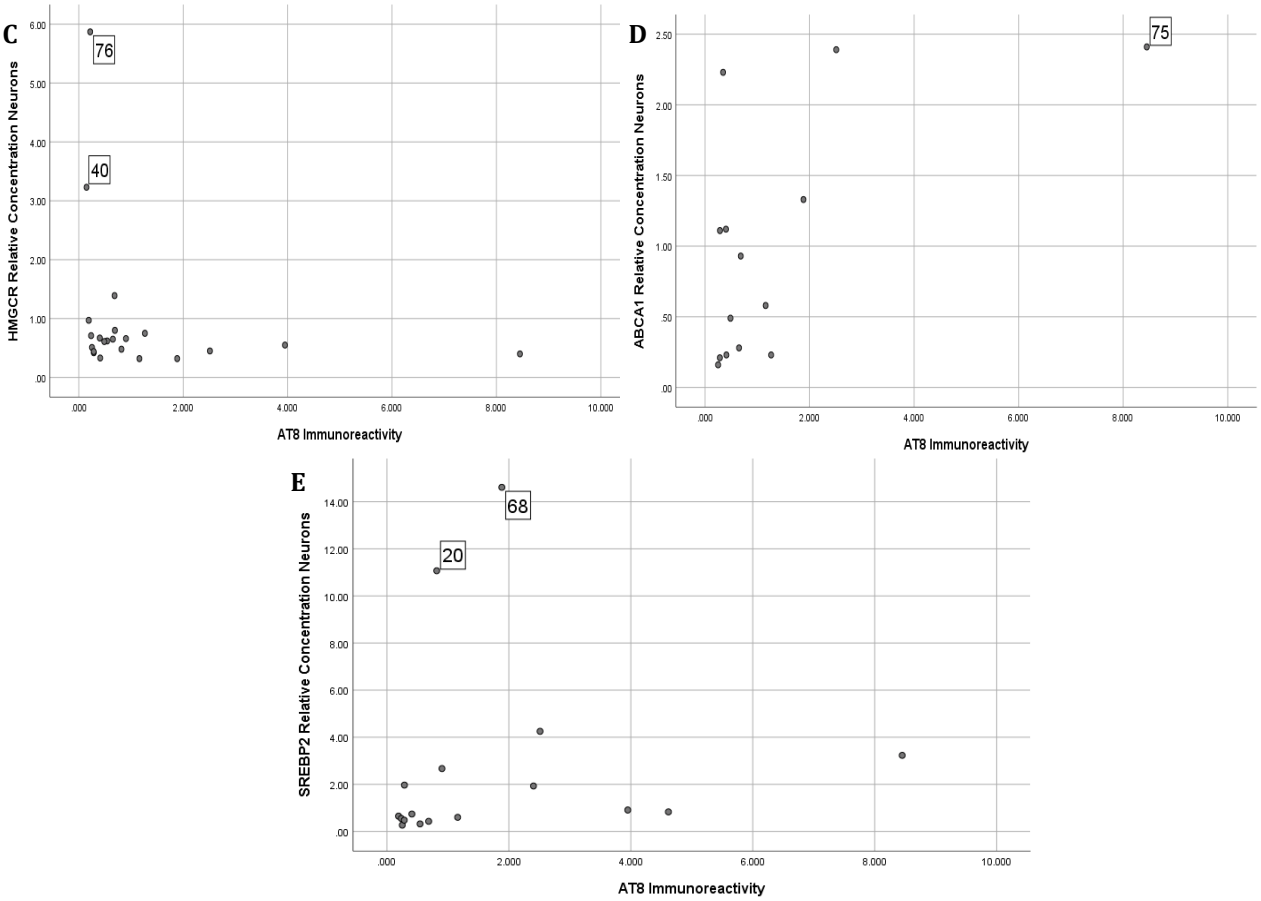

Figure 3.16. HMGCR, ABCA1 and SREBP2 gene relative concentration in neurons does correlate with AT8 immunoreactivity: Spearmen's rank correlation test was carried out to determine any correlations between relative concentration values for cholesterol biosynthetic genes from astrocytes (A) and neurons (B) with Aβ and AT8 immunoreactivity. Where r is the correlation coefficient and p is the significance value. Scatter plots showing the neuronal relative concentration (y-axis) for *HMGCR, ABCA1* and *SREBP2* respectively against AT8 immunoreactivity (x-axis) (C-E). Relative concentration values for each gene were calculated relative to Braak and Braak group 1.

A

	H2AX Astrocytes	H2AX Neurons	8-OHdG Astrocytes	MDA
HMGCR Astrocytes	r = 0.043 p = 0.879	r = -0.083 p = 0.770	r = -0.233 p = 0.422	r = 0.143 p = 0.736
CYP46A1 Astrocytes	r = -0.046 p = 0.906	r = -0.255 p = 0.507	r = -0.563 p = 0.146	r = 0.359 p = 0.553
ABCA1 Astrocytes	r = -0.036 p = 0.933	r = 0.000 p = 1.000	r = -0.690 p = 0.058	r = -0.600 p = 0.400
SREBP2 Astrocytes	r = -0.164 p = 0.674	r = 0.029 p = 0.940	r = -0.265 p = 0.491	r = 0.348 p = 0.499

B

	H2AX Astrocytes	H2AX Neurons	8-OHdG Astrocytes	MDA
HMGCR Neurons	r = 0.220 p = 0.313	r = 0.419* p = 0.046*	r = -0.142 p = 0.529	r = -0.100 p = 0.769
CYP6A1 Neurons	r = -0.297 p = 0.204	r = -0.075 p = 0.753	r = -0.394 p = 0.095	r = -0.067 p = 0.865
ABCA1 Neurons	r = 0.004 p = 0.988	r = -0.305 p = 0.289	r = -0.212 p = 0.487	r = -0.143 p = 0.787
SREBP2 Neurons	r = -0.025 p = 0.925	r = -0.326 p = 0.202	r = -0.176 p = 0.498	r = -0.119 p = 0.779

C

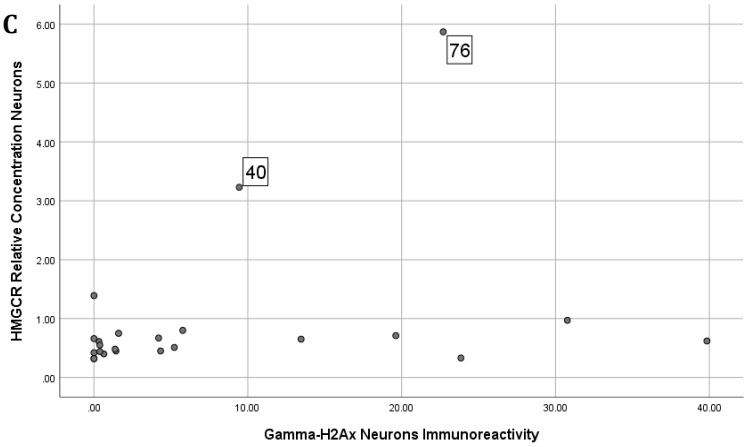

Figure 3.17. HMGCR gene relative concentration in neurons correlates to markers of DNA damage in neurons: Spearmen's rank correlation test was carried out to determine any correlations between relative concentration values for cholesterol biosynthetic genes from astrocytes (A) and neurons (B) with markers of oxidative stress (MDA protein levels and 8-OHdG immunoreactivity) and markers of DNA damage (H2AX immunoreactivity). Where r is the correlation coefficient and p is the significance value. Scatter plots showing the neuronal relative concentration (y-axis) for *HMGCR* against H2AX immunoreactivity in neurons (x-axis) (C). Relative concentration values for each gene were calculated relative to Braak and Braak group 1.

A

	MHC	CD68	GFAP
HMGCR Astrocytes	r = -0.027 p = 0.937	r = 0.093 p = 0.762	r = -0.055 p = 0.852
CYP46A1 Astrocytes	r = 0.126 p = 0.788	r = 0.060 p = 0.888	r = -0.494 p = 0.177
ABCA1 Astrocytes	r = -0.371 p = 0.468	r = -0.643 p = 0.086	r = -0.071 p = 0.867
SREBP2 Astrocytes	r = -0.143 p = 0.760	r = 0.059 p = 0.881	r = 0.109 p = 0.781

B

	MHC	CD68	GFAP
HMGCR Neurons	r = 0.490* p = 0.039*	r = 0.183 p = 0.453	r = -0.123 p = 0.587
CYP6A1 Neurons	r = -0.114 p = 0.685	r = 0.087 p = 0.740	r = -0.111 p = 0.650
ABCA1 Neurons	r = -0.042 p = 0.897	r = 0.368 p = 0.216	r = 0.213 p = 0.464
SREBP2 Neurons	r = -0.332 p = 0.246	r = 0.158 p = 0.589	r = 0.124 p = 0.649

C

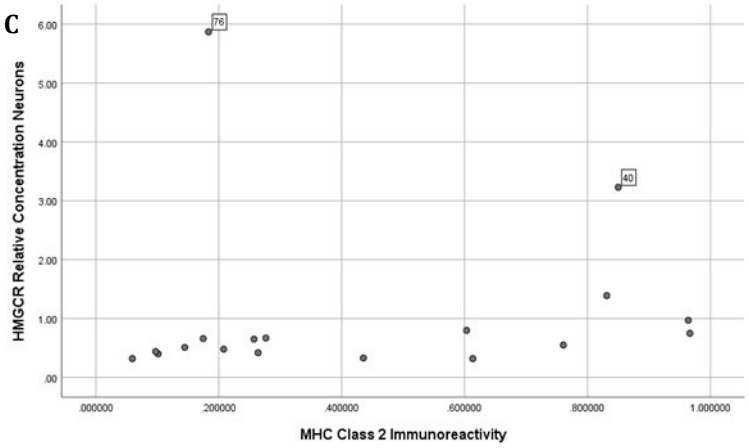

Figure 3.18. HMGCR gene relative concentration in neurons correlates to markers of neuroinflammation: Spearmen's rank correlation test was carried out to determine any correlations between relative concentration values for cholesterol biosynthetic genes from astrocytes (A) and neurons (B) with markers of neuroinflammation (MHCII and CD68 immunoreactivity) and gliosis (GFAP immunoreactivity). Where r is the correlation coefficient and p is the significance value. Scatter plots showing the neuronal relative concentration (y-axis) for *HMGCR* against MHCII immunoreactivity in neurons (x-axis) (C). Relative concentration values for each gene were calculated relative to Braak and Braak group 1.

3.4.15 Removal of outliers to confirm significant results

Outlying data points were removed to ensure significant data was not a result of statistical artefacts from extreme data points. Outliers were identified based on distribution displayed on a histogram and box plots and extreme data points with a relative gene concentration value (relative to Braak and Braak group 1 and Thal phase 1) greater than 3 and one standard deviation from the upper quartile. Outliers met all conditions to be removed from subsequent reanalysis. The outlier's removed were: RH43 from HMGCR in astrocytes (RC=4.37); RH40 and RH76 from HMGCR in neurons (RC=3.23 and RC=5.87, respectively); RH41 from CYP46A1 in neurons (RC=6.94); RH43 from ABCA1 in astrocytes (RC=4.50); RH68 and RH20 from SREBP2 in neurons (RC=14.61 and RC=11.07, respectively). Exclusion of outlier's led to the loss of significance for some variable and added significance for other variables (Table 3.6). Significant increase in *SREBP2* expression in neurons with Braak and Braak group was lost (including outlier's KW, p=0.040; excluding outlier's KW, p=0.174). A trend to decrease with tangle pathology and *HMGCR* expression in neurons (including outlier's JT, p=0.022; excluding outlier's JT, p=0.057). Significant decrease in *HMGCR* expression in neurons and plaque pathology was also lost (including outlier's KW, p=0.040; excluding outlier's KW, p=0.174). Significant correlations were also lost in neuronal *HMGCR* expression and AT8 and neuronal γH2AX immunoreactivity (including outlier's r=-0.458, p=0.032; r=0.419, p=0.046; excluding outlier's r=-0.284, p=0.224; r=0.335, p=0.138, respectively). New significant correlations also emerged following the removal of outlier's: *HMGCR* expression in neurons showed significant correlations with Aβ immunoreactivity and 24S-OHC levels in CSF (including outlier's r=-0.351, p=0.101; r=0.454, p=0.089; excluding outlier's r=-0.443, p=0.044; r=0.567, p=0.022, respectively); *CYP46A1* expression in neurons showed significant correlations with astrocytic γH2AX immunoreactivity (including outlier's r=-0.297, p=0.204; excluding outlier's r=-0.513, p=0.025).

A

	HMGCR	24S-OHC
HMGCR Astrocytes	r = 0.482 p = 0.069	r = 0.405 p = 0.320
CYP46A1 Astrocytes	r = 0.142 p = 0.715	r = 0.400 p = 0.600
ABCA1 Astrocytes	r = 0.357 p = 0.385	r = 0.200 p = 0.747
SREBP2 Astrocytes	r = -0.042 p = 0.915	r = 0.600 p = 0.400

B

	HMGCR	24S-OHC
HMGCR Neurons	r = -0.062 p = 0.779	r = 0.454 p = 0.089
CYP6A1 Neurons	r = 0.035 p = 0.885	r = 0.055 p = 0.858
ABCA1 Neurons	r = 0.106 p = 0.719	r = -0.176 p = 0.627
SREBP2 Neurons	r = -0.132 p = 0.613	r = -0.261 p = 0.467

Table 3.5. Correlation matrix between cholesterol biosynthetic gene expression in astrocytes and neurons with HMGCR and 24S-OHC: Spearmen's rank correlation test was carried out to determine any correlations between relative concentration values for cholesterol biosynthetic genes from astrocytes (A) and neurons (B) with HMGCR immunoreactivity and 24S-OHC CSF levels. Where r is the correlation coefficient and p is the significance value. Relative concentration values for each gene were calculated relative to Braak and Braak group 1.

A

Variables	Test	Inc outlier/ (p=)	Ex outlier / (p=)
SREBP2 Ast vs Braak Group	KW	0.120	0.120
	JT	0.031*	0.031*
SREBP2 Neu vs Braak group	KW	0.040*	0.174
	JT	0.011*	0.056
HMGCR Neu vs Tangle score	KW	0.059	0.207
	JT	0.022*	0.057
SREBP2 Neu vs Tangle score	KW	0.022*	0.056
	JT	0.005*	0.018*
HMGCR Neu vs Plaque score	KW	0.022*	0.057
	JT	0.020*	0.057

B

Variables	Inc outlier	Ex outlier
HMGCR Neu vs AT8	r = -0.458* p = 0.032*	r = -0.284 p = 0.224
HMGCR Neu vs A Beta	r = -0.351 p = 0.101	r = -0.443* p = 0.044*
ABCA1 Neu vs AT8	r = 0.541* p = 0.046*	r = 0.541* p = 0.046*
SREBP2 Neu vs AT8	r = 0.574* p = 0.016*	r = 0.593* p = 0.020*
HMGCR Neu vs H2AX Neu	r = 0.419* p = 0.046*	r = 0.335 p = 0.138
CYP46A1 Neu vs H2AX Ast	r = -0.297 p = 0.204	r = -0.513* p = 0.025*
HMGCR Neu vs MHC	r = 0.490* p = 0.039*	r = 0.567* p = 0.022*
HMGCR Neu vs 24S-OHC	r = 0.454 p = 0.089	r = 0.608* p = 0.027*

Table 3.6. Changes to significance following outlier exclusion: The significance of data changed following exclusion of outliers. The table shows changes in differences and trends with AD pathology (A). The table shows changes in correlations with AD pathology and markers of oxidative stress, neuroinflammation and cholesterol metabolism (B).

3.4.16 Tissue cholesterol concentration not normally distributed in temporal cortex

Temporal cortex tissue cholesterol concentration was determined using the Amplex red cholesterol assay. Distribution of tissue cholesterol concentration was tested for normality using a Kolmogorov-Smirnov (KS) test. A histogram was plotted to visualise the distribution of tissue cholesterol concentration in post-mortem human temporal cortex tissue (Figure 3.19). A non-parametric approach was used because although the KS values were not significant indicating a normal distribution however, inspection of histograms suggests that the data was not normally distributed. As a quality control measure, the effects of pH and post-mortem delay (PMD) on tissue cholesterol concentration were assessed using Spearman's rank correlation test. Only weak correlations between tissue cholesterol concentration with pH ($r=0.262$, $p=0.041$) and PMD ($r=-0.278$, $p=0.033$) were found (Figure 3.20 A). Plotting scatter graphs of tissue cholesterol concentration against pH (Figure 3.20 B) and PMD (Figure 3.20 C) showed that the correlation between these two variables was very weak and skewed by a few data points.

3.4.17 Tissue cholesterol concentration does not change with Braak and Braak stage

To determine how tissue cholesterol concentration related to NFT progression, we examined the relationship to Braak and Braak groups. No significant differences or trends were observed between tissue cholesterol concentrations with Braak and Braak groups (Figure 3.21).

3.4.18 Tissue cholesterol concentration does not change with Thal Aβ phase.

To determine whether tissue cholesterol concentration relates to Aβ progression, we examined the relationship to Thal Aβ phases. No significant differences or trends were observed between tissue cholesterol concentrations with Thal Aβ groups (Figure 3.22).

3.4.19 Tissue cholesterol concentration does not correlate with Aβ and AT8 immunoreactivity in temporal cortex

To assess whether tissue cholesterol concentration was related to local AD pathology we examined the relationship of two classical markers of AD pathology; Aβ and AT8 immunoreactivity, previously determined in our lab group (J E Simpson

et al., 2010). No significant correlations between tissue cholesterol concentration and markers of classical AD pathology were observed (Table 3.7).

3.4.20 Tissue cholesterol concentration does not correlate with markers of cholesterol biosynthesis and metabolism.

To assess whether tissue cholesterol concentration was related to markers of cholesterol biosynthesis and metabolism, we examined the relationship of HMGCR immunoreactivity and 24S-OHC levels in CSF, previously determined in our lab group (Simpson *et al.*, 2016). This study found that no significant correlations between tissue cholesterol concentration and HMGCR immunoreactivity and 24S-OHC CSF levels (Table 3.8).

3.4.21 Tissue cholesterol concentration does not correlate with relative gene expression of genes involved in cholesterol biosynthesis and metabolism.

To assess whether tissue cholesterol concentration was related to relative gene expression of genes involved in cholesterol biosynthesis and metabolism, we examined the relationship between gene expression of *HMGCR, CYP6A1, ABCA1* and SREBP2 isolated from astrocytes and neurons from post-mortem temporal cortex tissue. This study found that no significant correlations between tissue cholesterol concentration and genes involved in cholesterol biosynthesis and metabolism (Table 3.9).

3.4.22 Tissue cholesterol concentration does not correlate with markers of oxidative stress and DNA damage

To assess whether the tissue cholesterol concentration was related to markers of oxidative stress and DNA damage, we examined the relationship of oxidative stress markers (Malondialdehyde [MDA], thioredoxin-2 [Trx2] and peroxiredoxin-3 [Prx3]) and DNA damage markers (γH2AX), previously determined in our lab group (J. E. Simpson *et al.*, 2010). This study found that no significant correlations between tissue cholesterol concentration and MDA protein expression and γH2AX immunoreactivity in astrocytes and neurons (Figure 3.23 A). No significant differences or trends were observed between tissue cholesterol concentrations with Trx2 and Prx3 immunoreactivity (unpublished data) (Figure 3.23 B-F).

A

	Cholesterol Concentration /µM/mg
n	63
Mean	16.28
SEM	1.53
Median	13.77
SD	12.15
IQR	9.01-20.52
KS	0.157

B

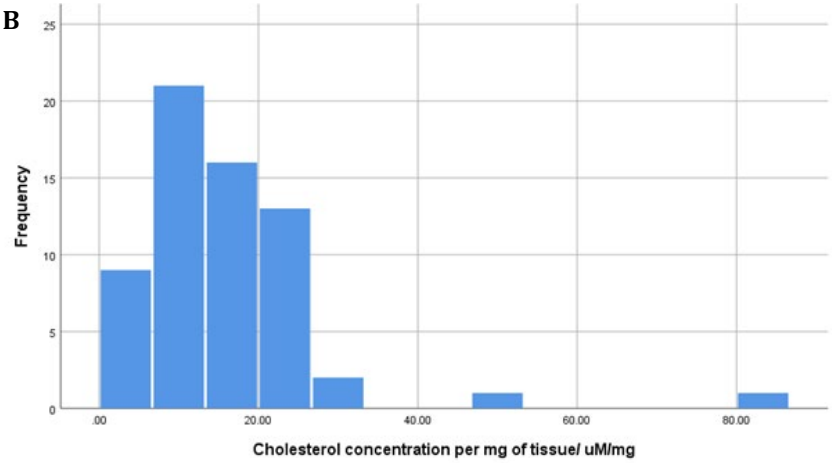

Figure 3.19. Distribution of tissue cholesterol concentration across cohort: The table shows the descriptive statistical values for cholesterol concentration per mg of tissue across the cohort (A). Data was tested for normality using Kolmogorov-Smirnov (KS). The distribution of tissue cholesterol concentration across the cohort displayed as a histogram

A

	pH	PMD
Cholesterol Concentration µM/mg	r = 0.262 p = 0.041*	r = -0.278 p = 0.033*

B

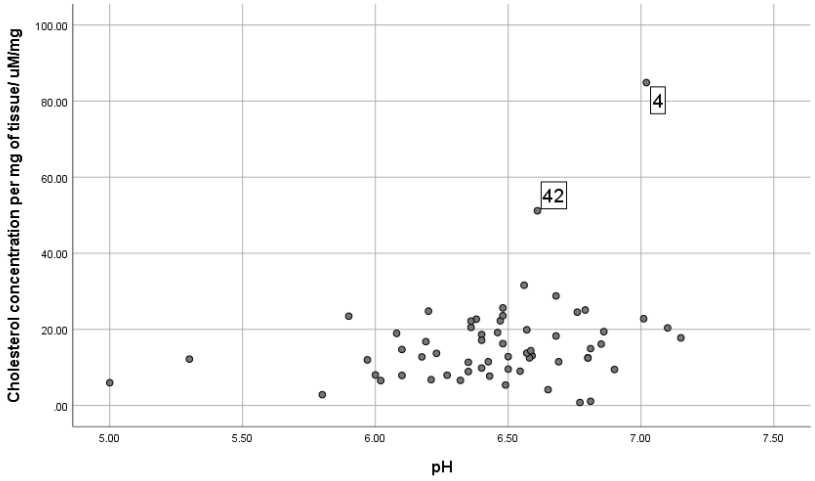

C

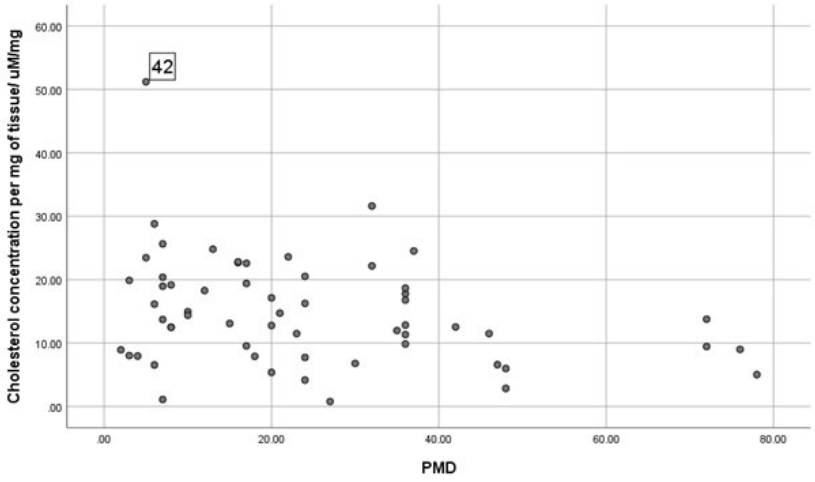

Figure 3.20. Tissue cholesterol concentration correlates with pH and PMD: Spearmen's rank correlation test was carried out to determine any correlations between tissue cholesterol concentration with pH and post-mortem delay (PMD). Where r is the correlation coefficient and p is the significance value. Scatter plots showing tissue cholesterol concentration (y-axis) for against pH (B) and PMD (C) (x-axis).

A

		Braak Groups			KW	JT
		0-II	III-IV	V-VI		
Cholesterol Concentration µM/mg	n	21	32	10	0.401	0.543
	Mean	16.07	17.68	2.19		
	SEM	2.16	2.57	0.16		
	Median	13.71	15.4	12.54		
	SD	9.89	14.52	6.92		
	Range	45.81	84.08	19.74		

B

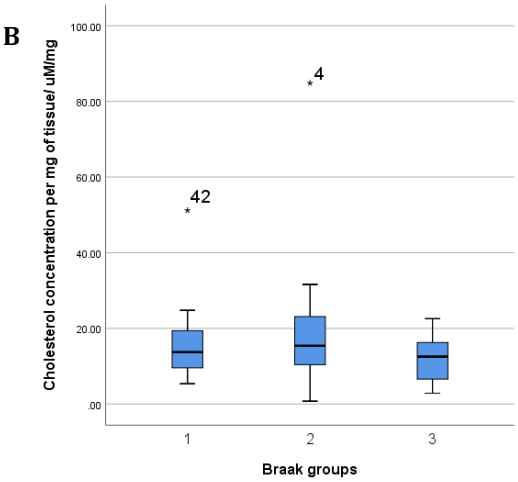

Figure 3.21. Tissue cholesterol concentration does not change with Braak and Braak groups: The table shows the descriptive statistical values for cholesterol concentration in each Braak and Braak group. The table also shows the p values for KW and JT tests to assess differences between tissue cholesterol concentration and Braak and Braak groups (A). Box plots show the distribution of tissue cholesterol concentration (y-axis) across Braak and Braak groups (x-axis) (B). No significant differences between tissue cholesterol concentration and Braak and Braak groups were identified.

A

		Thal Groups			KW	JT
		0-1	2-3	4-5		
Cholesterol Concentration µM/mg	n	16	27	20	0.813	0.985
	Mean	15.42	17.95	14.70		
	SEM	2.98	2.89	1.65		
	Median	12.66	14.95	13.74		
	SD	11.99	15.01	7.40		
	Range	50.41	78.88	25.95		

B

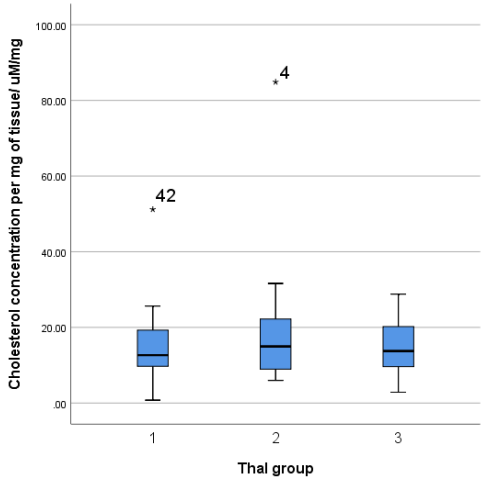

Figure 3.22. Tissue cholesterol concentration does not change with Thal groups: The table shows the descriptive statistical values for cholesterol concentration in each Thal group. The table also shows the p values for KW and JT tests to assess differences between tissue cholesterol concentration and Thal groups (A). Box plots show the distribution of tissue cholesterol concentration (y-axis) across Thal groups (x-axis) (B). No significant differences between tissue cholesterol concentration and Thal groups were identified.

	A Beta	AT8
Cholesterol Concentration µM/mg	r = 0.095 p =0.478	r = -0.095 p = 0.476

Table 3.7. Tissue cholesterol concentration does not correlate with Aβ and AT8 immunoreactivity: Spearmen's rank correlation test was carried out to determine any correlations between tissue cholesterol concentration with Aβ and AT8 immunoreactivity. Where r is the correlation coefficient and p is the significance value.

	HMGCR	24S-OHC
Cholesterol Concentration µM/mg	r = 0.237 p = 0.061	r = 0.134 p = 0.442

Table 3.8. Correlation matrix between tissue cholesterol concentration with HMGCR and 24S-OHC: Spearmen's rank correlation test was carried out to determine any correlations between tissue cholesterol concentration with HMGCR immunoreactivity and 24S-OHC CSF levels. Where r is the correlation coefficient and p is the significance value.

	HMGCR RC Astrocytes	HMGCR RC Neurons	CYP46A1 RC Astrocytes	CYP46A1 RC Neurons	ABCA1 RC Astrocytes	ABCA1 RC Neurons	SREBP2 RC Astrocytes	SREBP2 Neurons
Cholesterol Concentration µM/mg	r = -0.286 p = 0.535	r = 0.217 p = 0.576	r = 0.800 p = 0.200	r= -0.146 p= 0.669	r= -0.600 p= 0.400	r=-0.300 p=0.624	r=0.600 p=0.285	r=-0.517 p=0.154

Table 3.9. Correlation matrix between tissue cholesterol concentration and cholesterol biosynthetic gene expression in astrocytes and neurons: Spearmen's rank correlation test was carried out to determine any correlations between tissue cholesterol concentration with relative concentration values for cholesterol biosynthetic genes from astrocytes and neurons. Where r is the correlation coefficient and p is the significance value.

A

	H2AX Astrocytes	H2AX Neurons	MDA
Cholesterol Concentration µM/mg	r = 0.047 p = 0.723	r = 0.117 p = 0.374	r = 0.245 p = 0.298

B

	Trx2 Neurons		Trx2 Glia		Prx3 Neurons		Prx3 Glia	
	KW	JT	KW	JT	KW	JT	KW	JT
Cholesterol Concentration µM/mg	0.634	0.966	0.346	0.966	0.602	0.830	0.183	0.822

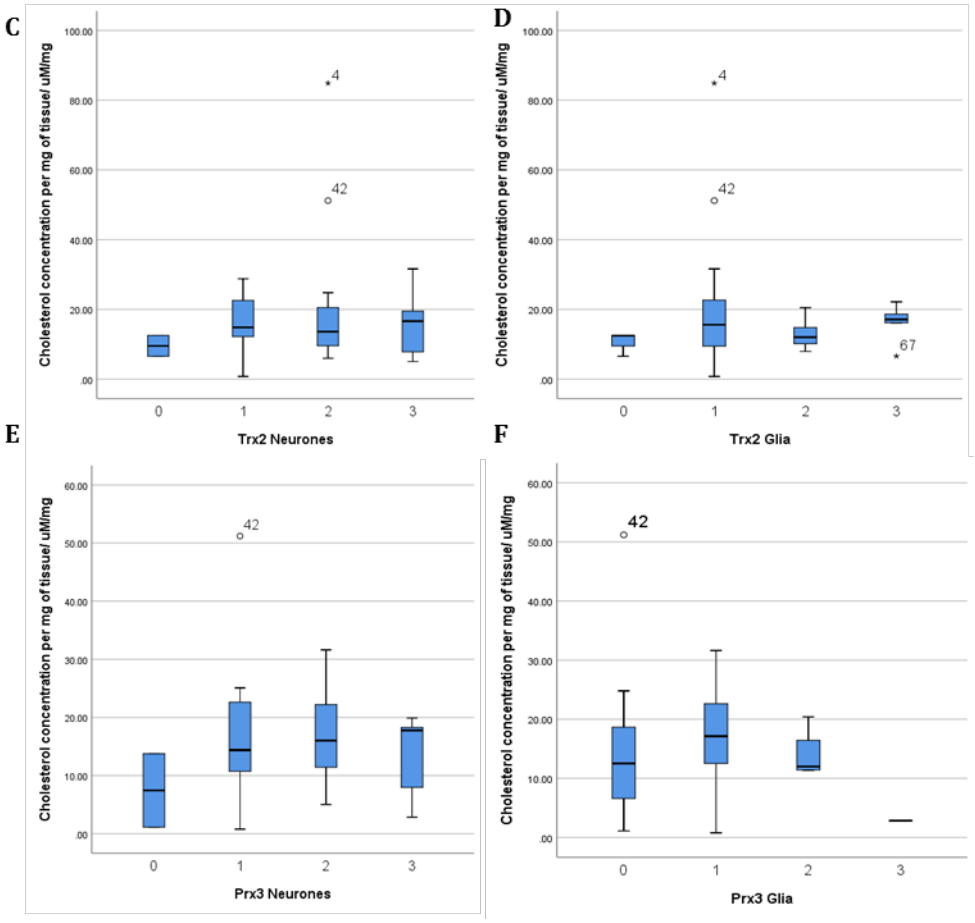

Figure 3.23. Tissue cholesterol concentration does not correlate to markers of oxidative stress: Spearmen's rank correlation test was carried out to determine any correlations between tissue cholesterol concentration with markers of oxidative stress (MDA protein levels) and markers of DNA damage (H2AX immunoreactivity) (A). Where r is the correlation coefficient and p is the significance value. The table also shows the p values for KW and JT tests to assess differences between tissue cholesterol concentration and Trx2 and Prx3 immunoreactivity (B). Box plots show the distribution of tissue cholesterol concentration (y-axis) across Trx2 immunoreactivity (C-D) and Prx3 immunoreactivity (E-F) (x-axis).

3.4.23 Tissue cholesterol concentration does not correlate with markers of neuroinflammation and gliosis

To assess whether tissue cholesterol concentration was related to markers of neuroinflammation and gliosis, we examined the relationship of neuroinflammation markers (MHC class 2 and CD68) and gliosis markers (GFAP), previously determined in our lab group (J. E. Simpson *et al.*, 2010). This study found that no significant correlations between tissue cholesterol concentration and MHCII, CD68 and GFAP immunoreactivity (Table 3.10).

3.4.24 Tissue cholesterol concentration does not change with markers of vascular pathology

To assess whether tissue cholesterol concentration was related to markers of vascular pathology, we examined the relationship of vascular pathology markers (cortical micro-infarct stage and CAA pathology) previously determined (Ince, 2001; Matthews *et al.*, 2009a). No significant differences or trends were observed between tissue cholesterol concentrations with cortical micro-infarct stage (Figure 3.24) and CAA pathology (Figure 3.25).

3.4.25 Tissue cholesterol concentration does not associate with various AD pathologies

Statistical analyses of various markers of contributors to AD pathology such as oxidative stress, neuroinflammation and vascular pathology. A summary of findings can be found in (Table 3.11).

	MHC	CD68	GFAP
Cholesterol Concentration µM/mg	r = 0.125 p = 0.377	r = -0.011 p = 0.940	r = 0.043 p = 0.745

Table 3.10. Tissue cholesterol concentration does not correlate to markers of neuroinflammation: Spearmen's rank correlation test was carried out to determine any correlations between tissue cholesterol concentration with markers of neuroinflammation (MHCII and CD68 immunoreactivity) and gliosis (GFAP immunoreactivity). Where r is the correlation coefficient and p is the significance value.

A

	Cortical micro-infarct stage	
	KW	JT
Cholesterol Concentration µM/mg	0.705	0.603

B

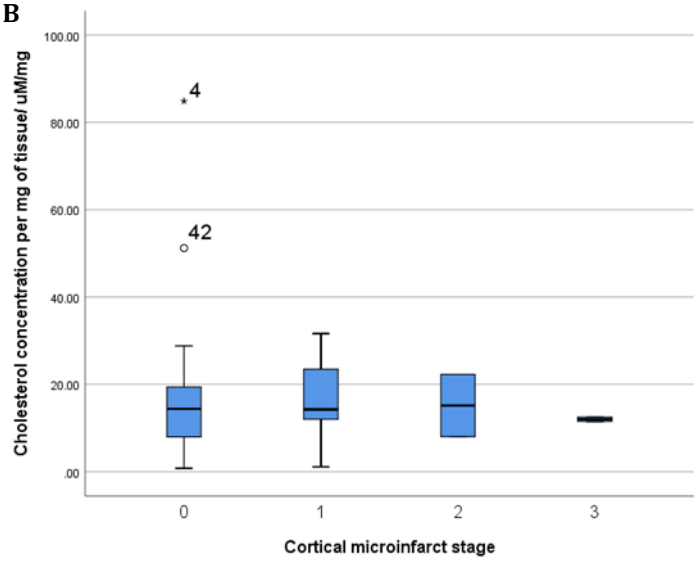

Figure 3.24. Tissue cholesterol concentration does not change with cortical micro infarct stage: The table also shows the p values for KW and JT tests to assess differences between tissue cholesterol concentration and cortical micro infarct stage (A). Box plots show the distribution of tissue cholesterol concentration (y-axis) across cortical micro infarct stage (x-axis) (B). No significant differences between tissue cholesterol concentration and cortical micro infarct stage were identified.

A

	CAA Pathology
	MW
Cholesterol Concentration µM/mg	0.735

B

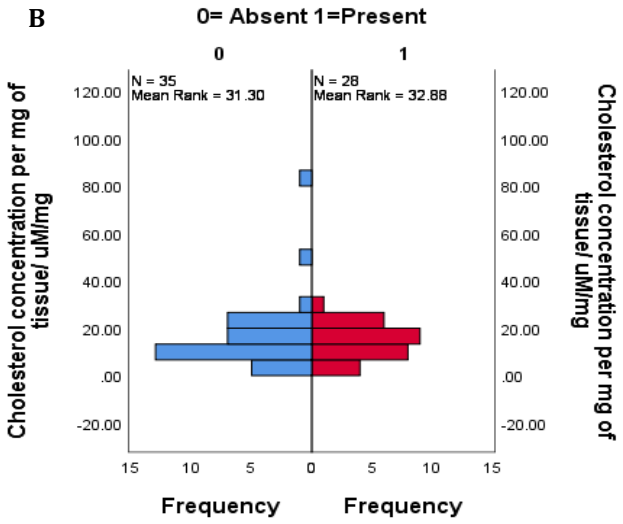

Figure 3.25. Tissue cholesterol concentration does not change with CAA pathology: The table also shows the p values for Mann-Whitney U (MW) test to assess differences between tissue cholesterol concentration and CAA pathology (A). Histogram shows the distribution of tissue cholesterol concentration (y-axis) in the absence (0-blue) and presence (1-red) of CAA pathology (B). No significant differences between tissue cholesterol concentration and Braak and Braak groups were identified.

Pathology	Measures									
AD Pathology	Braak Stage KW=0.401 JT=0.543		Thal Phase KW=0.813 JT=0.985		Aβ r = 0.095 p =0.478		AT8 r = -0.095 p = 0.476			
Oxidative Stress	γH2AX Neurons r = 0.117 p = 0.374	γH2AX Astrocytes r = 0.047 p = 0.723	MDA r = 0.245 p = 0.298	Trx2 Neurons KW= 0.634 JT=0.966	Trx2 Glia KW=0.346 JT=0.966	Prx3 Neurons KW=0.602 JT=0.830	Prx3 Glia KW=0.183 JT=0.822			
Neuroinflammation	CD68 r = -0.011 p = 0.940		MHCII r = 0.125 p = 0.377		GFAP r = 0.043 p = 0.745					
Vascular Pathology	CAA KW=0.705 JT=0.603				Cortical Micro-infarcts MW=0.735					
Cholesterol Homeostasis	HMGCR IR r = 0.237 p = 0.061	HMGCR RC Astrocytes r = -0.286 p = 0.535	HMGCR RC Neurons r = 0.217 p = 0.576	SREBP2 RC Astrocytes r=0.600 p=0.285	SREBP2 RC Neurons r=-0.517 p=0.154	ABCA1 RC Astrocytes r= -0.600 p= 0.400	ABCA1 RC Neurons r=-0.300 p=0.624	CYP46A1 RC Astrocytes r = 0.800 p = 0.200	CYP46A1 RC Neurons r= -0.146 p= 0.669	24-OHC CSF r = 0.134 p = 0.442

Table 3.11. Tissue cholesterol concentration does not associate with AD pathologies: A summary of the various measures carried to determine relationships of tissue cholesterol concentration with various AD pathologies. Where r is the Spearmen's rank correlation coefficient and p is the significance value. The table also shows the p values for KW (Kruskal-Wallis), JT (Jonckheere-Terpstra) and MW (Mann-Whitney U) tests. All tests were two tailed and the $p<0.05$ was set as the level for significance.

3.4.26 Moderate and high tissue cholesterol concentration is associated with dementia status

To determine if the variation in brain tissue cholesterol concentration associated with dementia status a Mann-Whitney U test was carried out. From the cases that cholesterol was measured (n=63), 40 cases had a dementia diagnosis before death (median=14.08, IQR= 9.06-21.76) and 21 cases had no dementia (median=12.84, IQR= 8.37-20.14) (Figure 3.26 A). The test showed that there was no significant difference between tissue cholesterol concentration and dementia status (MW, p=0.95). The distribution of tissue cholesterol concentration by dementia status across specific Braak and Braak stages and Thal phases was determined (Figure 3.26 B and C). A pairwise comparison of means using Tukey's adjustment found no significant difference between tissue cholesterol concentration and dementia status at specific Braak and Braak stages and Thal phases. The effect of tissue cholesterol concentration on risk of dementia was analysed using logistic regression (Figure 3.26 D). A univariate model adjusted for only age at death and sex as covariates, as well as a multivariate model adjusted for Braak and Braak, Thal and CAA pathology was produced. Tissue cholesterol concentration was analysed as continuous scales and categorically divided into tertiles. When modelled continuously no effect was seen in tissue cholesterol concentration. However, when tissue cholesterol was divided into tertiles, point estimates showed increased risk of dementia in moderate (univariate OR:1.58, 95% CI: 0.39-6.43; multivariate OR: 1.43 95% CI: 0.31-6.53) and high cholesterol groups (univariate OR:1.44, 95% CI: 0.35-5.85; multivariate OR: 1.21 95% CI: 0.29-5.08). In contrast the estimate for continuous cholesterol measure shows no effect with a more precise 95% CI (OR: 0.98, 95% CI: 0.93-1.03). Statistical analysis in relation to dementia status was carried out by Connor Richardson, University of Newcastle.

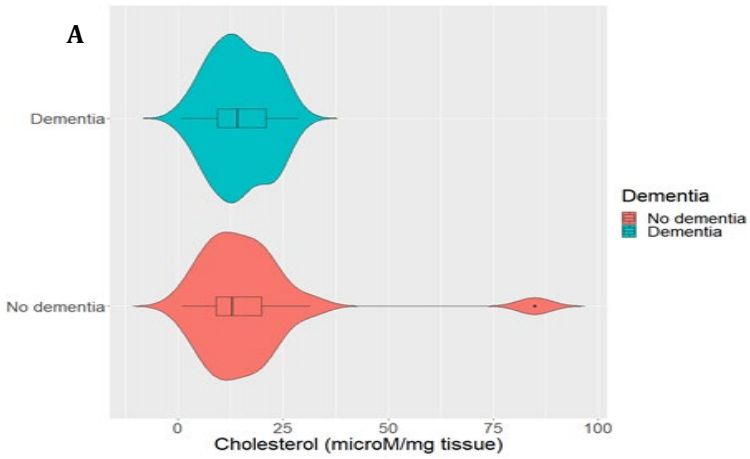

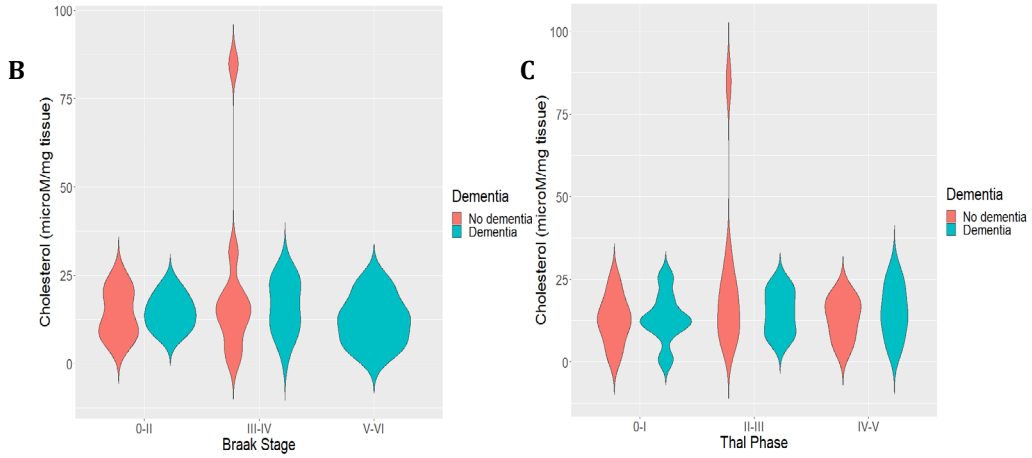

D

	Unadjusted (univariate)			Adjusted (multivariate)		
	OR	95% CI	p=	OR	95% CI	p=
Cholesterol	0.98	0.93-1.03	0.39	0.98	0.93-1.03	0.33
Tertiles						
Moderate	1.58	0.39-6.43	0.52	1.43	0.31-6.53	0.65
High	1.44	0.35-5.85	0.61	1.21	0.29-5.08	0.80

Figure 3.26. Moderate and high tissue cholesterol concentration is associated with dementia status: Tissue cholesterol concentration was compared to dementia status. Box and violin plots displaying the distribution and probability density of tissue cholesterol concentration by dementia status (A). Box plots show median, IQR and range, area around the box displays the probability density. Wider sections of the violin plots represent a higher probability that members of the population will take on the given value; narrower sections represent a lower probability. Violin plots showing the distribution of tissue cholesterol concentration by dementia status at specific Braak and Braak stage (C) and Thal phase (D). No significant difference between tissue cholesterol concentration and dementia status was found. Table D shows the output from logistic regression modelling (D). A univariate model adjusted for age at death and sex, multivariate models adjusted for Braak and Braak, Thal and CAA pathology. Tissue cholesterol concentration was modeled on a continuous scale and categorically by tertiles. Results are presented as odd ratios (OR) with 95% confidence intervals (CI) and p values. Statistical analysis and violin plots courtesy of Connor Richardson,

3.5 Discussion

In this chapter, the relative expression of four key genes (*HMGCR, CYP46A1, ABCA1* and *SREBP2*) involved in the cholesterol biosynthesis pathway and cholesterol metabolism were characterised using qPCR. In this study, we found that the relative expression of *HMGCR* in neuronal populations was decreased with tangle and plaque scores suggesting a decrease in expression as AD pathology progresses. This was supported by the negative correlation between percentage tau area-immunoreactivity and *HMGCR* expression in neurons. There were also positive correlations with neuronal *HMGCR* expression and markers of DNA damage (γH2AX) and neuroinflammation (MHCII). Furthermore, this study also found that *SREBP2* expression in enriched neuronal RNA was significantly increased with AD progression and pathology specifically with tau tangle pathology where an increase in relative expression is observed. We also found a significant moderate positive correlation between neuronal *ABCA1* expression and tau immunoreactivity. In astrocytic cell enrichment samples, we found a significant trend to decrease with *SREBP2* and Braak and Braak stages. No other statistically significant associations or correlations were observed in astrocyte isolations and markers of AD neuropathology progression, oxidative stress and neuroinflammatory markers. In this chapter, the total cholesterol concentration per mg of tissue from frozen human post-mortem temporal cortex was determined using the Amplex red cholesterol assay. This study found that there were no significant changes or trends with tissue cholesterol concentration and tangle and plaque progression. No significant correlations between local AD pathology, oxidative stress markers, neuroinflammation markers and markers of vascular pathology. Interestingly, no significant correlations were observed between tissue cholesterol concentration with HMGCR immunoreactivity and relative gene concentration of *HMGCR* and *SREBP2*. No significant correlations were found between tissue cholesterol concentration and CSF 24-OHC levels and relative gene concentration of *ABCA1* and *CYP46A1*. Data from *this current study* also showed that there was no significant association between temporal cortex cholesterol concentration and dementia status. However, when tissue cholesterol concentration was categorically divided into tertiles and modelled using logistic regression analysis, moderate and high tissue cholesterol concentration was associated with dementia.

3.5.1 LCM of immune-positive cells from post-mortem temporal cortex can produce an RNA sample enriched for neuronal and glial RNA.

LCM was used to isolate neurons and astrocytes from frozen temporal cortex sections from the CFAS Cambridge cohort. Once isolated, RNA was extracted from the cells and quality of RNA was assessed using Agilent RNA 6000 Pico Chip analysis which assigns the sample a RIN value. A RIN value was also obtained before carrying out LCM. This degradation between the RNA samples was expected as the first sample was extracted from an entire section of tissue so more high-quality RNA is expected and post-LCM an enriched but not homogenous cell population was obtained. Previous work within our lab group has found that following LCM the RIN value decreased by 1.5, however this remained of sufficient quality for downstream analysis (Waller *et al.*, 2012).

There are limitations to the use of post-mortem tissue, especially when extracting RNA from tissue. Conditions experienced at the time of death have an impact on RNA quality. Brain pH is a good indicator of levels of mRNA degradation, as a low pH (<6.5) indicates a slow death and a prolonged period within the agonal phase of donor prior to death (Kingsbury *et al.*, 1995). Nevertheless, the pH values obtained from human post-mortem brain tissue are sufficiently good for molecular investigations (Monoranu *et al.*, 2009). Hypoxia, pyrexia and terminal coma also lead to a decrease in mRNA stability (Harrison *et al.*, 1991; Waller *et al.*, 2012). Hence, for this study the criteria for inclusion within the sub-cohort was based on brain pH, PMD as well Braak and Braak stage.

The peaks at 28s and 18s from the Picochip analysis are used to determine the quality of RNA and help determine how much degradation has occurred. These peaks represent the level of RNA digestion that has occurred; if no peaks are present this indicates that all the RNA has been digested (Ogura *et al.*, 1998). A small level of degradation is expected due to the fact that RNA degradation may occur during the brief freeze thaw process that occurs during sectioning and the LCM process such as duration of capture and immunolabelling of sections may also contribute to RNA degradation (Waller *et al.*, 2012). However, despite the degradation in RNA, the RNA extracts are sufficient for downstream expression analysis as demonstrated by previous work undertaken within our lab (Simpson *et al.*, 2011, 2015, 2016).

Due to the intimate microarchitecture found within the brain, the LCM method helps isolate an enriched cell sample. To confirm neuronal enrichment, RNA from neuronal cell isolations was amplified to detect NeuN. NeuN is a neuronal nuclear protein, which is localised to the nucleus and is a marker for post-mitotic neurons and is expressed by most types of neurons except; Cajal-Retzius cells, inferior olive neurons, γ-motor neurons and Purkinje cells (Gusel'nikova and Korzhevskiy, 2015). Presence of a band in within the NeuN well, confirmed neuronal cell enrichment. Astrocytic enrichment was confirmed by amplification of RNA to detect GFAP. GFAP is a component of intermediate filaments found within astrocytes and is overexpressed in reactive astrocytes (Carter *et al.*, 2019). Presence of a band in within the GFAP well, confirmed astrocyte cell enrichment.

The use of FFPE tissue could help eliminate factors leading to RNA degradation that are associated with frozen brain tissue. One advantage of using FFPE would be the preserved morphology of the tissue, making isolation easier as specific cells can be identified using morphology in addition to immunostaining, leading to a more enriched population of single cell type (S. Shi *et al.*, 2008). However, during the fixation process both RNA and DNA are degraded making nucleic acid extraction challenging although transcription expression studies have been carried out on RNA extracted from FFPE tissue using LCM (Joseph and Gnanapragasam, 2011). Another method that could potentially be used to isolate specific cell populations from a section of tissue is flow-cytometry. A novel method has been developed by Martin et al (2017) in which they are able to sort cells from murine brains that have been fixed in formalin, they were also able to extract mRNA from the sections and perform qPCR after isolating cells and they found that they had high purity of isolated cell populations (Martin *et al.*, 2017).

3.5.2 *HMGCR* expression in neurons decreases with increasing AD pathology

HMGCR is an enzyme involved in the cholesterol biosynthesis pathway and the activity of this enzyme determines the rate of cholesterol production (Sharpe and Brown, 2013b). Immunohistochemical investigation in this study shows that HMGCR is expressed in the pyramidal neurons of the temporal cortex and the expression of HMGCR at a protein level, HMGCR immunoreactivity was also observed in glial population within the cortex and white matter boundary (2.4.3). The gene expression

studies confirm *HMGCR* expression at an mRNA level in astrocytes and neuron populations isolated from the temporal cortex at all Braak and Braak stages.

The data from this current study showed that neuronal *HMGCR* expression showed a trend to decrease with increasing tangle pathology and a significant moderate negative correlation with AT8 immunoreactivity. One study investigated the effects of different splice variants of the *HMGCR* gene in post-mortem tissue from AD patients (Leduc *et al.*, 2016). *HMGCR* gene has two possible alleles G and A, alternative splicing leads to full length and a variant containing a single nucleotide polymorphism (SNP) at locus rs3846662 which results in alternative splicing of exon 13. The skipping of exon 13 (Δ13) is more common in A allele rather than the G allele. The exact effect of the SNP remains unknown but it is suggested that it may result in a reduced or lack of enzymatic activity (Johnson *et al.*, 2003; Burkhardt *et al.*, 2008; Medina and Krauss, 2009; Yu *et al.*, 2014). The study by Leduc *et al*, (2016) found that Δ13 mRNA levels in the frontal cortex positively correlate with NFT and within the cerebellum Δ13 mRNA levels negatively correlate with Aβ, suggesting a link between *HMGCR* gene expression and AD pathology (Leduc *et al.*, 2016). However, these differences in brain regions could be accounted for by the varying cell populations as the frontal cortex has a higher ratio of glial cells compared to neuronal cells and vice versa within the cerebellum. So this would suggest that within the frontal cortex glial expression of Δ13 mRNA positively correlates with NFT and within the cerebellum neuronal expression of Δ13 mRNA negatively correlates with Aβ (Leduc *et al.*, 2016). Additionally, Δ13 splice variant did not have an impact on HMGCR protein levels and no significant correlations were observed with full length *HMGCR* mRNA levels in both frontal and cerebellar cortices and NFT and Aβ.

In *this current study,* we found that the expression of *HMGCR* within neurons decreased with increasing plaque pathology. One study investigated the effects of lovastatin *in vitro* on Aβ production and APP processing (Mendoza-Oliva *et al.*, 2015). Treating human neuroblastoma cells with lovastatin reduced the protein expression of HMGCR and increased levels of degraded HMGCR. Furthermore, APP levels were increased but secretion of Aβ1-40 and Aβ1-42 was significantly reduced; however, prolonged exposure to lovastatin induced cell death (Mendoza-Oliva *et al.*, 2015). This suggests that the initial degradation in HMGCR expression could be a protective effect to reduce the production of Aβ. However this sustained reduction

may later lead to neuronal cell death as HMGCR is crucial for other cellular functions such a protein prenylation and isoprenoid synthesis (Cahoy *et al.*, 2008b; Zhang *et al.*, 2014; Moutinho, Nunes and Rodrigues, 2017).

3.5.3 *HMGCR* expression in neurons correlates with markers of DNA damage

Data from this current study shows that the relative concentration of *HMGCR* in neurons showed a moderate positive correlation with γH2AX immunoreactivity in neurons. This suggests oxidative DNA damage in the form of double stranded DNA breaks in neurons alters *HMGCR* expression in neurons. A microarray study in which human neuroblastoma cells were exposed to xanthine/xanthine oxidase (X-XOD) which induces oxidative stress found overexpression of cholesterol biosynthetic genes and a fold change of 1.8 in *HMGCR* gene expression in cells treated with X-XOD (Recuero *et al.*, 2009). Previous microarray analysis from our lab group also found overexpression of *HMGCR* in neurons isolated from frontal cortex of low Braak and Braak cases that had high DNA damage response as a result of oxidative stress (Simpson *et al.*, 2016). Both these studies suggest a link between DNA damage as a result of oxidative stress and an increase in *HMGCR* expression as a protective mechanism to combat a decline in membrane cholesterol levels as a result of ROS damage, the data from this current study supports these findings. However, the data from this study showed no significant correlation with *HMGCR* expression and other markers of oxidative stress such as MDA and 8-OHdG.

3.5.4 *HMGCR* expression in neurons correlates with markers of neuroinflammation

The data from this current study found that the relative concentration of *HMGCR* in neurons showed a moderate positive correlation with MHCII immunoreactivity, but no significant correlation was observed with CD68 and GFAP immunoreactivity. Major MHCII is a molecule which is expressed by activated microglia which occurs during neuronal injury (Neumann, 2001). This suggests that an increase in *HMGCR* expression in neurons correlates with an increase in microglial activation. A study by Chen *et al* (2018) investigated the effect of a high cholesterol diet in young and aged mice and found that the protein expression of CD68 was significantly increased in aged mice fed on a high cholesterol diet compared to control young mice. A similar increase in CD68 protein expression was also observed in young mice fed on a high cholesterol diet compared to control young mice suggesting that a high cholesterol

diet may induce neuroinflammation by activating microglia (Chen *et al.*, 2018). This study also found an up regulation in both pro- and anti-inflammatory cytokines at mRNA level in aged mice on a high cholesterol diet; this suggests that there may be a more complex interplay between cholesterol biosynthesis and regulation of a neuroinflammatory response.

3.5.5 *HMGCR* expression in neurons does not correlate with markers of cholesterol biosynthesis

Data from this current study shows that the expression of *HMGCR* in astrocytes and neurons isolated from the temporal cortex does not have any significant correlations with HMGCR immunoreactivity. The lack of significant correlation highlights the limitations of IHC as a method to determine protein levels as opposed to protein localisation. Furthermore, the IHC method does not provide a liner assessment of protein concentration this makes it difficult to assess HMGCR protein levels based solely on percentage immunoreactivity as this method only takes into account the number of pixels that contain the chromogen and not the absolute amount of chromogen present (Matkowskyj *et al.*, 2003).

3.5.6 *SREBP2* expression in neurons is associated with markers of AD pathology

SREBP2 is a major regulatory transcription factor for cholesterol biosynthesis pathway (Zhang and Liu, 2015). Immunohistochemistry showed that SREBP2 is localised to astrocytes and neurons in the human temporal cortex (2.4.6). Gene expression analysis now confirmed *SREBP2* mRNA expression in both astrocyte and neuron isolations from the temporal cortex at all Braak and Braak stages, with an increase of *SREBP2* expression in neurons with Braak and Braak stage, tangle pathology and AT8 percentage area immunoreactivity. Although, a significant trend to decrease was observed in *SREBP2* expression in astrocytes with increasing Braak and Braak stage, it is difficult to make any biological conclusions due to the small number of valid cases within this data set.

Other studies have shown that *SREBP2* alters with classical markers of AD pathology. One study in which *SREBP2* was overexpressed in APP/PS1 mice found that Aβ accumulation was accelerated in the triple transgenic mice compared to APP/PS1 mice (Barbero-Camps *et al.*, 2013). Another study demonstrated that in high fat diet rats, activation of SREBP2 was observed and an increase in BACE1 was correlated with activation of SREBP2 (Mastrocola *et al.*, 2011). This data

suggests that activation of SREPB2 is associated with promoting the formation of Aβ. However, contradictory evidence has also been found in several other studies. One study found that Aβ inhibits the activation of SREBP2, in this study primary rat neurons were treated with oligomeric Aβ and found reduced levels of SREBP2 as well as decreased activated SREBP2 (Mohamed *et al.*, 2018b). Furthermore, in AD patient derived fibroblasts, astrocytoma and hepatic cells cleavage of APP with α-secretase stimulated SREBP2 signalling whereas β-secretase cleavage had an inhibitory effect (Mastrocola *et al.*, 2011). This data suggests that both APP and SREBP2 are involved in a physiological feedback loop regulating growth via cholesterol homeostasis. However, the data from this current study found no significant differences or correlations with Aβ or plaque pathology.

Wang *et al,* (2019) found that the N-terminal of SREBP2 was localised in the cytoplasm of pyramidal neurons from the hippocampus in AD brains, compared to age-matched control brains where the N-terminal of SREBP2 was localised to the nucleus. Furthermore, a significant reduction in neuronal nuclear locaisation in the N-terminal of SREBP2 was observed in AT8 immunopositive cases (Wang *et al.*, 2019). *In vivo* studies in triple transgenic mice models, which develop tau pathology, found that once NFT pathology starts to manifest a reduction in the neuronal nuclear locaisation in the N-terminal of SREBP2 was observed, this was further validated in another mouse model which overexpressed mutant tau where SREBP2 N-terminal was localised to the cytoplasm (Wang *et al.*, 2019). Therefore, this study suggests that there is a negative association between phosphorylated tau and nuclear localisation of SREBP2 is observed in pyramidal neurons of the hippocampus in AD brains suggesting that cholesterol biosynthesis is not being induced. Our study demonstrates a positive correlation between *SREBP2* expression in neurons and AT8 immunoreactivity and tangle pathology and evidence from the study by Wang *et al,* (2019) validates this finding as they found the C-terminal fragment expression increased significantly in AD patients. The primer used in our study was specific for exons 15-16 which is located within the central portion of the gene which forms part of the cytoplasmic fragment.

3.5.7 *ABCA1* expression in neurons correlates with tau immunoreactivity

ATP binding cassette transporter A1 (ABCA1) is a membrane bound protein which plays a role in regulating cellular cholesterol homeostasis (Phillips, 2018). ABCA1 is

ubiquitous and localised to the plasma membrane of cells and has also been observed to traffic between the plasma membrane, intracellular vesicles and early and late endosomes (Neufeld *et al.*, 2001). In the brain ABCA1 is mainly expressed in the endothelial cell membranes, playing a role in cholesterol efflux and redistributing phospholipids in the membrane and via apoE (Schinkel and Jonker, 2003; Bartels, 2011).

Cholesterol efflux mechanisms differ in expression and activity in both neurons and astrocytes. One study demonstrated an increased mRNA expression of *ABCA1* in rat primary cortical neurons compared to rat primary cortical astrocytes however, when the cells were treated with ethanol there was increased cholesterol efflux in astrocytes compared to neurons (Chen *et al.*, 2013). ABCA1 protein is expressed in neurons however, the exact physiological function of the transporter in neurons is yet to be elucidated. A study by Matsuda *et al* (2013) suggests that ABCA1 may play a role in 24S-OHC removal from neurons. The study found that the treatment of SH-SY5Y cells with 24S-OHC induced *ABCA1* gene expression and cholesterol efflux within the neurons was HDL- dependent (Matsuda *et al.*, 2013). Although, this study does not help ascertain the physiological function of ABCA1 as SH-SY5Y cells do not endogenously express it. Furthermore, 24S-OHC generates free radicals which induce apoptosis within neurons, making it neurotoxic, hence the action of ABCA1 in removing 24S-OHC may be a survival mechanism rather than a normal physiological mechanism (Kölsch *et al.*, 2001b). ABCA1 plays a crucial role in cholesterol transport within astrocytes. In one study, *ABCA1* gene knockout in primary mouse astrocytes showed an overall decrease in cholesterol efflux and a significant reduction in cholesterol efflux to apoE4 was observed (Hirsch-Reinshagen *et al.*, 2004). Furthermore, silencing of *ABCA1* in astrocytes, showed a decrease in apoE secretion and consequently intracellular cholesterol accumulation was also observed. This data suggests that ABCA1 plays a role in transporting cholesterol out of astrocytes and into apoE *in vitro* and lack of ABCA1 may impact apoE dependent cholesterol transport to neurons.

The data from this study showed a moderate positive correlation with AT8 immunoreactivity and *ABCA1* expression in neurons, suggesting that an increase in AT8 immunoreactivity correlates with an increase in *ABCA1* expression. ABCA1 expression has been shown to alter tau pathology. In one study, transgenic mice

expressing both human apoE3 and apoE4 were treated with a peptide (CS-6253) which directly increased ABCA1 activity. The study found that treatment with CS-6253 significantly decreased the AT8 immunoreactivity in murine hippocampal neurons compared to apoE3 treated and apoE4 untreated mice. Localisation of the peptide was found to accumulate in astrocytes within the hippocampus and treatment increased the lipidation of apoE4 and a significant reversal in cognitive decline was also observed (Boehm-Cagan *et al.*, 2016). This suggests that ABCA1 activation in astrocytes may play a role in the reversal of AD pathology, however the data from our study showed a significant correlation with neuronal *ABCA1* expression rather than astrocytic expression.

Studies have demonstrated a link between Aβ and ABCA1. One study treated primary mouse cortical neurons with oligomeric Aβ and microarray analysis showed an increase in *ABCA1* by a fold change of 4 (Malik *et al.*, 2012). In APP23 mice the knockout of *ABCA1* resulted in an increase in Aβ deposition within the brain (Koldamova, Staufenbiel and Lefterov, 2005). Overexpressing of *ABCA1* has been shown to reduce Aβ deposition. A study by Wahrle *et al* (2008) overexpressed *ABCA1* in an AD mouse model which overexpressed mutant human APP gene and found that there was a significant reduction in Aβ deposition (Wahrle *et al.*, 2008). Activation of liver X receptors in murine neuroblastoma cells expressing the Swedish mutant of APP showed an increase in ABCA1 protein expression leading to a decrease in Aβ formation (Sun *et al.*, 2003). Additionally, when apoE was added a profound decrease in Aβ was observed and a decrease in γ-secretase activity was also observed (Sun *et al.*, 2003). These studies suggest that ABCA1 may have a role to play in the formation of Aβ depositions the exact mechanism in which this is regulated is currently unknown. One possible way in which Aβ formation may be regulated by ABCA1 is preventing γ-secretase activity which in turn prevents APP cleavage from forming the amyloidogenic Aβ42 fragment. Another possibility is the activity of ABCA1 changes the cholesterol composition of the membrane, which favours the non-amyloidogenic processing of APP. However, in our study we found that there was no significant correlation with *ABCA1* expression in neurons and astrocyte isolations from temporal cortex with Aβ immunoreactivity, plaque and tangle pathology in the temporal cortex.

3.5.8 Tissue cholesterol concentration does not change with AD progression and does not correlate to markers of classical AD neuropathology

This study found that there were no significant changes in brain tissue cholesterol concentration in relation to AD neuropathology progression. One study found that in AD transgenic mice brains (Tg2576 and 3xTg-AD) cholesterol accumulates in hippocampal regions undergoing Aβ deposition compared to wild-type mice, which displayed a more homogeneous distribution of cholesterol. The cholesterol granules were not intimately associated with single Aβ deposits but spread over regions where Aβ accumulates (Solé-Domènech *et al.*, 2013). Another study found that cholesterol co-localised with fibrillar Aβ plaques but not diffuse plaques in mutant APP and PS1 transgenic mice (Burns *et al.*, 2003). Studies in transgenic mice expressing the human isoform of tau and *APOE* knockout mice found that neurons affected by tau had higher levels of unesterified cellular cholesterol compared neurons without tau pathology (Glöckner and Ohm, 2014). These studies demonstrate a clear link between cellular cholesterol concentration and classical AD pathology, whereas *this current study* found no significant changes in tissue cholesterol concentration with AD pathology and progression. One possible explanation for this difference is whole tissue cholesterol concentration does not consider changes occurring at an intracellular level. Furthermore, these studies mainly focused on mouse hippocampal regions where AD pathology has a more pronounced effect compared to temporal regions (Belfiore *et al.*, 2019).

3.5.9 Tissue cholesterol concentration does not correlate with markers of cholesterol biosynthesis

This study found that there were no significant correlations in brain tissue cholesterol concentration and markers of cholesterol biosynthesis. Correlations to cholesterol biosynthesis was assessed by comparing tissue cholesterol concentration with percentage immunoreactivity of HMGCR (2.4.1) and relative gene expression of *HMGCR* and *SREBP2* in neurons and astrocytes. The lack of correlation could be explained by the limitations of IHC quantification mentioned previously (2.5.7). Briefly, the number of pixels containing the chromogen is not directly proportional to the amount of protein and the detection system used by the program is not linear (Matkowskyj *et al.*, 2003). Another possible explanation as to why HMGCR immunoreactivity and gene expression does not correlate with tissue cholesterol concentration is that the mevalonate arm of the cholesterol biosynthesis pathway is

also used by neurons to synthesis isoprenoids rather than cholesterol (Cahoy *et al.*, 2008b; Zhang *et al.*, 2014; Moutinho, Nunes and Rodrigues, 2017).

3.5.10 Tissue cholesterol concentration does not correlate with markers of cholesterol metabolism

This study found that there were no significant correlations in brain tissue cholesterol concentration and markers of cholesterol metabolism. Correlations to cholesterol metabolism was assessed by comparing tissue cholesterol concentration with CSF 24-OHC levels (Simpson *et al.*, 2016) and relative gene expression of *ABCA1* and *CYP46A1* in neurons and astrocytes. Studies in human volunteers have found that 24-OHC flux into CSF and then into the jugular vein is calculated to be <1% this suggests that 99% of 24-OHC flux occurs via the BBB (Lütjohann *et al.*, 1996b; Lütjohann, 2006). Thus, measuring plasma 24-OHC levels may be providing a more accurate assessment of cholesterol metabolism within the brain.

3.5.11 Tissue cholesterol concentration does not correlate with markers of oxidative stress

This study found that there were no significant correlations in brain tissue cholesterol concentration and markers of oxidative stress. DNA damage was assessed by γH2AX immunoreactivity (J. E. Simpson *et al.*, 2010), H2AX is a core histone molecule, and is recruited at sites of double stranded breaks where it is phosphorylated on the 139th serine residue to form γH2AX foci (Kuo and Yang, 2008). Oxidative stress was assessed by MDA protein levels and immunoreactivity of thioredoxin2 (Trx2) and peroxiredoxin3 (Prx3). MDA is the product of lipid peroxidation caused by free radicals in cells and is commonly used as a marker of oxidative stress (Torun *et al.*, 2009). Trx2 and Prx2 are involved in the reduction of H_2O_2 into H_2O to maintain mitochondrial redox status and thus a marker ROS induced oxidative stress (Yin *et al.*, 2016). Studies have shown that in AD brains the expression of Prx3 is significantly lower compared to normal brains and Trx2 expression is significantly reduced in the hippocampus of AD brains (Kim *et al.*, 2001; Arodin *et al.*, 2014). One study found that excitatory neurotransmission mechanisms were linked to cholesterol loss in ageing. In primary rat hippocampal neurons excitatory neurotransmission via N-methyl-D-aspartate (NMDA) lead to the generation of ROS and membrane cholesterol loss (Sodero *et al.*, 2011). This study

suggests that a link between oxidative stress via ROS and cholesterol concentration, however in *this current study* no correlation was observed.

3.5.12 Tissue cholesterol concentration does not correlate with markers of neuroinflammation

This study found that there were no significant correlations in brain tissue cholesterol concentration and markers of neuroinflammation. To measure neuroinflammation the immunoreactivity of CD68, GFAP and MHCII from previous studies was used (J. E. Simpson *et al.*, 2010). CD68 is a glycosylated type 1 transmembrane glycoprotein localised to endosomal/lysosomal compartments and is expressed on the surface of macrophages (Chistiakov *et al.*, 2017). Major histocompatibility complex class 2 (MHCII) is a molecule which is expressed by activated microglia which occurs during neuronal injury (Neumann, 2001). GFAP is a protein, which makes up the intermediate filaments of the astrocytic cytoskeletal, in reactive astrocytes this protein is overexpressed (Carter *et al.*, 2019). A study in high cholesterol-fed rabbits found an increase in activated microglia and astrocytes alongside neuropathological features of AD (Zatta *et al.*, 2002). A more recent study investigated the effect of a high cholesterol diet in young and old mice and found that in aged mice on a normal diet microglial activation was observed and in mice fed with a high cholesterol diet showed a further increase in microglial activation and secretion of inflammatory cytokines such a IL-1β, IL-6 and TNF-α (Chen *et al.*, 2018). These studies suggest a relationship between high cholesterol diet and neuroinflammation via microglial activation, however the data from *this study* does not demonstrate this relationship.

3.5.13 Tissue cholesterol concentration does not correlate with markers of vascular pathology

This study found that there were no significant changes or trends in brain tissue cholesterol concentration and markers of vascular pathology. Vascular pathology was assessed by comparing tissue cholesterol concentration with the presence of cortical micro-infarcts and cerebra amyloid angiopathy (CAA) (Ince, 2001; Matthews *et al.*, 2009a). Early studies have shown a decrease in white matter cholesterol levels in brains diagnosed with AD and vascular dementia (Wallin *et al.*, 1989). A more recent population based study has found no significant differences between late life plasma HDL levels and presence of vascular pathologies such as CAA and cerebral microinfarcts (Bettcher *et al.*, 2017). This supports the findings from *this*

current study, however it is important to note that Bettcher *et al* (2017) measured blood plasma cholesterol levels in two ways: the first way was to predict the cholesterol level at age 70; and the second was to predict cholesterol levels 10 years prior to death (Bettcher *et al.*, 2017). Whereas in *this current study* brain tissue cholesterol concentration was directly measured.

3.5.14 Moderate and high tissue cholesterol concentration is associated with dementia status

Data from this current study showed that there was no significant association between temporal cortex cholesterol concentration and dementia status. However, when tissue cholesterol concentration was categorically divided into tertiles and modelled using logistic regression analysis moderate and high tissue cholesterol concentration was associated with dementia. A high degree of uncertainty surrounds this estimate due to the wide 95% confidence intervals which suggest that the current sample size is small, and a larger sample size would provide greater certainty. A longitudinal nationwide population study in Korea (Korean National Health insurance Service- Health Screening Cohort) measured the total cholesterol levels in blood of patients in the cohort during health examinations and the total cholesterol variability was determined from at least three measurements. They found that visit-to-visit total cholesterol variability was a risk factor for the development of all types of dementia (Chung *et al.*, 2019). In another large case-control study in China which measured total blood cholesterol from patients. This study found that a higher serum total cholesterol level was positively associated with the risk of dementia (Chen *et al.*, 2019). In a separate ageing population study in USA measured the total plasma cholesterol levels and then used these values to predict cholesterol levels in later life (Bettcher *et al.*, 2017). In this study, blood plasma cholesterol levels were predicted in two ways: the first way was to predict the cholesterol level at age 70; and the second was to predict cholesterol levels 10 years prior to death. This study found no significant associations between blood cholesterol in late life and AD neuropathology (Bettcher *et al.*, 2017). These studies show the that there is a complicated relationship blood plasma cholesterol levels and dementia however, it is worth noting that these studies investigated blood plasma cholesterol whereas, *this current study* looked at temporal cortex tissue cholesterol concentration.

3.5.15 Limitations of qPCR

There are limitations to the use of qPCR as a reliable method to study changes in gene expression. The qPCR data can be quantified by either absolute quantification or relative quantification (Rao *et al.*, 2013). Absolute quantification was calculated against a standard curve whereas relative quantification is when gene expression is calculated relative to a reference sample. In this study we used relative quantification to analyse our qPCR data using the $2^{-\Delta\Delta Ct}$ method, which determines relative concentration of gene by determining the number of PCR cycles that occur at which fluorescence levels reach a threshold level and is then normalised to reference gene expression and then further normalised to the control sample gene expression and raised to the power of two to give a liner value. In this study the relative concentration values for each gene were calculated relative to the mean ΔCt expression for Braak and Braak group 1 or Thal group 1 for each cell type. The reference gene selected for this study was β-actin, as this was the same housekeeping gene used in the preceding microarray study from which this study is derived from (Simpson *et al.*, 2016). However, in a study by Chen *et al* (2013), the expression of *ABCA1* in both astrocytes and neurons was normalised to the expression of hypoxanthine phosphoribosyl transferase 1 (HPRT1). This was because β-actin expression in primary rat cortical neurons was 0.475 fold of the expression in primary rat cortical astrocytes, whereas HPRT1 expression in neurons was 0.92 fold of astrocytic expression, this allowed for a better comparison in expression of cholesterol transporters between the two cell types (Chen *et al.*, 2013). When carrying out relative quantification it is based on two main assumptions; first of which is that the PCR amplification efficiency is 100% across all samples and genes; and secondly background fluorescence from probes is consistent across all primers (Rao *et al.*, 2013).

3.5.16 Limitations of cholesterol assay

There are some limitations associated with the cholesterol assay which need to be considered. The aim of the study was to determine the cholesterol concentration in temporal cortex tissue however, due to the nature of the frozen blocks that were available it was difficult to isolate the cortical regions. Therefore, the cholesterol concentration values also include cholesterol from white matter regions. Furthermore, according to the manufacturers protocol the assay is designed to detect cholesterol concentrations between 0 μM-20 μM (Amundson and Zhou, 1999). However, during

optimisation of this assay, we found that the fluorescent plate reader would oversaturate at 10 µM and so to maintain accuracy and reproducibility, tissue cholesterol extracts were diluted 500 fold to ensure they were within the standard curve range and a standard curve ranging from 0 µM-7.5 µM was used to determine cholesterol concentration.

3.6 Conclusion

In *this current study,* we confirmed the expression of four key genes (*HMGCR, CYP46A1, ABCA1* and *SREBP2*) involved in the cholesterol biosynthesis pathway and cholesterol metabolism in neurons and astrocyte populations isolated from the temporal cortex. This suggests that neurons possess the machinery to carry out *de novo* cholesterol biosynthesis. Neuronal *HMGCR* relative gene expression was found to have a trend to decrease with increasing tangle pathology and a significant moderate negative correlation with AT8 immunoreactivity. Furthermore, *SREBP2* relative gene expression in enriched neuronal populations isolated from human temporal cortex was found to increase with Braak and Braak stage, tangle pathology and AT8 immunoreactivity. A significant moderate positive correlation between neuronal *ABCA1* expression and tau immunoreactivity was also observed. This data suggests that the gene expression of key regulators of the cholesterol biosynthesis pathway in neurons may be altered by NFT pathology. However, these changes in cholesterol biosynthetic gene expression were not translated to a change in cholesterol concentration and no significant correlation was observed with tissue cholesterol concentration and NFT tangle progression and AT8 immunoreactivity. Although NFT pathology is altering cholesterol biosynthetic gene expression in neurons, it is not having an impact on overall temporal cortex tissue cholesterol concentration suggesting that NFT pathology may be redirecting the cholesterol biosynthesis pathway to provide a different product. In astrocytes we found a significant trend to decrease with *SREBP2* relative concentration and Braak and Braak stages. Furthermore, no significant correlations were observed between tissue cholesterol concentration with HMGCR immunoreactivity and relative gene concentration of *HMGCR* and *SREBP2*. Data from *this current study* also showed that there was no significant association between temporal cortex cholesterol concentration and dementia status. However, when tissue cholesterol concentration was categorically divided into tertiles and modelled using logistic regression analysis,

moderate and high tissue cholesterol concentration was associated with dementia. This suggests that the accumulation of cholesterol within the brain could increase the risk of dementia.

4.0 *In vitro* characterisation of the effects of oxidative stress on the cholesterol biosynthesis pathway in human neurons and astrocytes

4.1 Introduction

Oxidative stress is a feature of brain ageing and may contribute to the pathogenesis of AD. It is defined as the imbalance between biochemical processes leading to reactive oxygen species (ROS) being produced and those processes responsible for the removal of ROS (Harman, 1981; Recuero *et al.*, 2009). Studies have shown that within the CNS there are many contributors to ROS production (Tönnies and Trushina, 2017). One of the main contributors to ROS production in the brain is from mitochondria during oxidative phosphorylation (Ray, Huang and Tsuji, 2012; Holmström and Finkel, 2014). The accumulation of ROS within the brain can have a detrimental impact on several cellular components and functions such as: protein oxidation, lipid peroxidation, membrane destabilisation, ER stress, calcium homeostasis and nuclear DNA damage (Tönnies and Trushina, 2017).

Aβ can also lead to the formation of ROS and contribute to oxidative stress within the brain (Hensley *et al.*, 1994; Varadarajan *et al.*, 2000). The literature suggests that Aβ can accumulate inside neurons and target mitochondria. Hansson Peterson *et al* (2008) showed that incubating human neuroblastoma cells with extracellular Aβ, lead to Aβ being internalised and localised to the inner mitochondrial membrane (Hansson Petersen *et al.*, 2008). This same study also found that Aβ accumulated in mitochondrial specimens obtained from biopsies from living patients undergoing neurosurgery for suspected normal pressure hydrocephalus. Studies using a Drosophila model of AD showed that Aβ42 induced mitochondrial mis-localisation with accumulation of mitochondria within the soma and a reduction in axons and dendrites of neurons (Iijima-Ando *et al.*, 2009). Together these studies suggest that Aβ may play a role in mitochondrial dysregulation, which may play a role in ROS accumulation and AD pathogenesis.

Accumulation of ROS within the brain can lead to the oxidation of nucleic acids resulting in DNA damage (oxidative DNA damage) (Halliwell and Cross, 1994). Aβ can directly cause oxidative DNA damage. Human NT2 teratocarcinoma cells incubated with Aβ showed an up-regulation of a gene implicated in DNA excision repair mechanisms (growth arrest and DNA damage-inducible gene- *gadd45*),

suggesting that Aβ may cause rapid DNA strand breaks (Santiard-Baron *et al.*, 1999). Oxidative DNA damage is higher in the temporal lobes of both AD and control brains compared to other brain regions (Lyras *et al.*, 1997).

Build-up of oxidative DNA damage within neurons can trigger neuronal death, and the failure of DNA damage repair mechanisms also contribute to neuronal death (Coppede and Migliore, 2009). The base excision repair (BER) system is a mechanism responsible for repairing DNA damage caused by oxidative stress (Kwiatkowski *et al.*, 2016). Patients with AD showed an increase in the level of DNA damage compared to control patients, and polymorphisms in genes involved in the BER response which may contribute to the increase in DNA damage were also observed (Kwiatkowski *et al.*, 2016). Reactivation of the cell cycle within neurons has been suggested to be an attempt to repair damaged DNA (Krantic *et al.*, 2005; Coppede and Migliore, 2009). Breast cancer type 1 susceptibility protein (BRCA1) is involved with both DNA damage response and cell cycle regulation (Wezyk and Zekanowski, 2018). The promoter region for *BRCA1* was hypomethylated in post-mortem brain tissue from AD patients, resulting in upregulation and mis-localisation of the BRCA1 protein (Mano *et al.*, 2017).

Previous studies from our lab have shown that at low Braak and Braak stages there is an increase in oxidative stress markers such as; γH2AX, 8-OHdG and DNA-dependent protein kinase compared to high Braak and Braak stages in the temporal cortex. Furthermore, high levels of oxidative stress were associated with a DNA damage response (DDR) (J. E. Simpson *et al.*, 2010). Microarray analysis on neurons isolated from frontal cortex sections from the CFAS population-derived neuropathology cohort with low and high DDR was utilised to investigate neuronal changes associated with the DDR (Simpson *et al.*, 2016). This study had included only low Braak and Braak stage (I-II) cases (n=39) from the cohort, so that confounding effects of AD pathology were not included, and the effects of AD were not examined by the paper. Up-regulation of *HMGCR* (fold change of 4.5, p=0.0008) and down-regulation in *SREBF2* (fold change of -1.1, p=0.001) was associated with a high DDR. Further work identified that there was an overexpression of *HMGCR* in cases with high neuronal DDR suggesting that there is a link with oxidative DNA damage and cholesterol biosynthesis (Simpson *et al.*, 2016). As a result, for *this study* four key genes involved in cholesterol homeostasis were investigated to

assess changes in relative gene expression following exposure to oxidative stress. The genes selected were *HMGCR, SREBP2, ABCA1* and *APOE*.

The involvement of *HMGCR, SREBP2 and ABCA1* in AD and cholesterol homeostasis are discussed previously (3.1). Apolipoprotein E (*APOE*) is found on chromosome 19 and has 3 alleles- ε2, ε3 and ε4- of which ε2 is said to be protective and ε4 increases the risk of AD(Corder et al. 1993; Strittmatter et al. 1993; Rosenthal & Kamboh 2014; Karch & Goate 2015). *APOE* codes for a glycoprotein which is 299 amino acids long and is involved in cholesterol transport, neuroplasticity and inflammation within the CNS (Kim, Basak and Holtzman, 2009; Karch and Goate, 2015). *APOE* is mainly expressed in astrocytes and microglia however, neurons are also able to express this gene during AD, although at a lower level than astrocytes (Metzger *et al.*, 1996; Xu *et al.*, 2006; Kim, Basak and Holtzman, 2009). ApoE interacts with Aβ and is involved in the clearance, aggregation and metabolism of Aβ, although the exact mechanisms are yet to be elucidated (Kim, Basak and Holtzman, 2009; Karch and Goate, 2015). ApoE is involved in the transport of cholesterol produced in astrocytes to neurons (Pfrieger, 2003). ABCA1 activity in astrocytes is critical to apoE protein lipidation to form the apoE HDL (Vance and Hayashi, 2010). The lack of lipidation of apoE4 makes it more prone to forming aggregates and developing AD pathology (Hatters *et al.*, 2006; Raulin *et al.*, 2019). Once the apoE HDL is formed it delivers cholesterol to neurons by binding to low-density lipoprotein receptors (LDLR) (Herz and Bock, 2002; Belloy, Napolioni and Greicius, 2019).

To investigate the effects of acute and chronic oxidative stress in neurons and astrocytes *in vitro,* a double stress model, previously optimised in our lab group was used (Irina Vázquez-Villaseñor, unpublished data). This model used Lund human mesencephalic cells (LUHMES), a conditionally immortalised human dopaminergic neuronal precursor cell line. The double stress model has shown to induce double stranded breaks in DNA which can been detected 96 hrs following the stress (Irina Vázquez-Villaseñor, unpublished data). This model can induce a more persistent oxidative DNA damage in cells, by the addition of H_2O_2 to the culture media. This same stress model was applied to primary human foetal astrocytes, to investigate the effects of acute and chronic oxidative stress. The use of this model allows the

characterisation of changes that occur in neurons and astrocytes when exposed to oxidative stress.

4.2 Aims and Objectives

The aim of this study is to examine the effects of acute and chronic oxidative stress on the expression of genes involved in cholesterol biosynthesis and metabolism in neurons and glia.

We hypothesise that exposure to acute and chronic oxidative stress leads to cholesterol dysregulation in neurons and astrocytes, whereby an initial compensatory mechanism occurs, which then fails following chronic oxidative stress.

The objectives of this chapter are:

- Characterise LUHMES differentiation and expression of genes involved in cholesterol biosynthesis and metabolism.
- Determine the expression of *HMGCR*, *SREBP2*, *ABCA1* and *APOE* following a single and double exposure to H_2O_2 in LUHMES and primary human foetal astrocytes.
- Visualise the effects of single and double exposure to H_2O_2 on DNA damage in LUHMES and primary human foetal astrocytes.
- Determine the effect on cell viability on primary human foetal astrocytes following single and double exposure to H_2O_2.

4.3 Methods

List of materials can be found in Appendix 6.1.2

4.3.1 LUHMES cell culture

Lund human mesencephalic (LUHMES) cells, a conditionally immortalised human dopaminergic neuronal precursor cell line, possess the ability to differentiate into post-mitotic neurons following a strict differentiation protocol. LUHMES were derived from an 8-week old human embryonic ventral mesencephalic tissue and immortalised using a LINX v-*myc* retroviral vector containing a tetracycline-controlled transactivator (tTA). Therefore, in the absence of tetracycline (tet) v-*myc* gene transcription is activated by tTA continuing the cell cycle and maintaining the cells in a proliferative state. The addition of tet to culture media causes binding of tet to tTA which inhibits v*myc* expression arresting the cell cycle and initiating differentiation so that after five days the LUHMES will be post-mitotic (Hoshimaru *et al.*, 1996; Lotharius *et al.*, 2002; Lotharius, 2005). A two-step differentiation protocol, by re-plating the LUHMES following two days of differentiation, allows for a homogeneous and synchronised population of post-mitotic cells following five days of differentiation. LUHMES have been shown to be maintain electrophysiological activity for a further five-six days after achieving the post-mitotic state (Scholz *et al.*, 2011).

During the proliferation phase, the LUHMES were grown in Advanced DMEM/F12 (advanced Dulbecco's Modified Eagle Medium/Nutrient Mixture F-12, Gibco) with 1% (v/v) N2-supplement (Gibco); 1% (v/v) L-glutamine (Lonza group Ltd); 1% (v/v) Penicillin/Streptomycin (P/S) (Lonza group Ltd) and supplemented with 40 ng/ml basic fibroblast growth factor (bFGF) (Peprotech EC Ltd, USA). Fresh media was added replacing bFGF with 1 µg/ml of tetracycline (Sigma-Aldrich) to induce differentiation and over five days the LUHMES differentiated and become post-mitotic, with a re-plating step being performed on the third day after adding the differentiation media. LUHMES were grown in T75 flasks coated with 50 µg/ml Poly-L-ornithine hydrobromide (pLo) (Sigma-Aldrich) and 1 µg/ml fibronectin (Sigma-Aldrich) in sterilised distilled water (d.H_2O). The flasks were coated for a minimum of 3 hrs at 37°C and washed with sterile 1x phosphate buffered saline (PBS), prior to seeding. LUHMES were maintained in T75 flasks or plates at 37°C with 5% CO_2. LUHMES were passaged when they reached an 80% confluency, they were

dissociated using 1x trypsin versene (Lonza Group Ltd) at 37°C for 5 minutes and centrifuged at 550 rpm for 5 minutes to form a pellet which was then re-suspended in 5 ml of fresh media and re-plated accordingly (Table 4.1).

Plate or Flask	Proliferating cell density (cells/well or flask)	Differentiating cell density (cells/well or flask)
T75 flask	$7.0x10^5$	$4.0x10^6$
6-well plate	$5.5x10^5$	$1.5x10^6$
12-well plate	$3.0x10^5$	$4.5x10^5$
24-well plate	$1.0x10^5$	$3.5x10^5$

Table 4.1: LUHMES seeding densities

4.3.2 Cryopreservation of LUHMES

LUHMES were dissociated from the flask as previously described in 4.4.1, pelleted and re-suspended in cryopreservation media consisting of 70% advanced DMEM/F12 (Gibco) supplemented with bFGF (40ng/ml) (Gibco) , 10% (v/v) Foetal Bovine Serum (FBS) (Biosera) and 20% (v/v) Dimethyl Sulphoxide (DMSO) (Gibco). The LUHMES were stored in labelled sterile cryogenic vials at a cell density of $1x10^6$ cells/ml and stored at -80°C for 24 hrs in CoolCell® SV2 (Biocision) before transferring to liquid nitrogen for long term storage.

4.3.3 Astrocyte cell culture

Primary human astrocytes isolated from human foetal cerebral cortex, were purchased from ScienceCell Research Laboratories (USA). Astrocytes were maintained in T75 flasks in Astrocyte media, supplemented with 2% (v/v) Foetal Bovine Serum (FBS), 1% (v/v) Astrocyte Growth Supplement (AGS) and 1% (v/v) Penicillin/Streptomycin (P/S) (all ScienceCell Research Laboratories, USA). Astrocytes were cultured at 37°C and 5% CO_2. Astrocyte media was changed every 3-4 days and astrocytes were passaged when cells reached 90% confluency. Astrocytes were dissociated from the flasks using 1x trypsin versene (Lonza Group Ltd) at 37°C for 5 minutes and centrifuged at 550 rpm for 5 minutes to form a pellet which was then re-suspended in 3 ml of fresh astrocyte media and re-plated according to the experiments.

4.3.4 H_2O_2 treatments

Both LUHMES and astrocytes were subjected to single and double stress experiments (Figure 4.1). For single stress experiments fully differentiated LUHMES or primary human astrocytes were treated with a single dose of 50μM H_2O_2 (Sigma-Aldrich, USA). This dose was chosen, as no significant impact on cell viability was detected after 2 hrs and a 27.1% reduction in cell viability after 24 hrs. This dose induced a DNA damage response in LUHMES which could be detected after 24 hrs after a single stress and 96 hrs after a double stress (Irina Vázquez-Villaseñor, unpublished data). An equal volume of sterile PBS was used as a control. The effects of single dose were assessed at 1 hr, 3 hr, 6 hr and 24 hrs (n=3). For double stress experiments a second dose of 50 μM H_2O_2 was added to the cells 6 hrs following the first dose. The effects of a double dose were assessed at 1 hr, 3 hrs, 6 hrs, 24 hrs, 48 hrs and 96 hrs (n=3).

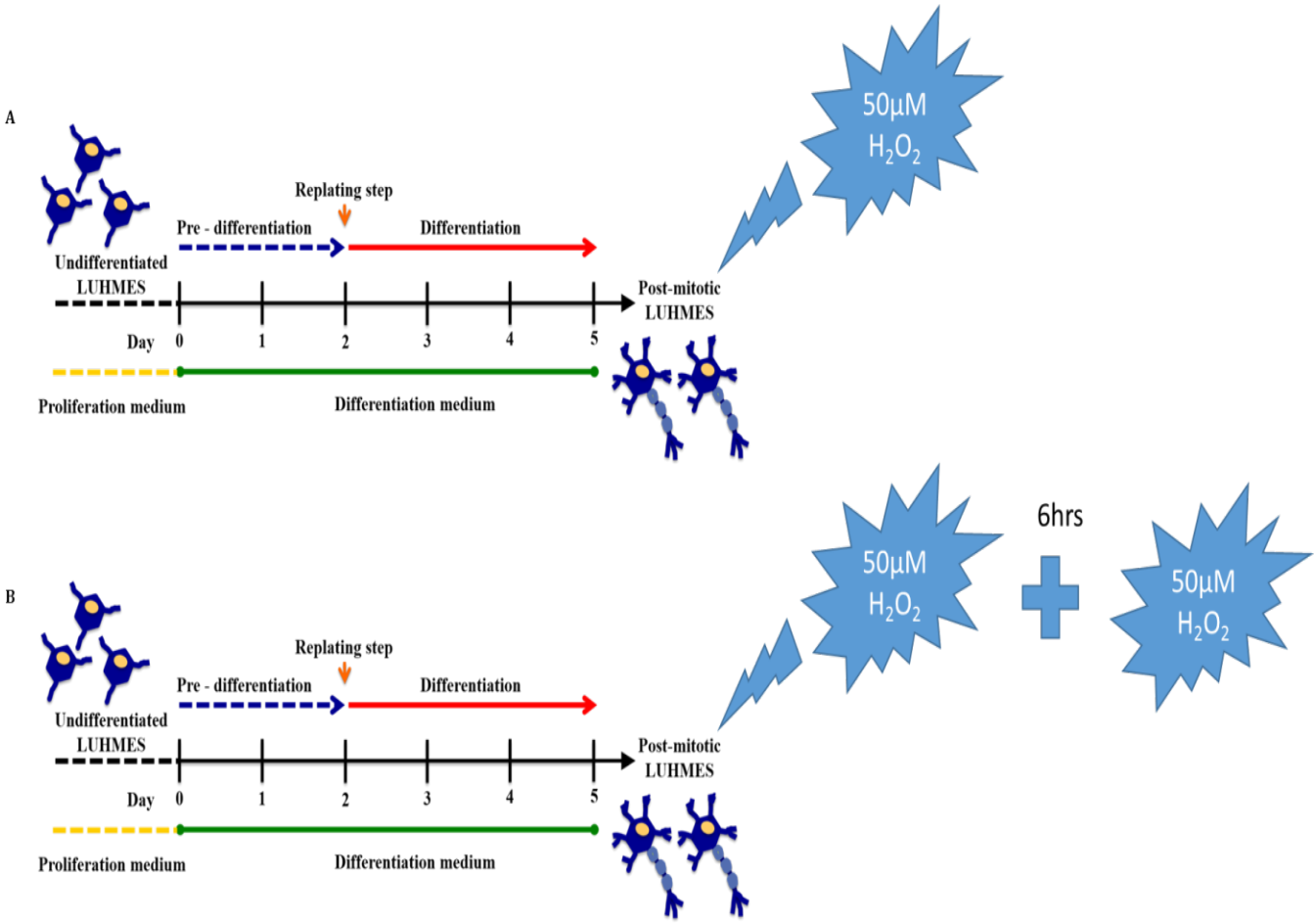

Figure 4.1. Double stress model. A diagram to illustrate the single (A) and double (B) dose of 50 µM H_2O_2 used in LUHMES and astrocytes to model the effects of acute and chronic oxidative stress on cholesterol biosynthesis.

4.3.5 RNA extraction from cells using TRIzol

For single and double stress in both astrocytes and neurons RNA was extracted from a combination of 4 wells, each condition yielding a final volume of 600 µl and 800 µl (astrocyte and neurons, respectively) of TRIzol extract per condition. Cells were scraped from the surface of the well and the TRIzol extracts were stored in labelled sterile tubes at -80°C. RNA extraction was carried out using the Direct-zol RNA MiniPrep extraction kit (Zymo Research, USA) according to the manufacturer's protocol. Briefly, TRIzol extracts were defrosted and mixed with equal volumes of 100% ethanol (LUHMES = 800 µl and astrocytes = 600 µl) and transferred to a Zymo-Spin IIC Column and centrifuged at 13,000g for 30 seconds at RT. The flow-through was discarded and the column was washed with Direct-Zol RNA PreWash and centrifuged at 13,000g for 30 seconds at RT twice followed by a wash with Direct-Zol RNA Wash Buffer and centrifuged at 13,000g for 2 minutes at RT. Following the washes, RNA was eluted from the columns using 50 µl of RNase free water and centrifuged at 13,000g for 30 seconds at RT into a sterile tube. The RNA was stored in a labelled sterile tube at -80°C. RNA concentration was determined by placing 1µl of RNA sample in the NanoDrop Spectrophotometer (ThermoFisher Scientific, USA). This also allowed determination of the purity of the RNA sample as a ratio was also measured. RNA integrity and degradation were determined using the Agilent RNA 6000 Nano Chip (Agilent Technologies, USA). Both methods helped determined the quality of the RNA that was used and would aid in downstream gene expression analysis via qPCR.

Following RNA extraction, cDNA synthesis, validation and q RT-PCR was carried out as outlined in previous chapter please refer to sections 3.3.7, 3.3.8 and 3.3.9. The PrimeTime qPCR assays (Integrated DNA Technologies) (Table 4.2) were used. Quantification of qPCR data was carried out using the ΔΔCt method relative to expression of control cells at the corresponding time points. Statistical analysis was carried out using GraphPad Prism 8.0 program (GraphPad Software, Inc., USA).

Gene	Prime Time® Assay ID	Reference	Exon	Primer Sequence	Probe Sequence
HMG Co Reductase (HMGCR)	Hs.PT.58.4048748	NM_001130996	15-16	1) 5'-CCTTTATATCCGTTTCCAGTCCA-3' 2) 5'-CCACTAACGGCTAGAATCTGC-3'	5'-/56-FAM/ATGTTCATC/ZEN/CCCATGGCATCCCC/3IABkFQ/-3'
Cytochrome P450 46A1 (CYP46A1)	Hs.PT.58.26445892	NM_006668	12-13	1) 5'-AAGAGTCGCTGAGGCTGTA-3' 2) 5'-CCTCAAAGTATGTGTCCATCCG-3'	5'-/56-FAM/CTCCTCTTC/ZEN/CAGCAGGCGAAAGG/3IABkFQ/-3'
ATP Binding Cassette A1 (ABCA1)	Hs.PT.58.11955	NM_005502	49-50	1) 5'-TGCTACAATACCAGCTTCCATC-3' 2) 5'-GTCCTTGGCAAAGTTCACAA-3'	5'-56-FAM/TCTCCCAGA/ZEN/GCAAAAAGCGACTCC/3IABkFQ/-3'
Acetyl-CoA acetyltransferase 1 (ACAT1)	Hs.PT.56a.22489703	NM_000019	11-12	1) 5'-CTGTTTCTCTGGGACATCCAA-3' 2) 5'-GAATTAGCATGGCAGAAGCAC-3'	5'-56-FAM/TCAAATGAC/ZEN/CAACAATCCTGGCTCCA/3IABkFQ/-3'
Sterol regulatory element binding transcription factor 2 (SREBF2)	Hs.PT.58.39417166	NM_004599	16-17	1) 5'-TTCCTTCTGCCATTGCGA-3' 2) 5'-ACAGTAGCAGGTCACAGGT-3'	5'-56-FAM/CTATGGAGC/ZEN/AGCCTCAACGTCAGT/3IABkFQ/-3'
SREBF chaperone (SCAP)	Hs.PT.58.1056408	NM_012235	18-19	1) 5'-CAGCAGCGAGGAGGTCT-3' 2) 5'-GAGAAGAAATCAAGGGAACCGT-3'	5'-56-FAM/CGTGCAGGCC/ZEN/ACAATCCTTTTGTCC/3IABkFQ/-3'
HMG Co Synthase 1 (HMGCS1)	Hs.PT.58.26937768.g	NM_002130	9-10	1) 5'-ATTCAAGAACTGGTGTGGCA-3' 2) 5'-AGTACCACGTTCCTTCAAAGAG-3'	5'-56-FAM/AACATGAAG/ZEN/CTCAGAGAGGACACCC/3IABkFQ/-3'
Mevalonate kinase (MVK)	Hs.PT.58.40379926	NM_001114185	8-10	1) 5'-CTGCTCAAGTTCCCAGAGAT-3' 2) 5'-TCATGTCAATGAGCTCTTCCA-3'	5'-56-FAM/CTTCCCCCA/ZEN/TCTCTCCCAGCAC/3IABkFQ/-3'
Mevalonate diphosphate decarboxylase (MVD)	Hs.PT.58.40165633.g	NM_002461	7-8	1) 5'-CATCTCCTGGCGCATCATC-3' 2) 5'-ACAAACTCAGCCACAGTGTC-3'	5'-56-FAM/CACCGCTTC/ZEN/AACGCCCACC/3IABkFQ/-3'
Farnesyl-diphosphate farnesyltransferase 1 (FDFT1)	Hs.PT.58.40218739	NM_004462	7-8	1) 5'-GGGCAAGCAGTGACCCT-3' 2) 5'-TGGTGGAGATGATCTGCCT-3'	5'-56-FAM/AGATTTATC/ZEN/ATAGAATCCCCGACTCAGACCC/3IABkFQ/-3'
Beta-Actin (ACTB)	Hs.PT.39a.22214847	NM_001101	1-2	1) 5'-ACAGAGCCTCGCCTTTG-3' 2) 5'-CCTTGCACATGCCGGAG-3'	5'-56-FAM/TCATCCATG/ZEN/GTGAGCTGGCGG/3IABkFQ/-3'
Apolipoprotein E (APOE)	Hs.PT.56a.3799446	NM_000041	3-4	1) 5'-TCTGAGCAGGTGCAGGA-3' 2) 5'-GTTGTTCCTCCAGTTCCGATT-3'	5'-56-FAM/CGTCCATCA/ZEN/GCGCCCTCAGTTC/3IABkFQ/-3'

Table 4.2: List of all Prime Time® qPCR Assays used for cholesterol biosynthetic gene expression investigation

4.3.6 Immunocytochemistry

Cells were washed once with PBS followed by fixation in 4% paraformaldehyde (PFA) (Sigma-Aldrich) for 5 minutes at 37°C. Cells were gently washed 3 times with PBS and permeabilised in 0.3% Triton-X-100 (Sigma-Aldrich) for 3 minutes at RT, washed again in PBS and coverslips were blocked in ICC blocking solution (3% (w/v) BSA diluted in PBS-T) for 30 minutes at RT. Coverslips were incubated with the primary antibodies diluted in ICC blocking solution, antibody details and incubation conditions are provided in table 4.3. Following primary antibody incubation, the coverslips were washed 3 times with PBS and then incubated with the appropriate species of secondary antibody diluted in ICC blocking solution (Table 4.4) for 1hr at RT followed by further washes in PBS. Nuclei were stained with Hoechst 33342 dye (Sigma-Aldrich) before mounting in ClearMount™ Mounting solution (Invitrogen). Rabbit and mouse isotype controls and omission of primary antibody (negative controls) were included to confirm antibody specificity. Cells were examined and imaged using a DsRi1 Eclipse microscope and camera (Nikon instruments, Japan).

Dual labelling immunocytochemistry was performed to determine the presence of γH2Ax foci within neuronal and astrocytic nuclei. Cells were fixed, permeabilised and non-specific binding blocked as described above. Cells were then incubated with a primary antibody against γH2AX (Table 4.3) washed in PBS and incubated with an anti-mouse secondary antibody (Table 4.4) at RT. From this point onwards, the remainder of the protocol was carried out in the absence of light. After removing the secondary antibody and washing in PBS, coverslips were again incubated in ICC blocking solution prior to an overnight incubation in the second primary antibody, which was cell specific; for LUHMES this was anti-β-III-tubulin and astrocytes anti-CD44 (Table 4.3). Coverslips were washed in PBS, incubated with the appropriate species of secondary antibody (Table 4.4) and nuclei were stained as outlined above. Negative and isotype controls were carried out as outlined above. Coverslips were mounted and imaged as outlined above.

Antibody	Species	Specificity	Dilutions and incubation conditions	Source
NeuN	Mouse monoclonal	Neuronal nuclei protein	1:100 (1hr, RT)	Merck Millipore, Germany
B-III-Tubulin	Chicken polyclonal	B-III tubulin peptide	1:1000 (1hr, RT)	Merck Millipore, Germany
Ki67	Mouse monoclonal	Ki67 Cell cycling antigen	1:50 (overnight, 4°C)	Leica microsystems, Germany
Map2	Rabbit polyclonal	Microtubule associated protein	1:100 (1hr, RT)	Sigma-Aldrich, USA
CD44	Rabbit polyclonal	CD44 Peptide	1:500 (overnight, 4°C)	Abcam, UK
γH2AX	Mouse monoclonal	Phosphorylated histone H2A.X at Ser139.	1:500 LUHMES (1hr, RT) Astrocytes (2hr, RT)	Merck Millipore, Germany

Table 4.3: Primary antibodies used for immunocytochemistry experiments

Antibody	Species	Dilution and incubation conditions	Source
488 Alexa Flour anti-chicken	Goat	1:1000 (1hr, RT)	Thermo Fisher Scientific, USA
568 Alexa Flour anti-mouse	Goat	1:1000 (1hr, RT)	Thermo Fisher Scientific, USA
568 Alexa Fluor anti-rabbit	Donkey	1:1000 (1hr, RT)	Thermo Fisher Scientific, USA

Table 4.4: Fluorescent secondary antibodies used for immunocytochemistry experiments

4.3.7 Lactate Dehydrogenase Assay

Lactate dehydrogenase (LDH) assay was carried out to assess cytotoxicity and cell viability in astrocytes after single and double exposure to 50 μM H_2O_2. This assay works on the principle that the LDH enzyme, a stable enzyme found in the cytoplasm of all cells, is released into the cell culture media following cell lysis. To quantify enzyme activity, NADH levels are measured through a coupled reaction where a yellow tetrazolium salt is converted into a red formazan product in the presence of NADH. Formazan levels are directly proportional to LDH levels, which is directly proportional to the number of damaged cells. Formazan levels are determined by measuring the absorbance of samples at 492 nm wavelength using a colorimetric plate reader (Kumar, Nagarajan and Uchil, 2018).

LDH cytotoxicity assay was purchased from Promega, USA and was carried out according to manufacturer's protocol. Astrocytes were grown in phenol red free astrocyte media in 12-well plates and stressed as outlined above (4.3.4). Following stresses, 3x 50 µl samples of media were transferred into a 96 well plate. The remaining media was collected, and the volume was measured. 150 µl of 1x lysis solution (provided in the kit) was added to each well and incubated at 37°C for 45 minutes. Following incubation, 850 µl of culture media was added to each well containing lysed astrocyte and 3 x 25 µl of lysed cell suspension was transferred into a 96 well plate and was made up to 50 µl using culture media. 50 µl of reaction mix was added to each well and was incubated for 30 minutes at RT in the dark. The assay was terminated by adding 50 µl of the stop solution (provided in the kit) into each well and the absorbance at 490 nm was measured using the PHERAStar spectrophotometer. The absorbance was normalised to positive controls and media controls on each plate and percentage cell death was calculated by working out the ratio of the absorbance at 490 nm of the media before and after lysis.

4.3.8 Statistical Analysis

Data obtained within *this study* was analysed with GraphPad Prism 8.0 (GraphPad Software, Inc., USA). All data was presented as mean ± standard error of the mean (SEM). One-way ANOVA was used to determine statistical significance of the data obtained from cholesterol biosynthesis gene expression in LUHMES during differentiation and cell viability experiments from astrocytes experiments. Post-hoc analysis of significant data was carried out using Tukeys multiple comparison test.

4.4 Results

4.4.1 Characterisation of LUHMES during proliferation and differentiation

To characterise LUHMES differentiation and confirm that the 2-step differentiation protocol outlined by Scholz *et al,* (2011) leads to post-mitotic neurons, immunocytochemistry for neuronal and cell cycle markers was carried out. NeuN expression in LUHMES was localised to the nucleus of the cells (Figure 4.2). During proliferation, NeuN expression was weak and was localised to the nucleus and cytoplasm as differentiation was initiated expression of NeuN was not detected during day 1 to day 2. Weak cytoplasmic staining was present on day 3 whilst on day 4 and 5 NeuN expression was detected in the nuclei of cells. During differentiation, the morphology of the nuclei within LUHMES was also altered, during proliferation nuclei appear to have a more ovoid morphology, whereas by day 5 LUHMES nuclei appear to have an oblong morphology. Microtubule-associated protein 2 (MAP2) is a protein involved in microtubule assembly and is abundantly expressed within the brain and is localised to somatodendritic compartments of neurons helping to stabilise dendrites (Harada *et al.*, 2002). MAP2 expression in LUHMES was detected during all stages of differentiation and proliferation. During proliferation, MAP2 staining was weak and near the nucleus, as the LUHMES differentiated expression of MAP2 was localised to small neurites structures which eventually formed longer neurites at days 4 and 5.

To characterise cell cycle status, Ki67 expression was determined in LUHMES. Antigen Ki67 is expressed in mammalian cells undergoing cell cycle, it is a nuclear protein which has been shown to be involved in heterochromatin organisation and is used as a cell proliferation marker (Sobecki *et al.*, 2016). When LUHMES are undergoing proliferation, the expression of Ki67 was localised to cell nuclei with most cells showing positive staining. Once differentiation had been initiated, the number of Ki67 positive nuclei decreased from day 1 to day 3 and after day 4 no Ki67 positive nuclei were observed. Staining for β-III-tubulin was also carried out to visualise morphological changes as β-III-tubulin is localised to the cytoskeleton. Within proliferating, day 1 and day 2, cells β-III-tubulin expression was present and displayed a change in morphology as small neurites formed. From day 3 onwards, neurites could be easily identified and were longer, a reduction in cell body size was also observed as differentiation took place.

4.4.2 Cholesterol biosynthetic gene expression in LUHMES during differentiation

To assess cholesterol biosynthesis in LUHMES during differentiation, expression of key genes involved in cholesterol homeostasis was determined as LUHMES differentiated. LUHMES were cultured and RNA was extracted at the same time point for each day and qPCR analysis for nine key genes was carried out and quantified using the ΔΔCt calculation relative to the mean expression in proliferating LUHMES (Figure 4.3). Between the samples, a lot of variation in relative gene expression was observed. *HMGCR* expression was observed at all stages of differentiation and remained consistent during differentiation with a small increase in expression seen on day 2 and day 5, no significant difference between *HMGCR* expression during differentiation and proliferation was observed (ANOVA, p=0.461). *ABCA1* expression increased during the first two days of differentiation followed by a sudden decrease in expression on day 3, followed by an increase in expression on day 4 and day 5, however the changes in *ABCA1* expression were not statistically significant (ANOVA, p=0.553). The expression of *ACAT1* shows a decrease in expression as LUHMES differentiate however, this decrease was not statistically significant (ANOVA, p=0.095). *SREBP2* expression increased during the first two days of differentiation followed by a sudden decrease in expression on day 3, followed by an increase in expression on day 4 and day 5, however the changes in *SREBP2* expression were not statistically significant (ANOVA, p=0.698). *SCAP* expression was significantly decreased in differentiating LUHMES compared to proliferating LUHMES (ANOVA, p=0.018), Tukey multiple comparisons showed that day 3, day 4 and day 5 were significantly decreased compared to proliferating cells (p=0.018, p=0.022, p=0.048 respectively). *HMGSC1* showed an initial decrease in expression and then following day 3 expression increased however, the changes were not statistically significant (ANOVA, p=0.103). The expression of both *MVK* and *MVD* had a similar profile with an initial decrease in expression until day 3 and then a plateau in expression, however these changes were not statistically significant (p=0.179, p=0.193 respectively). *FDFT1* expression decreased as LUHMES differentiated, the expression decreased until day 3 after which the expression stayed constant. This decrease was statistically significant (ANOVA, p=0.040) and Tukey's multiple comparisons showed that the expression at day 3 was significantly lower compared to proliferating LUHMES (p=0.043).

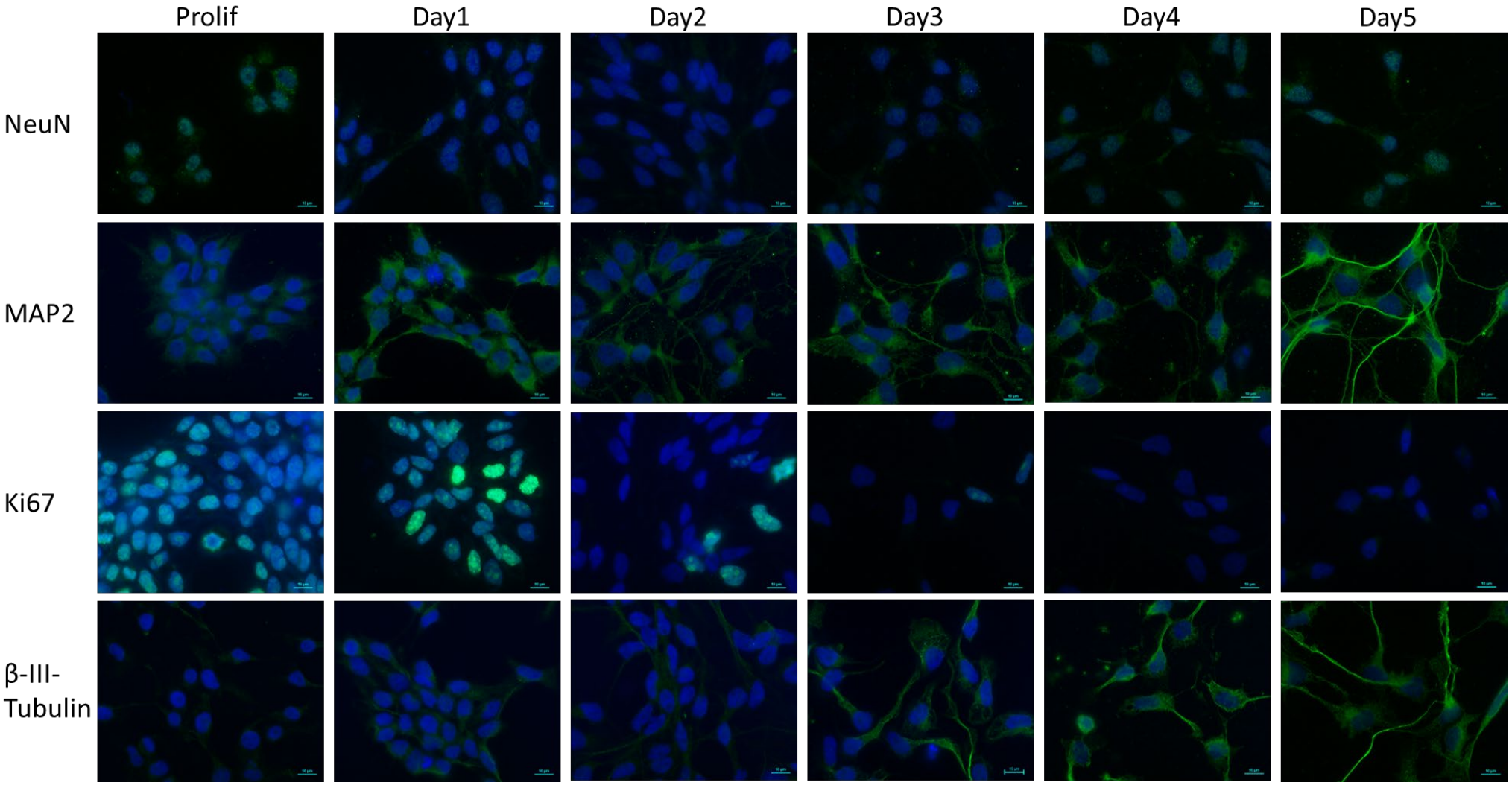

Figure 4.2. Characterisation of proliferating and differentiating LUHMES. Tetracycline was added to LUHMES to inactivate the v-*myc* transgene and induce terminal differentiation and the expression of key proliferative and neuronal markers was determined using immunocytochemistry. LUHMES were fixed with 4% PFA on each day of the differentiation process and immunolabelled with antibodies NeuN (green-top row), MAP2 (green-second row), Ki67 (green-third row) and β-III-tubulin (green-bottom row). Nuclei were stained with a nuclear dye Bisbenzimide (blue). Scale bar represents 10μm.

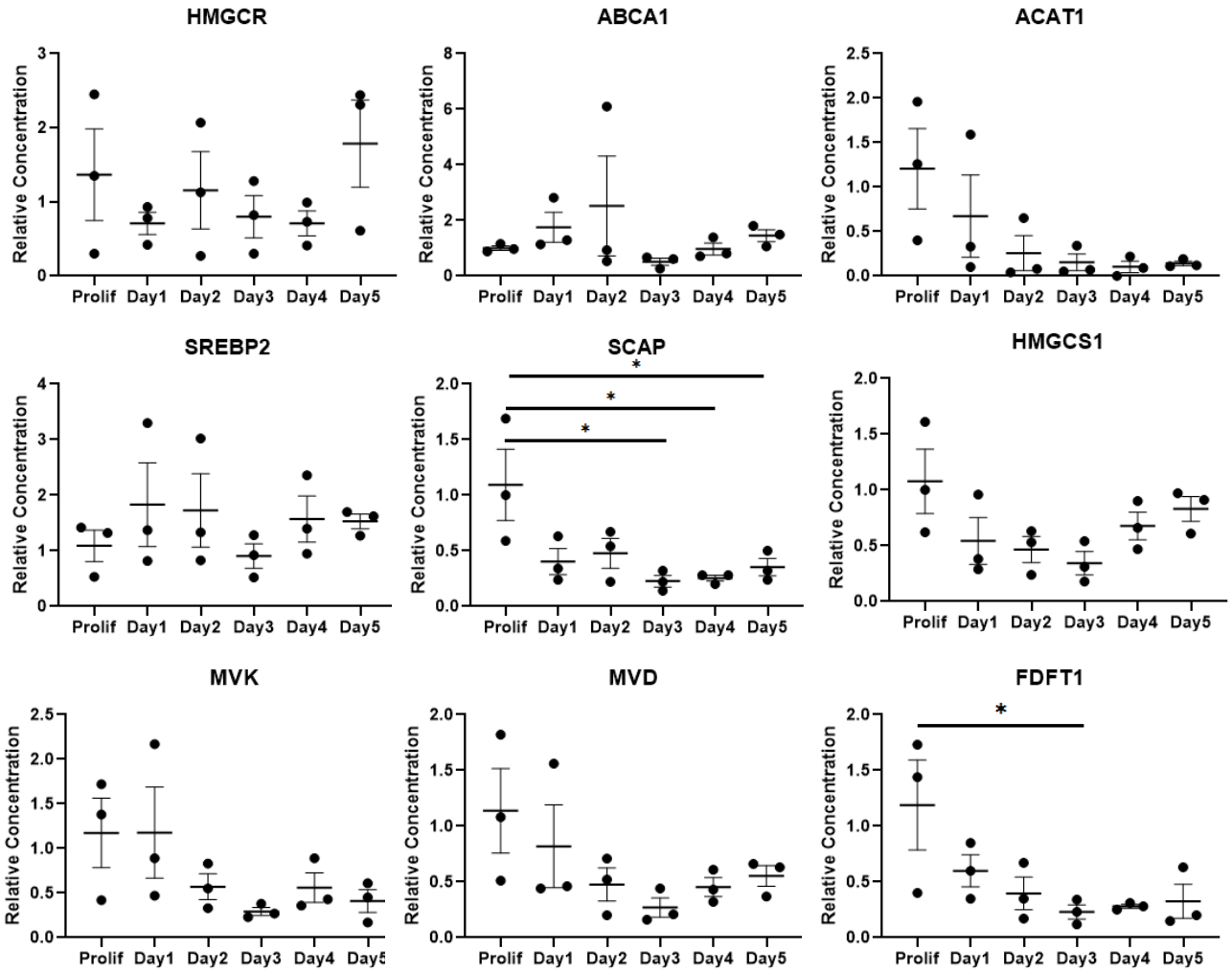

Figure 4.3. Cholesterol biosynthetic gene expression during LUHMES differentiation: The relative expression of genes involved in cholesterol biosynthesis was determined during LUHMES differentiation. Relative concentration values were calculated using the ΔΔCt calculation relative to the mean expression in proliferating LUHMES. A significant decrease in expression was observed in SCAP and FDFT1. N=3

4.4.3 Single and double exposure to H_2O_2 leads to the presence of γH2AX foci in post-mitotic LUHMES

To investigate the effects of oxidative stress on cholesterol biosynthesis, LUHMES were cultured on glass coverslips and exposed to either a single or double dose of 50 μM H_2O_2. Immunocytochemistry for γH2AX foci demonstrated that at all time points with both a single and double exposure to 50 μM H_2O_2, γH2AX foci was detected in the nuclei of LUHMES over 24 hrs and 96 hrs respectively (Figure 4.4).

4.4.4 Single exposure to H_2O_2 shows no significant changes in cholesterol biosynthetic relative gene expression in post-mitotic LUHMES

Post-mitotic LUHMES were exposed to a single dose of 50 μM H_2O_2 and the expression of four genes (*HMGCR, ABCA1, SREBF2* and *APOE*) involved in cholesterol biosynthesis and metabolism was determined using qPCR over 24 hrs. Preliminary data shows that all four genes were expressed in control and treated cells at all time-points. The current data suggests that there was a reduction in *ABCA1* expression and an increase in *SREBP2* expression following treatment with H_2O_2. However, due to the COVID-19 pandemic and a lack of technical replicates we found that the data is inconclusive (Figure 4.5).

4.4.5 Double exposure to H_2O_2 shows no significant changes in cholesterol biosynthetic relative gene expression in post-mitotic LUHMES

Post-mitotic LUHMES were exposed to a single dose of 50 μM H_2O_2 followed by another dose of 50 μM H_2O_2 6 hrs later. The expression of four genes (*HMGCR, ABCA1, SREBF2* and *APOE*) involved in cholesterol biosynthesis and metabolism was determined using qPCR over 96 hrs. Preliminary data shows that all four genes were expressed in control and treated cells at all time-points. The current data suggests that there is an increase in *HMGCR* expression with both a single and a double stress for the first 48 hrs, which stabilises at 96 hrs. However, due to the COVID-19 pandemic and a lack of technical replicates we found that the data is inconclusive (Figure 4.6-4.9).

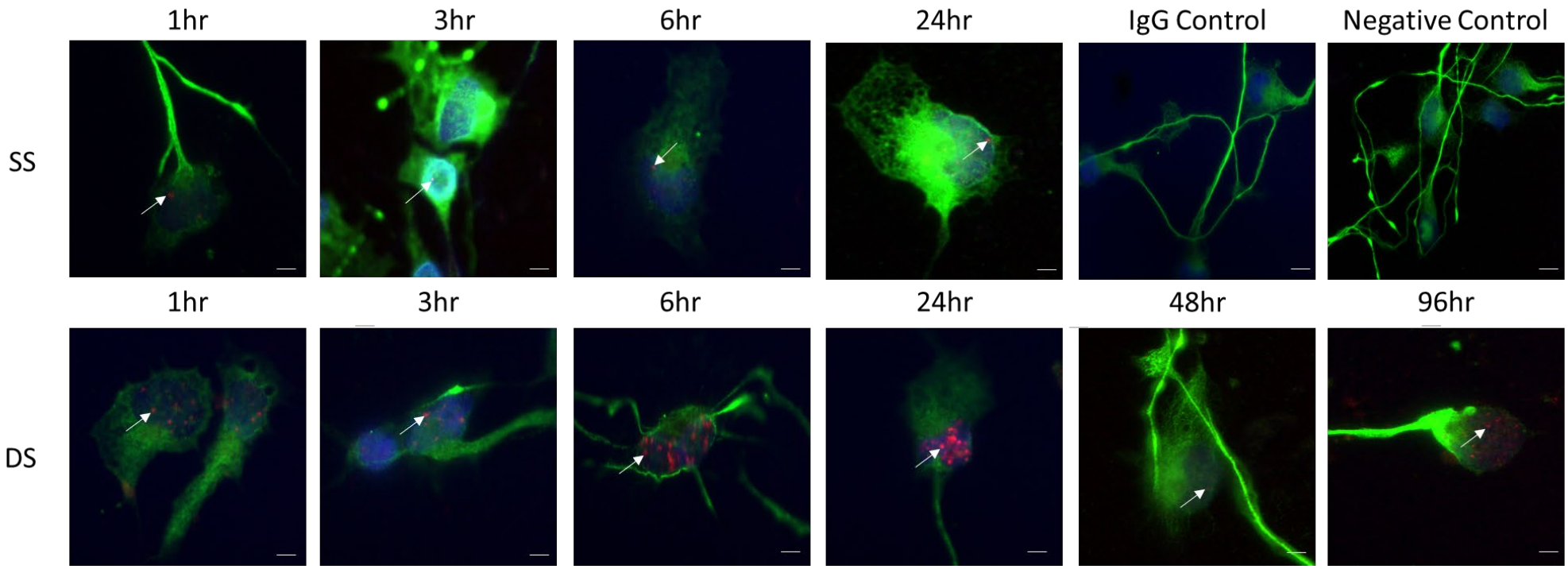

Figure 4.4. γH2AX foci expression in single and double stressed post-mitotic LUHMES: Immunocytochemistry was used to localise γH2AX foci expression (white arrows) as a marker of DNA damage during a single exposure to 50 μM H_2O_2 over a 24 hrs time period (top row, SS) and during double exposure to 50 μM H_2O_2 over a 96 hrs time period (bottom row, DS). Cells were stained with γH2AX (red) and counterstained with β-III-tubulin (green). Nuclei were stained with nuclear dye Hoechst H3342 (blue). Scale bar represents 10 μm.

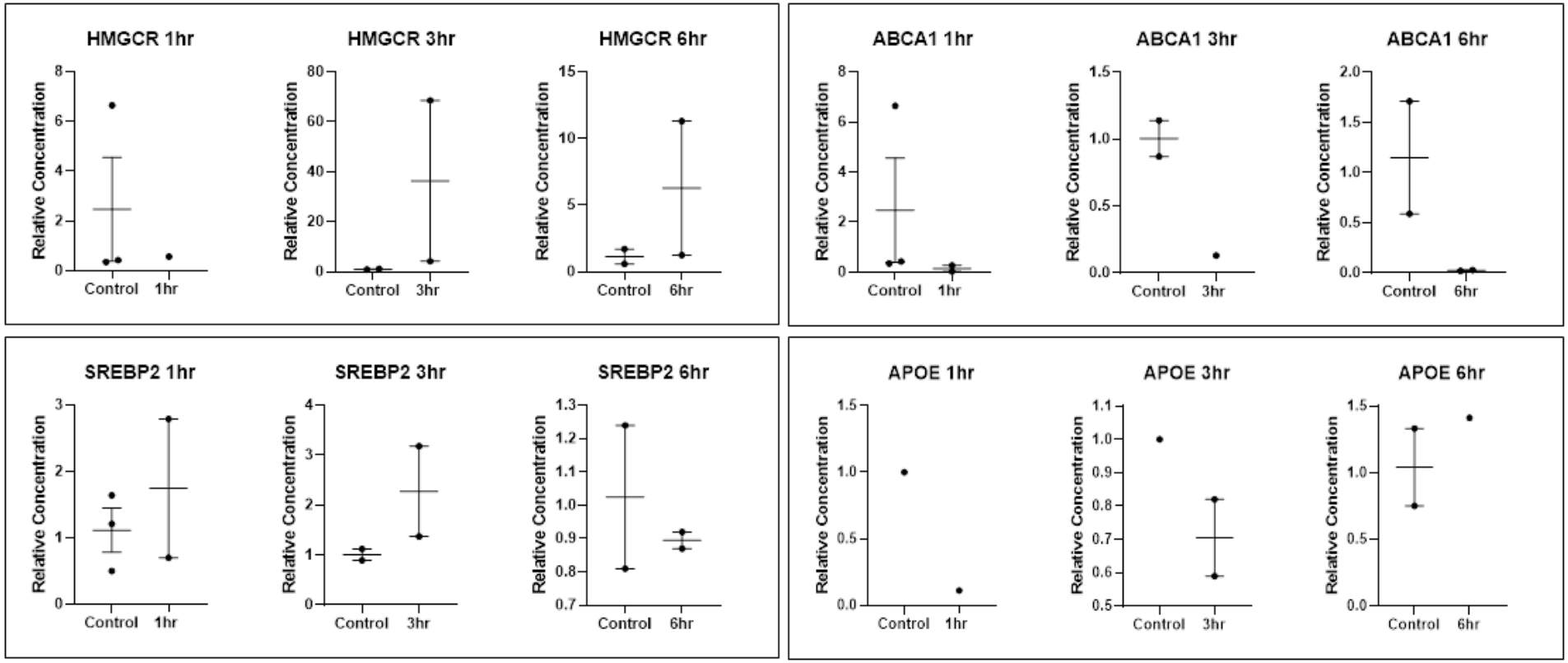

Figure 4.5. Expression of cholesterol biosynthetic genes in post-mitotic LUHMES after a single exposure to H_2O_2: The expression of four key genes (*HMGCR, ABCA1, SREBP2* and *APOE* respectively) involved in cholesterol biosynthesis was determined during a single exposure to 50 μM H_2O_2 in post-mitotic LUHMES over a 6 hrs time period. Relative concentration values for each gene were calculated relative to the control. Each point on the graph represents an individual biological replicate.

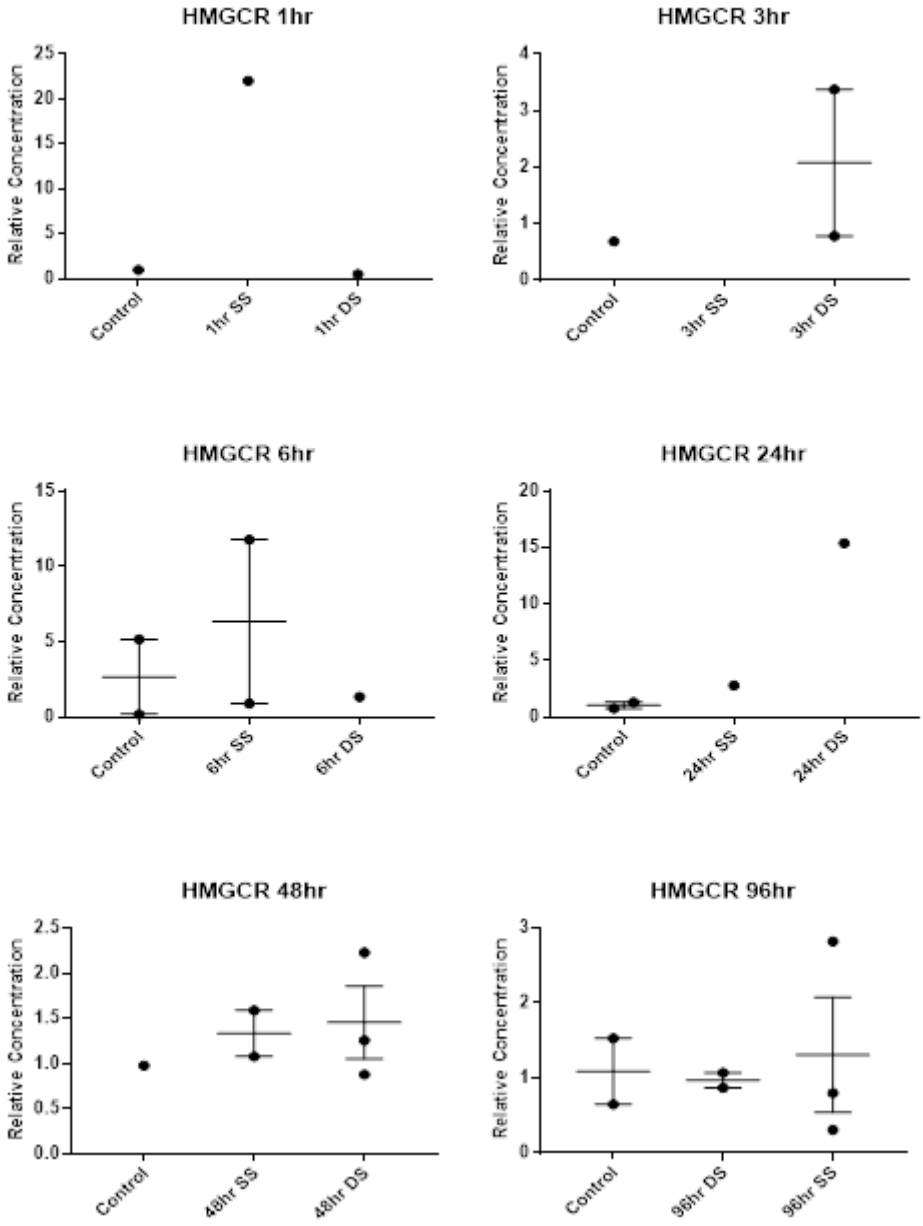

Figure 4.6. Expression of HMGCR in LUHMES after a single and double exposure to H_2O_2 over a 96 hrs time period: The expression of *HMGCR* was determined during single and double exposures to 50 μM H_2O_2 in LUHMES over a 96 hrs time period. RNA was extracted from LUHMES, cDNA was synthesised, and *HMGCR* expression was determined using qPCR. Each point on the graph represents an individual biological replicate.

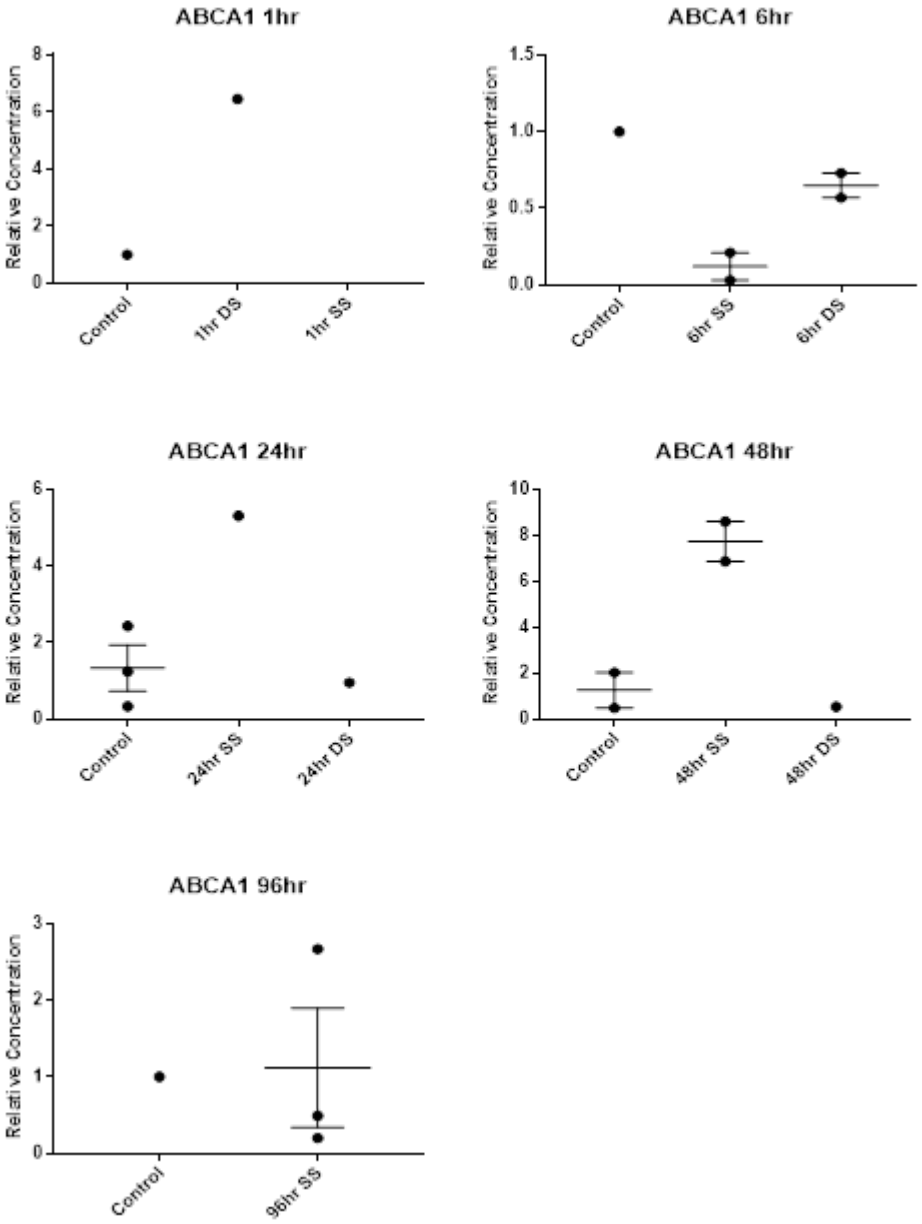

Figure 4.7. Expression of ABCA1 in LUHMES after a single and double exposure to H_2O_2 over a 96 hrs time period: The expression of *ABCA1* was determined during single and double exposures to 50 μM H_2O_2 in LUHMES over a 96 hrs time period. RNA was extracted from LUHMES, cDNA was synthesised, and *ABCA1* expression was determined using qPCR. Each point on the graph represents an individual biological replicate.

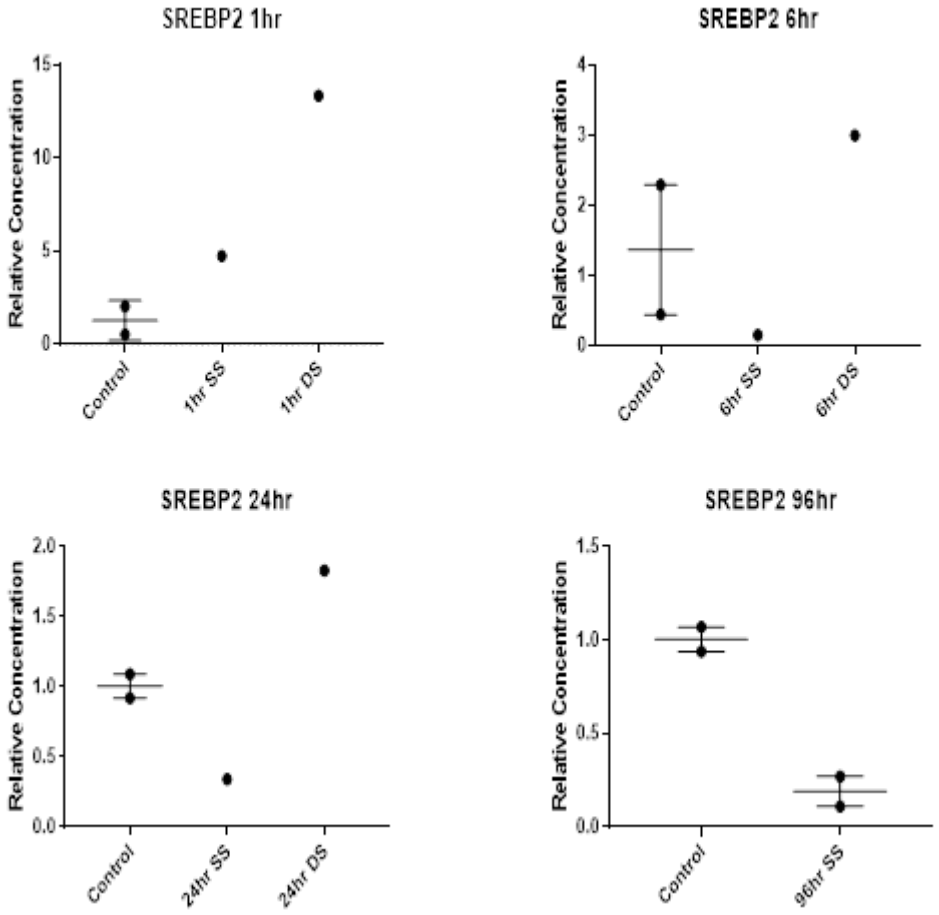

Figure 4.8. Expression of SREBP2 in LUHMES after a single and double exposure to H_2O_2 over a 96 hrs time period: The expression of *SREBP2* was determined during single and double exposures to 50 μM H_2O_2 in LUHMES over a 96 hrs time period. RNA was extracted from LUHMES, cDNA was synthesised, and *SREBP2* expression was determined using qPCR. Each point on the graph represents an individual biological replicate.

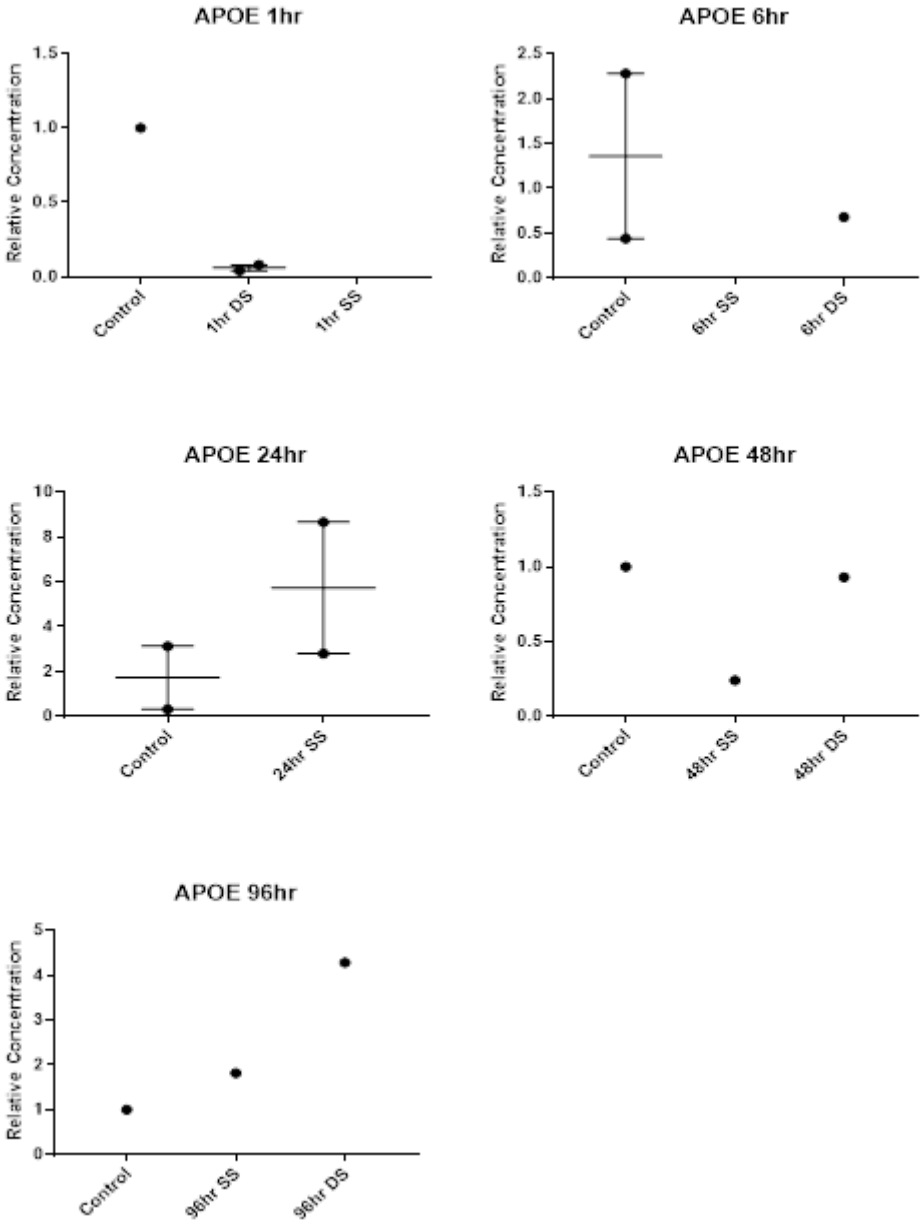

Figure 4.9. Expression of APOE in LUHMES after a single and double exposure to H_2O_2 over a 96 hrs time period: The expression of *APOE* was determined during single and double exposures to 50 μM H_2O_2 in LUHMES over a 96 hrs time period. RNA was extracted from LUHMES, cDNA was synthesised, and *APOE* expression was determined using qPCR. Each point on the graph represents an individual biological replicate.

4.4.6 Single and double exposure to H_2O_2 leads to the presence of γH2AX foci in astrocytes

To investigate the effects of oxidative stress on cholesterol biosynthesis a single and double stress model was previously developed within our lab group for LUHMES was adapted for use on primary human astrocytes. Astrocytes were cultured on glass coverslips and exposed to either a single or double dose of 50 μM H_2O_2 Immunocytochemistry for γH2AX foci demonstrated that at all time points with both a single and double exposure to H_2O_2, γH2AX foci were detected in the nuclei of astrocytes over 24 hrs and 96 hrs respectively (Figure 4.10).

4.4.7 Single and double exposure to H_2O_2 does not change the cell viability of astrocytes

To determine the toxicity and effects of a single and double dose of 50 μM H_2O_2 on cell viability an LDH assay was performed. The data shows that there were no significant changes to astrocyte cell viability following a single and double exposure to 50 μM H_2O_2 over 24 hrs and 96 hrs respectively (ANOVA, single stress p=0.981; double stress p=0.945) (Figure 4.11).

4.4.8 Single exposure to H_2O_2 shows no significant changes in cholesterol biosynthetic relative gene expression in astrocytes

Astrocytes were exposed to a single dose of 50 μM H_2O_2 and the expression of four genes (*HMGCR, ABCA1, SREBP2* and *APOE*) involved in cholesterol biosynthesis and metabolism was determined using qPCR over 24 hrs. Preliminary data shows that all four genes were expressed in control and treated cells at all time-points. The current data suggests that there are no changes in *APOE* expression following H_2O_2 treatment in astrocytes over 24 hrs. However, due to the COVID-19 pandemic and a lack of technical replicates we found that the data is inconclusive (Figure 4.12).

4.4.9 Double exposure to H_2O_2 shows no significant changes in cholesterol biosynthetic relative gene expression in astrocytes

Astrocytes were exposed to a single dose of 50 μM H_2O_2 followed by another dose of 50 μM H_2O_2 6 hrs later. The expression of four genes (*HMGCR, ABCA1, SREBP2* and *APOE*) involved in cholesterol biosynthesis and metabolism was determined using qPCR over 96 hrs. Preliminary data shows that all four genes were expressed in control and treated cells at all time-points. The current data suggests that *SREBP2* expression is consistent at 1 hr following single and double exposure to H_2O_2 and an increased expression at 3 hrs in single stressed and a further increased expression

following a double stress. At 6 hrs we see a decrease in *SREBP2* expression in both single and double stresses astrocytes, where the double stressed cells had a larger decrease compared to controls. At 24 hrs an increase in *SREBP2 expression* was observed in both single and double stressed cells. Followed by a decrease in *SREBP2* expression at 6 hrs in single and double stressed cells. At both 48 hrs and 96 hrs an increase in *SREBP2* expression was observed in single stressed cells, however in double stressed cells there was no change in *SREBP2* expression compared to the controls. Due to the COVID-19 pandemic and a lack of technical replicates we found that the data is inconclusive (Figure 4.13- 4.16).

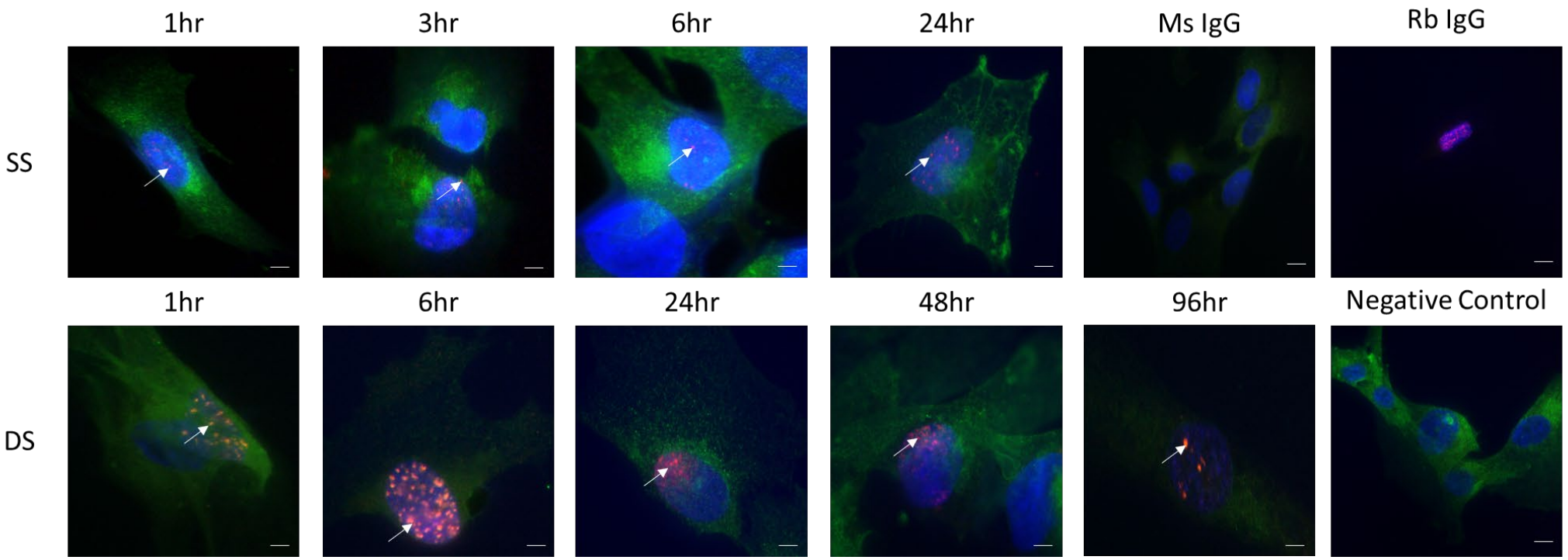

Figure 4.10. γH2AX foci expression in single and double stressed astrocytes: Immunocytochemistry was used to localise γH2AX foci expression (white arrows) as a marker of DNA damage during a single exposure to 50 μM H_2O_2 over a 24 hrs time period (top row, SS) and during double exposure to 50 μM H_2O_2 over a 96 hrs time period (bottom row, DS). Cells were stained with γH2AX (red) and counterstained with CD44 (green). Nuclei were stained with nuclear dye Hoechst H3342 (blue). Scale bar represents 10μm.

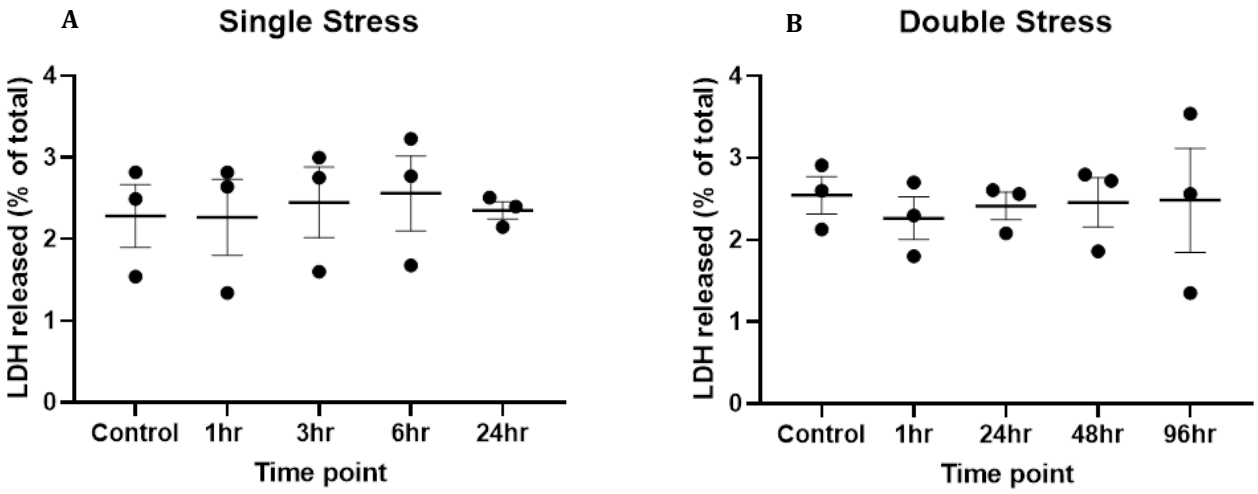

Figure 4.11. Cell viability in astrocytes following single and double exposure to H_2O_2: LDH assay was carried out to determine the effect on cell viability following a single and double exposure to 50 µM H_2O_2 in astrocytes. (A) Shows the percentage of LDH released h after a single exposure over a 24 hrs time period. (B) Shows the percentage of LDH released after a double exposure over a 96 hrs time period. Each point on the graph represents an average from triplicates from an individual biological replicate N=1.

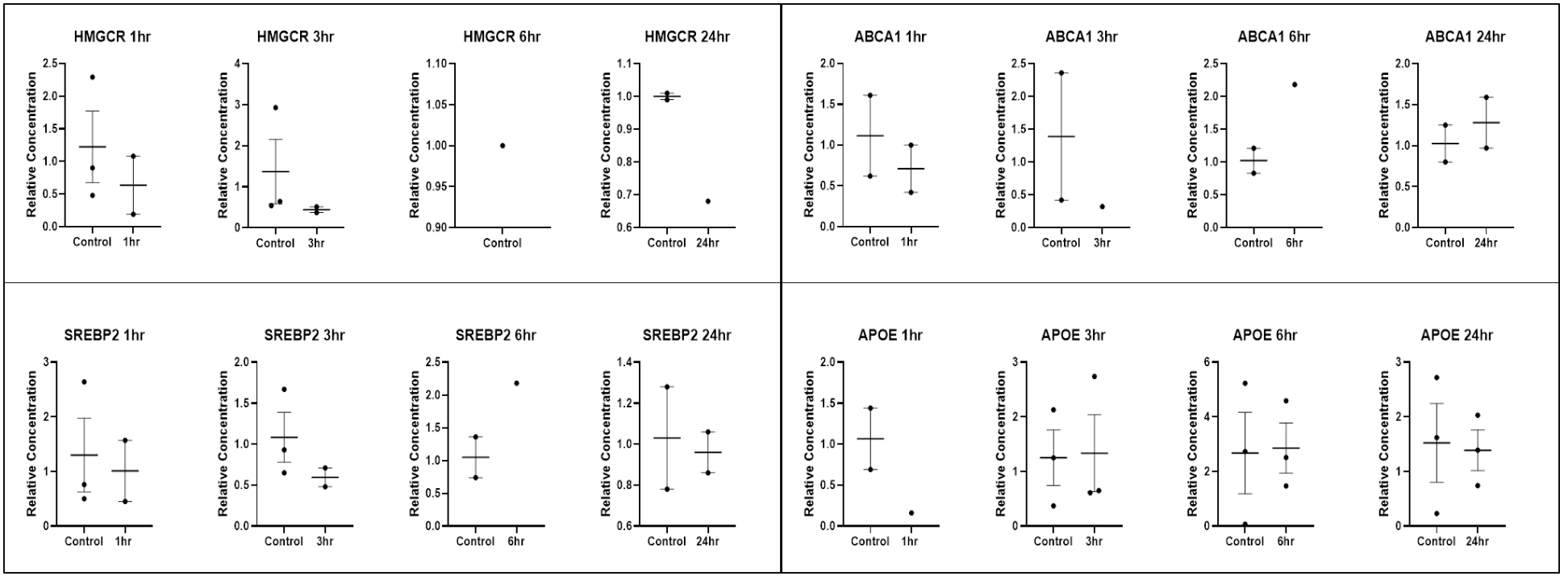

Figure 4.12. Expression of cholesterol biosynthetic genes in astrocytes after a single exposure to H_2O_2: The expression of four key genes (*HMGCR, ABCA1, SREBP2* and *APOE* respectively) involved in cholesterol biosynthesis was determined during a single exposure to 50 μM H_2O_2 in astrocytes over a 24 hrs time period. Relative concentration values for each gene were calculated relative to the control. Each point on the graph represents an individual biological replicate.

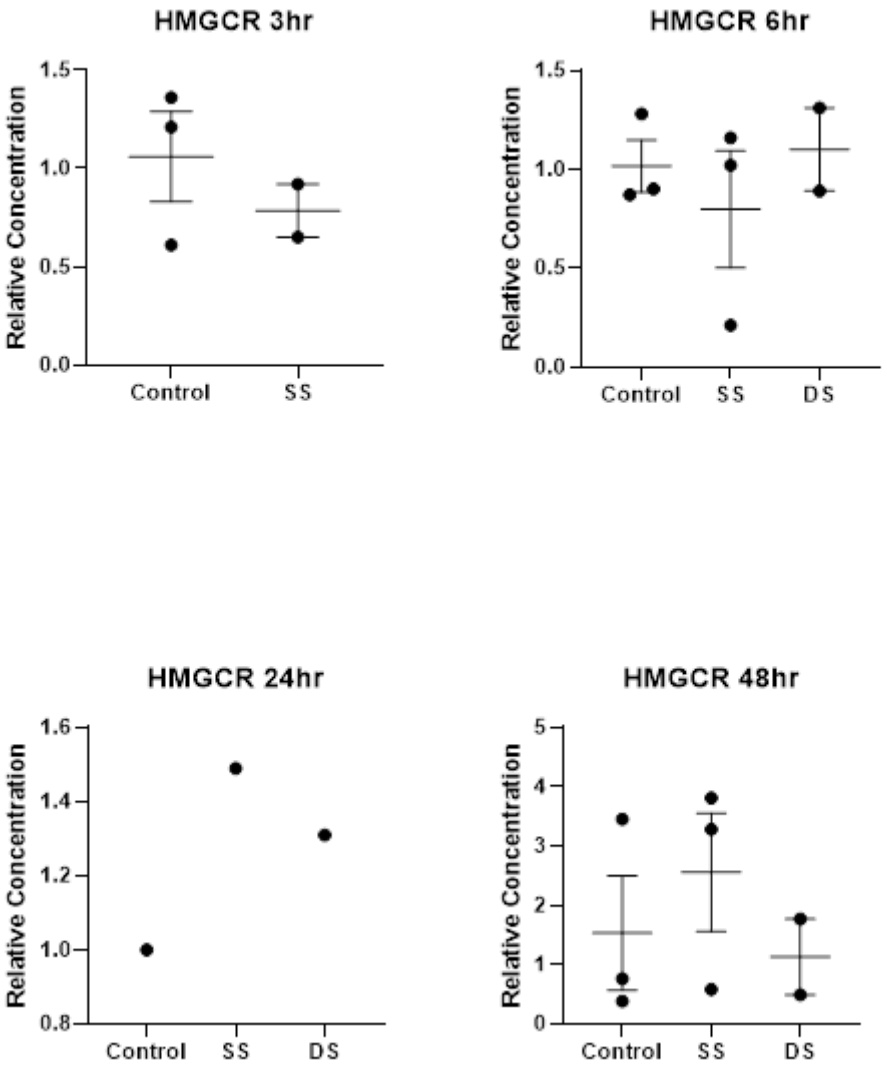

Figure 4.13. Expression of HMGCR in astrocytes after a single and double exposure to H_2O_2 over a 96 hrs time period: The expression of *HMGCR* was determined during single and double exposures to 50 μM H_2O_2 in astrocytes over a 96 hrs time period. RNA was extracted from astrocytes, cDNA was synthesised, and *HMGCR* expression was determined using qPCR. Each point on the graph represents an individual biological

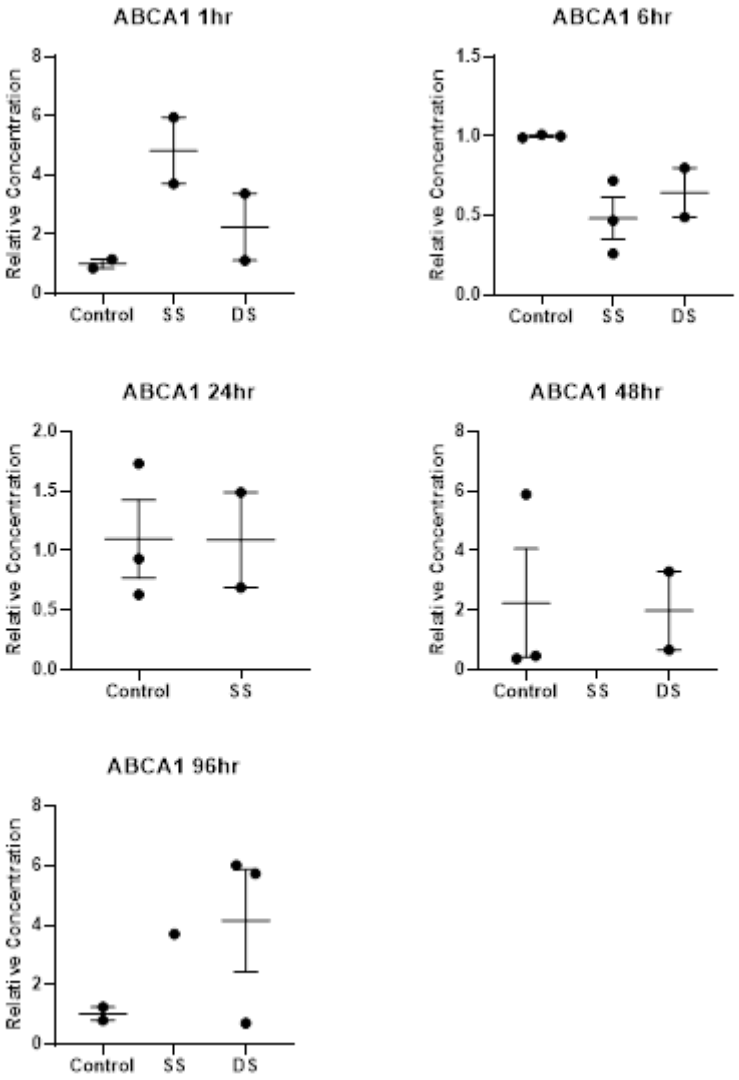

Figure 4.14. Expression of ABCA1 in astrocytes after a single and double exposure to H_2O_2 over a 96 hrs time period: The expression of *ABCA1* was determined during single and double exposures to 50 μM H_2O_2 in astrocytes over a 96 hrs time period. RNA was extracted from astrocytes, cDNA was synthesised, and *ABCA1* expression was determined using qPCR. Each point on the graph represents an individual biological replicate.

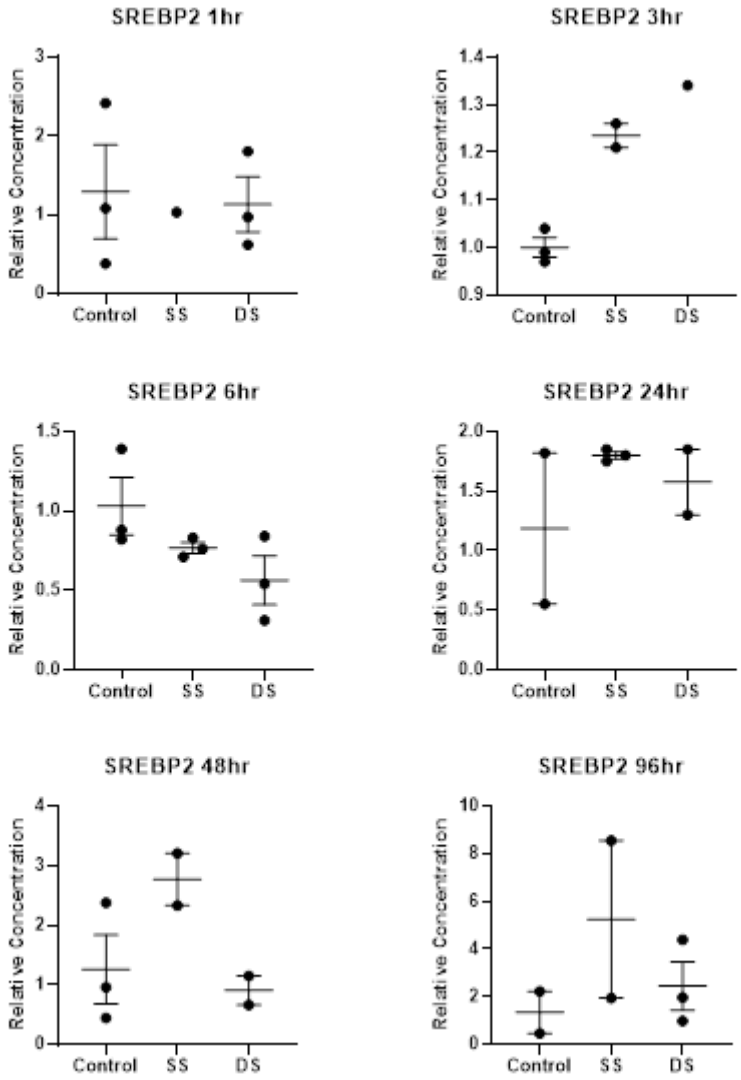

Figure 4.15. Expression of SREBP2 in astrocytes after a single and double exposure to H_2O_2 over a 96 hrs time period: The expression of *SREBP2* was determined during single and double exposures to 50 μM H_2O_2 in astrocytes over a 96 hrs time period. RNA was extracted from astrocytes, cDNA was synthesised, and *SREBP2* expression was determined using qPCR. Each point on the graph represents an individual

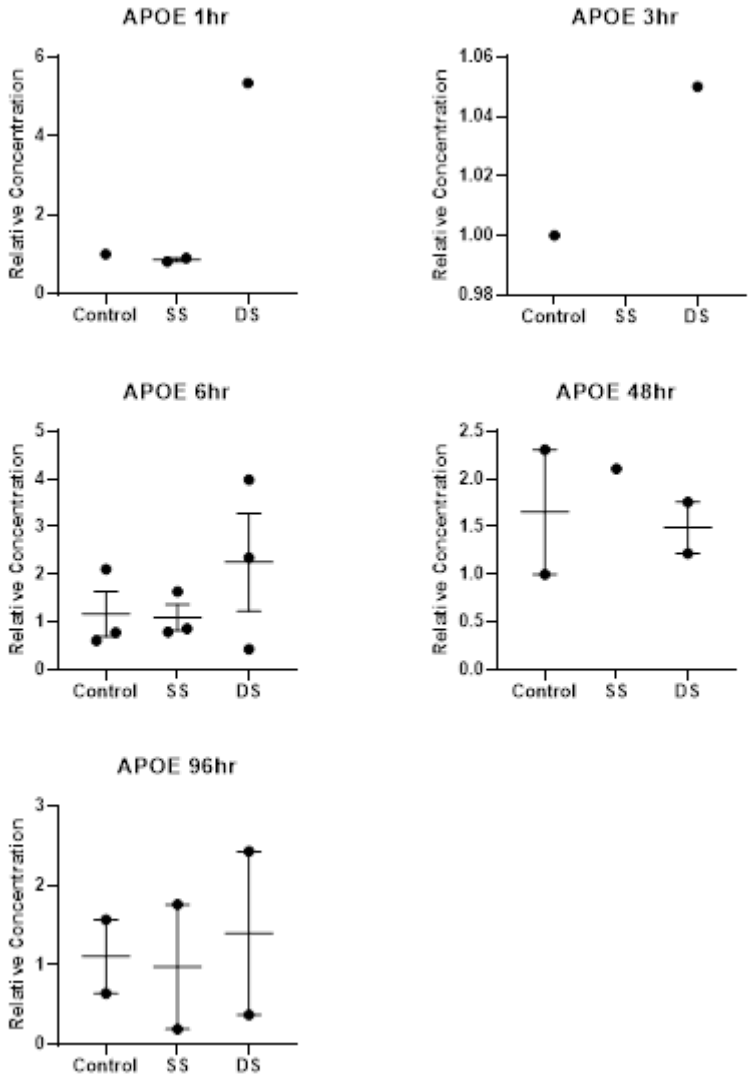

Figure 4.16. Expression of APOE in astrocytes after a single and double exposure to H_2O_2 over a 96 hrs time period: The expression of *APOE* was determined during single and double exposures to 50 μM H_2O_2 in astrocytes over a 96 hrs time period. RNA was extracted from astrocytes, cDNA was synthesised, and *APOE* expression was determined using qPCR. Each point on the graph represents an individual biological replicate.

4.5 Discussion

In this chapter, the effects of acute and chronic oxidative stress on cholesterol biosynthesis in neurons and astrocytes *in vitro* were investigated. The expression of cholesterol biosynthetic genes was characterised in LUHMES during differentiation. We found that genes involved in cholesterol biosynthesis were expressed in LUHMES during differentiation. *This study* also found a significant decrease in *SCAP* and *FDFT1* expression during differentiation. A single and double stress model was used to determine the changes in expression of four keys genes (*HMGCR, APOE, ABCA1* and *SREBP2*) involved in the cholesterol biosynthesis pathway and cholesterol metabolism were characterised using qPCR. We found that the four key genes were expressed in both neurons and astrocytes following a single and a double dose of H_2O_2. *This current study* also found that a single and double exposure to oxidative stress, in the form of H_2O_2, can lead to the formation of double stranded breaks in neurons and astrocytes and persists for up to 24 hrs and 96 hrs respectively.

4.5.1 Cholesterol biosynthetic genes are expressed in LUHMES during differentiation

The expression of cholesterol biosynthetic genes was characterised for LUHMES cell line during differentiation. Lund human mesencephalic (LUHMES) cells, a conditionally immortalised human dopaminergic neuronal precursor cell line, possess the ability to differentiate into post-mitotic neurons (Hoshimaru *et al.*, 1996; Lotharius *et al.*, 2002; Lotharius, 2005). A two-step differentiation protocol, by re-plating the LUHMES following two days of differentiation, allows for a homogeneous and synchronised population of post-mitotic cells on completion of differentiation following five days of differentiation (Scholz *et al.*, 2011). *This study* demonstrated that genes involved in cholesterol biosynthesis were expressed in neurons during neuronal differentiation, suggesting that neurons possess the machinery to carry out cholesterol biosynthesis. Murine cortical neurons have shown that during neuronal differentiation *de novo* cholesterol biosynthetic mechanisms are active. Primary mice cortical neurons grown in cholesterol free media showed accumulation of cholesterol within the cell and cholesterol is released into the media (Genaro-Mattos *et al.*, 2019b). This suggests that neurons *in vitro* are capable of synthesising cholesterol and supports the findings from *this current study*. The neuronal expression of

HMGCR in vitro further validates our finding from *in vivo* studies in post-mortem human temporal cortex tissue (Chapter 2 and 3).

Cartocci *et al* (2016) found that during neuronal differentiation in mice neuroblastoma cell line a reduction in HMGCR activity and the down-regulation of the mevalonate arm of the cholesterol biosynthesis pathway was observed (Cartocci *et al.*, 2016). However, the data from *our study* showed that there were no significant changes in the expression of genes within the mevalonate pathway (*HMGCR, HMGCS1, ACAT1*). Cartocci *et al* (2016) also found a reduction in the cleaved form of SREBP2 protein, whereas the data from *this study* showed no significant change in total *SREBP2* expression. However, a significant decrease in *SCAP* expression was observed in *this study*, suggesting that over a longer period this may translate to a decrease in total *SREBP2* expression. These differences could be accounted for by the re-plating step that occurs on day 2 during LUHMES differentiation which may alter cholesterol biosynthesis gene expression. Furthermore, the mice neuroblastoma cells were observed over eight days compared to just five days with the LUHMES, therefore a reduction within the mevalonate pathway could potentially be observed on later days as gene expression changes in LUHMES have also been observed at day 10-12 following differentiation (Scholz *et al.*, 2011). In the study by Cartocci *et al* (2016) the murine cell line N1E-115 was used and is an ideal model for studying neuronal differentiation but do not become post-mitotic, compared to LUHMES which become post-mitotic after five days which could also account for the differences observed in *this study* (Kranenburg *et al.*, 1995; Shim *et al.*, 2006; Cartocci *et al.*, 2016).

4.5.2 Acute and chronic stress models induced oxidative DNA damage in LUHMES

In *this study*, we used a previously optimised model of inducing acute and chronic stress to investigate the effects of oxidative DNA damage on the expression of four key genes involved in cholesterol homeostasis (Irina Vázquez-Villaseñor, unpublished data). We found that this model induced oxidative DNA damage, which was visualised using γ-H2AX foci as a marker of double stranded DNA breaks, the DNA damage persisted for 24 hrs following an acute stress and 96 hrs following a more chronic stress. Preliminary gene expression results are inconclusive due to the lack of repeats because of limitation of laboratory access due to the COVID-19

pandemic. The aim was to carry out three biological repeats with three technical repeats. For primary cells the biological repeats would require the experiments to be carried out on three different primary cell lines, however with immortalised cell lines biological repeats would be determined by carrying out the experiments at different passage numbers. Technical repeats would be carried out to remove the effects of errors caused by the protocols (Tsvetkov *et al.*, 2019).

Clement *et al* (2009) exposed cloned murine hippocampal cells to long-term treatment of sub-lethal doses of H_2O_2 to develop resistance to H_2O_2-induced oxidative stress. Compared to wild type cells, resistant cells showed an increase in cholesterol and cholesterol precursor levels; however, a decrease in *ABCA1* and *HMGCR* mRNA levels was detected, suggesting a decrease in cholesterol efflux and synthesis. Cholesterol also accumulated within the lysosomes of resistant cells, suggesting that this could be a neuroprotective effect as it prevents changes to plasma membrane rigidity preventing cellular degeneration (Clement *et al.*, 2009). In another study using LUHMES, the effect of oxidative stress induced by silver nanoparticles on cholesterol homeostasis was determined during both the proliferative and post-mitotic state. Zuberek *et* al (2018) found that *ABCA1* mRNA expression increased during differentiation and treatment of proliferating cells with silver nanoparticles also showed an increase in *ABCA1* mRNA expression (Zuberek *et al.*, 2018). This data suggests that an increase in ABCA1 turnover may be a neuroprotective effect because of oxidative stress. If a similar response was observed in our experiments, then in our current study, we would also predict a decrease in expression of *HMGCR, SREBP2* and *ABCA1* when exposed to a more chronic stress.

4.5.3 Acute and chronic stress models induced oxidative DNA damage in astrocytes

In *this study* we found that a single and double stress model that had been previously optimised in LUHMES also induced oxidative DNA damage in primary human foetal astrocytes. The presence of γH2AX, a marker of DNA damage (Kuo and Yang, 2008), foci within the nuclei of astrocytes after 24 hrs and 96 hrs following a single and double exposure, respectively, suggests that method can be used to measure the effects of a DNA damage response following exposure to acute and chronic oxidative stress within astrocytes. Measuring cell viability following single

and double exposure showed that there were no significant changes to cell viability suggesting that 50 μM of H_2O_2 is not a lethal dose to the astrocytes but is strong enough to induce oxidative DNA damage. Preliminary gene expression results are inconclusive due to the lack of technical repeats as a result of the COVID-19 pandemic.

Prieto and Alonso (1999) investigated the effect of varying H_2O_2 concentration on immature (E-14 embryonic origin) and mature (10-day-old) rat cortical astrocytes. Mature astrocytes showed no significant changes in LDH release as H_2O_2 concentration increased. However, in immature astrocytes low concentrations of H_2O_2 (30 μM and 50 μM) showed no significant changes in LDH release but higher concentrations of H_2O_2 (100 μM- 1000 μM) showed a significant increase in LDH release compared to controls (Prieto and Alonso, 1999). This data suggests that mature astrocytes can cope better with H_2O_2 induced oxidative stress, compared to immature astrocytes and at 50 μM of H_2O_2 no significant changes to cell viability are observed, supporting the findings from *our stu*dy.

Ito *et al* (2013), treated primary rat astrocytes with 100 μM and 300 μM H_2O_2 for 1 and 4 hrs and showed a significant decrease in percentage LDH release after 4 hrs, suggesting a decrease in cell viability. However, treating the astrocytes with 100 μM H_2O_2 for 4 hrs showed no significant decrease in LDH release compared to no treatment suggesting that cell viability does not significantly decrease (Ito *et al.*, 2013). Furthermore, following a 10 minutes treatment of 100 μM H_2O_2, caused a significant decrease in cholesterol synthesis for the first 6 hrs following treatment, and cholesterol synthesis was restored approximately 24 hrs after the stress. This would suggest that within *our study* a decrease in expression of *HMGCR* and *SREBP2* would be predicted. Further studies have shown that in rat astrocytes treating cells with 100 μM H_2O_2 leads to an increase in cholesterol released from the plasma membrane (Ito *et al.*, 2015). Further evidence from THP-1 macrophage treatment with H_2O_2 has shown a decrease in *ABCA1* mRNA expression (Marcil *et al.*, 2006). This suggests that in astrocytes, H_2O_2 treatment may lead to a decrease in *ABCA1* mRNA expression.

4.5.4 Limitations

There are certain limitations that need to be considered when interpreting the data from *this study*. One limitation of the double stress model is that it is unclear as to how much oxidative stress is present over the time period investigated. Previous work carried out within our lab group had showed that in LUHMES following a single stress only 5% of LUHMES were positive for γH2AX foci after 24 hrs and following a double stress 18% of LUHMES were positive for γH2AX foci after 96 hrs (Irina Vázquez-Villaseñor, unpublished data). These are very low percentages of cells which are positive for γH2AX foci and therefore any changes caused by persistent DNA damage could be masked by the fact that the sample would be enriched with LUHMES and astrocytes with no DNA damage present. The clearance of H_2O_2 within foetal astrocytic cultures and the impact H_2O_2 doses have on the generation of double stranded breaks and γH2AX foci needs to be determined. This will then allow a better assessment of the impact of the double stress model on astrocytes.

Another limitation of *this study* is that both cell lines are of embryonic origin making it difficult to assess the specific effects of ageing as well as oxidative stress on cholesterol biosynthesis. To study the effects of aging these experiments could be repeated in adult astrocytes and neurons. Another approach could involve the use of patient derived fibroblasts that are reprogrammed to form induced neuronal stem cells (iNSCs) which can be differentiated to form neurons and astrocytes or directly reprogrammed fibroblast cells to produce iNeurons and iAstrocytes. These reprogrammed cells (iNSCs, iNeurons, iAstrocytes) will contain specific age-associated changes, such as accumulation of DNA damage, compared to induced pluripotent stem cells (iPSCs) which may lose some of the epigenetic changes associated with ageing. These directly reprogrammed cells will help give a better understanding to how cholesterol synthesis is impacted during oxidative stress and AD (Erharter *et al.*, 2019; Traxler, Edenhofer and Mertens, 2019). However, one advantage of using foetal cells is that it allows a more thorough examination of the cholesterol biosynthesis pathway within neurons and astrocytes, as currently the process of *de novo* cholesterol biosynthesis within the CNS is yet to be fully elucidated (Pfrieger and Ungerer, 2011; Zhang and Liu, 2015).

Most *in vitro* neuronal studies make use of human neuroblastoma or murine derived cortical neurons however, in *this study* we used LUHMES. The advantages of using

LUHMES are that they are of human origin and cells can survive in a proliferative and post-mitotic phase with a relatively simple and quick differentiation protocol allowing for a synchronous population of cells to develop. However, LUHMES are very vulnerable to stresses associated with cell culture such as cell density, pH and temperature and can alter proliferation and differentiation of LUHMES. Previous work has shown that sub-confluent cultures are more vulnerable to oxidative stress and reduced clearance of H_2O_2 (Irina Vázquez-Villaseñor, unpublished data). Many studies make use of rodent derived astrocytes, however data shows that human astrocytes are much more complex and can better address questions related to human disease (Oberheim *et al.*, 2006).

Besides the limitations of qPCR quantification methods previously mentioned (3.6.13). Briefly, qPCR was quantified using relative quantification, when gene expression is calculated relative to a reference sample using the $2^{-\Delta\Delta Ct}$ method. In *this study*, the relative concentration values for each gene were calculated relative to the mean ΔCt expression for control wells at each time point. The reference gene selected for *this study* was β-actin, as this was the same housekeeping gene used in previous studies involving LUHMES and astrocytes (Ratcliffe *et al.*, 2018). The efficiency and handling prior to qPCR can be further improved by making use of a novel "zero-step" RT-qPCR (Chovancova *et al.*, 2017). This novel method does not require an RNA extraction step and allows qPCR reaction mix to be prepared directly from cell lysates. This method allows for quicker and easier determination of gene expression and enables a more accurate assessment of gene expression at shorter and longer time points.

4.6 Future work

Due to COVID-19 pandemic, the forced closure of labs prevented experiments from being repeated and completed. Repeating the single and double stress experiments in both LUHMES and astrocytes would be upmost priority to attain sufficient biological repeats. Followed by optimisation of the double stress model to simulate the effects of oxidative stress in a co-culture model previously developed in our lab (Ratcliffe *et al.*, 2018). Further technical validation of the double stress model in foetal astrocytes would also be required such as determining the clearance of H_2O_2 depending on cell density. Furthermore, determining the lasting effects of the double

stress model will help assess astrocyte recovery in relation to oxidative stress. To further validate gene expression data, determining the levels of cellular cholesterol within LUHMES and astrocyte cultures following single and double stress will enable us to determine if changes in cholesterol biosynthetic gene expression translated to a change in overall cellular cholesterol levels.

The literature suggests that within the CNS neurons and astrocytes work together to ensure overall homeostasis. Some evidence is suggesting that impairment in cholesterol transport from astrocytes and astrocytic cholesterol synthesis impairment could be involved in neurodegeneration. We hypothesise that dysregulation of cholesterol biosynthesis in the neuron-astrocyte unit contributes to dementia by impairing neuronal function due to impaired cholesterol metabolism and through generation of pro-oxidative stress metabolites. This hypothesis could be investigated within the co-culture system by pre-treating astrocytes using statins thereby, impairing cholesterol synthesis, and investigating the effect on neuronal health when the system is exposed to oxidative stress.

4.7 Conclusion

In *this study*, we found that *in vitro* neurons express genes involved in cholesterol biosynthesis suggesting that they are capable of producing their own cholesterol. We also found that a single and double exposure to H_2O_2 lead to the formation of double stranded breaks leading of oxidative DNA damage in both neurons and astrocytes. The effects of a single exposure to H_2O_2 are detected 24 hrs after the dose and the effects of a double exposure to H_2O_2 are detected 96 hrs after the dose in both cell types. Preliminary data from stress experiments showed that the four key genes involved in cholesterol homeostasis (*HMGCR, ABCA1, SREBP2* and *APOE*) were expressed at all-time points following a single and double exposure to H_2O_2 in both cell types. The expression of these cholesterol biosynthetic genes in neurons suggests that cholesterol biosynthesis may be directly affected by oxidative stress, highlighting the importance oxidative stress plays in neurodegeneration in particular its effect on cholesterol. In *this study* a double stress model was employed to model the effects of chronic oxidative stress, compared to other studies which model the effects of acute oxidative stress.

5.0 General discussion and future work

5.1 General Discussion

The overall aim of this thesis was to characterise how cholesterol production and cholesterol metabolism changed during the progression of AD. The overall hypothesis is that cholesterol dysregulation in the brain contributes to dementia and to progression of AD. We found that NFT pathology correlates with changes in gene expression of genes involved in cholesterol biosynthesis however, these changes in gene expression were not translated to changes in tissue cholesterol concentration. Immunohistochemical characterisation of key regulators of the cholesterol biosynthesis pathway (HMGCR and SREBP2) were localised to the neurons and astrocytes within the temporal cortex. However, quantification of HMGCR immunoreactivity and subsequent statistical analysis found that there were no significant associations with AD neuropathology progression and dementia status. This study found that moderate and high levels of brain cholesterol are associated with dementia. However, the confidence intervals were wide suggesting uncertainty around this association. Therefore, further studies with a larger sample size would be required in order to confirm a real association. If a real association is present, then *this study* suggests that the effect of brain cholesterol on dementia is small. In conclusion, the findings of this study suggest that cholesterol biosynthesis and metabolism are dysregulated in the brain however, whether this dysregulation contributes to dementia or AD progression remains unknown.

5.2 Neuronal expression of HMGCR

One of the key findings of *this study* was the neuronal expression of the enzyme HMGCR. Immunohistochemical characterisation of HMGCR in human post-mortem temporal cortex and frontal cortex tissue showed positive immunolabelling in pyramidal neurons. This staining pattern was observed across a pan- Braak and Braak cohort and an ageing series, from young to old, this suggests that the staining pattern is not a consequence of aging or neurodegeneration. Furthermore, HMGCR expression was confirmed at protein level in whole tissue protein extracts and in protein lysates from LUHMES cells demonstrating that HMGCR is expressed *in vivo* and *in vitro* in neurons. HMGCR expression was also found at an mRNA level in isolated neuronal populations from the temporal cortex and LUHMES. This is a novel

finding in human brain, as many studies have shown glial cells tend to undertake the bulk of the cholesterol production within the brain, whereas this study suggests that neurons possess the mechanisms to synthesise cholesterol (Pfrieger, 2003; Nieweg, Schaller and Pfrieger, 2009; Pfrieger and Ungerer, 2011; Zhang and Liu, 2015). To investigate this suggestion, HMGCR immunoreactivity and HMGCR mRNA expression in the temporal cortex was compared to temporal cortex total tissue cholesterol concentration, but no significant correlations were observed. The lack of correlation could be due to the limitations of the methods used. As mentioned before, IHC detection is not linear and therefore positive immunolabelling does not represent exact amount of antigen present (Matkowskyj *et al.*, 2003). Additionally, gene expression data was calculated relative to the expression of β-actin over Braak and Braak group 1 using the $2^{-\Delta\Delta Ct}$ method which is not an absolute measurement of HMGCR expression (Rao *et al.*, 2013). Furthermore, tissue cholesterol concentration was determined using frozen temporal cortex blocks rather than an enriched population of neurons, hence other cells within the temporal cortex and white matter regions contribute to the total cholesterol concentration.

One possible biological explanation for the lack of correlation between HMGCR expression and cholesterol concentration, could be that HMGCR activity is used to produce isoprenoids rather than cholesterol (Eckert *et al.*, 2009). Isoprenoids such as farnesyl pyrophosphate (FPP) and geranylgeranyl pyrophosphate (GGPP) are involved in the prenylation of proteins, a post-translational modification, allowing insertion into membranes and determining their function and localisation. FPP is formed from the mevalonate arm of the cholesterol biosynthesis pathway and is a precursor for both cholesterol and GGPP (Eckert *et al.*, 2009). Neurons have been shown to maintain and activate the mevalonate pathway to produce isoprenoids and protein prenylation (Moutinho, Nunes and Rodrigues, 2017). One study showed that a product of protein prenylation, Rho GTPases, are essential for neuronal development playing a key role in axonal and dendritic outgrowth and stabilisation and synapse formation (Govek, Newey and Van Aelst, 2005). Interestingly, levels of FPP and GGPP are higher in the brain compared to other organs and in aged mice a reduction in association of Rho GTPases in the membranes of aged mice (Hooff *et al.*, 2010; Afshordel *et al.*, 2014). These studies demonstrate the crucial role of isoprenoids in the brain. A study in aged mice found that levels of FPP and GGPP

protein levels were significantly increased in aged mice (23 months old) compared to young mice (3 months old) (Hooff *et al.*, 2012). A separate study showed that FPP and GGPP levels were significantly increased in AD brains compared to age matched controls in the frontal cortex (Hooff *et al.*, 2008).

Changes in isoprenoids have been observed in ageing and neurodegeneration (Edlund, Söderberg and Kristensson, 1994). One study found that treating primary rat basal forebrain neurons with oligomeric Aβ showed a significant reduction in Rab and Ras protein prenylation (Mohamed *et al.*, 2012). A similar effect was also observed in cortical regions of a transgenic mouse model of AD compared to age-matched wild type controls. The decrease in prenylation by Aβ was attributed to a reduction in GGPP supply and inhibition of protein prenylation has been suggested to be involved in the mechanisms of neuronal death (Mohamed *et al.*, 2012). One study reported the involvement of GGPP in γ-secretase activity in SH-SY5Y neuroblastoma cells; and FPP and GGPP increase the Aβ levels in H4 neuroglioma cells by increasing γ-secretase activity (Kukar *et al.*, 2005; Urano *et al.*, 2005).

5.3 Cholesterol biosynthesis gene expression is altered with tau pathology

In *this study,* the variation in neuronal HMGCR immunoreactivity was not associated with dementia status and AD pathology. However, *HMGCR* relative gene expression in enriched neuronal populations isolated from human temporal cortex tissue was found to decrease with increasing tangle pathology and there was a significant moderate negative correlation with AT8 immunoreactivity. Furthermore, *SREBP2* relative gene expression in enriched neuronal populations isolated from human temporal cortex was increased with Braak and Braak stage, local cortical tangle pathology and AT8 immunoreactivity. This data suggests that the gene expression of key regulators of the cholesterol biosynthesis pathway (HMGCR and SREBP2) may be altered by NFT pathology. A decrease in *HMGCR* expression suggests that cholesterol levels may be optimum or accumulating hence a reduced mRNA expression to prevent an accumulation of cholesterol. However, the increase in *SREBP2* expression suggests that an increase in SREBP2 cleavage and turnover and so an increase in SREBP2 expression has occurred to maintain SREBP2 homeostasis. Interestingly, the changes in gene expression in the enriched neuronal population were not translated to a change in cholesterol concentration. Another possible explanation for the changes in *SREBP2* expression could be that this could

be a compensatory mechanism as cholesterol levels are not altered. However, considering the fact that SREBP2 expression shows a trend to increase it may later lead to an increase in expression of SREBP2 target genes such as HMGCR (Sharpe and Brown, 2013b). Therefore, from this data alone it is difficult to determine the specific impact of AD neuropathology and dementia on neuronal cholesterol biosynthesis as mRNA or protein expression of HMGCR alone does not determine cholesterol biosynthesis, as mentioned earlier, HMGCR activity has also been shown to be involved in the protein prenylation and isoprenoid synthesis (Eckert *et al.*, 2009).

5.4 The impact of oxidative stress on cholesterol biosynthesis

This current study also investigated the impact of oxidative stress on cholesterol biosynthesis. In post-mortem human temporal cortex tissue, we found that HMGCR immunoreactivity did not correlate to markers of oxidative DNA damage. However, in enriched neuronal populations isolated from the temporal cortex *HMGCR* expression showed a moderate positive correlation with oxidative DNA damage markers (γH2AX). Further work found that *HMGCR* mRNA expression was observed following exposure to acute and a more chronic oxidative stress in neuronal monocultures. This data suggests that oxidative stress may have an impact on cholesterol biosynthesis. Previous work from our lab has shown overexpression of *HMGCR* in neurons isolated from frontal cortex of low Braak and Braak cases that had high DNA damage response as a result of oxidative stress (Simpson *et al.*, 2016). Exposing human neuroblastoma cells to oxidative stress also found an increase in *HMGCR* expression (Recuero *et al.*, 2009). These studies also show that oxidative stress induces expression of *HMGCR* in neurons. Studies have shown that cholesterol influences the processing of APP, cholesterol enriched regions of the membrane favour the production of amyloidogenic Aβ and APP has also been shown to inhibit cleavage of SREBP2, preventing the nuclear localisation of the transcription factor domain (Cordy *et al.*, 2003; Grimm, Rothhaar and Hartmann, 2012, Pierrot *et al.*, 2013b). The deposition of Aβ plaques is a source of oxidative stress leading to DNA damage within neurons (Kwiatkowski *et al.*, 2016). This suggests that APP prevents the expression of SREBP2 target genes however, the presence of Aβ plaques leads to the generation of ROS and oxidative stress, which may induce *HMGCR* expression. This may lead to the aberrant activation of

cholesterol biosynthesis and cholesterol accumulation in cells, which increases the generation of Aβ.

5.5 High brain cholesterol is associated with dementia

This study found that moderate and high brain cholesterol was associated with increased risk of dementia. In *this study* the association with dementia was assessed independently of any presumed pathological basis. This effect was observed in both a univariate analysis adjusted for age at death and sex as well as a multivariate analysis adjusted for AD pathologies such as Braak and Braak, Thal and CAA pathology. Given the wide confidence intervals it suggests a weak and uncertain relationship and if any significant effect was present the effect is likely to be small. This study does not provide sufficient evidence to suggest that brain cholesterol modification, such as statins, would be an important therapeutic target for treating dementia. This is because it is still unclear whether the accumulation of cholesterol is bad for the neuron or whether the accumulation is a result of secondary changes due to other pathologies. However, considering the potential downstream functions associated with the cholesterol biosynthesis pathway, would provide important avenues for further investigation for targeting dementia.

5.6 Future work

To determine whether the mevalonate arm of the cholesterol biosynthesis pathway is being diverted to isoprenoid synthesis rather than cholesterol synthesis, characterisation of isoprenoids such as FFP and GGPP should be carried out. Immunohistochemical characterisation will determine the expression and localisation of isoprenoids in the temporal cortex. Dual labelling of isoprenoids and HMGCR would help determine if neuronal HMGCR immunoreactivity is associated with the non-sterol pathway. Immunohistochemical characterisation using both the CFAS and Edinburgh ageing cases will help determine if changes in isoprenoid expression are associated with aging and dementia status and pathology. Furthermore, isolating neurons from temporal cortex tissue using laser capture microdissection will help determine the changes that occur within both the mevalonate pathway and the isoprenoid synthesis pathway at an mRNA level.

The cholesterol biosynthetic gene expression in temporal cortex isolations should be further validated in temporal cortex using immunohistochemistry to determine the localisation of CYP46A1 and ABCA1. Extending gene expression studies to different

areas of the brain such as the hippocampus and frontal cortex will help elucidate the changes that occur in cholesterol biosynthesis in different brain regions during AD. This will also demonstrate the role of cholesterol homeostasis in different brain regions and may highlight similarities and differences between the regions. Measuring cholesterol concentration in an ageing cohort will help also determine the effects of aging on tissue cholesterol concentration in specific regions of the brain.

Another approach could involve the use of AD patient derived fibroblasts that are reprogrammed to form induced neuronal stem cells (iNSCs) which can be differentiated to form neurons and astrocytes or directly reprogrammed fibroblast cells to produce iNeurons and iAstrocytes. These reprogrammed cells (iNSCs, iNeurons, iAstrocytes) will contain specific age-associated changes, such as accumulation of DNA damage, compared to induced pluripotent stem cells (iPSCs) which may lose some of the epigenetic changes associated with ageing. These directly reprogrammed cells will help give a better understanding to how cholesterol biosynthesis is impacted in response to Aβ, tau and other contributing AD pathologies such as oxidative stress and neuroinflammation (Erharter *et al.*, 2019; Traxler, Edenhofer and Mertens, 2019).

In vivo models of AD can also be used to determine changes in cholesterol biosynthesis alongside AD neuropathology progression, this can be achieved using transgenic mice models. Transgenic mice models of AD usually consist of overexpressing human forms of wild type or mutant genes that are known to be involved in the formation of plaques and tangles (*APP*, *MAP2*, *APOE*, *PSN1*) (Myers and McGonigle, 2019). These models will allow the assessment of AD pathology on the cholesterol biosynthesis within the brain as LCM or cell sorting can be used to isolate neurons and astrocytes and determine the gene expression and protein levels of key regulators of the cholesterol biosynthesis pathway. Furthermore, transgenic mice models can also be used to determine the changes in brain tissue cholesterol in response to AD neuropathology. Certain limitations and considerations need to be considered when using transgenic mice models. First and foremost are the ethical consideration surround *in vivo* animal work and whether a different model may be more appropriate. Furthermore, wild type mice do not develop AD and mouse homologs of AD associated protein differ from human homologs. Also the expression patterns and phenotypes of microglia differ between the two species

hence, transgenic mice do not necessarily have the disease and does not accurately simulate the cognitive changes found in AD (Sasaguri *et al.*, 2017).

6.0 Appendix

6.1 Materials

All chemicals/solutions were stored at room temperature (RT) unless stated otherwise.

All chemicals were purchased from Sigma-Aldrich Ltd, (UK), unless stated otherwise.

6.1.1 Histology materials

6.1.1.1 Immunohistochemistry

1x Tris-buffered Saline (TBS) pH 7.6 was prepared using 6.05 g of Tris base (Fisher Scientific, New Jersey, US) and 8.50 g of Sodium Chloride (Alfa Aesar, USA) in 1 L of distilled water.

Xylene (Fisher Scientific, UK)

Ethanol (VWR Chemicals, France)

pH 9.5 buffer for antigen retrieval (Menarini Diagnostics, UK)

Endogenous peroxidase blocking solution 3% (v/v) H_2O_2/Methanol (Fisher Scientific UK)/ (Fisher Scientific UK)

Vectastain elite ABC Rabbit IgG kit (Vector Laboratories, UK). The goat blocking serum was prepared in 10 ml of TBS with 150 µl of serum. The secondary biotinylated antibody was prepared in 10 ml of 1.5% (v/v) goat serum with 50 µl of antibody solution. The avidin biotinylated complex horseradish peroxidase (ABC-HRP) solution was prepared in 10 ml of TBS with 100 µl of both reagent A and reagent B, at least 30 minutes before use.

3,3'-diaminobenzidine (DAB) (Vector Laboratories, UK). The DAB solution was prepared in 2.5 ml of d.H_2O in which 50 µl of DAB buffer, 50 µl H_2O_2 and 100 µl of DAB substrate were added.

Harris haematoxylin (Cell Path, UK)

Scotts Tap water was prepared using 3.5 M of Sodium bicarbonate (Fisher Scientific, UK) and 20 M of Magnesium Sulphate (Fisher Scientific, UK) in 1 L of tap water.

DPX mountant (Cell Path, UK)

Antibodies used for IHC can be found in Table 2.3

6.1.1.2 Frozen Immunohistochemistry

Acetone (VWR chemicals, France) and stored at 4°C

6.1.1.3 Dual labelling immunohistochemistry

Vectastain ABC-AP kit, Vector Laboratories, UK. Alkaline phosphatase-conjugated avidin-biotin complex (ABC-AP) was prepared by adding 100 µl of reagent 'A' and 100 µl of reagent 'B' into 5 ml 1x TBS, prepared at least 30 minutes prior to use.

Vector Red Alkaline Phosphatase substrate kit, Vector Laboratories, UK. Alkaline phosphatase substrate was prepared by adding 100 µl of reagents 1, 2, and 3 into 5 ml Tris-HCL, 100mM.

6.1.1.4 Bicinchoninic acid assay (BCA)

BCA protein assay kit was purchased from ThermoFisher Scientific, USA.

Extra strong lysis buffer was prepared in ultrapure H_2O using 10 mM Tris-HCL (pH 7.5), 0.5% (w/v) sodium dodecyl sulphate (SDS), 0.5% (w/v) sodium deoxycholate, 1% (v/v) Triton X-100, 75 mM sodium chloride, 10 mM ethylenediaminetetraacetic acid, 2 mM sodium orthovandate, 1.25 mM sodium fluoride. Protease inhibitor cocktail (Roche, Germany) for mammalian tissues, 1 tablet was used for 10 ml of extra strong lysis buffer.

Bovine serum albumin (BSA) standard was purchased from Thermo Scientific™Pierce™ Albumin standard (Pierce Endogen, USA).

6.1.1.5 SDS-polyacrylamide gel electrophoresis (SDS-PAGE)

30% Acrylamide solution (Bio-Rad Laboratories Ltd, UK).

Ammonium Persulphate (APS).

Tetramethylethylenediamine (TEMED) (Thermo Scientific, UK).

Resolving buffer was prepared using 1.5 M Tris-HCL pH 8.8 and 4% (v/v) of 10% (v/v) SDS solution.

Stacking buffer was prepared using 0.5 M Tris-HCL pH 6.8 and 4% (v/v) of 10% (v/v) SDS solution.

Running buffer was prepared using 24.8 mM Tris base, pH 8.3 and 192 mM glycine.

4x Lammeli sample buffer was prepared using 40 mM Tris, pH 6.8, 12% (w/v) SDS, 47% (v/v) glycerol, 0.12% (v/v) beta-mercaptoethanol and 0.6 M DTT.

The Precision Plus Dual Colour Protein Standard was used as the standard for Western Blot analysis (Bio-Rad Laboratories Ltd, UK).

6.1.1.6 Western Blotting

1x Phosphate buffered Saline (PBS) pH 7.4 was prepared using 8 M sodium chloride, 0.2 M potassium chloride, 1.44 M sodium phosphate dibasic and 0.24 M potassium phosphate monobasic diluted in ultrapure H_2O.

Western blotting transfer buffer was prepared using 25 mM Tris, 100 mM glycine and 10% (v/v) methanol.

Nitrocellulose membrane (GE Healthcare, UK)

Milk-PBST blocking solution was prepared using 5% (w/v) marvel original dried skimmed milk and 0.01% (v/v) tween 20 in 1x PBS

Ponceau red was prepared using 0.1% (w/v) Ponceau S in 5% (v/v) acetic acid diluted in ddH_2O.

PBS-T wash buffer was prepared using 0.01% (v/v) Tween-20 in 1x PBS.

Enhanced chemiluminescent substrate (ECL) (EZ-ECL Biological Industries, Israel).

6.1.1.7 RNA Extraction from Post-Mortem Tissue

Trizol (Fisher Scientific, UK) and stored at 4°C.

Chloroform (Sigma-Aldrich, UK).

Isopropanol (Fisher Scientific, UK).

Ethanol (VWR Chemicals, France).

RNAase free water (Zymo research, US).

6.1.1.8 Rapid Immunohistochemistry for laser capture microdissection

Acetone (VWR chemicals, France) and stored at 4°C.

6.1.1.9 Toluidine Blue staining for neurons

Toluidine blue is prepared using 1 g/l of Toluidine blue (TCS Biosciences LTD, UK) in dH_2O.

Diethylpyrocarbonate (EMD Biosciences, UK) add 1 ml of 0.1% (v/v) Diethylpyrocarbonate (DEPC) to 1 L dH_2O and mix well. Autoclave and cool to RT prior to use.

6.1.1.10 Laser Capture Micro-dissection (LCM)

LCM caps (Arcturus, life technology, US).

Picopure RNA isolation kit (Thermo fisher scientific, UK).

6.1.1.11 cDNA synthesis

Q-script (Quanta biosciences, US) and stored at -20°C.

6.1.1.12 Cell enrichment validation

5x Green firepole PCR mix (Solis Biodyne, Estonia) and stored at -20°C.

Validation primers (Eurofins Genomics, Germany) reconstituted and stored at -20°C. Primer sequences can be found in table 3.1.

6.1.1.13 Agarose Gel Electrophoresis

Agarose (Bioline, UK).

1x TAE buffer is used which has 0.04 M Tris-Acetate and 0.001 M EDTA in triple red pure water.

Hyperladder V (Bioline, UK) and stored at 4°C.

Ethidium Bromide (Sigma-Aldrich, UK).

6.1.1.14 Quantitative real time PCR (q RT-PCR)

PrimeTime qPCR assays were purchased from Integrated DNA Technologies (USA). Standard qPCR assays were reconstituted in 500 µl 1x TE buffer, the primer probe sequence can be found in table 3.2.

TE Buffer, pH8, was prepared using 10 mM Tris and 0.1 mM EDTA in triple red pure water.

1x LUNA universal probe qPCR master mix (New England Biolabs, UK).

6.1.1.15 Amplex Red cholesterol Assay

Amplex Red cholesterol assay kit was purchased from (Thermo fisher scientific, UK).

96-well black polypropylene microplates were purchased from Merck, Germany. (M9685-100EA).

6.1.2 Cell culture materials

6.1.2.1 LUHMES cell culture

Poly-L-Ornithine (p-L-o) was prepared using 50 µg/ml p-L-o in 1x PBS.

Fibronectin was prepared using 1 µg/ml fibronectin in 1x PBS.

Proliferation media was prepared using Advanced Dulbecco's Modified Eagle Medium/Nutrient Mixture F-12, (Gibco, Thermo Fisher Scientific, UK), 1% (v/v) N2-supplement (Gibco, Thermo Fisher Scientific, UK), 1% (v/v) L-glutamine (Lonza group Ltd, Switzerland), 1% (v/v) Penicillin/streptomycin (Lonza group Ltd, Switzerland) and supplemented with 40 ng/ml basic fibroblast growth factor (bFGF) (Peprotech EC Ltd, USA).

Differentiation media was prepared using Advanced Dulbecco's Modified Eagle Medium/Nutrient Mixture F-12, (Gibco, Thermo Fisher Scientific, UK), 1% (v/v) N2-supplement (Gibco, Thermo Fisher Scientific, UK), 1% (v/v) L-glutamine (Lonza group Ltd, Switzerland), 1% (v/v) Penicillin/streptomycin (Lonza group Ltd, Switzerland) and supplemented with 1 µg/ml tetracycline (Sigma-Aldrich, UK).

Trypsin-versene (Lonza group Ltd, Switzerland).

6.1.2.2 Cryopreservation of LUHMES

Foetal Bovine Serum (FBS) (Biosera, France).

Dimethyl sulphoxide (DMSO) (Sigma-Aldrich, UK).

6.1.2.3 Astrocyte cell culture

Astrocyte media was purchased from ScienceCell Research Laboratories (USA) and supplemented with 2% (v/v) FBS, 1% (v/v) astrocyte growth supplement (AGS) and 1% (v/v) penicillin/streptomycin all purchased from ScienceCell Research Laboratories, USA.

6.1.2.4 H_2O_2 treatments

30% H_2O_2 (v/v) (Sigma-Aldrich, UK).

6.1.2.5 RNA extraction from cells using Trizol extracts

Direct-zol RNA MiniPrep extraction kit (Zymo Research, USA).

6.1.2.6 Immunocytochemistry

4% Paraformaldehyde was prepared using 4% (w/v) Paraformaldehyde (Sigma-Aldrich, UK) in 1x PBS and sterile filtered through 0.45 µM filter.

0.3% (v/v) Triton-X100 (Sigma-Aldrich, UK) in 1x PBS.

Blocking solution was prepared using 3% (v/v) Albumin bovine fraction V (BSA) (Melford Laboratories Ltd, UK), 0.01% Tween20 (Sigma-Aldrich, UK) in 1x PBS.

Hoechst (33342) 10 mg/ml bisbenzimide H 33342 trihydrochloride (Sigma-Aldrich, UK).

ClearMount^{TM} mounting solution (Invitrogen, UK).

Primary and secondary antibodies used for ICC can be found in table 4.2 and 4.3 respectively.

6.1.2.7 Lactate Dehydrogenase Assay (LDH)

Cytotoxicity/ LDH assay kit was purchased from Promega, USA.

6.2 HMGCR antibody optimisation

To study the protein expression and localisation of HMGCR, antigen retrieval and antibody dilution were optimised for human post-mortem formalin fixed paraffin embedded brain tissue from the CFAS Cambridge cohort. Weak specific immunolabelling of pyramidal neurons was observed at the 1:100 and 1:50 antibody dilutions with both pressure cooker antigen retrieval conditions. Immunolabelling was not observed with both antibody dilutions with either microwave antigen retrieval conditions. Overall, a 1 hr antibody incubation time at RT showed a weak immunoreactivity for the pressure cooker treated sections while no immunoreactivity was present with microwave treated sections (Figure 6.1), indicating the pressure cooker antigen retrieval with a longer antibody incubation time would be required. No specific immunoreactivity was observed in IgG and negative controls.

After an overnight incubation at 4°C, HMGCR immunoreactivity was strong for the 1:50 antibody dilution, although a high amount of non-specific background immunoreactivity was also present for both pH6 and pH9 antigen retrieval buffers (Figure 6.2 E & F). An antibody dilution of 1:100 gave a very similar level of immunoreactivity as the 1:50 dilution but there appeared to be less non-specific background staining for both pH6 and pH9 buffers (Figure 6.2 A and B). Thus, optimal conditions for HMGCR IHC were the use of a pressure cooker with an alkaline (pH9) buffer. Optimal antibody conditions were a 1:100 with a 24hr incubation period at 4°C.

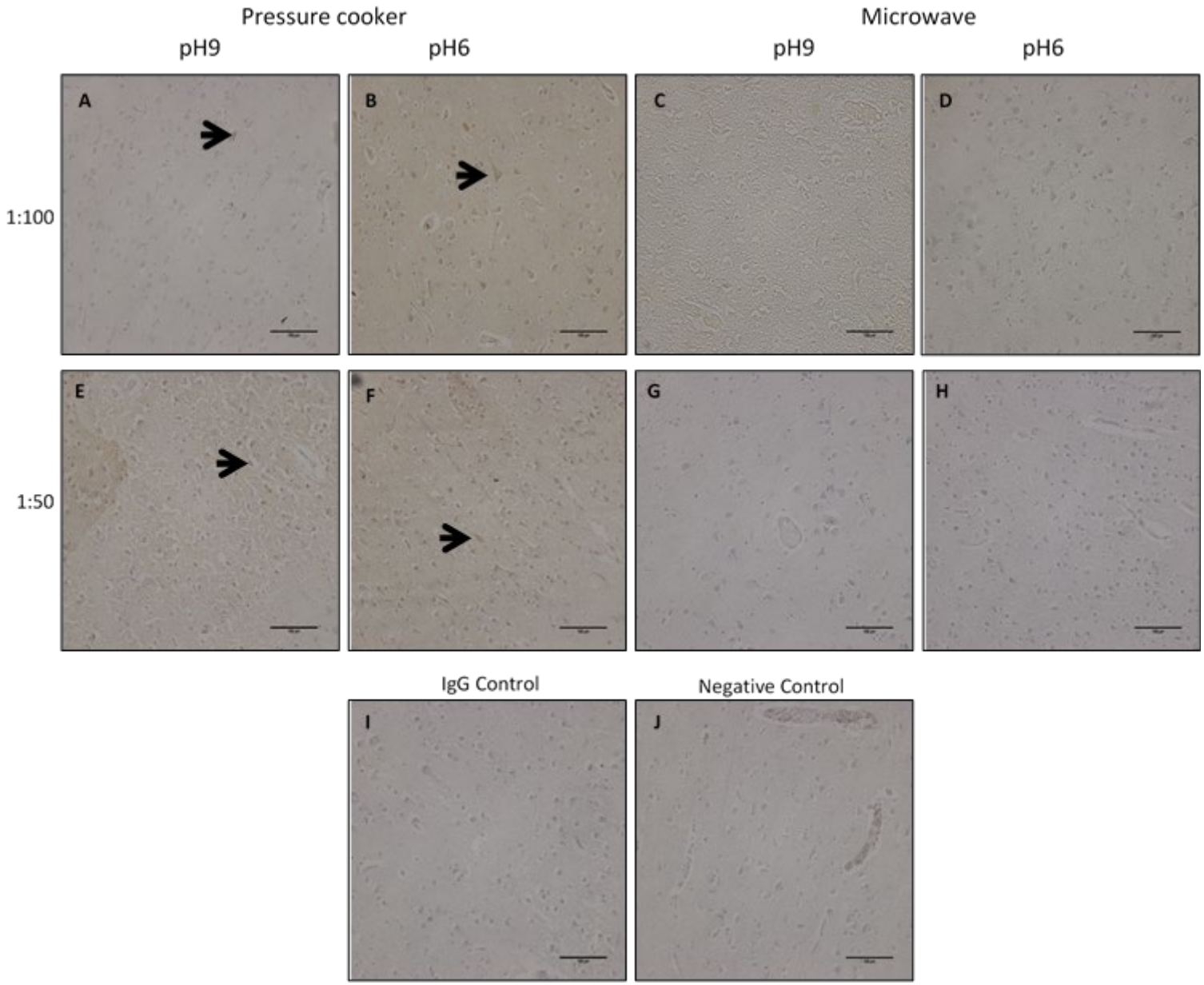

Figure 6.1. HMGCR antibody optimisation, 1hr incubation at room temperature. Pressure cooker antigen retrieval at pH9 , 1:100 (A), 1;50 (E), pressure cooker antigen retrieval at pH6 1:100 (B), 1:50 (F), microwave antigen retrieval using EDTA buffer (pH8) 1;100 (C), 1:50 (G), and microwave antigen retrieval using tris sodium citrate buffer (pH6) 1:100 (D), 1:50 (H). Weak specific immunolabelling of pyramidal neurons (as indicated by the black arrows) was observed at the 1:100 and 1:50 antibody dilutions with both pressure cooker antigen retrieval conditions (A, B, E & F). Immunolabelling was not observed with both antibody dilutions with either microwave antigen retrieval condition (C, D, G, H) No specific immunostaining was observed in either IgG isotype control (I) or negative control (J). Scale bar represents 100µm.

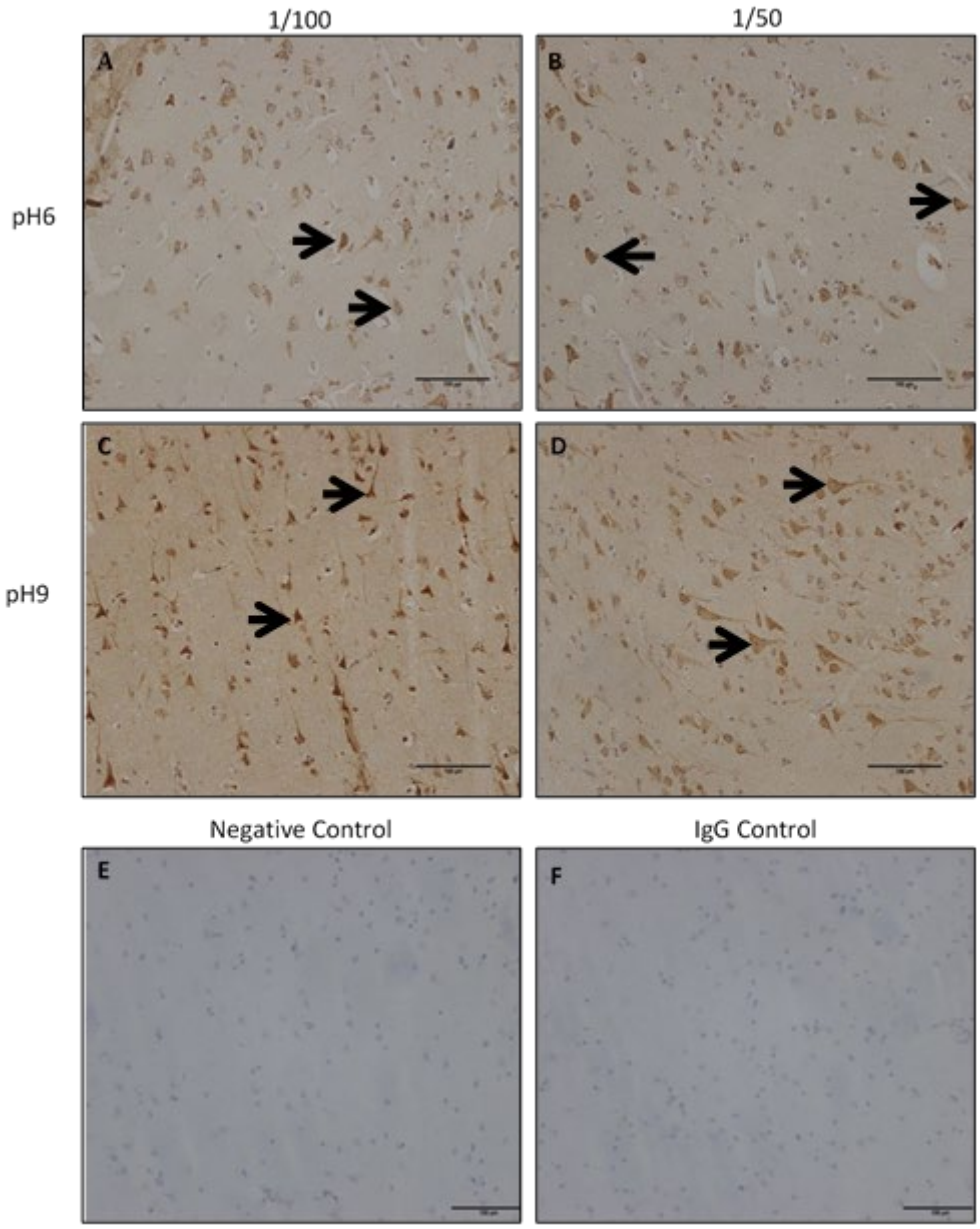

Figure 6.2. HMGCR antibody optimisation, overnight incubation at 4°C. The sections were incubated overnight at 4°C with the primary antibody. Both pressure cooker antigen retrieval at pH6, 1:100 (A) and 1:50 (B) showed weak immunostaining (black arrows). Pressure cooker antigen retrieval at pH9, 1:100 (C) and 1:50 (D) showed strong punctate immunostaining in pyramidal neurons (black arrows). No specific immunostaining was observed with either rabbit IgG isotype control (E) or negative control (F). Scale bar represents 100µm.

6.3 CFAS Ethical approval

NHS
Health Research Authority
NRES Committee South West - Frenchay
Level 3, Block B
Whitefriars
Lewins Mead,
Bristol BS1 2NT
Email: nrescommittee.southwest-frenchay@nhs.net

10 August 2015

Professor Stephen B Wharton
Professor and Honorary Consultant in Neuropathology
University of Sheffield
Sheffield Institute for Translational Neuroscience
385A Glossop Road
Sheffield
S10 2HQ

Dear Professor Wharton

Study title:	**Cognitive Function and Ageing Studies: Diabetes, Defective Nutrient Signalling and Dementia: an Epidemiological Neuropathology approach.**
REC reference:	**15/SW/0246**
IRAS project ID:	**184134**

The Proportionate Review Sub-committee of the NRES Committee South West - Frenchay reviewed the above application on 10 August 2015.

We plan to publish your research summary wording for the above study on the HRA website, together with your contact details. Publication will be no earlier than three months from the date of this favourable opinion letter. The expectation is that this information will be published for all studies that receive an ethical opinion but should you wish to provide a substitute contact point, wish to make a request to defer, or require further information, please contact the REC Manager Mrs Naazneen Nathoo, nrescommittee.southwest-frenchay@nhs.net. Under very limited circumstances (e.g. for student research which has received an unfavourable opinion), it may be possible to grant an exemption to the publication of the study.

Ethical opinion

On behalf of the Committee, the sub-committee gave a favourable ethical opinion of the above research on the basis described in the application form, protocol and supporting documentation, subject to the conditions specified below.

CFAS
Cognitive Function & Ageing Study

FOR CFAS OFFICE USE

Tissue request no. 16/04

AUTHORISATION TO USE TISSUE FROM THE COGNITIVE FUNCTION AND AGEING STUDY (CFAS) BIOLOGICAL RESOURCE

FOLLOWING CONSIDERATION BY THE CFAS MANAGEMENT COMMITTEE (CMC) AND BIOLOGICAL RESOURCE ADVISORY COMMITTEE (BRAC):

Study Title: Cholesterol dysregulation in the neurovascular unit as an early contributor to neuronal dysfunction in Alzheimer's disease

Head of proposed study

Title:Professor

Name: Steve Wharton
Additional investigator: Hemant Mistry

Organisation:
Address: Sheffield Institute for Translational Neuroscience, 385A Glossop Road, Sheffield, S10 2HQ

Telephone No: 0114 222 2235

Email: s.wharton@sheffield.ac.uk

CFAS TISSUE REQUEST NUMBER**: 16/04**

This project was reviewed by both CMC and BRAC committees and approval was given to release the requested tissue under the following REC approval:

Title of Ethical application: Cognitive Function and Ageing Studies: Diabetes, Defective Nutrient Signalling and Dementia: an Epidemiological Neuropathology approach.

REC No: 15/SW/0246
IRAS No: 184134

Professor Carol Brayne
Chief Investigator CFAS

Date: 27/07/2017

Sample demographics	Men, n = 37	Women, n = 60	Total, n = 97
Age at death/ years			
70-74	5	5	10
75-79	5	5	10
80-84	9	9	18
85-89	10	18	28
90+	8	23	31
Average age at death/ years	83	83	83
Median post-mortem delay / hrs	21	15	17
Median brain pH	6.43	6.54	6.50
Dementia status/ n			
No Dementia	16	21	37
Dementia	19	39	58

Table 6.3.1: CFAS Cambridge temporal cortex case demographics

6.4 Edinburgh Ethical approval

CCBS
Centre for Clinical Brain Sciences

Ms Chris-Anne McKenzie
Brain Bank Manager
Department of Academic Neuropathology
Centre for Clinical Brain Sciences
University of Edinburgh
Chancellor's Building
49 Little France Crescent
Edinburgh
EH16 4SB
0131 242 6521

Mr H Mistry
Sheffield Institute of Translational Neuroscience
385A Glossop Road
Sheffield
South Yorkshire
S10 2HQ

Dear Mr Mistry 31/07/2019

Re; Cholesterol *dysregulation in the neurone-astrocyte unit as an early contributor to neuronal dysfunction in Alzheimer 's disease*.

Thank you for your recent request for use of unstained slides.
I can confirm that the local management group has approved your request.

Yours sincerely

Chris-Anne McKenzie
Brain Bank Manager

Age-group	Age	Sex	pH	Post Mortem Delay/ hr	Cause of Death	Neuropathology
16-30	20	F	6.5	71	Suspension by ligature	None
	29	M	6.5	44	Suspension by ligature	Focal Tau, no neuritic plaques
	30	M	6.4	71	Unascertained	None
31-45	32	F	6.3	63	Cardiomyopathy, Marfan's syndrome	None
	39	F	6.4	43	Suspension by ligature	None
	42	M	6.4	61	IHD	None
46-60	46	M	6.5	52	IHD	None
	48	M	6.3	72	CAD	None
	50	M	6.3	45	IHD/CAD	None
	52	M	6.4	91	Road traffic collision	None
	57	M	6.5	66	IHD/CAD	None
61-75	63	F	6.3	35	IHD/CAD	Mild amyloid tangles and plaques
	70	F	6.5	79	Ruptured aneurysm	Large vessel arteriosclerosis and ischaemic white matter pathology. Mild tau threads and tangles. Mild vascular amyloid, tangles and plaques.
	71	F	6.5	41	IHD	Mild and focal vascular tau. Mild amyloid tangles and plaques
	74	M	6.3	66	IHD/CAD	White matter pallor, mild tau tangles, plaques and treads
75+	75	M	6.4	78	IHD/CAD	Mild tau tangles and treads

Table 6.4.1: Edinburgh Medical Research Council sudden death prefrontal association cortex cohort case demographics.

7.0 Bibliography

A. Armstrong, R. (2014) ‘A critical analysis of the “amyloid cascade hypothesis”’, *Folia Neuropathologica*, 3(3), pp. 211–225. doi: 10.5114/fn.2014.45562.

Afshordel, S. *et al.* (2014) ‘Impaired geranylgeranyltransferase-I regulation reduces membrane-associated Rho protein levels in aged mouse brain’, *Journal of Neurochemistry*. Blackwell Publishing Ltd, 129(4), pp. 732–742. doi: 10.1111/jnc.12654.

Ahmed, M. *et al.* (2019) ‘Current Agents in Development for Treating Behavioral and Psychological Symptoms Associated with Dementia’, *Drugs and Aging*. Springer International Publishing, pp. 589–605. doi: 10.1007/s40266-019-00668-7.

Ajikumar, A. *et al.* (2019) ‘Neutrophil-derived microvesicle induced dysfunction of brain microvascular endothelial cells in vitro’, *International Journal of Molecular Sciences*. MDPI AG, 20(20). doi: 10.3390/ijms20205227.

American Psychological Association (APA) (2013) *Diagnostic and Statistical Manual of Mental Disorders: Depressive Disorders*, *Diagnostic and Statistical Manual of Mental Disorders,*. American Psychiatric Publishing, Inc. doi: 10.1176/appi.books.9780890425596.dsm04.

Amundson, D. M. and Zhou, M. (1999) ‘Fluorometric method for the enzymatic determination of cholesterol’, *Journal of Biochemical and Biophysical Methods*. Elsevier, 38(1), pp. 43–52. doi: 10.1016/S0165-022X(98)00036-0.

Andersen, O. M. *et al.* (2005) ‘Neuronal sorting protein-related receptor sorLA/LR11 regulates processing of the amyloid precursor protein.’, *Proceedings of the National Academy of Sciences of the United States of America*. National Academy of Sciences, 102(38), pp. 13461–6. doi: 10.1073/pnas.0503689102.

Andreadis, A. (2005) ‘Tau gene alternative splicing: Expression patterns, regulation and modulation of function in normal brain and neurodegenerative diseases’, *Biochimica et Biophysica Acta - Molecular Basis of Disease*. Elsevier, pp. 91–103. doi: 10.1016/j.bbadis.2004.08.010.

Arima, K. (2006) ‘Ultrastructural characteristics of tau filaments in tauopathies: Immuno-electron microscopic demonstration of tau filaments in tauopathies’, *Neuropathology*. John Wiley & Sons, Ltd, 26(5), pp. 475–483. doi: 10.1111/j.1440-1789.2006.00669.x.

Arispe, N. (2004) ‘Architecture of the Alzheimer’s AβP Ion Channel Pore’, *Journal of Membrane Biology*. Springer, 197(1), pp. 33–48. doi: 10.1007/s00232-003-0638-7.

Arodin, L. *et al.* (2014) ‘Alteration of thioredoxin and glutaredoxin in the progression of Alzheimer’s disease’, *Journal of Alzheimer’s Disease*. IOS Press, 39(4), pp. 787–797. doi: 10.3233/JAD-131814.

Ball, M. J. and Lo, P. (1977) ‘GRANULOVACUOLAR DEGENERATION IN THE AGEING BRAIN AND IN DEMENTIA’, *Journal of Neuropathology and Experimental Neurology*. Oxford Academic, 36(3), pp. 474–487. doi: 10.1097/00005072-197705000-00006.

Ballabh, P., Braun, A. and Nedergaard, M. (2004) ‘The blood-brain barrier: An overview: Structure, regulation, and clinical implications’, *Neurobiology of Disease*. Academic Press, pp. 1–13. doi: 10.1016/j.nbd.2003.12.016.

Barber, R. C. and C., R. (2012) ‘The genetics of Alzheimer’s disease.’, *Scientifica*. Hindawi Publishing Corporation, 2012, p. 246210. doi: 10.6064/2012/246210.

Barbero-Camps, E. *et al.* (2013) ‘APP/PS1 mice overexpressing SREBP-2 exhibit combined Aβ accumulation and tau pathology underlying Alzheimer’s disease’, *Human Molecular Genetics*, 22(17), pp. 3460–3476. doi: 10.1093/hmg/ddt201.

Barbiero, L. *et al.* (2003) 'BACE-2 is overexpressed in Down's syndrome', *Experimental Neurology*. Academic Press Inc., 182(2), pp. 335–345. doi: 10.1016/S0014-4886(03)00049-9.
Barrientos, A. *et al.* (1997) 'Reduced steady-state levels of mitochondrial RNA and increased mitochondrial DNA amount in human brain with aging.', *Brain research. Molecular brain research*, 52(2), pp. 284–9. Available at: http://www.ncbi.nlm.nih.gov/pubmed/9495550 (Accessed: 4 January 2017).
Bartels, A. L. (2011) 'Blood-Brain Barrier P-Glycoprotein Function in Neurodegenerative Disease', *Current Pharmaceutical Design*. Bentham Science Publishers Ltd., 17(26), pp. 2771–2777. doi: 10.2174/138161211797440122.
Bartzokis, G. (2011) 'Alzheimer's disease as homeostatic responses to age-related myelin breakdown', *Neurobiology of Aging*, 32(8), pp. 1341–1371. doi: 10.1016/j.neurobiolaging.2009.08.007.
Belfiore, R. *et al.* (2019) 'Temporal and regional progression of Alzheimer's disease-like pathology in 3xTg-AD mice', *Aging Cell*. Blackwell Publishing Ltd, 18(1). doi: 10.1111/acel.12873.
Bell, R. D. *et al.* (2012) 'Apolipoprotein e controls cerebrovascular integrity via cyclophilin A', *Nature*. Nature Publishing Group, 485(7399), pp. 512–516. doi: 10.1038/nature11087.
Belloy, M. E., Napolioni, V. and Greicius, M. D. (2019) 'A Quarter Century of APOE and Alzheimer's Disease: Progress to Date and the Path Forward', *Neuron*, 101(5), pp. 820–838. doi: 10.1016/j.neuron.2019.01.056.
Bettcher, B. M. *et al.* (2017) 'Association between cholesterol exposure and neuropathological findings: The ACT Study', *Journal of Alzheimer's Disease*. IOS Press, 59(4), pp. 1307–1315. doi: 10.3233/JAD-161224.Association.
Binder, L. I., Frankfurter, A. and Rebhun, L. I. (1985) 'The distribution of tau in the mammalian central nervous system.', *The Journal of Cell Biology*, 101(4).
Björkhem, I., Meaney, S. and Fogelman, A. M. (2004) 'Brain Cholesterol: Long Secret Life behind a Barrier', *Arteriosclerosis, Thrombosis, and Vascular Biology*, pp. 806–815. doi: 10.1161/01.ATV.0000120374.59826.1b.
Blalock, E. M. *et al.* (2004) 'Incipient Alzheimer's disease: Microarray correlation analyses reveal major transcriptional and tumor suppressor responses', *Proceedings of the National Academy of Sciences of the United States of America*. National Academy of Sciences, 101(7), pp. 2173–2178. doi: 10.1073/pnas.0308512100.
Boehm-Cagan, A. *et al.* (2016) 'ABCA1 Agonist Reverses the ApoE4-Driven Cognitive and Brain Pathologies', *Journal of Alzheimer's Disease*, 54(3), pp. 1219–1233. doi: 10.3233/JAD-160467.
Boutajangout, A. and Wisniewski, T. (2014) 'Tau-based therapeutic approaches for Alzheimer's disease - a mini-review.', *Gerontology*. Karger Publishers, 60(5), pp. 381–5. doi: 10.1159/000358875.
Boveris, A. and Navarro, A. (2008) 'Brain mitochondrial dysfunction in aging.', *IUBMB life*, 60(5), pp. 308–14. doi: 10.1002/iub.46.
Braak, H. *et al.* (2006) 'Staging of Alzheimer disease-associated neurofibrillary pathology using paraffin sections and immunocytochemistry', *Acta Neuropathologica*. Springer-Verlag, 112(4), pp. 389–404. doi: 10.1007/s00401-006-0127-z.
Braak, H. and Braak, E. (1991) 'Acta H ' pathologica Neuropathological stageing of Alzheimer-related changes', *Acta Neuropathol*, 82, pp. 239–259.
Bradl, M. and Hohlfeld, R. (2003) 'Molecular pathogenesis of neuroinflammation', *Journal of Neurology, Neurosurgery and Psychiatry*. BMJ Publishing Group, pp.

1364–1370. doi: 10.1136/jnnp.74.10.1364.
Brayne, C., McCracken, C. and Matthews, F. E. (2006) 'Cohort profile: The medical research council cognitive function and ageing study (CFAS)', *International Journal of Epidemiology*, 35(5), pp. 1140–1145. doi: 10.1093/ije/dyl199.
Bretillon, L. *et al.* (2000) 'Plasma levels of 24S-hydroxycholesterol reflect the balance between cerebral production and hepatic metabolism and are inversely related to body surface', *Journal of Lipid Research*. American Society for Biochemistry and Molecular Biology, 41(5), pp. 840–845.
Brown, A. J. and Jessup, W. (2009) 'Oxysterols: Sources, cellular storage and metabolism, and new insights into their roles in cholesterol homeostasis', *Molecular Aspects of Medicine*. Mol Aspects Med, pp. 111–122. doi: 10.1016/j.mam.2009.02.005.
Brown, J., Theisler, C., Silberman, S., Magnuson, D., Gottardi-Littell, N., Lee, John M, *et al.* (2004) 'Differential expression of cholesterol hydroxylases in Alzheimer's disease.', *The Journal of biological chemistry*, 279(33), pp. 34674–81. doi: 10.1074/jbc.M402324200.
Brown, J., Theisler, C., Silberman, S., Magnuson, D., Gottardi-Littell, N., Lee, John M., *et al.* (2004) 'Differential expression of cholesterol hydroxylases in Alzheimer's disease', *Journal of Biological Chemistry*. American Society for Biochemistry and Molecular Biology, 279(33), pp. 34674–34681. doi: 10.1074/jbc.M402324200.
Brown, M. S. and Goldstein, J. L. (1997) 'The SREBP pathway: Regulation of cholesterol metabolism by proteolysis of a membrane-bound transcription factor', *Cell*, 89(3), pp. 331–340. doi: 10.1016/S0092-8674(00)80213-5.
Burkhardt, R. *et al.* (2008) 'Common SNPs in HMGCR in micronesians and whites associated with LDL-cholesterol levels affect alternative splicing of exon13', *Arteriosclerosis, Thrombosis, and Vascular Biology*. Arterioscler Thromb Vasc Biol, 28(11), pp. 2078–2084. doi: 10.1161/ATVBAHA.108.172288.
Burns, M. P. *et al.* (2003) 'Co-localization of cholesterol, apolipoprotein E and fibrillar Aβ in amyloid plaques', *Molecular Brain Research*. Elsevier, 110(1), pp. 119–125. doi: 10.1016/S0169-328X(02)00647-2.
Bushong, E. A. *et al.* (2002) 'Protoplasmic astrocytes in CA1 stratum radiatum occupy separate anatomical domains', *Journal of Neuroscience*, 22(1), pp. 183–192. doi: 10.1523/jneurosci.22-01-00183.2002.
Caceres, A. and Kosik, K. S. (1990) 'Inhibition of neurite polarity by tau antisense oligonucleotides in primary cerebellar neurons', *Nature*. Nature Publishing Group, 343(6257), pp. 461–463. doi: 10.1038/343461a0.
Cahoy, J. D. *et al.* (2008a) 'A transcriptome database for astrocytes, neurons, and oligodendrocytes: A new resource for understanding brain development and function', *Journal of Neuroscience*. Society for Neuroscience, 28(1), pp. 264–278. doi: 10.1523/JNEUROSCI.4178-07.2008.
Cahoy, J. D. *et al.* (2008b) 'Cellular/Molecular A Transcriptome Database for Astrocytes, Neurons, and Oligodendrocytes: A New Resource for Understanding Brain Development and Function', *Journal of Neuroscience*, 28(1). doi: 10.1523/JNEUROSCI.4178-07.2008.
Cai, Z. *et al.* (2018) 'Role of Blood-Brain Barrier in Alzheimer's Disease', *Journal of Alzheimer's Disease*. IOS Press, pp. 1223–1234. doi: 10.3233/JAD-180098.
Carson, M. J. *et al.* (2006) 'CNS immune privilege: Hiding in plain sight', *Immunological Reviews*. NIH Public Access, pp. 48–65. doi: 10.1111/j.1600-065X.2006.00441.x.
Carter, C. J. (2007) 'Convergence of genes implicated in Alzheimer's disease on the

cerebral cholesterol shuttle: APP, cholesterol, lipoproteins, and atherosclerosis', *Neurochemistry International*. Pergamon, pp. 12–38. doi: 10.1016/j.neuint.2006.07.007.
Carter, S. F. *et al.* (2019) 'Astrocyte Biomarkers in Alzheimer's Disease', *Trends in Molecular Medicine*. Elsevier Ltd, pp. 77–95. doi: 10.1016/j.molmed.2018.11.006.
Cartocci, V. *et al.* (2016) 'Modulation of the Isoprenoid/Cholesterol Biosynthetic Pathway During Neuronal Differentiation In Vitro', *Journal of cellular biochemistry*. Wiley-Blackwell, 117(9), pp. 2036–2044. doi: 10.1002/jcb.25500.
Chang, T. Y. *et al.* (2017) 'Cellular cholesterol homeostasis and Alzheimer's disease', *Journal of Lipid Research*. American Society for Biochemistry and Molecular Biology Inc., 58(12), pp. 2239–2254. doi: 10.1194/jlr.R075630.
de Chaves, E. P. and Narayanaswami, V. (2008) 'Apolipoprotein E and cholesterol in aging and disease in the brain', *Future Lipidology*, pp. 505–530. doi: 10.2217/17460875.3.5.505.
Chen, H. *et al.* (2019) 'Association between serum cholesterol levels and Alzheimer's disease in China: a case-control study', *International Journal of Food Sciences and Nutrition*. Taylor and Francis Ltd, 70(4), pp. 405–411. doi: 10.1080/09637486.2018.1508426.
Chen, J. *et al.* (2013) 'Cholesterol efflux is differentially regulated in neurons and astrocytes: Implications for brain cholesterol homeostasis', *Biochimica et Biophysica Acta - Molecular and Cell Biology of Lipids*. Elsevier, 1831(2), pp. 263–275. doi: 10.1016/j.bbalip.2012.09.007.
Chen, Y. *et al.* (2018) 'Pro- and Anti-inflammatory effects of high cholesterol diet on aged brain', *Aging and Disease*. International Society on Aging and Disease, 9(3), pp. 374–390. doi: 10.14336/AD.2017.0706.
Chistiakov, D. A. *et al.* (2017) 'CD68/macrosialin: Not just a histochemical marker', *Laboratory Investigation*. Nature Publishing Group, 97(1), pp. 4–13. doi: 10.1038/labinvest.2016.116.
Chovancova, P. *et al.* (2017) 'Reverse-transcription quantitative PCR directly from cells without RNA extraction and without isothermal reverse-transcription: A "zero-step" RT-qPCR protocol', *Biology Methods and Protocols*. Oxford University Press, 2(1). doi: 10.1093/biomethods/bpx008.
Chung, H. S. *et al.* (2019) 'Variability in Total Cholesterol Concentration Is Associated With the Risk of Dementia: A Nationwide Population-Based Cohort Study', *Frontiers in Neurology*. Frontiers Media S.A., 10(MAY), p. 441. doi: 10.3389/fneur.2019.00441.
Clement, A. B. *et al.* (2009) 'Adaptation of neuronal cells to chronic oxidative stress is associated with altered cholesterol and sphingolipid homeostasis and lysosomal function', *Journal of Neurochemistry*, 111(3), pp. 669–682. doi: 10.1111/j.1471-4159.2009.06360.x.
Cline, E. N. *et al.* (2018) 'The Amyloid-β Oligomer Hypothesis: Beginning of the Third Decade', *Journal of Alzheimer's Disease*. IOS Press, pp. S567–S610. doi: 10.3233/JAD-179941.
Colonna, M. (2003) 'Trems in the immune system and beyond', *Nature Reviews Immunology*. Nature Publishing Group, pp. 445–453. doi: 10.1038/nri1106.
Colonna, M. and Wang, Y. (2016) *TREM2 variants: new keys to decipher Alzheimer disease pathogenesis*. doi: 10.1038/nrn.2016.7.
Condello, C. *et al.* (2015) 'Microglia constitute a barrier that prevents neurotoxic protofibrillar Aβ42 hotspots around plaques', *Nature Communications*. Nature Publishing Group, 6, p. 6176. doi: 10.1038/ncomms7176.

Coppede, F. and Migliore, L. (2009) ‘DNA Damage and Repair in Alzheimers Disease’, *Current Alzheimer Research*, 6(1), pp. 36–47. doi: 10.2174/156720509787313970.
Cordy, J. M. *et al.* (2003) ‘Exclusively targeting β-secretase to lipid rafts by GPI-anchor addition up-regulates β-site processing of the amyloid precursor protein’, *Proceedings of the National Academy of Sciences of the United States of America*, 100(20), pp. 11735–11740. doi: 10.1073/pnas.1635130100.
Coric, V. *et al.* (2015) ‘Targeting Prodromal Alzheimer Disease With Avagacestat’, *JAMA Neurology*. American Medical Association, 72(11), p. 1324. doi: 10.1001/jamaneurol.2015.0607.
Cruts, M., Theuns, J. and Van Broeckhoven, C. (2012) ‘Locus-specific mutation databases for neurodegenerative brain diseases’, *Human Mutation*. Wiley Subscription Services, Inc., A Wiley Company, 33(9), pp. 1340–1344. doi: 10.1002/humu.22117.
Daneschvar, H. L., Aronson, M. D. and Smetana, G. W. (2015) ‘Do statins prevent Alzheimer’s disease? A narrative review ☆’, *European Journal of Internal Medicine*, 26(9), pp. 666–669. doi: 10.1016/j.ejim.2015.08.012.
Dawkins, E. and Small, D. H. (2014) ‘Insights into the physiological function of the β-amyloid precursor protein: Beyond Alzheimer’s disease’, *Journal of Neurochemistry*, 129(5), pp. 756–769. doi: 10.1111/jnc.12675.
Dean, M., Hamon, Y. and Chimini, G. (2001) ‘The human ATP-binding cassette (ABC) transporter superfamily’, *Journal of Lipid Research*. American Society for Biochemistry and Molecular Biology, pp. 1007–1017. doi: 10.1101/gr.184901.
DeBose-Boyd, R. A. (2008) ‘Feedback regulation of cholesterol synthesis: Sterol-accelerated ubiquitination and degradation of HMG CoA reductase’, *Cell Research*. NIH Public Access, 18(6), pp. 609–621. doi: 10.1038/cr.2008.61.
DeMattos, R. B. *et al.* (2001) ‘Peripheral anti-A beta antibody alters CNS and plasma A beta clearance and decreases brain A beta burden in a mouse model of Alzheimer’s disease.’, *Proceedings of the National Academy of Sciences of the United States of America*. National Academy of Sciences, 98(15), pp. 8850–8855. doi: 10.1073/pnas.151261398.
DeMattos, R. B. (2004) ‘Apolipoprotein E dose-dependent modulation of beta-amyloid deposition in a transgenic mouse model of Alzheimer’s disease.’, *Journal of molecular neuroscience : MN*, 23(3), pp. 255–62. doi: 10.1385/JMN:23:3:255.
Deming, Y. *et al.* (2016) *A potential endophenotype for Alzheimer’s disease: cerebrospinal fluid clusterin*, *Neurobiology of Aging*. doi: 10.1016/j.neurobiolaging.2015.09.009.
Deture, M. A. and Dickson, D. W. (2019) ‘The neuropathological diagnosis of Alzheimer’s disease’, *Molecular Neurodegeneration*. BioMed Central Ltd. doi: 10.1186/s13024-019-0333-5.
Dickson, D. W. *et al.* (2002) ‘Office of rare diseases neuropathologic criteria for corticobasal degeneration’, *Journal of Neuropathology and Experimental Neurology*. American Association of Neuropathologists Inc., 61(11), pp. 935–946. doi: 10.1093/jnen/61.11.935.
Dickson, D. W. (2006) ‘Pick’s Disease: A Modern Approach’, *Brain Pathology*. Blackwell Publishing Ltd, 8(2), pp. 339–354. doi: 10.1111/j.1750-3639.1998.tb00158.x.
Dickson, D. W., Rademakers, R. and Hutton, M. L. (2007) ‘Progressive supranuclear palsy: Pathology and genetics’, in *Brain Pathology*. John Wiley & Sons, Ltd, pp. 74–82. doi: 10.1111/j.1750-3639.2007.00054.x.

Dietschy, J. M. (2009) ‘Central nervous system: Cholesterol turnover, brain development and neurodegeneration’, *Biological Chemistry*. NIH Public Access, pp. 287–293. doi: 10.1515/BC.2009.035.
Dixit, R. *et al.* (2008) ‘Differential Regulation of Dynein and Kinesin Motor Proteins by Tau’, *Science*, 319(5866).
Do, T. M. *et al.* (2015) ‘Age-dependent regulation of the blood-brain barrier influx/efflux equilibrium of amyloid-β peptide in a mouse model of Alzheimer’s disease (3xTg-AD)’, *Journal of Alzheimer’s Disease*. IOS Press, 49(2), pp. 287–300. doi: 10.3233/JAD-150350.
Doody, R. S. *et al.* (2013) ‘A phase 3 trial of semagacestat for treatment of Alzheimer’s disease’, *New England Journal of Medicine*, 369(4), pp. 341–350. doi: 10.1056/NEJMoa1210951.
Doody, R. S. *et al.* (2014) ‘Phase 3 trials of solanezumab for mild-to-moderate Alzheimer’s disease.’, *The New England journal of medicine*, 370(4), pp. 311–21. doi: 10.1056/NEJMoa1312889.
Dubrac, S. *et al.* (2005) ‘Role of CYP27A in cholesterol and bile acid metabolism’, *Journal of Lipid Research*. American Society for Biochemistry and Molecular Biology, 46(1), pp. 76–85. doi: 10.1194/jlr.M400219-JLR200.
Eckert, G. P. *et al.* (2009) ‘Regulation of the brain isoprenoids farnesyl- and geranylgeranylpyrophosphate is altered in male Alzheimer patients’, *Neurobiology of disease*, 35(2), pp. 251–257. Available at: https://www.sciencedirect.com/science/article/pii/S0969996109001028?via%3Dihub (Accessed: 20 December 2019).
Edlund, C., Söderberg, M. and Kristensson, K. (1994) ‘Isoprenoids in aging and neurodegeneration’, *Neurochemistry International*. Pergamon, 25(1), pp. 35–38. doi: 10.1016/0197-0186(94)90050-7.
Engel, K. B. and Moore, H. M. (2011) ‘Effects of preanalytical variables on the detection of proteins by immunohistochemistry in formalin-fixed, paraffin-embedded tissue’, *Archives of Pathology and Laboratory Medicine*, 135(5), pp. 537–543. doi: 10.1043/2010-0702-RAIR.1.
Erharter, A. *et al.* (2019) ‘Take the shortcut – direct conversion of somatic cells into induced neural stem cells and their biomedical applications’, *FEBS Letters*. Wiley Blackwell, pp. 3353–3369. doi: 10.1002/1873-3468.13656.
Fadul, M. M. *et al.* (2020) ‘NDRG2 Expression Correlates with Neurofibrillary Tangles and Microglial Pathology in the Ageing Brain’, *International Journal of Molecular Sciences*, 21(1), p. 340. doi: 10.3390/ijms21010340.
Famer, D. *et al.* (2007) ‘Regulation of α- and β-secretase activity by oxysterols: Cerebrosterol stimulates processing of APP via the α-secretase pathway’, *Biochemical and Biophysical Research Communications*, 359(1), pp. 46–50. doi: 10.1016/j.bbrc.2007.05.033.
Families Author, O. *et al.* (1993) ‘Gene Dose of Apolipoprotein E Type 4 Allele and the Risk of Alzheimer’s Disease in Late’, *Source: Science, New Series*, 261(13), pp. 921–923. Available at: http://www.jstor.org/stable/2882127 (Accessed: 8 December 2016).
Fassbender, K. *et al.* (2002) ‘Effects of statins on human cerebral cholesterol metabolism and secretion of Alzheimer amyloid peptide.’, *Neurology*, 59(8), pp. 1257–1258. doi: 10.1212/WNL.59.8.1257.
Ferris, H. A. *et al.* (2017) ‘Loss of astrocyte cholesterol synthesis disrupts neuronal function and alters whole-body metabolism’, *Proceedings of the National Academy of Sciences of the United States of America*. National Academy of Sciences, 114(5),

pp. 1189–1194. doi: 10.1073/pnas.1620506114.
Fester, L. *et al.* (2009) ‘Cholesterol-promoted synaptogenesis requires the conversion of cholesterol to estradiol in the hippocampus’, *Hippocampus*, 19(8), pp. 692–705. doi: 10.1002/hipo.20548.
Fillenbaum, G. G. *et al.* (2008) ‘Consortium to Establish a Registry for Alzheimer’s Disease (CERAD): The first twenty years’, *Alzheimer’s and Dementia*, pp. 96–109. doi: 10.1016/j.jalz.2007.08.005.
Finger, E. C. (2016) ‘Frontotemporal dementias’, *CONTINUUM Lifelong Learning in Neurology*. Lippincott Williams and Wilkins, pp. 464–489. doi: 10.1212/CON.0000000000000300.
Flügge, G. *et al.* (2014) ‘NDRG2 as a marker protein for brain astrocytes’, *Cell and Tissue Research*. Springer Verlag, 357(1), pp. 31–41. doi: 10.1007/s00441-014-1837-5.
Fünfschilling, U. *et al.* (2007) ‘Survival of adult neurons lacking cholesterol synthesis in vivo’, *BMC Neuroscience*, 8(1), p. 1. doi: 10.1186/1471-2202-8-1.
Fünfschilling, U. *et al.* (2012) ‘Critical time window of neuronal cholesterol synthesis during neurite outgrowth’, *Journal of Neuroscience*, 32(22), pp. 7632–7645. doi: 10.1523/JNEUROSCI.1352-11.2012.
Furgerson, M. *et al.* (2014) ‘Hirano body expression impairs spatial working memory in a novel mouse model’, *Acta Neuropathologica Communications*. BioMed Central Ltd. doi: 10.1186/s40478-014-0131-9.
Gabuzda, D. *et al.* (1994) ‘Inhibition of energy metabolism alters the processing of amyloid precursor protein and induces a potentially amyloidogenic derivative.’, *The Journal of biological chemistry*, 269(18), pp. 13623–8. Available at: http://www.ncbi.nlm.nih.gov/pubmed/8175797 (Accessed: 4 January 2017).
Gale, S. A., Acar, D. and Daffner, K. R. (2018) ‘Dementia’, *American Journal of Medicine*, 131(10), pp. 1161–1169. doi: 10.1016/j.amjmed.2018.01.022.
Galvão, F. *et al.* (2019) ‘The amyloid precursor protein (APP) processing as a biological link between Alzheimer’s disease and cancer’, *Ageing Research Reviews*. Elsevier Ireland Ltd, pp. 83–91. doi: 10.1016/j.arr.2018.11.007.
Gamba, P. *et al.* (2015) ‘Oxidized cholesterol as the driving force behind the development of Alzheimer’s disease’, *Frontiers in Aging Neuroscience*, 7(JUN), pp. 1–21. doi: 10.3389/fnagi.2015.00119.
Genaro-Mattos, T. C. *et al.* (2019a) ‘Cholesterol Biosynthesis and Uptake in Developing Neurons’, *ACS Chemical Neuroscience*, 10(8), pp. 3671–3681. doi: 10.1021/acschemneuro.9b00248.
Genaro-Mattos, T. C. *et al.* (2019b) ‘Cholesterol Biosynthesis and Uptake in Developing Neurons’, *ACS Chemical Neuroscience*, 10(8), pp. 3671–3681. doi: 10.1021/acschemneuro.9b00248.
Gendreau, K. L. and Hall, G. F. (2013) ‘Tangles, Toxicity, and Tau Secretion in AD – New Approaches to a Vexing Problem’, *Frontiers in Neurology*. Frontiers, 4, p. 160. doi: 10.3389/fneur.2013.00160.
Gibson, P. H. and Tomlinson, B. E. (1977) ‘Numbers of Hirano bodies in the hippocampus of normal and demented people with Alzheimer’s disease’, *Journal of the Neurological Sciences*. J Neurol Sci, 33(1–2), pp. 199–206. doi: 10.1016/0022-510X(77)90193-9.
Giri, M., Zhang, M. and Lü, Y. (2016) ‘Genes associated with Alzheimer’s disease: an overview and current status.’, *Clinical interventions in aging*. Dove Press, 11, pp. 665–81. doi: 10.2147/CIA.S105769.
Glöckner, F. and Ohm, T. G. (2014) ‘Tau pathology induces intraneuronal cholesterol

accumulation', *Journal of Neuropathology and Experimental Neurology*. Lippincott Williams and Wilkins, 73(9), pp. 846–854. doi: 10.1097/NEN.0000000000000103.
Goldstein, J. L., DeBose-Boyd, R. A. and Brown, M. S. (2006) 'Protein sensors for membrane sterols', *Cell*. Elsevier, pp. 35–46. doi: 10.1016/j.cell.2005.12.022.
Goldstein, J. L., Rawson, R. B. and Brown, M. S. (2002) 'Mutant mammalian cells as tools to delineate the sterol regulatory element-binding protein pathway for feedback regulation of lipid synthesis', *Archives of Biochemistry and Biophysics*. Academic Press Inc., 397(2), pp. 139–148. doi: 10.1006/abbi.2001.2615.
Gong, J.-S. *et al.* (2002) 'Apolipoprotein E (ApoE) isoform-dependent lipid release from astrocytes prepared from human ApoE3 and ApoE4 knock-in mice.', *The Journal of biological chemistry*, 277(33), pp. 29919–26. doi: 10.1074/jbc.M203934200.
Gong, J. S. *et al.* (2002) 'Amyloid β-protein affects cholesterol metabolism in cultured neurons: Implications for pivotal role of cholesterol in the amyloid cascade', *Journal of Neuroscience Research*, 70(3), pp. 438–446. doi: 10.1002/jnr.10347.
Goritz, C., Mauch, D. H. and Pfrieger, F. W. (2005) 'Multiple mechanisms mediate cholesterol-induced synaptogenesis in a CNS neuron', *Molecular and Cellular Neuroscience*, 29(2), pp. 190–201. doi: 10.1016/j.mcn.2005.02.006.
Govek, E. E., Newey, S. E. and Van Aelst, L. (2005) 'The role of the Rho GTPases in neuronal development', *Genes and Development*. Cold Spring Harbor Laboratory Press, pp. 1–49. doi: 10.1101/gad.1256405.
Greeve, I. *et al.* (2000) 'The human DIMINUTO/DWARF1 homolog seladin-1 confers resistance to Alzheimer's disease-associated neurodegeneration and oxidative stress.', *The Journal of neuroscience : the official journal of the Society for Neuroscience*, 20(19), pp. 7345–52. Available at: http://www.ncbi.nlm.nih.gov/pubmed/11007892 (Accessed: 5 January 2017).
Grimm, M. O. W., Rothhaar, T. L. and Hartmann, T. (2012) 'The role of APP proteolytic processing in lipid metabolism', *Experimental Brain Research*, pp. 365–375. doi: 10.1007/s00221-011-2975-6.
Guerreiro, R. *et al.* (2013) 'TREM2 Variants in Alzheimer's Disease ', *New England Journal of Medicine*. New England Journal of Medicine (NEJM/MMS), 368(2), pp. 117–127. doi: 10.1056/nejmoa1211851.
Gusel'nikova, V. V. and Korzhevskiy, D. E. (2015) 'NeuN as a neuronal nuclear antigen and neuron differentiation marker', *Acta Naturae*, 7(2), pp. 42–47. doi: 10.32607/20758251-2015-7-2-42-47.
Gyure, K. A. *et al.* (2001) *Intraneuronal A-Amyloid Precedes Development of Amyloid Plaques in Down Syndrome*, *Arch Pathol Lab Med*. Allen Press. doi: 10.1043/0003-9985(2001)125<0489:IAAPDO>2.0.CO;2.
Haass, C. *et al.* (2012) 'Trafficking and Proteolytic Processing of APP', *Cold Spring Harbor perspectives in medicine*. Cold Spring Harbor Laboratory Press, 2(5), p. a006270. doi: 10.1101/cshperspect.a006270.
Halliday, M. R. *et al.* (2016) 'Accelerated pericyte degeneration and blood-brain barrier breakdown in apolipoprotein E4 carriers with Alzheimer's disease', *Journal of Cerebral Blood Flow and Metabolism*. Nature Publishing Group, 36(1), pp. 216–227. doi: 10.1038/jcbfm.2015.44.
Halliwell, B. and Cross, C. E. (1994) 'Oxygen-derived species: their relation to human disease and environmental stress.', *Environmental Health Perspectives*. National Institute of Environmental Health Sciences, 102(suppl 10), pp. 5–12. doi: 10.1289/ehp.94102s105.
Hänggi, J. *et al.* (2011) 'A CYP46 T/C SNP modulates parahippocampal and

hippocampal morphology in young subjects', *Neurobiology of Aging*, 32(6), pp. 1023–1032. doi: 10.1016/j.neurobiolaging.2009.07.001.
Hansson Petersen, C. A. *et al.* (2008) 'The amyloid β-peptide is imported into mitochondria via the TOM import machinery and localized to mitochondrial cristae', *Proceedings of the National Academy of Sciences of the United States of America*. National Academy of Sciences, 105(35), pp. 13145–13150. doi: 10.1073/pnas.0806192105.
Harada, A. *et al.* (2002) 'MAP2 is required for dendrite elongation, PKA anchoring in dendrites, and proper PKA signal transduction', *Journal of Cell Biology*. The Rockefeller University Press, 158(3), pp. 541–549. doi: 10.1083/jcb.200110134.
Hardy, J. A. and Higgins, G. A. (1992) 'Alzheimer's disease: the amyloid cascade hypothesis.', *Science (New York, N.Y.)*, 256(5054), pp. 184–5. doi: 10.1126/science.1566067.
Harman, D. (1981) 'The aging process.', *Proceedings of the National Academy of Sciences of the United States of America*, 78(11), pp. 7124–8. Available at: http://www.ncbi.nlm.nih.gov/pubmed/6947277 (Accessed: 5 January 2017).
Harrison, P. J. *et al.* (1991) 'Terminal coma affects messenger RNA detection in post mortem human temporal cortex', *Molecular Brain Research*, 9, pp. 161–164. Available at: http://ac.els-cdn.com/0169328X9190143L/1-s2.0-0169328X9190143L-main.pdf?%7B_%7Dtid=dfab3580-6ae8-11e7-9cdb-00000aacb361%7B&%7Dacdnat=1500293587%7B_%7Dfe5944b11fee74d9e3a2b0e9d8818da3 (Accessed: 17 July 2017).
Hatters, D. M. *et al.* (2006) 'Amino-terminal Domain Stability Mediates Apolipoprotein E Aggregation into Neurotoxic Fibrils', *Journal of Molecular Biology*. Academic Press, 361(5), pp. 932–944. doi: 10.1016/j.jmb.2006.06.080.
Hayashi, H. (2011) 'Lipid Metabolism and Glial Lipoproteins in the Central Nervous System', *Biological & Pharmaceutical Bulletin*. The Pharmaceutical Society of Japan, 34(4), pp. 453–461. doi: 10.1248/bpb.34.453.
Hayden, E. Y. and Teplow, D. B. (2013) 'Amyloid β-protein oligomers and Alzheimer's disease', *Alzheimer's Research and Therapy*. BioMed Central, p. 60. doi: 10.1186/alzrt226.
He, X. *et al.* (2006) 'Lovastatin modulates increased cholesterol and oxysterol levels and has a neuroprotective effect on rat hippocampal neurons after kainate injury', *Journal of Neuropathology and Experimental Neurology*. Oxford Academic, 65(7), pp. 652–663. doi: 10.1097/01.jnen.0000225906.82428.69.
Head, E. *et al.* (2018) 'Down syndrome, beta-amyloid and neuroimaging', *Free Radical Biology and Medicine*. Elsevier Inc., pp. 102–109. doi: 10.1016/j.freeradbiomed.2017.09.013.
Hebert, L. E. *et al.* (2013) 'Alzheimer disease in the United States (2010-2050) estimated using the 2010 census', *Neurology*. American Academy of Neurology, 80(19), pp. 1778–1783. doi: 10.1212/WNL.0b013e31828726f5.
Hendrickx, D. A. E. *et al.* (2017) 'Staining of HLA-DR, Iba1 and CD68 in human microglia reveals partially overlapping expression depending on cellular morphology and pathology', *Journal of Neuroimmunology*. Elsevier B.V., 309, pp. 12–22. doi: 10.1016/j.jneuroim.2017.04.007.
Heneka, M. T. *et al.* (2015) 'Neuroinflammation in Alzheimer's disease', *The Lancet Neurology*. Lancet Publishing Group, pp. 388–405. doi: 10.1016/S1474-4422(15)70016-5.
Hensley, K. *et al.* (1994) 'A model for β-amyloid aggregation and neurotoxicity based on free radical generation by the peptide: Relevance to Alzheimer disease',

Proceedings of the National Academy of Sciences of the United States of America. National Academy of Sciences, 91(8), pp. 3270–3274. doi: 10.1073/pnas.91.8.3270.
Herrup, K. (2015) 'The case for rejecting the amyloid cascade hypothesis', *Nature Neuroscience*. Nature Research, 18(6), pp. 794–799. doi: 10.1038/nn.4017.
Herz, J. and Bock, H. H. (2002) 'Lipoprotein Receptors in the Nervous System', *Annual Review of Biochemistry*. Annual Reviews, 71(1), pp. 405–434. doi: 10.1146/annurev.biochem.71.110601.135342.
Heverin, M. *et al.* (2004) 'Changes in the levels of cerebral and extracerebral sterols in the brain of patients with Alzheimer's disease.', *Journal of lipid research*, 45(1), pp. 186–93. doi: 10.1194/jlr.M300320-JLR200.
Heverin, M. *et al.* (2005) 'Crossing the barrier: Net flux of 27-hydroxycholesterol into the human brain', *Journal of Lipid Research*. American Society for Biochemistry and Molecular Biology, 46(5), pp. 1047–1052. doi: 10.1194/jlr.M500024-JLR200.
Hirano, A. (1994) 'Hirano bodies and related neuronal inclusions', *Neuropathology and Applied Neurobiology*. Blackwell Publishing Ltd, pp. 3–11. doi: 10.1111/j.1365-2990.1994.tb00951.x.
Hirsch-Reinshagen, V. *et al.* (2004) 'Deficiency of ABCA1 impairs apolipoprotein E metabolism in brain', *Journal of Biological Chemistry*. American Society for Biochemistry and Molecular Biology, 279(39), pp. 41197–41207. doi: 10.1074/jbc.M407962200.
Holmes, C. *et al.* (2008) 'Long-term eff ects of Aβ 42 immunisation in Alzheimer's disease: follow-up of a randomised, placebo-controlled phase I trial', *Articles 216 www.thelancet.com*.
Holmström, K. M. and Finkel, T. (2014) 'Cellular mechanisms and physiological consequences of redox-dependent signalling', *Nature Reviews Molecular Cell Biology*. Nature Publishing Group, pp. 411–421. doi: 10.1038/nrm3801.
Holton, P. *et al.* (2013) 'Initial Assessment of the Pathogenic Mechanisms of the recently identified Alzheimer Risk Loci', *Ann Hum Genet*, 77(2), pp. 85–105. doi: 10.1111/ahg.12000.
Hooff, G. P. *et al.* (2008) 'Isoprenoid quantitation in human brain tissue: A validated HPLC-fluorescence detection method for endogenous farnesyl- (FPP) and geranylgeranylpyrophosphate (GGPP)', *Analytical and Bioanalytical Chemistry*. Europe PMC Funders, 392(4), pp. 673–680. doi: 10.1007/s00216-008-2306-3.
Hooff, G. P. *et al.* (2010) 'Isoprenoids, small GTPases and Alzheimer's disease', *Biochimica et Biophysica Acta - Molecular and Cell Biology of Lipids*. Elsevier, 1801(8), pp. 896–905. doi: 10.1016/j.bbalip.2010.03.014.
Hooff, G. P. *et al.* (2012) 'Brain isoprenoids farnesyl pyrophosphate and geranylgeranyl pyrophosphate are increased in aged mice', *Molecular Neurobiology*. Humana Press Inc., 46(1), pp. 179–185. doi: 10.1007/s12035-012-8285-6.
Hoover, B. R. *et al.* (2010) 'Tau Mislocalization to Dendritic Spines Mediates Synaptic Dysfunction Independently of Neurodegeneration', *Neuron*. Neuron, 68(6), pp. 1067–1081. doi: 10.1016/j.neuron.2010.11.030.
Horton, J. D. *et al.* (2003) 'Combined analysis of oligonucleotide microarray data from transgenic and knockout mice identifies direct SREBP target genes', *Proceedings of the National Academy of Sciences of the United States of America*, 100(21), pp. 12027–12032. doi: 10.1073/pnas.1534923100.
Horton, J. D., Goldstein, J. L. and Brown, M. S. (2002) 'SREBPs', *Most*, 109(9), pp. 1125–1131. doi: 10.1172/JCI200215593.Lipid.
Hoshimaru, M. *et al.* (1996) 'Differentiation of the immortalized adult neuronal progenitor cell line HC2S2 into neurons by regulatable suppression of the v-myc

oncogene', *Proceedings of the National Academy of Sciences of the United States of America*. National Academy of Sciences, 93(4), pp. 1518–1523. doi: 10.1073/pnas.93.4.1518.
Hou, X. *et al.* (2018) 'Age- and disease-dependent increase of the mitophagy marker phospho-ubiquitin in normal aging and Lewy body disease', *Autophagy*. Taylor and Francis Inc., 14(8), pp. 1404–1418. doi: 10.1080/15548627.2018.1461294.
Hua, X. *et al.* (1995) 'Hairpin orientation of sterol regulatory element-binding protein-2 in cell membranes as determined by protease protection', *Journal of Biological Chemistry*, 270(49), pp. 29422–29427. doi: 10.1074/jbc.270.49.29422.
Hua, Xianxin *et al.* (1995) 'Structure of the human gene encoding sterol regulatory element binding protein-1 (SREBF1) and localization of SREBF1 and SREBF2 to chromosomes 17p11.2 and 22q13', *Genomics*, 25(3), pp. 667–673. doi: 10.1016/0888-7543(95)80009-B.
Huefner, A. *et al.* (2013) 'Intracellular SERS nanoprobes for distinction of different neuronal cell types', *Nano Letters*. American Chemical Society, 13(6), pp. 2463–2470. doi: 10.1021/nl400448n.
Hughes, T. M. *et al.* (2013) 'Brain cholesterol metabolism, oxysterols, and dementia.', *Journal of Alzheimer's disease : JAD*. NIH Public Access, 33(4), pp. 891–911. doi: 10.3233/JAD-2012-121585.
Hussain, I. *et al.* (2000) 'Asp1 (BACE2) cleaves the amyloid precursor protein at the β-secretase site', *Molecular and Cellular Neuroscience*. Academic Press Inc., 16(5), pp. 609–619. doi: 10.1006/mcne.2000.0884.
Hwang, S. *et al.* (2016) 'Contribution of accelerated degradation to feedback regulation of 3-hydroxy-3-methylglutaryl coenzyme A reductase and cholesterol metabolism in the liver', *Journal of Biological Chemistry*. American Society for Biochemistry and Molecular Biology Inc., 291(26), pp. 13479–13494. doi: 10.1074/jbc.M116.728469.
Iadanza, M. G. *et al.* (2018) 'A new era for understanding amyloid structures and disease', *Nature Reviews Molecular Cell Biology*. Springer US, 19(12), pp. 755–773. doi: 10.1038/s41580-018-0060-8.
Iijima-Ando, K. *et al.* (2009) 'Mitochondrial mislocalization underlies aβ42-induced neuronal dysfunction in a drosophila model of alzheimer's disease', *PLoS ONE*. Public Library of Science, 4(12), p. 8310. doi: 10.1371/journal.pone.0008310.
Ince, P. G. (2001) 'Pathological correlates of late-onset dementia in a multicentre, community-based population in England and Wales', *Lancet*, 357(9251), pp. 169–175. doi: 10.1016/S0140-6736(00)03589-3.
Ingelsson, M. *et al.* (2004) 'Lack of association of the cholesterol 24-hydroxylase (CYP46) intron 2 polymorphism with Alzheimer's disease', *Neuroscience Letters*, 367(2), pp. 228–231. doi: 10.1016/j.neulet.2004.06.011.
Iqbal, K. *et al.* (2009) 'Mechanisms of tau-induced neurodegeneration', *Acta Neuropathologica*. Springer-Verlag, 118(1), pp. 53–69. doi: 10.1007/s00401-009-0486-3.
Irina Vázquez-Villaseñor (2018) 'An in vivo and in vitro study of stress-induced senescence in neurones and its role in neurodegeneration', p. 321. Available at: https://pdfs.semanticscholar.org/d668/ff43c7fbfba6f9c49fca594c37fefb15f3fd.pdf.
Istvan, E. S. and Deisenhofer, J. (2000) 'The structure of the catalytic portion of human HMG-CoA reductase', *Biochimica et Biophysica Acta - Molecular and Cell Biology of Lipids*. Elsevier, pp. 9–18. doi: 10.1016/S1388-1981(00)00134-7.
Ito, J. I. *et al.* (2013) 'Enhancement of FGF-1 release along with cytosolic proteins from rat astrocytes by hydrogen peroxide', *Brain Research*. Elsevier, 1522, pp. 12–

21. doi: 10.1016/j.brainres.2013.05.035.
Ito, J. I. *et al.* (2015) 'Biochemical properties in membrane of rat astrocytes under oxidative stress', *Brain Research*. Elsevier B.V., 1615, pp. 1–11. doi: 10.1016/j.brainres.2015.04.008.
Jiang, C. H. *et al.* (2001) 'The effects of aging on gene expression in the hypothalamus and cortex of mice.', *Proceedings of the National Academy of Sciences of the United States of America*. National Academy of Sciences, 98(4), pp. 1930–4. doi: 10.1073/pnas.98.4.1930.
Johnson, J. M. *et al.* (2003) 'Genome-Wide Survey of Human Alternative Pre-mRNA Splicing with Exon Junction Microarrays', *Science*. Science, 302(5653), pp. 2141–2144. doi: 10.1126/science.1090100.
Jones, S. E. and Jomary, C. (2002) 'Clusterin', *The International Journal of Biochemistry & Cell Biology*, 34(5), pp. 427–431. doi: 10.1016/S1357-2725(01)00155-8.
Jonsson, T. *et al.* (2012) 'A mutation in APP protects against Alzheimer's disease and age-related cognitive decline', *Nature*, 488(7409), p. 96. doi: 10.1038/nature11283.
Jonsson, T. *et al.* (2013) ' Variant of TREM2 Associated with the Risk of Alzheimer's Disease ', *New England Journal of Medicine*. New England Journal of Medicine (NEJM/MMS), 368(2), pp. 107–116. doi: 10.1056/nejmoa1211103.
Joseph, A. and Gnanapragasam, V. J. (2011) 'Laser-capture microdissection and transcriptional profiling in archival FFPE tissue in prostate cancer', *Methods in Molecular Biology*. Humana Press, 755, pp. 291–300. doi: 10.1007/978-1-61779-163-5_24.
van der Kant, R. *et al.* (2019) 'Cholesterol Metabolism Is a Druggable Axis that Independently Regulates Tau and Amyloid-β in iPSC-Derived Alzheimer's Disease Neurons', *Cell Stem Cell*. Elsevier, 24(3), pp. 363-375.e9. doi: 10.1016/j.stem.2018.12.013.
Karch, C. M. and Goate, A. M. (2015) 'Alzheimer's Disease Risk Genes and Mechanisms of Disease Pathogenesis', *Biological Psychiatry*, 77(1), pp. 43–51. doi: 10.1016/j.biopsych.2014.05.006.
Khan, S. S. and Bloom, G. S. (2016) 'Tau: The Center of a Signaling Nexus in Alzheimer's Disease', *Frontiers in Neuroscience*. Frontiers, 10, p. 31. doi: 10.3389/fnins.2016.00031.
Kim, J., Basak, J. M. and Holtzman, D. M. (2009) 'The Role of Apolipoprotein E in Alzheimer's Disease', *Neuron*, 63(3), pp. 287–303. doi: 10.1016/j.neuron.2009.06.026.
Kim, S. H. *et al.* (2001) 'Protein levels of human peroxiredoxin subtypes in brains of patients with Alzheimer's disease and Down Syndrome', *Journal of Neural Transmission, Supplement*. Springer Wien, (61), pp. 223–235. doi: 10.1007/978-3-7091-6262-0_18.
Kim, W. S. *et al.* (2010) 'Increased ATP-binding cassette transporter A1 expression in Alzheimer's disease hippocampal neurons', *Journal of Alzheimer's Disease*, 21(1), pp. 193–205. doi: 10.3233/JAD-2010-100324.
Kingsbury, A. E. *et al.* (1995) 'Tissue pH as an indicator of mRNA preservation in human post-mortem brain', *Molecular Brain Research*, 28, pp. 311–318. Available at: http://ac.els-cdn.com/0169328X94002195/1-s2.0-0169328X94002195-main.pdf?_tid=bc100eca-6ae8-11e7-95fa-00000aacb360&acdnat=1500293528_b77b2ec3a413a2dbb7ca86f28376b443 (Accessed: 17 July 2017).

Klenyaeva, A. N. *et al.* (2014) 'Development of mouse fibroblast cell line expressing human tau protein and evaluation of tau-dependent cytotoxity', *Biochemistry (Moscow) Supplement Series A: Membrane and Cell Biology*. Pleiades Publishing, 8(3), pp. 232–239. doi: 10.1134/S1990747814020111.
Koldamova, R., Staufenbiel, M. and Lefterov, I. (2005) 'Lack of ABCA1 considerably decreases brain ApoE level and increases amyloid deposition in APP23 mice', *Journal of Biological Chemistry*. American Society for Biochemistry and Molecular Biology, 280(52), pp. 43224–43235. doi: 10.1074/jbc.M504513200.
Kölsch, H. *et al.* (1999) 'The neurotoxic effect of 24-hydroxycholesterol on SH-SY5Y human neuroblastoma cells', *Brain Research*. Elsevier, 818(1), pp. 171–175. doi: 10.1016/S0006-8993(98)01274-8.
Kölsch, H. *et al.* (2001a) 'Neurotoxicity of 24-hydroxycholesterol, an important cholesterol elimination product of the brain, may be prevented by vitamin E and estradiol-17β', *Journal of Neural Transmission*. Springer-Verlag, 108(4), pp. 475–488. doi: 10.1007/s007020170068.
Kölsch, H. *et al.* (2001b) 'Neurotoxicity of 24-hydroxycholesterol, an important cholesterol elimination product of the brain, may be prevented by vitamin E and estradiol-17β', *Journal of Neural Transmission*. Springer, 108(4), pp. 475–488. doi: 10.1007/s007020170068.
Kölsch, H. *et al.* (2002) 'Polymorphism in the cholesterol 24S-hydroxylase gene is associated with Alzheimer's disease', *Molecular Psychiatry*. Nature Publishing Group, 7(8), pp. 899–902. doi: 10.1038/sj.mp.4001109.
van den Kommer, T. N. *et al.* (2012) 'The role of extracerebral cholesterol homeostasis and ApoE e4 in cognitive decline', *Neurobiology of Aging*. Elsevier Inc., 33(3), pp. 622.e17-622.e28. doi: 10.1016/j.neurobiolaging.2011.02.019.
Koschack, J. *et al.* (2009) 'Serum 24S-hydroxycholesterol and hippocampal size in middle-aged normal individuals', *Neurobiology of Aging*. Neurobiol Aging, 30(6), pp. 898–902. doi: 10.1016/j.neurobiolaging.2007.10.010.
Koss, D. J. *et al.* (2016) 'Soluble pre-fibrillar tau and β-amyloid species emerge in early human Alzheimer's disease and track disease progression and cognitive decline', *Acta Neuropathologica*. Springer Berlin Heidelberg, 132(6), pp. 875–895. doi: 10.1007/s00401-016-1632-3.
Kovacs, G. G. (2015) 'Invited review: Neuropathology of tauopathies: Principles and practice', *Neuropathology and Applied Neurobiology*, 41(1), pp. 3–23. doi: 10.1111/nan.12208.
Kranenburg, O. *et al.* (1995) 'Inhibition of cyclin-dependent kinase activity triggers neuronal differentiation of mouse neuroblastoma cells', *Journal of Cell Biology*, 131(1), pp. 227–234. doi: 10.1083/jcb.131.1.227.
Krantic, S. *et al.* (2005) 'Molecular basis of programmed cell death involved in neurodegeneration', *Trends in Neurosciences*. Elsevier Current Trends, pp. 670–676. doi: 10.1016/j.tins.2005.09.011.
Kreilaus, F. *et al.* (2015) 'Evidence for altered cholesterol metabolism in Huntington's disease post-mortem brain tissue', *Neuropathology and Applied Neurobiology*, p. n/a-n/a. doi: 10.1111/nan.12286.
Kukar, T. *et al.* (2005) *Diverse compounds mimic Alzheimer disease-causing mutations by augmenting Aβ42 production*, *NATURE MEDICINE*. Available at: http://www.nature.com/naturemedicine (Accessed: 26 December 2019).
Kumar, P., Nagarajan, A. and Uchil, P. D. (2018) 'Analysis of cell viability by the lactate dehydrogenase assay', *Cold Spring Harbor Protocols*, 2018(6), pp. 465–468. doi: 10.1101/pdb.prot095497.

Kumar, V. *et al.* (2019) 'Inhibition of human 3-hydroxy-3-methylglutaryl CoA reductase by peptides leading to cholesterol homeostasis through SREBP2 pathway in HepG2 cells', *Biochimica et Biophysica Acta (BBA) - Proteins and Proteomics*. Elsevier, 1867(6), pp. 604–615. doi: 10.1016/J.BBAPAP.2019.04.002.
Kuo, L. J. and Yang, L.-X. (2008) 'Phosphorylation of H2AX and its Related Molecules', *in vivo*, 22(3), pp. 305–310. Available at: http://iv.iiarjournals.org/content/22/3/305.full.pdf (Accessed: 4 November 2019).
Kwiatkowski, D. *et al.* (2016) 'Associations between DNA damage, DNA base excision repair gene variability and Alzheimer's disease risk', *Dementia and Geriatric Cognitive Disorders*, 41(3–4), pp. 152–171. doi: 10.1159/000443953.
Langlet, C. *et al.* (2000) 'Membrane rafts and signaling by the multichain immune recognition receptors.', *Current opinion in immunology*, 12(3), pp. 250–5. Available at: http://www.ncbi.nlm.nih.gov/pubmed/10781401 (Accessed: 3 January 2017).
Leduc, V. *et al.* (2015) 'HMGCR is a genetic modifier for risk, age of onset and MCI conversion to Alzheimer's disease in a three cohorts study', *Molecular Psychiatry*. Nature Publishing Group, 20(7), pp. 867–873. doi: 10.1038/mp.2014.81.
Leduc, V. *et al.* (2016) 'Effects of rs3846662 Variants on HMGCR mRNA and Protein Levels and on Markers of Alzheimer's Disease Pathology', *Journal of Molecular Neuroscience*. Springer New York LLC, 58(1), pp. 109–119. doi: 10.1007/s12031-015-0666-7.
Leoni, V. and Caccia, C. (2011) 'Oxysterols as biomarkers in neurodegenerative diseases', *Chemistry and Physics of Lipids*. Elsevier Ireland Ltd, 164(6), pp. 515–524. doi: 10.1016/j.chemphyslip.2011.04.002.
Licastro, F. *et al.* (2010) 'Multivariable network associated with cognitive decline and dementia', *Neurobiology of Aging*. Elsevier, 31(2), pp. 257–269. doi: 10.1016/j.neurobiolaging.2008.03.019.
Lipman, N. S. *et al.* (2005) 'Monoclonal Versus Polyclonal Antibodies: Distinguishing Characteristics, Applications, and Information Resources', *ILAR Journal*, 46(3), pp. 258–268. doi: 10.1093/ilar.46.3.258.
Lomnitski, L. *et al.* (1999) 'Antioxidant mechanisms in apolipoprotein E deficient mice prior to and following closed head injury.', *Biochimica et biophysica acta*, 1453(3), pp. 359–68. Available at: http://www.ncbi.nlm.nih.gov/pubmed/10101254 (Accessed: 5 January 2017).
López-Otín, C. *et al.* (2013) 'The Hallmarks of Aging', *Cell*, 153(6), pp. 1194–1217. doi: 10.1016/j.cell.2013.05.039.
Lotharius, J. *et al.* (2002) 'Effect of mutant alpha-synuclein on dopamine homeostasis in a new human mesencephalic cell line.', *The Journal of biological chemistry*. American Society for Biochemistry and Molecular Biology, 277(41), pp. 38884–94. doi: 10.1074/jbc.M205518200.
Lotharius, J. (2005) 'Progressive Degeneration of Human Mesencephalic Neuron-Derived Cells Triggered by Dopamine-Dependent Oxidative Stress Is Dependent on the Mixed-Lineage Kinase Pathway', *Journal of Neuroscience*. Society for Neuroscience, 25(27), pp. 6329–6342. doi: 10.1523/JNEUROSCI.1746-05.2005.
Lund, E G, Guileyardo, J. M. and Russell, D. W. (1999) 'cDNA cloning of cholesterol 24-hydroxylase, a mediator of cholesterol homeostasis in the brain.', *Proceedings of the National Academy of Sciences of the United States of America*. National Academy of Sciences, 96(13), pp. 7238–43. doi: 10.1073/PNAS.96.13.7238.
Lund, Erik G., Guileyardo, J. M. and Russell, D. W. (1999) 'cDNA cloning of cholesterol 24-hydroxylase, a mediator of cholesterol homeostasis in the brain', *Proceedings of the National Academy of Sciences of the United States of America*.

National Academy of Sciences, 96(13), pp. 7238–7243. doi: 10.1073/pnas.96.13.7238.
Lütjohann, D. *et al.* (1996a) 'Cholesterol homeostasis in human brain: Evidence for an age-dependent flux of 24S-hydroxycholesterol from the brain into the circulation', *Proceedings of the National Academy of Sciences of the United States of America*. National Academy of Sciences, 93(18), pp. 9799–9804. doi: 10.1073/pnas.93.18.9799.
Lütjohann, D. *et al.* (1996b) 'Cholesterol homeostasis in human brain: Evidence for an age-dependent flux of 24S-hydroxycholesterol from the brain into the circulation', *Proceedings of the National Academy of Sciences of the United States of America*. National Academy of Sciences, 93(18), pp. 9799–9804. doi: 10.1073/pnas.93.18.9799.
Lütjohann, D. *et al.* (2000) 'Plasma 24S-hydroxycholesterol (cerebrosterol) is increased in Alzheimer and vascular demented patients', *Journal of Lipid Research*. American Society for Biochemistry and Molecular Biology, 41(2), pp. 195–198.
Lütjohann, D. (2006) 'Cholesterol metabolism in the brain: Importance of 24S-hydroxylation', *Acta Neurologica Scandinavica*, 114(SUPPL. 185), pp. 33–42. doi: 10.1111/j.1600-0404.2006.00683.x.
Lyman, M. *et al.* (2014) 'Neuroinflammation: The role and consequences', *Neuroscience Research*. Elsevier, pp. 1–12. doi: 10.1016/j.neures.2013.10.004.
Lyras, L. *et al.* (1997) 'An assessment of oxidative damage to proteins, lipids, and DNA in brain from patients with Alzheimer's disease', *Journal of Neurochemistry*. Blackwell Publishing Ltd, 68(5), pp. 2061–2069. doi: 10.1046/j.1471-4159.1997.68052061.x.
Makrides, V. *et al.* (2003) 'Microtubule-dependent oligomerization of tau. Implications for physiological tau function and tauopathies.', *The Journal of biological chemistry*, 278(35), pp. 33298–304. doi: 10.1074/jbc.M305207200.
Malik, B. *et al.* (2012) 'Oligomeric amyloid-β peptide affects the expression of genes involved in steroid and lipid metabolism in primary neurons', *Neurochemistry International*. Pergamon, 61(3), pp. 321–333. doi: 10.1016/j.neuint.2012.05.006.
Maloney, J. A. *et al.* (2014) 'Molecular mechanisms of Alzheimer disease protection by the A673T allele of amyloid precursor protein.', *The Journal of biological chemistry*. American Society for Biochemistry and Molecular Biology, 289(45), pp. 30990–1000. doi: 10.1074/jbc.M114.589069.
Mano, T. *et al.* (2017) 'Neuron-specific methylome analysis reveals epigenetic regulation and tau-related dysfunction of BRCA1 in Alzheimer's disease', *Proceedings of the National Academy of Sciences of the United States of America*. National Academy of Sciences, 114(45), pp. E9645–E9654. doi: 10.1073/pnas.1707151114.
Marcil, V. *et al.* (2006) 'Oxidative stress influences cholesterol efflux in THP-1 macrophages: Role of ATP-binding cassette A1 and nuclear factors', *Cardiovascular Research*. Elsevier, 72(3), pp. 473–482. doi: 10.1016/j.cardiores.2006.08.024.
Maria Giudetti, A. *et al.* (2015) 'The Role of Brain Cholesterol and its Oxidized Products in Alzheimer's Disease', *Current Alzheimer Research*, 13(2), pp. 198–205. doi: 10.2174/1567205012666150921103426.
Martin, D. *et al.* (2017) 'Neurocytometry: Flow Cytometric Sorting of Specific Neuronal Populations from Human and Rodent Brain', *ACS Chemical Neuroscience*, 8(2), pp. 356–367. doi: 10.1021/acschemneuro.6b00374.
Martin, M., Dotti, C. G. and Dolores, M. (2010) 'Brain cholesterol in normal and pathological aging', *BBA - Molecular and Cell Biology of Lipids*. Elsevier B.V.,

1801(8), pp. 934–944. doi: 10.1016/j.bbalip.2010.03.011.
Mastrocola, R. *et al.* (2011) 'Dysregulation of SREBP2 induces BACE1 expression', *Neurobiology of Disease*. Academic Press, 44(1), pp. 116–124. doi: 10.1016/j.nbd.2011.06.010.
Matkowskyj, K. A. *et al.* (2003) 'Quantitative immunohistochemistry by measuring cumulative signal strength accurately measures receptor number.', *The journal of histochemistry and cytochemistry : official journal of the Histochemistry Society*, 51(2), pp. 205–14. doi: 10.1177/002215540305100209.
Matsuda, A. *et al.* (2013) '24(S)-hydroxycholesterol is actively eliminated from neuronal cells by ABCA1', *Journal of Neurochemistry*, 126(1), pp. 93–101. doi: 10.1111/jnc.12275.
Matthews, F. E. *et al.* (2009a) 'Epidemiological pathology of dementia: Attributable-risks at death in the medical research council cognitive function and ageing study', *PLoS Medicine*, 6(11). doi: 10.1371/journal.pmed.1000180.
Matthews, F. E. *et al.* (2009b) 'Epidemiological Pathology of Dementia: Attributable-Risks at Death in the Medical Research Council Cognitive Function and Ageing Study', *PLoS Medicine*. Edited by S. Gandy. Public Library of Science, 6(11), p. e1000180. doi: 10.1371/journal.pmed.1000180.
Mazein, A. *et al.* (2013) 'A comprehensive machine-readable view of the mammalian cholesterol biosynthesis pathway', *Biochemical Pharmacology*, 86(1), pp. 56–66. doi: 10.1016/j.bcp.2013.03.021.
McGuinness, B. *et al.* (2014) 'Statins for the treatment of dementia', in McGuinness, B. (ed.) *Cochrane Database of Systematic Reviews*. Chichester, UK: John Wiley {&} Sons, Ltd. doi: 10.1002/14651858.CD007514.pub3.
McLaurin, J. A. *et al.* (2000) 'Inositol stereoisomers stabilize an oligomeric aggregate of alzheimer amyloid β peptide and inhibit Aβ-induced toxicity', *Journal of Biological Chemistry*. American Society for Biochemistry and Molecular Biology, 275(24), pp. 18495–18502. doi: 10.1074/jbc.M906994199.
Medina, M., Hernández, F. and Avila, J. (2016) 'New features about tau function and dysfunction', *Biomolecules*. MDPI AG. doi: 10.3390/biom6020021.
Medina, M. W. and Krauss, R. M. (2009) 'The Role of HMGCR Alternative Splicing in Statin Efficacy', *Trends in Cardiovascular Medicine*. Elsevier, pp. 173–177. doi: 10.1016/j.tcm.2009.10.003.
Mendez, M. F. (2019) 'Early-onset Alzheimer disease and its variants', *CONTINUUM Lifelong Learning in Neurology*. Lippincott Williams and Wilkins, pp. 34–51. doi: 10.1212/CON.0000000000000687.
Mendoza-Oliva, A. *et al.* (2015) 'Lovastatin Differentially Affects Neuronal Cholesterol and Amyloid-β Production in vivo and in vitro', *CNS Neuroscience and Therapeutics*. Blackwell Publishing Ltd, 21(8), pp. 631–641. doi: 10.1111/cns.12420.
Metzger, R. E. *et al.* (1996) 'Neurons of the human frontal cortex display apolipoprotein E immunoreactivity: implications for Alzheimer's disease.', *Journal of neuropathology and experimental neurology*, 55(3), pp. 372–80. Available at: http://www.ncbi.nlm.nih.gov/pubmed/8786396 (Accessed: 10 July 2017).
Michel, D. *et al.* (1997) 'Stress-induced transcription of the clusterin/apoJ gene.', *The Biochemical journal*. Portland Press Ltd, (Pt 1), pp. 45–50. Available at: http://www.ncbi.nlm.nih.gov/pubmed/9359832 (Accessed: 21 December 2016).
Mitsche, M. A. *et al.* (2015) 'Flux analysis of cholesterol biosynthesis in vivo reveals multiple tissue and cell-type specific pathways.', *eLife*. eLife Sciences Publications, Ltd, 4, p. e07999. doi: 10.7554/eLife.07999.
Mohamed, A. *et al.* (2012) 'β-amyloid inhibits protein prenylation and induces

cholesterol sequestration by impairing SREBP-2 cleavage', *Journal of Neuroscience*. Society for Neuroscience, 32(19), pp. 6490–6500. doi: 10.1523/JNEUROSCI.0630-12.2012.
Mohamed, A. *et al.* (2018a) 'Aβ inhibits SREBP-2 activation through Akt inhibition', *Journal of Lipid Research*. American Society for Biochemistry and Molecular Biology Inc., pp. 1–13. doi: 10.1194/jlr.M076703.
Mohamed, A. *et al.* (2018b) 'Aβ inhibits SREBP-2 activation through Akt inhibition', *Journal of Lipid Research*. American Society for Biochemistry and Molecular Biology Inc., pp. 1–13. doi: 10.1194/jlr.M076703.
Monoranu, C. M. *et al.* (2009) 'PH measurement as quality control on human post mortem brain tissue: A study of the BrainNet Europe consortium', *Neuropathology and Applied Neurobiology*. Blackwell Publishing Ltd, 35(3), pp. 329–337. doi: 10.1111/j.1365-2990.2008.01003a.x.
Montagne, A. *et al.* (2015) 'Blood-Brain barrier breakdown in the aging human hippocampus', *Neuron*. Cell Press, 85(2), pp. 296–302. doi: 10.1016/j.neuron.2014.12.032.
Moreira, P. I. *et al.* (2005) 'Oxidative stress mechanisms and potential therapeutics in Alzheimer disease.', *Journal of neural transmission (Vienna, Austria : 1996)*, 112(7), pp. 921–32. doi: 10.1007/s00702-004-0242-8.
Moutinho, M., Nunes, M. J. and Rodrigues, E. (2017) 'The mevalonate pathway in neurons: It's not just about cholesterol', *Experimental Cell Research*, pp. 55–60. doi: 10.1016/j.yexcr.2017.02.034.
Müller, U. C. and Zheng, H. (2012) 'Physiological functions of APP family proteins', *Cold Spring Harbor Perspectives in Medicine*. Cold Spring Harbor Laboratory Press, 2(2), p. a006288. doi: 10.1101/cshperspect.a006288.
Myers, A. and McGonigle, P. (2019) 'Overview of Transgenic Mouse Models for Alzheimer's Disease', *Current Protocols in Neuroscience*. Blackwell Publishing Inc. doi: 10.1002/cpns.81.
Navarro, A. and Boveris, A. (2007) 'The mitochondrial energy transduction system and the aging process.', *American journal of physiology. Cell physiology*, 292(2), pp. C670-86. doi: 10.1152/ajpcell.00213.2006.
Nelson, T. J. and Alkon, D. L. (2005) 'Oxidation of cholesterol by amyloid precursor protein and β-amyloid peptide', *Journal of Biological Chemistry*. American Society for Biochemistry and Molecular Biology, 280(8), pp. 7377–7387. doi: 10.1074/jbc.M409071200.
Neufeld, E. B. *et al.* (2001) 'Cellular Localization and Trafficking of the Human ABCA1 Transporter', *Journal of Biological Chemistry*. American Society for Biochemistry and Molecular Biology, 276(29), pp. 27584–27590. doi: 10.1074/jbc.M103264200.
Neumann, H. (2001) 'Control of glial immune function by neurons', *Glia*, 36(2), pp. 191–199. doi: 10.1002/glia.1108.
Neymeyer, V., Tephly, T. R. and Miller, M. W. (1997) 'Folate and 10-formyltetrahydrofolate dehydrogenase (FDH) expression in the central nervous system of the mature rat', *Brain Research*. Elsevier, 766(1–2), pp. 195–204. doi: 10.1016/S0006-8993(97)00528-3.
Nieweg, K., Schaller, H. and Pfrieger, F. W. (2009) 'Marked differences in cholesterol synthesis between neurons and glial cells from postnatal rats', *Journal of Neurochemistry*. John Wiley & Sons, Ltd (10.1111), 109(1), pp. 125–134. doi: 10.1111/j.1471-4159.2009.05917.x.
Nikolaev, A. *et al.* (2009) 'APP binds DR6 to trigger axon pruning and neuron death

via distinct caspases', *Nature*. Nature Publishing Group, 457(7232), pp. 981–989. doi: 10.1038/nature07767.
Nishitsuji, K. *et al.* (2011) 'Apolipoprotein E regulates the integrity of tight junctions in an isoform-dependent manner in an in vitro blood-brain barrier model', *Journal of Biological Chemistry*. American Society for Biochemistry and Molecular Biology, 286(20), pp. 17536–17542. doi: 10.1074/jbc.M111.225532.
O'Brien, J. T. *et al.* (2003) 'Vascular cognitive impairment', *Lancet Neurology*, 2(2), pp. 89–98. doi: 10.1016/S1474-4422(03)00305-3.
Oberheim, N. A. *et al.* (2006) 'Astrocytic complexity distinguishes the human brain.', *Trends in neurosciences*. Elsevier, 29(10), pp. 547–53. doi: 10.1016/j.tins.2006.08.004.
Offe, K. *et al.* (2006) 'The lipoprotein receptor LR11 regulates amyloid beta production and amyloid precursor protein traffic in endosomal compartments.', *The Journal of neuroscience : the official journal of the Society for Neuroscience*. NIH Public Access, 26(5), pp. 1596–603. doi: 10.1523/JNEUROSCI.4946-05.2006.
Ogura, M. *et al.* (1998) 'RNA chip: Quality assessment of RNA by microchannel linear gel electrophoresis in injection-molded plastic chips', *Clinical Chemistry*, 44(11), pp. 2249–2255. Available at: http://clinchem.aaccjnls.org/content/clinchem/44/11/2249.full.pdf (Accessed: 17 July 2017).
Ohyama, Y. *et al.* (2006) 'Studies on the transcriptional regulation of cholesterol 24-hydroxylase (CYP46A1): marked insensitivity toward different regulatory axes.', *The Journal of biological chemistry*, 281(7), pp. 3810–20. doi: 10.1074/jbc.M505179200.
Overk, C. R. and Masliah, E. (2014) 'Pathogenesis of synaptic degeneration in Alzheimer's disease and Lewy body disease', *Biochemical Pharmacology*. Elsevier Inc., pp. 508–516. doi: 10.1016/j.bcp.2014.01.015.
Papassotiropoulos, A. *et al.* (2000) 'Plasma 24S-hydroxycholesterol: A peripheral indicator of neuronal degeneration and potential state marker for Alzheimer's disease', *NeuroReport*. Neuroreport, 11(9), pp. 1959–1961. doi: 10.1097/00001756-200006260-00030.
Papassotiropoulos, A. *et al.* (2003) 'Increased brain β-amyloid load, phosphorylated tau, and risk of Alzheimer disease associated with an intronic CYP46 polymorphism', *Archives of Neurology*. American Medical Association, 60(1), pp. 29–35. doi: 10.1001/archneur.60.1.29.
Pardridge, W. (2015) 'Targeted delivery of protein and gene medicines through the blood-brain barrier', *Clinical Pharmacology & Therapeutics*. John Wiley & Sons, Ltd, 97(4), pp. 347–361. doi: 10.1002/cpt.18.
Park, M. H. *et al.* (2012) 'Mutant presenilin 2 increases beta-secretase activity through reactive oxygen species-dependent activation of extracellular signal-regulated kinase', *Journal of neuropathology and experimental neurology*, 71(2), pp. 130–139. doi: 10.1097/NEN.0b013e3182432967.
Park, S. E. *et al.* (2011) 'Kaempferol acts through mitogen-activated protein kinases and protein kinase B/AKT to elicit protection in a model of neuroinflammation in BV2 microglial cells', *British Journal of Pharmacology*. Wiley-Blackwell, 164(3), pp. 1008–1025. doi: 10.1111/j.1476-5381.2011.01389.x.
Pataj, Z. *et al.* (2016) 'Quantification of oxysterols in human plasma and red blood cells by liquid chromatography high-resolution tandem mass spectrometry', *Journal of Chromatography A*. Elsevier B.V., 1439, pp. 82–88. doi: 10.1016/j.chroma.2015.11.015.
Perl, D. P. (2010) 'Neuropathology of Alzheimer's disease', *Mount Sinai Journal of*

Medicine. NIH Public Access, pp. 32–42. doi: 10.1002/msj.20157.
Pfrieger, F. W. (2003) 'Outsourcing in the brain: Do neurons depend on cholesterol delivery by astrocytes?', *BioEssays*, 25(1), pp. 72–78. doi: 10.1002/bies.10195.
Pfrieger, F. W. and Ungerer, N. (2011) 'Cholesterol metabolism in neurons and astrocytes', *Progress in Lipid Research*, 50(4), pp. 357–371. doi: 10.1016/j.plipres.2011.06.002.
Phillips, M. C. (2018) 'Is ABCA1 a lipid transfer protein?', *Journal of Lipid Research*. American Society for Biochemistry and Molecular Biology Inc., pp. 749–763. doi: 10.1194/jlr.R082313.
Pierrot, N. *et al.* (2013a) 'Amyloid precursor protein controls cholesterol turnover needed for neuronal activity', *EMBO Molecular Medicine*, 5(4), pp. 608–625. doi: 10.1002/emmm.201202215.
Pierrot, N. *et al.* (2013b) 'Amyloid precursor protein controls cholesterol turnover needed for neuronal activity', *EMBO Molecular Medicine*, 5(4), pp. 608–625. doi: 10.1002/emmm.201202215.
Piguet, O. *et al.* (2009) 'White matter loss in healthy ageing: A postmortem analysis', *Neurobiology of Aging*. Elsevier, 30(8), pp. 1288–1295. doi: 10.1016/j.neurobiolaging.2007.10.015.
Porcellini, E. *et al.* (2007) *The hydroxy-methyl-glutaryl CoA reductase promoter polymorphism is associated with Alzheimer's risk and cognitive deterioration*, *Neuroscience Letters*. doi: 10.1016/j.neulet.2007.01.046.
Prasher, V. P. *et al.* (1998) 'Molecular mapping of Alzheimer-type dementia in Down's syndrome.', *Annals of neurology*, 43(3), pp. 380–3. doi: 10.1002/ana.410430316.
Prieto, M. and Alonso, G. (1999) 'Differential sensitivity of cultured tanycytes and astrocytes to hydrogen peroxide toxicity', *Experimental Neurology*. Academic Press Inc., 155(1), pp. 118–127. doi: 10.1006/exnr.1998.6970.
Quan, G. *et al.* (2003) 'Ontogenesis and regulation of cholesterol metabolism in the central nervous system of the mouse', *Developmental Brain Research*. Elsevier, 146(1–2), pp. 87–98. doi: 10.1016/j.devbrainres.2003.09.015.
Raihan, O. *et al.* (2018) 'The Age-dependent Elevation of miR-335-3p Leads to Reduced Cholesterol and Impaired Memory in Brain', *Neuroscience*. Elsevier Ltd, 390, pp. 160–173. doi: 10.1016/j.neuroscience.2018.08.003.
Rao, X. *et al.* (2013) 'An improvement of the 2ˆ(-delta delta CT) method for quantitative real-time polymerase chain reaction data analysis.', *Biostatistics, bioinformatics and biomathematics*. NIH Public Access, 3(3), pp. 71–85. Available at: http://www.ncbi.nlm.nih.gov/pubmed/25558171 (Accessed: 15 March 2020).
Ratcliffe, L. E. *et al.* (2018) 'Loss of IGF1R in Human Astrocytes Alters Complex I Activity and Support for Neurons', *Neuroscience*. Elsevier Ltd, 390, pp. 46–59. doi: 10.1016/j.neuroscience.2018.07.029.
Raulin, A. C. *et al.* (2019) 'The Molecular Basis for Apolipoprotein E4 as the Major Risk Factor for Late-Onset Alzheimer's Disease', *Journal of Molecular Biology*. Academic Press, 431(12), pp. 2248–2265. doi: 10.1016/j.jmb.2019.04.019.
Rawat, V. *et al.* (2019) 'ApoE4 Alters ABCA1 Membrane Trafficking in Astrocytes', *The Journal of neuroscience : the official journal of the Society for Neuroscience*, 39(48), pp. 9611–9622. doi: 10.1523/JNEUROSCI.1400-19.2019.
Ray, P. D., Huang, B. W. and Tsuji, Y. (2012) 'Reactive oxygen species (ROS) homeostasis and redox regulation in cellular signaling', *Cellular Signalling*. NIH Public Access, pp. 981–990. doi: 10.1016/j.cellsig.2012.01.008.
Recuero, M. *et al.* (2009) 'A free radical-generating system induces the cholesterol

biosynthesis pathway: A role in Alzheimer's disease', *Aging Cell*, 8(2), pp. 128–139. doi: 10.1111/j.1474-9726.2009.00457.x.
Refolo, L. M. *et al.* (2001) 'A cholesterol-lowering drug reduces beta-amyloid pathology in a transgenic mouse model of Alzheimer's disease.', *Neurobiology of disease*, 8(5), pp. 890–9. doi: 10.1006/nbdi.2001.0422.
Replogle, J. M. *et al.* (2015) 'A TREM1 variant alters the accumulation of alzheimer-related amyloid pathology', *Annals of Neurology*. John Wiley and Sons Inc., 77(3), pp. 469–477. doi: 10.1002/ana.24337.
Roher, A. E. *et al.* (2017) 'APP/Aβ structural diversity and Alzheimer's disease pathogenesis', *Neurochemistry International*. Elsevier Ltd, pp. 1–13. doi: 10.1016/j.neuint.2017.08.007.
Rosenthal, S. L. and Kamboh, M. I. (2014) 'Late-Onset Alzheimer's Disease Genes and the Potentially Implicated Pathways.', *Current genetic medicine reports*. Springer, 2(2), pp. 85–101. doi: 10.1007/s40142-014-0034-x.
Saher, G. *et al.* (2005) 'High cholesterol level is essential for myelin membrane growth', *Nature Neuroscience*, 8(4), pp. 468–475. doi: 10.1038/nn1426.
Saher, G. and Stumpf, S. K. (2015) 'Cholesterol in myelin biogenesis and hypomyelinating disorders', *Biochimica et Biophysica Acta - Molecular and Cell Biology of Lipids*. Elsevier, pp. 1083–1094. doi: 10.1016/j.bbalip.2015.02.010.
Sakai, J. *et al.* (1996) 'Sterol-regulated release of SREBP-2 from cell membranes requires two sequential cleavages, one within a transmembrane segment', *Cell*, 85(7), pp. 1037–1046. doi: 10.1016/S0092-8674(00)81304-5.
Sakai, J. *et al.* (1997) 'Identification of complexes between the COOH-terminal domains of sterol regulatory element-binding proteins (SREBPS) and SREBP cleavage-activating protein', *Journal of Biological Chemistry*, 272(32), pp. 20213–20221. doi: 10.1074/jbc.272.32.20213.
Salloway, S. *et al.* (2011) 'A phase 2 randomized trial of ELND005, scyllo-inositol, in mild to moderate Alzheimer disease.', *Neurology*. American Academy of Neurology, 77(13), pp. 1253–62. doi: 10.1212/WNL.0b013e3182309fa5.
Salloway, S. *et al.* (2014) 'Two Phase 3 Trials of Bapineuzumab in Mild-to-Moderate Alzheimer's Disease', *New England Journal of Medicine*. Massachusetts Medical Society , 370(4), pp. 322–333. doi: 10.1056/NEJMoa1304839.
Sano, M. *et al.* (2011) 'A randomized, double-blind, placebo-controlled trial of simvastatin to treat Alzheimer disease.', *Neurology*. American Academy of Neurology, 77(6), pp. 556–563. doi: 10.1212/WNL.0b013e318228bf11.
Santiard-Baron, D. *et al.* (1999) 'Identification of β-amyloid-responsive genes by RNA differential display: Early induction of a DNA damage-inducible gene, gadd45', *Experimental Neurology*. Academic Press Inc., 158(1), pp. 206–213. doi: 10.1006/exnr.1999.7076.
Sapir, T. *et al.* (2012) 'Tau's role in the developing brain: implications for intellectual disability.', *Human molecular genetics*, 21(8), pp. 1681–92. doi: 10.1093/hmg/ddr603.
Sasaguri, H. *et al.* (2017) ' APP mouse models for Alzheimer's disease preclinical studies ', *The EMBO Journal*. EMBO, 36(17), pp. 2473–2487. doi: 10.15252/embj.201797397.
Savva, G. M. *et al.* (2009) 'Age , Neuropathology , and Dementia for the Medical Research Council Cognitive Function and Ageing Study', *N Engl J Med*. Massachusetts Medical Society, 360(22), pp. 2302–9. doi: 10.1056/NEJMoa0806142.
Schinkel, A. H. and Jonker, J. W. (2003) 'Mammalian drug efflux transporters of the

ATP binding cassette (ABC) family: An overview', *Advanced Drug Delivery Reviews*. Elsevier, 55(1), pp. 3–29. doi: 10.1016/S0169-409X(02)00169-2.
Scholz, D. *et al.* (2011) 'Rapid, complete and large-scale generation of post-mitotic neurons from the human LUHMES cell line', *Journal of Neurochemistry*. Blackwell Publishing Ltd, 119(5), pp. 957–971. doi: 10.1111/j.1471-4159.2011.07255.x.
Sealey, M. A. *et al.* (2017) 'Distinct phenotypes of three-repeat and four-repeat human tau in a transgenic model of tauopathy', *Neurobiology of Disease*. Academic Press Inc., 105, pp. 74–83. doi: 10.1016/j.nbd.2017.05.003.
Selkoe, D. J. (2000) 'Toward a comprehensive theory for Alzheimer's disease. Hypothesis: Alzheimer's disease is caused by the cerebral accumulation and cytotoxicity of amyloid beta-protein.', *Annals of the New York Academy of Sciences*. Blackwell Publishing Ltd, 924(1), pp. 17–25. doi: 10.1111/j.1749-6632.2000.tb05554.x.
Selkoe, D. J. (2019) 'Alzheimer disease and aducanumab: adjusting our approach', *Nature Reviews Neurology*. Nature Publishing Group, 15(7), pp. 365–366. doi: 10.1038/s41582-019-0205-1.
Selkoe, D. J. and Hardy, J. (2016) 'The amyloid hypothesis of Alzheimer's disease at 25 years.', *EMBO molecular medicine*. Wiley-Blackwell, 8(6), pp. 595–608. doi: 10.15252/emmm.201606210.
Serrano-Pozo, A. *et al.* (2010) 'Beneficial effect of human anti-amyloid-b active immunization on neurite morphology and tau pathology'. doi: 10.1093/brain/awq056.
Serrano-Pozo, A., Frosch, M. P., *et al.* (2011) 'Neuropathological alterations in Alzheimer disease', *Cold Spring Harbor Perspectives in Medicine*. Cold Spring Harbor Laboratory Press, 1(1). doi: 10.1101/cshperspect.a006189.
Serrano-Pozo, A., Mielke, M. L., *et al.* (2011) 'Reactive glia not only associates with plaques but also parallels tangles in Alzheimer's disease', *American Journal of Pathology*. Am J Pathol, 179(3), pp. 1373–1384. doi: 10.1016/j.ajpath.2011.05.047.
Sever, N. *et al.* (2003) 'Accelerated degradation of HMG CoA reductase mediated by binding of insig-1 to its sterol-sensing domain', *Molecular Cell*, 11(1), pp. 25–33. doi: 10.1016/S1097-2765(02)00822-5.
Sevigny, J. *et al.* (2016) 'The antibody aducanumab reduces Aβ plaques in Alzheimer's disease', *Nature*. Nature Publishing Group, 537(7618), pp. 50–56. doi: 10.1038/nature19323.
Shabab, T. *et al.* (2017) 'Neuroinflammation pathways: a general review', *International Journal of Neuroscience*. Taylor and Francis Ltd, 127(7), pp. 624–633. doi: 10.1080/00207454.2016.1212854.
Sharpe, L. J. and Brown, A. J. (2013a) 'Controlling cholesterol synthesis beyond 3-hydroxy-3-methylglutaryl-CoA reductase (HMGCR)', *Journal of Biological Chemistry*. American Society for Biochemistry and Molecular Biology, 288(26), pp. 18707–18715. doi: 10.1074/jbc.R113.479808.
Sharpe, L. J. and Brown, A. J. (2013b) 'Controlling cholesterol synthesis beyond 3-hydroxy-3-methylglutaryl-CoA reductase (HMGCR)', *Journal of Biological Chemistry*, 288(26), pp. 18707–18715. doi: 10.1074/jbc.R113.479808.
Shea, Y. F. *et al.* (2016) 'A systematic review of familial Alzheimer's disease: Differences in presentation of clinical features among three mutated genes and potential ethnic differences', *Journal of the Formosan Medical Association*, pp. 67–75. doi: 10.1016/j.jfma.2015.08.004.
Shen, L. *et al.* (2008) 'Immunohistochemical detection of Ndrg2 in the mouse nervous system', *NeuroReport*, 19(9), pp. 927–931. doi: 10.1097/WNR.0b013e32830163d0.

Shi, S. *et al.* (2008) ‘Evaluation of the Value of Frozen Tissue Section Used as “ Gold Standard ” for Immunohistochemistry’, pp. 358–366. doi: 10.1309/7CXUYXT23E5AL8KQ.
Shi, S. R. *et al.* (2008) ‘Evaluation of the value of frozen tissue section used as “gold standard” for immunohistochemistry’, *American Journal of Clinical Pathology*, 129(3), pp. 358–366. doi: 10.1309/7CXUYXT23E5AL8KQ.
Shim, K. S. *et al.* (2006) ‘Bach2 is involved in neuronal differentiation of N1E-115 neuroblastoma cells’, *Experimental Cell Research*. Academic Press Inc., 312(12), pp. 2264–2278. doi: 10.1016/j.yexcr.2006.03.018.
Simons, K. and Ikonen, E. (1997) ‘Functional rafts in cell membranes.’, *Nature*, 387(6633), pp. 569–72. doi: 10.1038/42408.
Simons, K. and Ilonen, E. (2000) ‘How Cells Handle Cholesterol’, 290(December), pp. 1721–1727.
Simons, K. and Sampaio, J. L. (2011) ‘Membrane organization and lipid rafts.’, *Cold Spring Harbor perspectives in biology*. Cold Spring Harbor Laboratory Press, 3(10), p. a004697. doi: 10.1101/cshperspect.a004697.
Simons, K. and Toomre, D. (2000) ‘Lipid rafts and signal transduction.’, *Nature reviews. Molecular cell biology*, 1(1), pp. 31–9. doi: 10.1038/35036052.
Simpson, J E *et al.* (2010) ‘Astrocyte phenotype in relation to Alzheimer-type pathology in the ageing brain’, *Neurobiology of Aging*. Elsevier Inc., 31(4), pp. 578–590. doi: 10.1016/j.neurobiolaging.2008.05.015.
Simpson, J. E. *et al.* (2010) ‘Population variation in oxidative stress and astrocyte DNA damage in relation to Alzheimer-type pathology in the ageing brain’, *Neuropathology and Applied Neurobiology*, 36(1), pp. 25–40. doi: 10.1111/j.1365-2990.2009.01030.x.
Simpson, J. E. *et al.* (2011) ‘Microarray analysis of the astrocyte transcriptome in the aging brain: Relationship to Alzheimer’s pathology and APOE genotype’, *Neurobiology of Aging*, 32(10), pp. 1795–1807. doi: 10.1016/j.neurobiolaging.2011.04.013.
Simpson, J. E. *et al.* (2015) ‘A neuronal DNA damage response is detected at the earliest stages of Alzheimer’s neuropathology and correlates with cognitive impairment in the Medical Research Council’s Cognitive Function and Ageing Study ageing brain cohort’, *Neuropathology and Applied Neurobiology*, 41(4), pp. 483–496. doi: 10.1111/nan.12202.
Simpson, J. E. *et al.* (2016) ‘Neuronal DNA damage response-associated dysregulation of signalling pathways and cholesterol metabolism at the earliest stages of Alzheimer-type pathology’, *Neuropathology and Applied Neurobiology*, 42(2), pp. 167–179. doi: 10.1111/nan.12252.
Simpson, J. E., Wharton, S. B. and Heath, P. R. (2018) ‘Immuno-laser-capture microdissection for the isolation of enriched glial populations from frozen post-mortem human brain’, in *Methods in Molecular Biology*. Humana Press Inc., pp. 273–284. doi: 10.1007/978-1-4939-7558-7_16.
Snaidero, N. and Simons, M. (2014) ‘Myelination at a glance.’, *Journal of cell science*, 127(Pt 14), pp. 2999–3004. doi: 10.1242/jcs.151043.
Sobecki, M. *et al.* (2016) ‘The cell proliferation antigen Ki-67 organises heterochromatin’, *eLife*. eLife Sciences Publications Ltd, 5(MARCH2016). doi: 10.7554/eLife.13722.
Söderberg, M. *et al.* (1990) ‘Lipid Compositions of Different Regions of the Human Brain During Aging’, *Journal of Neurochemistry*, 54(2), pp. 415–423. doi: 10.1111/j.1471-4159.1990.tb01889.x.

Sodero, A. O. *et al.* (2011) 'Cellular stress from excitatory neurotransmission contributes to cholesterol loss in hippocampal neurons aging in vitro', *Neurobiology of Aging*. Elsevier, 32(6), pp. 1043–1053. doi: 10.1016/j.neurobiolaging.2010.06.001.
Sogorb-Esteve, A. *et al.* (2018) 'Inhibition of γ-Secretase Leads to an Increase in Presenilin-1', *Molecular Neurobiology*. Springer US, 55(6), pp. 5047–5058. doi: 10.1007/s12035-017-0705-1.
Solé-Domènech, S. *et al.* (2013) 'Localization of cholesterol, amyloid and glia in Alzheimer's disease transgenic mouse brain tissue using time-of-flight secondary ion mass spectrometry (ToF-SIMS) and immunofluorescence imaging', *Acta Neuropathologica*, 125(1), pp. 145–157. doi: 10.1007/s00401-012-1046-9.
Spampinato, S. F. *et al.* (2017) 'Astrocytes contribute to Aβ-induced blood-brain barrier damage through activation of endothelial MMP9', *Journal of Neurochemistry*. Blackwell Publishing Ltd, 142(3), pp. 464–477. doi: 10.1111/jnc.14068.
Sparks, D. L. *et al.* (1994) 'Induction of Alzheimer-like beta-amyloid immunoreactivity in the brains of rabbits with dietary cholesterol.', *Experimental neurology*. BioMed Central, pp. 88–94. doi: 10.1006/exnr.1994.1044.
Sparks, D. L. *et al.* (2006) 'Circulating cholesterol levels, apolipoprotein E genotype and dementia severity influence the benefit of atorvastatin treatment in Alzheimer's disease: results of the Alzheimer's Disease Cholesterol-Lowering Treatment (ADCLT) trial', *Acta Neurologica Scandinavica*. Blackwell Publishing Ltd, 114(s185), pp. 3–7. doi: 10.1111/j.1600-0404.2006.00690.x.
Stamer, K. *et al.* (2002) 'Tau blocks traffic of organelles, neurofilaments, and APP vesicles in neurons and enhances oxidative stress', *The Journal of Cell Biology*, 156(6).
Stancu, C. and Sima, A. (2001) 'Statins: Mechanism of action and effects', *Journal of Cellular and Molecular Medicine*. Journal of Cellular and Molecular Medicine, 5(4), pp. 378–387. doi: 10.1111/j.1582-4934.2001.tb00172.x.
Steele, M. L. and Robinson, S. R. (2012) 'Reactive astrocytes give neurons less support: Implications for Alzheimer's disease', *Neurobiology of Aging*. Elsevier Inc., pp. 423.e1-423.e13. doi: 10.1016/j.neurobiolaging.2010.09.018.
Steinberg, S. *et al.* (2015) 'Loss-of-function variants in ABCA7 confer risk of Alzheimer's disease', *Nature Publishing Group*, 47(5). doi: 10.1038/ng.3246.
Stelzmann, R. A., Norman Schnitzlein, H. and Reed Murtagh, F. (1995) 'An english translation of alzheimer's 1907 paper, ?????ber eine eigenartige erkankung der hirnrinde???', *Clinical Anatomy*, 8(6), pp. 429–431. doi: 10.1002/ca.980080612.
Strittmatter, W. J. *et al.* (1993) 'Binding of human apolipoprotein E to synthetic amyloid ,B peptide: Isoform-specific effects and implications for late-onset Alzheimer disease', *Medical Sciences*, 90, pp. 8098–8102.
Sun, J. H., Yu, J. T. and Tan, L. (2015) 'The Role of Cholesterol Metabolism in Alzheimer's Disease', *Molecular Neurobiology*. Humana Press Inc., pp. 947–965. doi: 10.1007/s12035-014-8749-y.
Sun, L. P. *et al.* (2005) 'Insig required for sterol-mediated inhibition of Scap/SREBP binding to COPII proteins in vitro', *Journal of Biological Chemistry*, 280(28), pp. 26483–26490. doi: 10.1074/jbc.M504041200.
Sun, Y. *et al.* (2003) 'Expression of liver X receptor target genes decreases cellular amyloid β peptide secretion', *Journal of Biological Chemistry*. American Society for Biochemistry and Molecular Biology, 278(30), pp. 27688–27694. doi: 10.1074/jbc.M300760200.
Suzuki, R. *et al.* (2010) 'Diabetes and insulin in regulation of brain cholesterol metabolism', *Cell Metabolism*. Elsevier Inc., 12(6), pp. 567–579. doi:

10.1016/j.cmet.2010.11.006.
Sweeney, M. D., Sagare, A. P. and Zlokovic, B. V. (2018) 'Blood-brain barrier breakdown in Alzheimer disease and other neurodegenerative disorders', *Nature Reviews Neurology*. Nature Publishing Group, pp. 133–150. doi: 10.1038/nrneurol.2017.188.
Swerdlow, R. H. (2011) 'Brain aging, Alzheimer's disease, and mitochondria', *Biochimica et Biophysica Acta (BBA) - Molecular Basis of Disease*, 1812(12), pp. 1630–1639. doi: 10.1016/j.bbadis.2011.08.012.
Tagami, S. *et al.* (2017) 'Semagacestat Is a Pseudo-Inhibitor of γ-Secretase', *Cell Reports*. Cell Press, 21(1), pp. 259–273. doi: 10.1016/j.celrep.2017.09.032.
Tamagno, E. *et al.* (2002) 'Oxidative stress increases expression and activity of BACE in NT2 neurons.', *Neurobiology of disease*, 10(3), pp. 279–88. Available at: http://www.ncbi.nlm.nih.gov/pubmed/12270690 (Accessed: 4 January 2017).
Tatarnikova, O. G., Orlov, M. A. and Bobkova, N. V. (2015) 'Beta-Amyloid and Tau-Protein: Structure, Interaction, and Prion-Like Properties', *Biochemistry (Moscow)*. Pleiades Publishing, 80(13), pp. 1800–1819. doi: 10.1134/S000629791513012X.
Teller, J. K. *et al.* (1996) 'Presence of soluble amyloid β-peptide precedes amyloid plaque formation in Down's syndrome', *Nature Medicine*. Presse Dienstleistungsgesellschaft mbH und Co. KG, 2(1), pp. 93–95. doi: 10.1038/nm0196-93.
Terao, A. *et al.* (2002) 'Immune response gene expression increases in the aging murine hippocampus', *Journal of Neuroimmunology*, 132(1), pp. 99–112. doi: 10.1016/S0165-5728(02)00317-X.
Terry, R. D. *et al.* (1991) 'Physical basis of cognitive alterations in alzheimer's disease: Synapse loss is the major correlate of cognitive impairment', *Annals of Neurology*. Ann Neurol, 30(4), pp. 572–580. doi: 10.1002/ana.410300410.
Thal, D. R. *et al.* (2002) 'Thal et al., 2002-Phases of Aß-deposition in the human brain and its relevance for the development of AD'.
Thelen, K. M. *et al.* (2006) 'Cholesterol synthesis rate in human hippocampus declines with aging', *Neuroscience Letters*, 403(1–2), pp. 15–19. doi: 10.1016/j.neulet.2006.04.034.
Tönnies, E. and Trushina, E. (2017) 'Oxidative Stress, Synaptic Dysfunction, and Alzheimer's Disease', *Journal of Alzheimer's Disease*. IOS Press, pp. 1105–1121. doi: 10.3233/JAD-161088.
Torun, A. N. *et al.* (2009) 'Serum total antioxidant status and lipid peroxidation marker malondialdehyde levels in overt and subclinical hypothyroidism', *Clinical Endocrinology*. John Wiley & Sons, Ltd, 70(3), pp. 469–474. doi: 10.1111/j.1365-2265.2008.03348.x.
Traxler, L., Edenhofer, F. and Mertens, J. (2019) 'Next-generation disease modeling with direct conversion: a new path to old neurons', *FEBS Letters*. Wiley Blackwell, pp. 3316–3337. doi: 10.1002/1873-3468.13678.
Trusler, D. (2011) 'Statin prescriptions in UK now total a million each week.', *BMJ (Clinical research ed.)*. British Medical Journal Publishing Group. doi: 10.1136/bmj.d4350.
Tsutsui, K. *et al.* (2000) 'Novel brain function: biosynthesis and actions of neurosteroids in neurons', *Neuroscience Research*, 36, pp. 261–273. Available at: www.elsevier.com/locate/neures (Accessed: 14 July 2017).
Tsvetkov, D. *et al.* (2019) 'Distinguishing Between Biological and Technical Replicates in Hypertension Research on Isolated Arteries', *Frontiers in Medicine*. Frontiers Media SA, 6, p. 126. doi: 10.3389/fmed.2019.00126.

Ulland, T. K. *et al.* (2017) 'TREM2 Maintains Microglial Metabolic Fitness in Alzheimer's Disease', *Cell*. Cell Press, 170(4), pp. 649-663.e13. doi: 10.1016/j.cell.2017.07.023.
Ulland, T. K. and Colonna, M. (2018) 'TREM2 — a key player in microglial biology and Alzheimer disease', *Nature Reviews Neurology*. Nature Publishing Group, pp. 667–675. doi: 10.1038/s41582-018-0072-1.
Ulrich, J. D. *et al.* (2017) 'Elucidating the Role of TREM2 in Alzheimer's Disease', *Neuron*. Cell Press, pp. 237–248. doi: 10.1016/j.neuron.2017.02.042.
Urano, Y. *et al.* (2005) 'Association of active γ-secretase complex with lipid rafts', *Journal of Lipid Research*, 46(5), pp. 904–912. doi: 10.1194/jlr.M400333-JLR200.
Urano, Y., Ochiai, S. and Noguchi, N. (2013) 'Suppression of amyloid-β production by 24S-hydroxycholesterol via inhibition of intracellular amyloid precursor protein trafficking', *FASEB Journal*, 27(10), pp. 4305–4315. doi: 10.1096/fj.13-231456.
Uto, Y. (2015) 'Imidazo[1,2-a]pyridines as cholesterol 24-hydroxylase (CYP46A1) inhibitors: A patent evaluation (WO2014061676)', *Expert Opinion on Therapeutic Patents*, 25(3), pp. 373–377. doi: 10.1517/13543776.2014.989214.
Valenza, M. *et al.* (2014) 'Disruption of astrocyte-neuron cholesterol cross talk affects neuronal function in Huntington's disease.', *Cell death and differentiation*. Nature Publishing Group, 22(4), pp. 1–13. doi: 10.1038/cdd.2014.162.
Vance, J. E. and Hayashi, H. (2010) 'Formation and function of apolipoprotein E-containing lipoproteins in the nervous system', *Biochimica et Biophysica Acta - Molecular and Cell Biology of Lipids*. Elsevier, pp. 806–818. doi: 10.1016/j.bbalip.2010.02.007.
Vance, J. E. and Vance, D. E. (1990) 'The assembly of lipids into lipoproteins during secretion.', *Experientia*, 46(6), pp. 560–9. Available at: http://www.ncbi.nlm.nih.gov/pubmed/2193819 (Accessed: 4 January 2017).
Varadarajan, S. *et al.* (2000) 'Review: Alzheimer's amyloid β-peptide-associated free radical oxidative stress and neurotoxicity', *Journal of Structural Biology*. Academic Press Inc., pp. 184–208. doi: 10.1006/jsbi.2000.4274.
Vega, G. L. *et al.* (2003) 'Reduction in levels of 24S-hydroxycholesterol by statin treatment in patients with Alzheimer disease', *Archives of Neurology*. American Medical Association, 60(4), pp. 510–515. doi: 10.1001/archneur.60.4.510.
Viggars, A. P. *et al.* (2011) 'Alterations in the blood brain barrier in ageing cerebral cortex in relationship to Alzheimer-type pathology: A study in the MRC-CFAS population neuropathology cohort', *Neuroscience Letters*. Elsevier Ireland Ltd, 505(1), pp. 25–30. doi: 10.1016/j.neulet.2011.09.049.
Vitali, C., Wellington, C. L. and Calabresi, L. (2014) 'HDL and cholesterol handling in the brain', *Cardiovascular Research*, 103(3), pp. 405–413. doi: 10.1093/cvr/cvu148.
Vyas, S. *et al.* (2016) 'Chronic stress and glucocorticoids: From neuronal plasticity to neurodegeneration', *Neural Plasticity*. Hindawi Limited. doi: 10.1155/2016/6391686.
Wahrle, S. E. *et al.* (2004) 'ABCA1 is required for normal central nervous system apoE levels and for lipidation of astrocyte-secreted apoE', *Journal of Biological Chemistry*. American Society for Biochemistry and Molecular Biology, 279(39), pp. 40987–40993. doi: 10.1074/jbc.M407963200.
Wahrle, S. E. *et al.* (2008) 'Overexpression of ABCA1 reduces amyloid deposition in the PDAPP mouse model of Alzheimer disease', *Journal of Clinical Investigation*. American Society for Clinical Investigation, 118(2), pp. 671–682. doi: 10.1172/JCI33622.
Wake, H. *et al.* (2009) 'Resting microglia directly monitor the functional state of synapses in vivo and determine the fate of ischemic terminals', *Journal of*

Neuroscience. J Neurosci, 29(13), pp. 3974–3980. doi: 10.1523/JNEUROSCI.4363-08.2009.
Waller, R. *et al.* (2012) 'Isolation of enriched glial populations from post-mortem human CNS material by immuno-laser capture microdissection', *Journal of Neuroscience Methods*, 208, pp. 108–113. doi: 10.1016/j.jneumeth.2012.04.014.
Wallin, A. *et al.* (1989) 'Decreased myelin lipids in Alzheimer's disease and vascular dementia', *Acta Neurologica Scandinavica*, 80(4), pp. 319–323. doi: 10.1111/j.1600-0404.1989.tb03886.x.
Walz, W. and Lang, M. K. (1998) 'Immunocytochemical evidence for a distinct GFAP-negative subpopulation of astrocytes in the adult rat hippocampus', *Neuroscience Letters*, 257(3), pp. 127–130. doi: 10.1016/S0304-3940(98)00813-1.
Wang, C. *et al.* (2019) 'The sterol regulatory element-binding protein 2 is dysregulated by tau alterations in Alzheimer disease', *Brain Pathology*, 29(4), pp. 530–543. doi: 10.1111/bpa.12691.
Wang, H. *et al.* (2016) 'The cytotoxicity of 27-hydroxycholesterol in co-cultured SH-SY5Y cells and C6 cells', *Neuroscience Letters*. Elsevier Ireland Ltd, 632, pp. 209–217. doi: 10.1016/j.neulet.2016.08.056.
Wang, W. *et al.* (2014) 'Amyloid precursor protein α- And β-cleaved ectodomains exert opposing control of cholesterol homeostasis via SREBP2', *FASEB Journal*. FASEB, 28(2), pp. 849–860. doi: 10.1096/fj.13-239301.
Waterham, H. R. *et al.* (2001) 'Mutations in the 3beta-hydroxysterol Delta24-reductase gene cause desmosterolosis, an autosomal recessive disorder of cholesterol biosynthesis.', *American journal of human genetics*, 69(4), pp. 685–94. doi: 10.1086/323473.
Wezyk, M. and Zekanowski, C. (2018) 'Role of BRCA1 in Neuronal Death in Alzheimer's Disease', *ACS Chemical Neuroscience*. American Chemical Society, 9(5), pp. 870–872. doi: 10.1021/acschemneuro.8b00149.
Wharton, S. B. *et al.* (2011) 'Epidemiological neuropathology: The MRC cognitive function and aging study experience', *Journal of Alzheimer's Disease*, 25(2), pp. 359–372. doi: 10.3233/JAD-2011-091402.
'WHO | Dementia' (2016) *WHO*. World Health Organization.
Wilson, M. R. and Easterbrook-Smith, S. B. (2000) 'Clusterin is a secreted mammalian chaperone', *Trends in Biochemical Sciences*, 25(3), pp. 95–98. doi: 10.1016/S0968-0004(99)01534-0.
Wisniewski, K. E., Wisniewski, H. M. and Wen, G. Y. (1985) 'Occurrence of neuropathological changes and dementia of Alzheimer's disease in Down's syndrome', *Annals of Neurology*. John Wiley & Sons, Ltd, 17(3), pp. 278–282. doi: 10.1002/ana.410170310.
Witman, G. B. *et al.* (1976) 'Tubulin requires tau for growth onto microtubule initiating sites (flagella/in vitro assembly/electron microscopy)', *Cell Biology*, 73(11), pp. 4070–4074.
Wu, L. *et al.* (2012) 'Early-onset familial Alzheimer's disease (EOFAD).', *The Canadian journal of neurological sciences. Le journal canadien des sciences neurologiques*, 39(4), pp. 436–45. Available at: http://www.ncbi.nlm.nih.gov/pubmed/22728850 (Accessed: 7 December 2016).
Wu, Z. *et al.* (2016) 'Nutrients, Microglia Aging, and Brain Aging', *Oxidative Medicine and Cellular Longevity*. Hindawi Limited. doi: 10.1155/2016/7498528.
Xiong, L. *et al.* (2018) 'Dementia incidence and predictors in cerebral amyloid angiopathy patients without intracerebral hemorrhage', *Journal of Cerebral Blood Flow and Metabolism*. SAGE Publications Ltd, 38(2), pp. 241–249. doi:

10.1177/0271678X17700435.
Xu, Q. *et al.* (2006) 'Profile and Regulation of Apolipoprotein E (ApoE) Expression in the CNS in Mice with Targeting of Green Fluorescent Protein Gene to the ApoE Locus', *Journal of Neuroscience*, 26(19), pp. 4985–4994. doi: 10.1523/JNEUROSCI.5476-05.2006.
Yang, T. *et al.* (2002) 'Crucial step in cholesterol homeostasis: Sterols promote binding of SCAP to INSIG-1, a membrane protein that facilitates retention of SREBPs in ER', *Cell*, 110(4), pp. 489–500. doi: 10.1016/S0092-8674(02)00872-3.
Yin, F. *et al.* (2016) 'Energy metabolism and inflammation in brain aging and Alzheimer's disease', *Free Radical Biology and Medicine*. Elsevier Inc., pp. 108–122. doi: 10.1016/j.freeradbiomed.2016.04.200.
Yu, C. Y. *et al.* (2014) 'HNRNPA1 regulates HMGCR alternative splicing and modulates cellular cholesterol metabolism', *Human Molecular Genetics*, 23(2), pp. 319–332. doi: 10.1093/hmg/ddt422.
Yuan, P. *et al.* (2016) 'TREM2 Haplodeficiency in Mice and Humans Impairs the Microglia Barrier Function Leading to Decreased Amyloid Compaction and Severe Axonal Dystrophy', *Neuron*. Cell Press, 90(4), pp. 724–739. doi: 10.1016/j.neuron.2016.05.003.
Zago, W. *et al.* (2012) 'Neutralization of soluble, synaptotoxic amyloid β species by antibodies is epitope specific.', *The Journal of neuroscience : the official journal of the Society for Neuroscience*. Society for Neuroscience, 32(8), pp. 2696–702. doi: 10.1523/JNEUROSCI.1676-11.2012.
Zatta, P. *et al.* (2002) 'Astrocytosis, microgliosis, metallothionein-I-II and amyloid expression in high cholesterol-fed rabbits', *Journal of Alzheimer's Disease*, 4(1), pp. 1–9. doi: 10.3233/JAD-2002-4101.
Zhang, J. and Liu, Q. (2015) 'Cholesterol metabolism and homeostasis in the brain', *Protein and Cell*, 6(4), pp. 254–264. doi: 10.1007/s13238-014-0131-3.
Zhang, X. *et al.* (2019) '27-hydroxycholesterol promotes Aβ accumulation via altering Aβ metabolism in mild cognitive impairment patients and APP/PS1 mice', *Brain Pathology*, 29(4), pp. 558–573. doi: 10.1111/bpa.12698.
Zhang, Y. *et al.* (2014) 'Cellular/Molecular An RNA-Sequencing Transcriptome and Splicing Database of Glia, Neurons, and Vascular Cells of the Cerebral Cortex', *Journal of Neuroscience*, 34(36). doi: 10.1523/JNEUROSCI.1860-14.2014.
Zhang, Z. *et al.* (2019) 'The Appropriate Marker for Astrocytes: Comparing the Distribution and Expression of Three Astrocytic Markers in Different Mouse Cerebral Regions', *BioMed Research International*. Hindawi Limited, 2019. doi: 10.1155/2019/9605265.
Zhu, X. C. *et al.* (2015) 'Rate of early onset Alzheimer's disease: A systematic review and meta-analysis', *Annals of Translational Medicine*. AME Publishing Company, 3(3), p. 38. doi: 10.3978/j.issn.2305-5839.2015.01.19.
Zhukareva, V. *et al.* (2002) 'Sporadic Pick's disease: A tauopathy characterized by a spectrum of pathological τ isoforms in gray and white matter', *Annals of Neurology*. John Wiley & Sons, Ltd, 51(6), pp. 730–739. doi: 10.1002/ana.10222.
Ziontz, J. *et al.* (2019) 'Tau pathology in cognitively normal older adults', *Alzheimer's and Dementia: Diagnosis, Assessment and Disease Monitoring*. Elsevier Inc, 11, pp. 637–645. doi: 10.1016/j.dadm.2019.07.007.
Zuberek, M. *et al.* (2018) 'Exposure of human neurons to silver nanoparticles induces similar pattern of ABC transporters gene expression as differentiation: Study on proliferating and post-mitotic LUHMES cells', *Mechanisms of Ageing and Development*. Elsevier Ireland Ltd, 171, pp. 7–14. doi: 10.1016/j.mad.2018.02.004.